Quantitative Magnetic Resonance Imaging in Muscular Dystrophies

Dr Alexander Peter Murphy

PhD thesis

The John Walton Muscular Dystrophy Research Centre

Institute of Genetic Medicine

Newcastle University

June 2018

Abstract

Muscular dystrophies are rare diseases characterised by progressive muscle wasting and weakness. Putative therapies are being evaluated; the slowly progressive nature makes outcome measures difficult to design. Four pathological hallmarks of muscular dystrophies include: muscle necrosis, inflammation, fibrosis, and adipose transformation. This thesis evaluates novel methods of quantifying pathological hallmarks of muscular dystrophy in both skeletal and cardiac muscle using magnetic resonance imaging (MRI).

To quantify fibrosis in a mouse model of Duchenne muscular dystrophy, EP3533, a collagen-specific contrast agent, was assessed in quantification of fibrosis in muscle. EP3533-measures correlated with functional tests and histological quantification of fibrosis.

Extracellular volume (ECV) was calculated in a limb muscular dystrophy type R9 cohort (LGMDR9), a Becker muscular dystrophy cohort and healthy controls. ECV was found comparable to traditional measures of cardiac dysfunction and demonstrated regional dysfunction.

A multicentre study followed up 24 participants with LGMDR9 over 6 years. The three-point Dixon method of fat fraction calculation was evaluated in this cohort and compared to functional assessments. All muscles showed significantly increased fat fractions over 6 years, which was more responsive than functional assessments.

As patients with muscular dystrophies can have difficulties remaining supine during scanning, a method of reducing acquisition time in measurement of left ventricular (LV) indices was evaluated. Accelerated images were compared to conventional imaging with accelerated imaging producing images with a high fidelity. No significant changes were seen in LV functional indices or cardiac tagging measures over five years was assessed in an LGMDR9 cohort, this may be due to confounding variables.

The MRI methods described can be successfully used to quantify progression of disease pathology in muscular dystrophies. These findings can be used to support further trials of EP3533 and ECV as an outcome measure in muscular dystrophies and to inform study design of future trials into LGMDR9.

Declaration

This PhD involved murine experiments and collaboration with the Newcastle University Institute of Cellular Medicine, UK. The technical protocol for MRI was designed by myself, with support from Dr Dara O'Hogain (Institute of Cellular Medicine, Newcastle University, UK) and Professor Andrew Blamire (Institute of Cellular Medicine, Newcastle University, UK). Animal handling was performed by myself and supported by Ms Elizabeth Greally (John Walton Muscular Dystrophy Research Centre, Newcastle University, UK). PK sampling was done by Ms Elizabeth Greally and Ms Brigid Griffin (Comparative Biology Centre, Newcastle University, UK). The contrast agent (EP3533) was supplied by our collaborator Professor Peter Caravan (Collagen LLC, Boston, United States).

The clinical part of this PhD involved firstly a multicentre study with participants with LGMDR9 from the following research groups: Professor Michael Hanna (University College London (UCL) Institute of Neurology, London); Professor Pierre Carlier and Dr Tanja Stojkovic (Institute of Myology, Paris, France); Professor John Vissing (Neuromuscular Research Unit, Copenhagen, Denmark) and Professor Volker Straub (John Walton Muscular Dystrophy Research Centre, Newcastle upon Tyne, UK).

The LGMDR9 muscle study protocol was based on the first study written by Dr Tracey Willis (2009) (Institute of Genetic Medicine, Newcastle University, UK). This was amended by myself with ethical approval obtained for UK based sites. Professor Carlier and Professor Vissing applied for local ethical approval for their respective institutions.

The protocol for quantitative MRI for the LGMDR9 6 year follow-up study was coordinated by Dr Kieren Hollingsworth, (Institute of Cellular Medicine, Newcastle University, UK).

Region of interest analysis was performed by myself, James Clark and Anna Beretsos (Faculty of Medical Sciences, Newcastle University, UK). Their assistance is gratefully acknowledged.

The manual for the standardised physical assessments was amended by myself and the research physiotherapists (John Walton Muscular Dystrophy Research Centre, Newcastle University, UK): Dr Michelle Eagle, Dr Anna Mayhew and Ms Meredith James. These physiotherapists also provided study specific teleconference training. Functional assessments were carried out by local physiotherapists with results sent to me for analysis.

Cardiac MRI analysis was analysed by myself with assistance from Dr Kieren Hollingsworth, James Clark and Anna Beretsos.

Radiographers Louise Ward, Tim Hodgson and Dorothy Wallace (Newcastle Magnetic Resonance Centre, Newcastle University, UK) performed all human MRI scans.

Participant recruitment, their care during the study, all study procedures (i.e. cannulation) and all other aspects apart from those mentioned previously were undertaken by myself.

The composition of this thesis is my work. The research contained within the thesis has not been submitted elsewhere for a PhD.

I dedicate this thesis to Holly, Georgia and Lexie

Acknowledgments

Firstly I would like to thank my supervisors, Dr John Bourke, Professor Straub and Dr Kieren Hollingsworth for their ongoing support and guidance.

Volker has been an incredibly supportive mentor and it has been an amazing opportunity to work within the John Walton muscular dystrophy research centre. He has been unflappable during all of the trials and tribulations of my work where he has always offered guidance.

I would especially like to thank Kieren who was kind enough (and patient enough) to give so many hours of his time to teach me about statistics, and scientific writing. Without his attention to detail and supervision I would not be able to have completed this work.

A special thank you must go to Elizabeth Greally who has been my sounding board and friend throughout the difficult times in the lab. She has taught me so much about academia, laboratory skills, and animal handling. She is a great friend, real grafter and an excellent teacher.

I would like to thank the whole team at the John Walton muscular dystrophy research centre, doctors, nurses, physios, and delivery staff who have helped me and supported me throughout this process. I'd like to thank the nurses at the CRF for taking care of me in Newcastle, they have been excellent friends to me during my whole time here.

I would like to thank all the participants who take part in clinical research. The bravery and commitment to forwarding research has been a real inspiration for me. I am always surprised by those participants (and healthy control participants) who take part in these studies.

I would like to thank my parents for giving me an excellent start in life and always pushing me to try my hardest.

I would like to thank Lexie and Georgia for being random, looking after their Mummy Girl while I was away, and drawing me pictures to put on my wall to make me smile when I have been lonely. Finally and most importantly, I would like to thank Holly for proof reading my work and being the most supportive partner I could wish for. She has always been amazing, putting me and our little family first. Without her infinite patience and support I have no doubt I would not have been able to write this. Thank you.

Contents

Figure List

Table List

Abbreviation

Abbreviation	Term
6MWT	Six minute walk test
10MWR	Ten metre walk or run
A	Anterior
AA	Apical anterior
Amy	Amyloidosis
AP	Apical posterior
AS	Aortic stenosis
ASA	Apical septal anterior
ASP	Apical septal posterior
ATP	Adenosine triphosphate
BA	Basal anterior
BFLH	Biceps femoris long head
BFSH	Biceps femoris short head
BH	Breath holding
BL10	Black 10 control mice
BLAST	Broad-use Linear Acquisition Speed-up Technique
BMD	Becker muscular dystrophy
BP	Basal posterior
Bpm	Beats per minute
BSA	Basal septal anterior
BSP	Basal septal posterior
cCSA	Contractile cross sectional area
CK	Creatine Kinase
CIRCUS	Circular cartesian undersampling
CMRI	Cardiac magnetic resonance imaging
CSA	Cross sectional area
CSPAMM	Complementary spatial modulation of magnetisation
CTGF	connective tissue growth factor
DAPI	4',6-Diamidine-2'-phenylindole dihydrochloride
DCM	Dilated cardiomyopathy
DMD	Duchenne muscular dystrophy
DMSO	Dimethyl sulfoxide
DTPA	Diethylenetriaminepentaacetic
DWI	Diffusion weighted imaging
ECM	Extracellular matrix
ECV	Extracellular volume
ETL	Echo train length
F	Foot
FA	Flip angle
FB	Free breathing
FF	Fat fraction
FKRP	Fukutin-related protein
FOV	Field of view
FVC	Forced vital capacity
GCN	Gastrocnemius
Gd	Gadolinium

Abbreviation	Term
gemsIR-LL	Gradient echo multi-slice inversion-recovery Look-Locker
Gr	Gracilis
GRE	3d gradient echo
H	Head
H&E	Haematoxylin and eosin
HCM	Hypertrophic obstructive cardiomyopathy
Hct	Haematocrit
HMS	Hamstrings
I	Inferior
ICD	Implantable cardioverter defibrillator
IGF	Insulin-like growth factor
IP	Intraperitoneal
IQR	Interquartile range
L	Left
LC-MS/MS	Liquid chromatography – mass spectrometry/mass spectrometry
LDH	Lactate dehydrogenase
LFT	Liver function tests
LG	Lateral gastrocnemius
LGE	Late gadolinium enhancement
LGMD	Limb girdle muscular dystrophies
LGMDR9	Limb girdle muscular dystrophy type R9
LOA	Limits of agreement
LV	Left ventricular
LVEDV	Left ventricular end diastolic volume
LVEF	Left ventricular ejection fraction
LVESV	Left ventricular end systolic volume
LVM	Left ventricular mass
LVSV	Left ventricular stroke volume
MCA	Mid cavity anterior
MCP	Mid cavity posterior
MCSA	Mid cavity septal anterior
MCSP	Mid cavity septal posterior
MEMRI	Manganese enhancement magnetic resonance imaging
MG	Medial gastrocnemius
MI	Myocardial infarction
MMT	Manual muscle testing
MOLLI	Modified Look Locker sequence
MRI	Magnetic resonance imaging
MRS	Magnetic resonance spectroscopy
MT	Masson's trichrome
NAcc	Net acceleration
N/A	Not applicable
NG	Not given
NIV	Non-invasive ventilation
NO	Nitric oxide
nNOS	Neuronal Nitric oxide synthetase
NS	Not significant
NSAA	North star ambulatory assessment
P	Posterior

Abbreviation	Term
PBS	Phosphate buffered saline
PCr	Phosphocreatine
PDGF	Platelet derived growth factor
PECS	Peak endocardial strain
PFA	Paraformaldehyde
PK	Pharmacokinetics
PL	Peroneus longus
PSIR	3D phase sensitive inversion recovery
PT	Peak torsion
PWWS	Peak whole wall circumferential strain
QMT	Quantitative muscle testing
QUADS	Quadriceps
R	Right
RF	Rectus femoris
ROI	Region of interest
RVEF	Right ventricular ejection fraction
S	Superior
Sar	Sartorius
SENSE	SENSitivity Encoding
SGd	Standard gadolinium agent
SM	Semimembranosus
SNR	Signal to noise ratio
Sol	Soleus
SRM	Standardised response mean
ST	Semitendinosus
STIR	Short T1 inversion recovery
TA	Tibialis anterior
TE	Echo time
TFE	Turbo field echo
TGF-ß1	Transforming growth factor beta one
TR	Repetition time
TSR	Torsion to strain ratio
UCL	University of central London
UK	United Kingdom
UNEW	Newcastle University
US	Ultrasound
UTE	Ultrashort echo time
VCG	Vectorcardiogram
VL	Vastus lateralis
VM	Vastus medialis
WMA	Wall motion abnormalities

Chapter 1. Introduction

1.1 Muscular dystrophies

Muscular dystrophies are heterogeneous inherited conditions that cause progressive muscular wasting and weakness. These conditions can present at any age from the antenatal period to late in adult life, and a similarly wide variation is seen in the rate of progression. While muscular dystrophies are associated with skeletal muscle weakness and loss of ambulation, certain muscular dystrophies involve cardiac and respiratory systems, leading to mortality due to respiratory failure, chest infections, arrhythmias or cardiomyopathy (Bushby et al., 2010b). The advent of international collaborative networking such as 'TREAT-NMD' and international policies have facilitated research into rare diseases, which when considered as a whole affect 8-10% of the population (Treat NMD, 2017, European commission, 2008). Over the past two decades advances in basic science and genetics have led to the development of several promising therapeutic avenues for muscular dystrophies (Qiao et al., 2014, Stevens et al., 2013, Richard et al., 2016, Svahn et al., 2015). The selection of appropriate outcome measures for clinical trials is of paramount importance in the pathway of translational research, and determines the value, power and feasibility of putative therapeutic agents. For a therapeutic agent to be licenced, trial design must maximise internal and statistical validity. When selecting clinical trial outcome measures, several factors have to be considered: what the intervention is aiming to improve, how best to measure this through existing outcome tools, and whether the outcome measure has sufficient sensitivity to detect change over time (longitudinal validity) (Liang, 2000, Coster, 2013). Among other barriers, muscular dystrophies are slowly progressive and therefore outcome measures may lack longitudinal sensitivity. Clinical trials into muscular dystrophies have also reported difficulty in demonstrating clinical efficacy outside of a narrow group of participants fulfilling specific inclusion criteria (Domingos and Muntoni, 2018).

The pathology of many of the muscular dystrophies is caused primarily by the loss of one of the many proteins that are essential to the healthy working of a myocyte. Alpha-dystroglycan is a peripheral membrane protein which, through the many bonds formed by glycosylation, is central to the structure of the myocyte and membrane stability. Dystrophinopathies such as Duchenne muscular dystrophy (DMD) and Becker muscular dystrophy (BMD) are caused by a defect in the dystrophin protein which bonds directly to α-dystroglycan to form the dystrophin-glycoprotein complex. Therefore, these conditions share a common pathway of pathogenesis with conditions affecting α-dystroglycan such as limb girdle muscular dystrophy type R9 *FKRP*-related (LGMDR9). Membrane instability and subsequent cation influx cause muscle fibre necrosis. Inflammation and

inability of the somatic repair mechanisms to manage the myocytic damage leads to fibrosis, replacement with adipocytes (fat replacement) and eventual muscular weakness. The four detectable hallmarks of muscular dystrophy pathology are: 1. Muscle fibre necrosis and inflammatory response, 2. Fibrosis, 3. Replacement of muscle with adipocytes, 4. Progressive muscle weakness. Outcome measures are typically based upon one or more of these hallmarks which demonstrate disease progression (Figure 1). Current approaches to quantification of disease pathology in muscular dystrophies are discussed in detail in Chapter 2.

In current clinical trials, the most commonly used primary outcome measures are functional due to their clinical relevance to patients. Criticisms of functional assessments include: subjectivity, improvement through training effects, dependence on age or comorbidity and lack of longitudinal sensitivity (Bushby and Connor, 2011). Magnetic resonance imaging (MRI) has been shown to have utility as a diagnostic tool in muscular dystrophies (Mercuri et al., 2007, Wattjes et al., 2010). Some techniques of quantitative MRI are well established as outcome measures, whereas other novel methods require *in vivo* validation (Ricotti et al., 2016, Wren et al., 2008, Finanger et al., 2012, Dixon, 1984). It has been shown that MRI has potential to non-invasively detect change in skeletal muscle over a shorter period of time than functional assessments, and is fully objective (Willis et al., 2013).
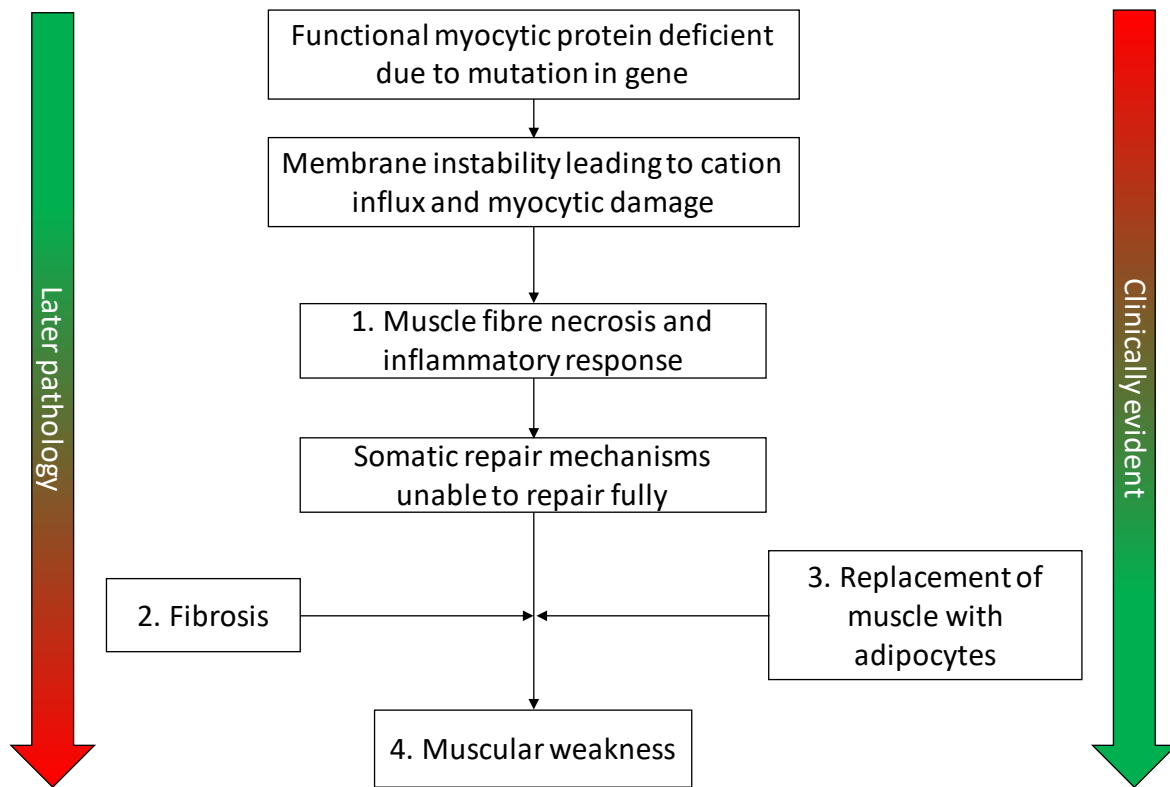
Figure 1. An overview of disease pathology in dystrophin-glycoprotein complex associated muscular dystrophies with reference to outcome measure design. Numbered boxes are current approaches to quantifiable outcome measures with number 4 functional weakness being the most clinically evident (shown by the arrow to the right of the diagram), but the latest detectable pathology (shown by the arrow to the left of the diagram). There are advantages to successful detection of early pathological changes, which may be more sensitive to the disease process before weakness is detectable; this can reduce duration of clinical trials or be used to increase study design power.

Muscular dystrophies are a heterogeneous group of rare genetic disorders. Muscular dystrophies encompass several different forms of inherited conditions, including DMD, BMD and the Limb girdle muscular dystrophies (LGMD). The LGMD were established as a separate entity from DMD in a seminal paper by Walton and Natrass in 1954 (Walton and Nattrass, 1954). DMD, BMD and LGMDR9 are caused by a defect of a gene which results in deficit of a functional protein essential in healthy myocytes. In the case of DMD and BMD there is a deficit of full-length functional dystrophin, a subsarcolemmal, cytoskeletal protein which assists in membrane stability (Kole and Krieg, 2015, Anthony et al., 2011). Most types of muscular dystrophy are not confined to skeletal muscle and can affect multiple organs. The most severe types cause congenital malformation and involve cardiac and respiratory muscles.

This first chapter provides an overview of the three types of muscular dystrophy that will feature in studies within this thesis, either as an animal model, or as clinical trial participants.

Chapter 2 details how outcome measures have been used in the past to quantify different aspects of muscular dystrophies, with focus on methodology used in this thesis. Chapter 3 describes the

methods used in subsequent chapters. Chapter 4 discusses murine experiments of a novel, collagen-specific contrast agent (EP3533) in quantification of fibrosis as an outcome measure in skeletal and cardiac muscle. Chapter 5 details how quantitative MRI and physiotherapy-based assessments can be used to detect disease progression as an outcome measure in LGMDR9. In Chapter 6, extra cellular volume (ECV) quantification of the heart is measured as a potential biomarker of diffuse fibrosis and inflammation in participants with LGMDR9 and BMD. Chapter 7 explores cardiac outcome measures in a LGMDR9 group over five years and evaluates whether a method of reducing acquisition time improves quantitative MRI as an outcome measure, whilst retaining image fidelity and providing accurate calculation of cardiac functional measures. Chapters 8 and 9 discuss the findings of the studies contained within this thesis and place these findings within the wider context of muscular dystrophies and clinical trials.

1.2 Overview of the muscular dystrophies involved within this thesis

1.2.1 Duchenne muscular dystrophy

DMD is an X-linked recessive disorder caused by mutations in the *DMD* gene. The *DMD* gene is located on the X-chromosome and measures 2.4Mb (Den Dunnen et al., 1992). Dystrophin is a sub-sarcolemmal protein found in several tissues including smooth, skeletal, and cardiac muscle. Dystrophin is important for the membrane stability of myocytes; the stress of contraction of muscle is thought to be absorbed in a way analogous to a spring, reducing mechanical shear forces and supporting the membrane (Kole and Krieg, 2015, Anthony et al., 2011). A deficit of dystrophin leads to membrane instability and damage, allowing extracellular cation influx, leading to oedema and inflammation (Klingler et al., 2012). Development of muscular fibrosis is a common pathological hallmark of progression, with higher levels associated with a poorer prognosis in terms of ambulation and cardiac function (Desguerre et al., 2009, Puchalski et al., 2009, Walcher et al., 2011). Dystrophin is expressed within neural tissue with reported signalling properties within the postsynaptic site of neurons (Hendriksen et al., 2015). Dystrophin expression within the brain may account for the higher incidence of learning difficulties, epilepsy, autism and attention deficit hyperactivity disorder found within this cohort (Donders and Taneja, 2009, Wicksell et al., 2004, Wu et al., 2005, Pane et al., 2013).

DMD has an estimated worldwide prevalence of 1 in 3,300-5,136 (Mendell et al., 2012, Moat et al., 2013, Emery, 2002). Newborn screening tests have been trialled in several countries though currently no country has a fully implemented ongoing neonatal screening programme for DMD

(Moat et al., 2013, Drousiotou et al., 1998, Beckmann et al., 1976, Greenberg et al., 1991). In the United Kingdom (UK), the mean age of diagnosis of DMD is 4.3 years old (Bushby et al., 1999). Onset of symptoms is typically much earlier (UK average of 2.7 years), with delayed gross motor milestones and development of Gowers' sign (van Ruiten et al., 2014). Typically patients with DMD reach their developmental milestones late, reaching a plateau of improvement in motor function between 5-7 years old. Patients with DMD are unable to keep up with their peers, with increased fatigability and exercise intolerance (Bushby et al., 2010a). Due to the higher incidence of learning difficulties and autism, speech and language delay may be the presenting complaint.

Without treatment, progressive muscle weakness leads to loss of ambulation; typically within the first to second decade of life. Weakness is more profound proximally in the hip and shoulder girdle muscles, with progression to distal muscles over a period of years. On examination, pseudo-hypertrophy of the calf causes the appearance of an enlargement in the lower leg muscles. Development of scoliosis is common in steroid naïve patients. Progressive contracture development also occurs without appropriate orthoses and physiotherapy. Rhabdomyolysis is uncommon but can occur, typically only after extended exercise. Respiratory muscle weakness is progressive and includes the diaphragm; many patients require ventilation in the second decade of life. Cardiac dysfunction is seen in almost all patients with DMD by the age of twenty, and is associated with a reduced life span (Jefferies et al., 2005, Ramaciotti et al., 2006, Barp et al., 2015, Eagle et al., 2002).

Patients with DMD have a reduced life span; without corticosteroids this can be restricted to the second decade of life (Eagle et al., 2002). The most common cause of death is due to respiratory insufficiency and chest infections, with an estimated 20% dying due to cardiac arrhythmias or cardiomyopathy (Passamano et al., 2012).

Several blood markers are likely to be abnormal in patients with DMD, but are not specific to this condition. These include serum creatine kinase (CK) activity, several liver function tests (LFT) and lactate dehydrogenase (LDH). Muscle biopsy with immuno-histochemical staining reveals an absence of dystrophin. The diagnosis of DMD is confirmed by identification of a mutation within the *DMD* gene on molecular genetic testing (Bushby et al., 2010a).

MRI is the most commonly used imaging modality to differentiate between neuromuscular disorders. In early DMD, standard T1 weighted imaging can have a normal appearance, with development of degenerative changes in the second half of the first decade of life (Lamminen, 1990, Nagao et al., 1991, Matsumura et al., 1988). T1 values and appearances change initially in the gluteus maximus and adductor magnus, followed by the quadriceps (QUADS), rectus femoris

(RF) and biceps femoris muscles. There is reported sparing of the sartorius (Sar), gracilis (Gr), semitendinosus (ST), and semimembranosus (SM) muscles. In the calf, the gastrocnemius (GCN) muscles are affected earlier than the soleus (Sol) and the peroneus longus (PL) muscles. Specialist MRI techniques such as T2 weighted short T1 inversion recovery imaging (STIR) reveal areas of inflammation and oedema in muscles as yet not affected by fatty replacement (Mercuri et al., 2007). In later stages of the disease, fatty replacement of the muscles almost eliminates all appearances of normal muscle.

Care standards for DMD suggest that management is multidisciplinary (Birnkrant et al., 2018a, Birnkrant et al., 2018c, Birnkrant et al., 2018d). Physiotherapy, occupational therapy and educational services are important to involve from an early age (Bushby et al., 2010b). Cardiac review is recommended annually over the age of ten, with those under the age of ten recommended every two years (Birnkrant et al., 2018a). Respiratory function is reviewed at least annually, with non-invasive ventilation (NIV) recommended once forced vital capacity (FVC) falls below recommended levels, or the patient becomes symptomatic of nocturnal hypoventilation (Bushby et al., 2010b, Birnkrant et al., 2018a).

Corticosteroids are the current recommended treatment for DMD. Beneficial effects of steroids have been shown even after loss of ambulation on respiratory and cardiac function (Matthews et al., 2016). To date, Translarna is the only UK licenced treatment which is specific to DMD with nonsense mutations. Eteplirsen has been approved by the Food and Drug Administration in the United States. With the advent of standards of care, current supportive treatments and corticosteroids, the course of DMD has changed over the past twenty years. Life expectancy has improved from 14.4 years in the 1960s to 25.3 years in the late twentieth century (Passamano et al., 2012).

1.2.2 The *mdx* mouse model

The *mdx* mouse is the best characterised and most widely used animal model of DMD. It has a point mutation within exon 23 of the *Dmd* gene, which leads to a premature stop codon. Other animal models of DMD include: piscene, rodent, feline, porcine, and canine (Bassett and Currie, 2003, Winand et al., 1994, Kornegay et al., 2012, Larcher et al., 2014, Klymiuk et al., 2013). The *mdx* mouse model has advantages over the majority of these other animal models, including speed of reproduction and overall cost. The average life span of an *mdx* mouse is reduced to over 20 months, compared to control mice (average life span over 25 months) (Chamberlain et al., 2007). Muscle

pathology is most pronounced in the first 3-4 weeks of life, with corresponding high serum CK levels (Collins and Morgan, 2003). Histological appearances are highly variable between mice but display diffuse extra cellular fibrosis with little adipose tissue deposition. The mild phenotype of *mdx* mice may be due to the relatively small housing environment, which reduces physical activity (Collins and Morgan, 2003).

1.2.3 Becker muscular dystrophy

BMD was identified in a paper in 1955 by Dr Peter Emil Becker, a German neurologist, psychiatrist and geneticist (Becker, 1955). Building on knowledge from an earlier family described in a publication with similar symptoms, he diagnosed a milder form of the X-linked DMD (Kostakow and Derix, 1937). In BMD, the *DMD* gene has in-frame deletion, allowing production of a truncated dystrophin protein. The truncated dystrophin protein imperfectly cushions the mechanical forces caused by myocyte contraction. Over time, myocytes go through the same pathophysiological processes as seen in DMD. Some studies have suggested that the severity of the phenotype of BMD is dependent on the location of the mutation in the *DMD* gene (Nicolas et al., 2015, Kaspar et al., 2009).

BMD is less common than DMD, with a suggested point prevalence of 7.29 per 100,000 population (Norwood et al., 2009a). BMD shows an incidence of 1 individual per 30,000 male births. In contrast to LGMDs, there isn't thought to be a significant ethnic variation in terms of prevalence (American Academy of Pediatics, 2005).

Motor symptoms commence at 11-12 years old on average, but with a wide age range (van den Bergen et al., 2014). Proximal muscle weakness, myalgia, difficulty in ascending stairs and exercise intolerance are common presenting complaints. Pseudo-hypertrophy of the calf muscles may be seen, and Gower's sign is often positive. Progression of weakness causes loss of ambulation at, on average, 27 years of age. Respiratory muscles are involved variably and deficiency may be progressive; respiratory failure may require NIV in the minority of patients. Cardiac dysfunction does not necessarily correlate to severity of skeletal muscle involvement, and can be very severe. Throughout their lives cardiac dysfunction has been suggested to be prevalent in up to 70% of patients with BMD (Nigro et al., 1995, Petri et al., 2015, Finsterer and Stöllberger, 2008).

Similar to DMD, CK, LDH and LFT are commonly raised. The diagnosis of BMD is confirmed by identification of an in-frame mutation within the *DMD* gene on molecular genetic testing (Bushby

et al., 2010a). Muscle histology and muscle MRI show broadly similar results to DMD though typically less severe.

There are only supportive treatments available for BMD, corticosteroids may have beneficial effects but are not routinely given due to side effects. Prevalence of cardiac dysfunction has been variably reported from 33-100% of patients throughout their lives; the most widely quoted prevalence is 70% (Nigro et al., 1995, Petri et al., 2015, Finsterer and Stöllberger, 2008). Unlike other muscular dystrophies, cardiac pathology is not necessarily related to the level of ambulation, with cardiac involvement the most common cause of mortality in BMD (Finsterer and Stöllberger, 2008). There is a wide variation in the progression of cardiac fibrosis within patients with BMD. Angiotensin converting enzyme inhibitors, beta blockers, mineralocorticoids and diuretics are the mainstays of treatment. In severe cases, left ventricular (LV) assist devices and cardiac transplantation have been performed with positive outcomes (Hollander et al., 2016, Wu et al., 2010).

1.2.4 Limb girdle muscular dystrophy

Limb girdle muscular dystrophy is an umbrella term used to denote a group of rare, autosomally-inherited diseases. The LGMD were first characterised in a seminal paper by Walton and Natrass in 1954 (Walton and Nattrass, 1954). To date, over thirty sub-types of LGMD exist (Pegoraro and Hoffman, 1993). Recessively inherited cases make up the majority of LGMDs. Consensus on the nomenclature and classification of the LGMD was formalised in 1995, with a number assigned depending on mode of inheritance, 1 is dominant or 2 for recessive; a letter is then added in order of discovery (Figure 2) (Bushby, 1995). A recent European neuromuscular centre workshop has revisited the definition and classification. Subtypes are categorised with the character R or D depending on whether the condition is recessive or dominant respectively, a number is then added in order of discovery. The related protein is included in the name (Straub et al., 2018).
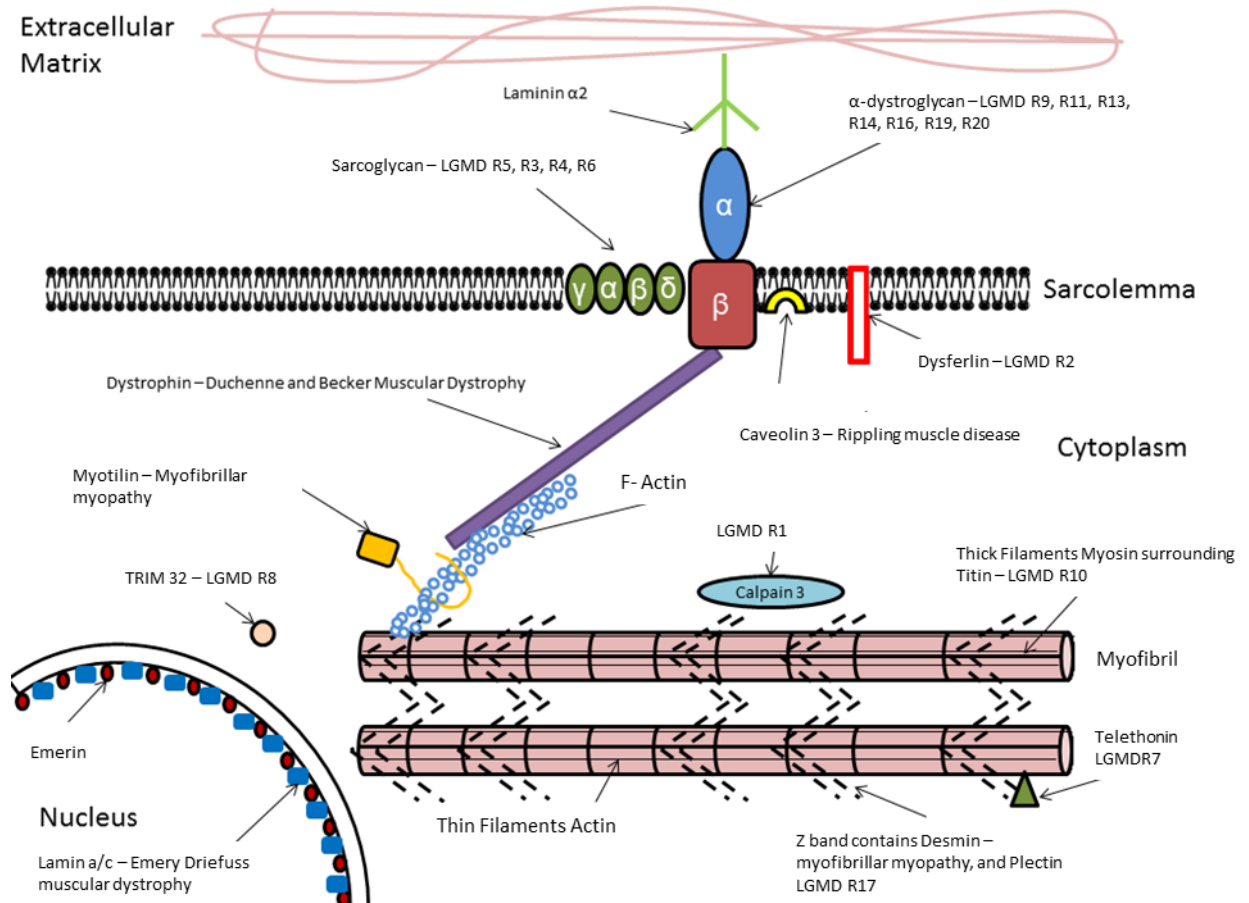
Figure 2. A depiction of the sarcolemma and LGMD subtypes associated with a defect in each protein. Modified to include the new classification from Murphy *et al.* (Murphy and Straub, 2015).

Overall prevalence of LGMD worldwide has been estimated to be 1 in 14,500-45,000 (van der Kooi et al., 1996, Norwood et al., 2009a). LGMD displays wide variation in prevalence between ethnicities, and it has been suggested that this may be due to founder mutations (Hicks et al., 2011, Norwood et al., 2009b, Emery, 1991, Walter et al., 2004a). Some of the most recently identified LGMD subtypes have only been described in one to two families worldwide (Preisler et al., 2013, Chardon et al., 2015).

LGMDR9 is one of the most common subtypes in northern Europe. Norwood *et al.* estimated that in the UK, of all of the LGMD subtypes the most common is LGMDR1 (26.5%), then LGMDR9 (19.1%) (Norwood et al., 2009b). LGMDR9 has an estimated prevalence of 0.43 per 100,000 in the UK (Norwood et al., 2009b).

The *Fukutin-Related Protein* (*FKRP*) gene was first discovered by Brockington *et al.* in 2001 (Brockington et al., 2001). FKRP has been implicated in the glycosylation of α-dystroglycan and is expressed in several tissues including skeletal and cardiac muscle, with several other tissues also containing this protein - however to a much smaller degree. Glycosylation is the process of adding

carbohydrates to proteins; glycosylation of α-dystroglycan through the addition of glycans allows multiple points of bonding and therefore greater structural support between the extracellular matrix (ECM) and the myocyte (Awano et al., 2015). Glycans have many possible structural configurations. Alpha-dystroglycan is a subtype of glycans known as an 'O-glycan'. Alpha-dystroglycan binds to important proteins such as laminin, perlecan, neurexin and agrin (Kanagawa et al., 2016).

Kanagawa *et al.* suggested that FKRP works in tandem with Fukutin protein to produce Ribitol-5 Phosphate, a substance essential in functional maturation of α-dystroglycan (Kanagawa et al., 2016). FKRP has been found within the Golgi apparatus and the rough endoplasmic reticulum and is present at the cell membrane (Beedle et al., 2007). FKRP modifies α-dystroglycan by addition of terminating glycans, thus stabilising the dystrophin-glycoprotein complex (Kanagawa et al., 2016, Beedle et al., 2007).

The most common mutation within the *FKRP* gene LGMDR9 population is the c.826C > A, p.Leu276Ile (L276I) (Walter et al., 2004a). Compound heterozygous mutations cause a more severe phenotype and have been likened in severity to the course of DMD (Sveen et al., 2006, Richard et al., 2016). Reported frequency of mutant alleles in Europe is estimated to be 1 in 200-600 (Sveen et al., 2006, Brockington et al., 2001, Walter et al., 2004b). Compound homozygous presentation is typically within the first decade of life, with ambulation lost during the second decade. In contrast to homozygous mutations cardiac involvement is seen in almost all patients, with respiratory support needed in almost all by the age of 30 (Richard et al., 2016, Poppe et al., 2004).

Since the most common mutation within the *FKRP* gene is L276I, description of the clinical presentation will focus on this genotype.

LGMDR9 can present between 2 to 40 years old, with the mean reported age of presentation with skeletal muscle weakness is at 15.2-18.0 years (Sveen et al., 2006, Poppe et al., 2004). The most common symptoms include proximal muscle weakness, myalgia, and exercise intolerance. One study suggested that in 45% of patients, initial onset of symptoms was proceeded by a viral illness (Richard et al., 2016). LGMDR9 affects the skeletal, respiratory, and cardiac muscles. Muscular weakness is progressive over the course of several years. Calf hypertrophy is evident in 66% of patients, with eventual loss of ambulation in an estimated 22% of patients (Sveen et al., 2006, Richard et al., 2016). Progression of muscular weakness has not been shown to correlate necessarily to respiratory or cardiac severity (Poppe et al., 2004, Petri et al., 2015, Richard et al., 2016).

Respiratory involvement is often variable but frequently progressive. One study suggested that above the age of twenty, predicted FVC drops by 6-20% over five years (Poppe et al., 2003). A relatively small proportion (5%) of patients require respiratory support (i.e. NIV) (Sveen et al., 2006).

There are significantly fewer studies investigating LGMDR9 cardiac dysfunction, and the development of fibrosis remains comparatively poorly characterised (Rosales et al., 2011, Petri et al., 2015). Poppe *et al.* suggested that cardiac involvement may be present in 38% of patients, with onset of cardiomyopathy seen most commonly after the third decade of life (Poppe et al., 2003). Onset of cardiomyopathy may be present in childhood (Rasmussen et al., 2014, D'Amico et al., 2008), and this demonstrates the importance of cardiac surveillance, which is recommended annually (Rasmussen et al., 2014). Treatment of cardiac manifestation secondary to LGMDR9 is based on the same principles and medication as for BMD. There have been isolated case reports of patients with LGMDR9 requiring surgical intervention for cardiac disease (D'Amico et al., 2008). It is not known whether the prognosis of LGMDR9 is dependent on cardiac involvement in the same way as in other NMDs (Eagle et al., 2002, Finsterer and Stöllberger, 2008).

Serum CK activity is between 10-20 times the upper limit of normal. Muscle MRI has an important utility in aiding differentiation between types of muscular dystrophies. The pattern of LGMDR9 muscle involvement does depend on the progression of the disease, with early involvement of the gluteus maximus, adductor magnus and biceps femoris (Wattjes et al., 2010, Willis et al., 2014). In the thigh the ST and SM muscles are also more commonly affected. The RF and vastus lateralis (VL) muscles are affected later in the disease, with the Sar and the Gr muscles reportedly relatively spared (Wattjes et al., 2010, Willis et al., 2014). In the calf, diffuse changes are seen in the GCN and Sol muscles. Eventually these become severely affected, with the tibialis anterior (TA) muscle relatively spared (Wattjes et al., 2010, Willis et al., 2014).

There is evidence of differences in manifestations of LGMDR9 along gender lines. Studies have found differences in patterns of muscles affected on MRI (Willis et al., 2014). The speed of ambulatory decline and cardiac involvement have been suggested to be less severe in affected females (Poppe et al., 2004).

Diagnosis may be suspected following a muscle biopsy with pathological levels of α-dystroglycan, though findings may be variable (Rasmussen et al., 2014). Genetic confirmation of mutations within the *FKRP* gene is diagnostic.

1.3 Conclusion

Research into muscular dystrophies has burgeoned; with several therapeutic avenues to be explored there is a pressing need for appropriate clinical outcome measures. Muscular dystrophies represent a cohort with unique challenges for the design of clinical trial outcome measures. Although functional assessments are the most commonly used primary outcome measure for therapeutic trials, quantitative MRI has several potential advantages in its ability to evaluate different hallmarks of muscular dystrophy non-invasively. This PhD explores several novel methods of how quantitative MRI can be used as an outcome measure for clinical trials.

Three forms of muscular dystrophy are described within this chapter, the most severe of which is DMD. BMD and LGMDR9 are often considered together in studies due to their phenotypic similarities. To date, few studies have investigated clinical outcome measures in the slowly progressive BMD or LGMDR9.

1.4 Aims

The overall aim of this thesis is to evaluate novel methods of quantification of the pathology of muscular dystrophy and to apply existing methods to a muscular dystrophy cohort.

Chapter-specific objectives are detailed below.

1. Quantification of fibrosis via a collagen-specific contrast agent: The first objective is threefold: firstly, to assess whether the novel collagen-specific contrast agent (EP3533) can be used to quantify the different levels of fibrosis found within control (BL10) and *mdx* mice cardiac and skeletal muscles. Secondly, to correlate skeletal muscle signal post-EP3533 to histological methods of fibrosis quantification. Thirdly, to use EP3533 to investigate whether fibrosis can be quantified and used to monitor disease progression in response to administration of an established anti-fibrotic (halofuginone).

2. To apply Dixon fat fraction (FF) quantification to a LGMDR9 cohort over a six year period. To compare this to how functional assessments can detect disease progression and to evaluate the most sensitive muscle groups or compound muscle groups, for analysis.

3. The third objective is to quantify the extracellular volume (ECV) for the measurement of fibrosis in cardiac muscle of patients with LGMDR9 and BMD. Comparing the ECV in different segments of the heart and correlating these to other methods of detecting global cardiac dysfunction such as left ventricular mass (LVM), left ventricular ejection fraction

(LVEF), measurements of cardiac strain, presence of late gadolinium enhancement (LGE), and wall motion abnormalities (WMA). To perform a preliminary evaluation of ECV as a measure of cardiac disease progression with reference to cardiac indices.

4. To evaluate accelerated imaging in the acquisition of LV indices in muscular dystrophies using Bland Altman analysis compared to conventional imaging techniques. The second objective is to assess whether LV indices and measures of strain and torsion significantly change over a five year period in a LGMDR9 group.

1.5 Hypotheses

1. Administration of EP3533 will cause a quantifiable change in signal to noise ratio (SNR) and R1 change within skeletal and cardiac muscle.

2. Quantification of fibrosis *ex vivo* demonstrates a statistically significant correlation with R1 change post-EP3533 administration in cardiac and skeletal muscles.

3. EP3533-derived R1 values will be able to quantify differences in disease progression following a 12-week administration of an established anti-fibrotic (halofuginone) compared to untreated mice.

4. In a LGMDR9 cohort there will be significant increases in skeletal muscle fat content from baseline to six years.

5. MRI measurement of FF is more sensitive to disease change compared to standardised functional assessments over six years.

6. ECV values will be higher in cardiac segments in BMD and LGMDR9 cohorts compared to control participants.

7. Segmental and global measurements of ECV correlate with other methods of detecting cardiac dysfunction such as ejection fraction, LGE, WMA, and cardiac strain and torsion.

8. Accelerated imaging demonstrates no significant bias in LV indices compared to conventional imaging with clinically acceptable LOA.

9. The accelerated imaging technique employed has a greater level of agreement with the conventional imaging technique compared to other studies utilising similar accelerated imaging techniques.

10. LV indices and measures of strain and torsion significantly decline over a six year period in a LGMDR9 group.

Chapter 2: Outcome measures in muscular dystrophy

2.1 Introduction

There are several putative therapies in development for the treatment of muscular dystrophies. Translarna is the only disease-specific medication currently licenced in the UK for the treatment of a muscular dystrophy, with therapy aiming to slow clinical deterioration (Haas et al., 2015). Therapeutic approaches include exon skipping (Clinical Trials.gov, 2017, Mendell et al., 2016, Charleston et al., 2018), gene therapy (Clinical Trials.gov, 2018d), myostatin inhibition (Clinical trials.gov, 2018b), histone deactylase inhibition (Clinical trials.gov, 2018a), and anti-fibrotics (Clinical Trials.gov, 2016, Kirschner et al., 2010, Buyse et al., 2015, Raman et al., 2015, Udelson et al., 2010). The pathology of muscular dystrophies has several hallmarks which may be used to demonstrate disease progression as an outcome measure or be targeted as a therapeutic avenue. A good outcome measure is repeatable, minimally invasive, has low inter and intra-observer variability, is clinically relevant, and sensitive to disease fluctuations over the short and long term. In the context of the slowly progressive muscular dystrophies, clinically meaningful outcome measures can be insufficiently sensitive to disease progression over short periods of time.

Muscle biopsy is used to quantify dystrophin in clinical trials targeting production of dystrophin (Charleston et al., 2018). Whilst muscle biopsy and subsequent histology allows measurement of dystrophin and can quantify other disease processes such as fibrosis (Beekman et al., 2018, Beekman et al., 2014, Pessina et al., 2014b), the test is invasive and involves standard surgical risks of infection and issues specific to neuromuscular disease around general anaesthetic (Blatter Joshua and Finder Jonathan, 2013). As pathology in muscular dystrophies is not uniform, with some areas of muscle affected by focal fibrosis, muscle biopsies run the risk of over- or underestimation of pathology. Kinali *et al.* assessed histology as an outcome measure against semi-quantitative MRI in assessing disease (Kinali et al., 2011). Muscle biopsy samples were taken from the extensor digitorum brevis muscle and were compared to muscle MRI findings using a semi-quantitative scale. The histological quantification of disease progression and fat replacement correlated significantly with the semi-quantitative MRI measurement (r=0.81 p<0.001, r=0.62 p<0.05 respectively) (Kinali et al., 2011). Due to the subjective nature of semi-quantitative scales of muscle involvement on MRI, and significant overlap between grading of muscles, such scales have largely been superseded by quantitative measures (Willis et al., 2013, Willis et al., 2014, Carlier et al., 2015, Forbes et al., 2014, Forbes et al., 2013, Diaz-Manera et al., 2018). Regarding muscle biopsy as an

outcome measure, other technologies (i.e. MRI) have potential to show disease progression in a less invasive manner, and potentially can show disease progression over larger areas of muscle.

The three muscular dystrophies discussed within this thesis DMD, BMD and LGMDR9 have similar mechanisms and hallmarks of pathology with a variable rate of progression. This chapter discusses the four hallmarks of muscular dystrophy pathology as detailed in the introduction (muscle fibre necrosis and inflammatory response, fibrosis, replacement of muscle with adipocytes and muscular weakness); identifying how these can be used as outcome measures, with a focus on previous work around methods used within this thesis.

2.2 Pathology of muscular dystrophies within this thesis

In DMD and BMD, weakness is an end-stage pathology due to reduced contractile skeletal muscle, increased fibrosis and adipose replacement. Dystrophin has been suggested to be analogous to a spring, cushioning mechanical forces during muscle contraction and reducing membrane instability. In the absence of fully functioning dystrophin, membrane instability leads to it becoming porous, allowing the influx of extracellular cations such as calcium and sodium. Changes of intracellular sodium concentration cause osmotic influx within myocytes (Klingler et al., 2012). Calcium overload occurs due to the newly established diffusion gradient, leading to mitochondrial uncoupling and eventual production of reactive oxygen species and acidic metabolites. Necrosis and apoptosis occurs within the myocyte, which in turn releases cytokines and causes further inflammation (Klingler et al., 2012). Transforming growth factor beta 1 (TGF-ß1) stimulates precursor cells to differentiate into fibroblasts and is thought to be one of the main mechanisms by which fibrosis occurs in DMD and BMD. TGF-ß1 is a cytokine which signals via receptor proteins, to allow phosphorylation of the downstream Smad 2/3 proteins. The Smad proteins are translocated into the nucleus, where they bind to DNA to regulate transcription of pro-fibrotic genes. Smad 3 is a strongly pro-fibrotic molecule, which has been suggested to be central to TGF-ß1-mediated fibrosis in pathological states (Zhao et al., 2002, Bonniaud et al., 2005).

Other inflammatory pathways include interleukin-6 release in response to increased irregular myocyte strain. This has been implicated in the placement of connective tissue, if not collagen directly. Platelet derived growth factor (PDGF), Insulin-like growth factor (IGF) and connective tissue growth factor (CTGF) are implicated in fibrosis formation and proliferation of myofibroblasts and satellite cells (Klingler et al., 2012, Wynn, 2007). Precursor myocytes are used to replace the damaged myocytes, and eventually the pool of satellite cells is exhausted (Rahimov and Kunkel,

2013). Fibro-fatty tissue increases within the ECM and replaces healthy muscle tissue (Barp et al., 2017).

Another possible mechanism of myocytic damage is due to vasoconstriction. Neuronal nitric oxide synthetase (nNOS) is important in the production of nitric oxide (NO), a powerful vasodilator. A reduction in nNOS is associated with an absence of dystrophin (Bia et al., 1999). This reduces the concentration of NO available to the microvasculature of the muscle, and may cause vasoconstriction and subsequent myocyte damage (Sander et al., 2000). To lend further support to the role of nNOS, animal models of DMD have been shown to be ameliorated by the replacement of nNOS (Wehling et al., 2001).

Central to the stability of the sarcolemma is the dystrophin-glycoprotein complex which links the cytoskeletal actin and the extracellular matrix. The dystrophin-glycoprotein complex is made up of α and β dystroglycan. An important factor in maintaining sarcolemmal membrane stability is the correct glycosylation of α-dystroglycan, which is modified by both N and O-linked glycosylation. FKRP is thought to be important in O-linked glycosylation of α-dystroglycan. Mutations in FKRP have been shown to reduce the molecular weight of α-dystroglycan (Esapa et al., 2002). Glycosylation of α-dystroglycan is also thought to be important in binding to laminin, neurexin and agrin. In LGMDR9, where there is an absence of functional FKRP, this leads to hypoglycosylation of α-dystroglycan. The structural link between extracellular matrix and cytoskeleton is weakened as there are fewer binding sites to important extracellular matrix proteins (Vannoy et al., 2017). The membrane is therefore less stable and becomes porous, this then follows the same pathway as seen in dystrophinopathies of: influx of extracellular cations, myocytic damage and necrosis, inflammatory response, eventual fibrosis, adipocyte replacement of muscle, and muscular weakness.

2.3 Pathological hallmarks of muscular dystrophies - Inflammation and somatic repair

Inflammatory response and subsequent repair is the earliest part of the mechanism of pathology in muscular dystrophies. Due to the many complex pathways of inflammation and repair, biomarkers based upon quantity of a single protein or enzyme may not reflect the disease progression fully. Levels of proteins and enzyme may vary throughout the disease process or due to the development of comorbidities.

2.3.1 Therapeutic avenues related to inflammation

Corticosteroids are the longest standing pharmacological agent aimed at amelioration of DMD (Bushby et al., 2010a, Birnkrant et al., 2018b). Corticosteroids reduce inflammation within muscle, thereby allowing more time for somatic mechanisms to repair myocytes before fibrosis and adipocyte replacement. A study of ciclosporin A, a targeted anti-inflammatory medication, had no success in a clinical trial aimed at reducing deterioration of ambulation (Kirschner et al., 2010).

2.3.2 Outcome measures related to inflammation and somatic repair mechanisms

CK is the most widely used serum biomarker used to assist in the diagnosis of DMD, with a specificity of 94% and sensitivity of 100% (Anaya-Segura et al., 2015). CK is raised in several muscular dystrophies, and therefore has limited value in differentiating between different muscular dystrophies. Liver enzyme tests are commonly raised in DMD; however, similarly to CK, levels are variable and not necessarily related to disease progression (Anaya-Segura et al., 2015).

Several serum biomarkers for DMD have been evaluated, mostly utilising elements of the inflammatory cascade to detect disease progression. Previously identified biomarkers include, among others, micro-ribonucleic acid (Cacchiarelli et al., 2011), interleukin-17 (De Pasquale et al., 2012), several types of serum matrix metalloproteinase (Nadarajah et al., 2011, Anaya-Segura et al., 2015), tissue inhibitor of metalloproteinases 1, myostatin and follistatin (Anaya-Segura et al., 2015). Proteomics, the large-scale assessment of proteins, has been used to identify several biomarkers of muscular dystrophies, which may be useful in the diagnosis or in following disease progression (Hathout et al., 2015, Spitali et al., 2018). Further studies are required to show correlation to existing outcome measures; greater understanding of how the serum proteins vary throughout the course of the disease has potential to demonstrate multifaceted disease progression or amelioration. Urinary biomarkers have been identified as significantly higher in DMD, including urinary ferritin (Rouillon et al., 2018) and amino terminal titin fragment (Robertson et al., 2017). These urinary molecules may have a link to the active disease process and reflect muscle breakdown. Longitudinal data on urinary molecules is lacking and such factors are likely to vary over the course of the disease.

Monitoring the progression of cardiac dysfunction primarily involves imaging technologies. Serum biomarkers such as troponins, and natriuretic peptides have been evaluated in the acute period and in monitoring of chronic dysfunction of several cardiac diseases (Bodor et al., 1997, Mori et al., 2002, Doust et al., 2005). Mori *et al.* found that in DMD cardiac biomarkers were only raised in the

presence of severe heart failure (fractional shortening <15% on echocardiogram), suggesting that these biomarkers were not sensitive enough for early detection of cardiac dysfunction (Mori et al., 2002). Rises in cardiac biomarkers are transient in response to myocytic damage, and have been used to stratify risk following acute events such as unstable angina or myocardial infarction (MI) (Morrow et al., 2000). In muscular dystrophies, cardiomyocyte damage is a chronic process and is asymptomatic until late stage heart failure (Bushby et al., 2003).

2.3.3 Imaging modalities

Most imaging technologies rely on the detection of tissue differences, due to a property of the tissue which alters the returning signal. To detect inflammation, the majority of imaging technologies rely on the detection of extracellular oedema or an increased extracellular space. Imaging technologies may be unable to differentiate between oedema and fibrosis unless they are contrast enhanced (Mavrogeni et al., 2017).

Ultrasound scanning (USS) has been shown to be a safe, painless, quick technique which is effective at imaging superficial and some deep tissues. Fat and skin transmit sound and the subtle changes in density allow recognition of borders between layers. Bone and more dense tissues reflect almost all of the sound back to the transducer, producing a high intensity signal and preventing deeper imaging.

USS is not widely used in the diagnosis of muscular dystrophies. Several studies have explored using USS as a diagnostic tool (Pillen et al., 2007, Zuberi et al., 1999, Brockmann et al., 2007), and some have suggested high positive predictive values of 88-91% (Brockmann et al., 2007, Pillen et al., 2007). These studies looked at a range of neuromuscular disorders, focussing on whether USS could differentiate between these conditions, which may have significantly different mechanisms of pathology (i.e. neurogenic versus myopathic) (Brockmann et al., 2007, Pillen et al., 2007). These studies had only a minority of participants with muscular dystrophies; one detailed a false negative result in a presymptomatic participant with DMD (Pillen et al., 2007). USS as a diagnostic tool in muscular dystrophies may therefore have limited utility as a way to non-invasively differentiate between diagnoses (Pillen et al., 2007).

USS studies in healthy children have established normal parameters for echo intensity, which appear to be more strongly correlated with height, weight and age than factors such as muscle strength (Jacobs et al., 2013). Quantification of fibrous and fatty tissues using backscatter and echo intensities has been trialled using semi-quantitative scales and grey scale analysis. These have been

shown in DMD to correlate significantly with both histological measures of fibrosis (Pillen et al., 2009) and function (Jacobs et al., 2013, Jansen et al., 2012). Zaidman *et al.* suggested that skeletal muscle USS modalities demonstrated disease progression when functional assessments continued to improve in younger patients with DMD (Zaidman et al., 2015). USS has been evaluated longitudinally as an outcome measure, demonstrating progressive increases in muscle echo-intensity under the age of 12 years. Echo intensity after this age reached a plateau and did not increase further, potentially due to extensive replacement of muscle by fibrosis and adipose tissue (Jansen et al., 2012). USS therefore has several advantages as an outcome measure: it is readily available, cheap and non-invasive. Several studies have suggested limited utility in diagnosis, and higher signal has been correlated to disease progression over time (Jacobs et al., 2013, Jansen et al., 2012). Unlike contrast-enhanced MRI, it lacks specificity for the disease processes and may reflect oedema rather than fat or fibrosis. There may also be a limit to the use of USS as an outcome measure longitudinally over 12 years of age, which may be due to the muscles examined – however further studies are required to confirm this (Jansen et al., 2012).

It is possible to ascertain the biochemical composition of tissue using magnetic resonance spectroscopy (MRS), and thereby assess skeletal muscle metabolism. MRS uses the properties of different metabolites to display unique resonances at different chemical shifts within a magnetic field. The chemical shift is used to discern different metabolites as each molecule appears at a different point along the x axis (measured in parts per million). Metabolites of interest include: creatine, phosphocreatine (PCr), phosphodiesters, and lipids.(Lamb et al., 1999, Canese et al., 2016, Kim et al., 2016).

Several studies have used MRS to investigate muscular dystrophies (Arpan et al., 2014, Carlier et al., 2016, Crilley et al., 2000, Hollingsworth et al., 2013b, Wary et al., 2015, Barnard et al., 2018), and abnormalities in MRS metabolites have been detected in patients with DMD, BMD, carriers of dystrophin mutations and LGMDR9 (Kemp et al., 1993, Hollingsworth et al., 2013b). Lower total amounts of certain phosphate-based compounds have been suggested to be due to loss of healthy muscle and replacement with fibro-fatty tissue (Carlier et al., 2016). Phosphodiesters and inorganic phosphate have been shown to be higher in dystrophic muscle, in the case of inorganic phosphate this may be due to a porous membrane with insufficient homeostatic mechanisms (Wary et al., 2012, Hooijmans et al., 2017). Altered ratios of metabolites such as PCr and adenosine triphosphate (ATP) have been found in dystrophic skeletal and cardiac muscle (Wokke et al., 2014a, Cui et al., 2015a). This has been found earlier in disease than other measures of dysfunction or fibrosis but have poor correlation to measurements of function and disease progression (Hollingsworth et al., 2013b, Crilley et al., 2000, Kim et al., 2015, Lodi et al., 1997). Changes in MRS metabolites have

been shown in DMD in response to corticosteroid therapy (Arpan et al., 2014), exon skipping (Le Guiner et al., 2014) and loss of ambulation (Wary et al., 2015). One study showed spectral abnormalities in BMD prior to detectable fat replacement, suggesting that MRS may be sensitive to early stages of the disease process (Wokke et al., 2014a). As with other biomarkers based on early pathology there is likely to be significant intra-subject variability in metabolite levels over time and volume of remaining functional muscle.

Some studies have suggested that native T1 weighted imaging is able to demonstrate disease pathology when comparing healthy controls to participants with muscular dystrophies in both cardiac and skeletal muscle (Fatehi et al., 2017, Florian et al., 2014c, Garrood et al., 2009, Soslow et al., 2016). Native T2 measurement has been extensively examined in muscular dystrophies, and is linked to fat replacement; this has been shown to significantly correlate to functional assessments (Kim et al., 2010, Kim et al., 2015, Willcocks et al., 2014, Wansapura et al., 2010, Mankodi et al., 2017). Native T1 and T2 measurement lacks specificity to the disease process reflecting overall pathology and oedema.

Diffusion weighted imaging (DWI) is a technique which has been used to demonstrate diffusion of water molecules and to evaluate structural changes in skeletal muscle fibres and has been linked to injury and repair (Zaraiskaya et al., 2006, Anneriet and Bruce, 2007). DWI metrics in skeletal muscle have been shown to correlate to a significant degree to functional measures and MRI calculated FF (Ponrartana et al., 2015, Li et al., 2016). It has been suggested that DWI can be affected by muscular lipid replacement due to fat-related artefacts and the low self-diffusion coefficient of lipids compared to water, which may reduce the accuracy of DWI in reflecting myofibre structure (Williams Sarah et al., 2013, Ponrartana et al., 2015).

Murine studies have suggested that sodium entry in *mdx* myofibers is higher than in controls (Hirn et al., 2008). Sodium-based MRI has been piloted, showing significantly higher signal intensity of intracellular sodium in skeletal muscle in individuals with DMD compared to healthy volunteers (Weber et al., 2011). To date, no large scale studies have investigated the use of sodium imaging; however initial studies have suggested potentially important features of the nature of muscular oedema (Weber et al., 2011).

Contrast-enhanced MRI may be able to infiltrate skeletal muscle in the presence of sarcolemmal damage or necrosis in animal models of DMD (Thibaud et al., 2007, Amthor et al., 2004). Garood *et al*. used a non-specific gadolinium (Gd) agent to attempt to quantify differences between normal and corticosteroid treated participants with DMD, further evaluating Gd enhancement post-

exercise. The relatively spared TA muscles were the only muscles to show a significant increase in enhancement post-exercise (Garrood et al., 2009).

Binding of Gd directly to monoclonal antibodies allows targeting of a specific protein (Boros et al., 2015, Caravan, 2006). A Gd-based probe with moderate affinity to albumin was evaluated by Lauffer *et al.* (Lauffer et al., 1998). Some preclinical studies have investigated an albumin-targeted contrast probe in dystrophic muscle. The albumin-specific contrast probe was able to diffuse into areas of tissues with damaged membranes (Amthor et al., 2004, Straub et al., 2000). Such probes were able to be used to detect fibre damage, and showed increases in signal intensity in several muscles. The authors of these studies suggested that probes of this type could be used as outcome measures or, with modification, as a therapeutic vector (Amthor et al., 2004, Straub et al., 2000). Another study, using a discrete targeted multimer agent, attempted to identify extracellular deoxyribonucleic acid (DNA) post-MI; this was potentially useful in monitoring levels of cell death (Huang et al., 2011). Targeted particle assembly method was used in *in vivo* experiments targeting fibrin (Flacke et al., 2001, Uppal et al., 2010). Using this method, only vascular targets are possible due to the relative molecular size of the Gd-based probe (Caravan, 2006). To date, none of these agents have been used to quantify disease progression. Such probes are reliant on myocytic membrane damage, which may vary over time.

Another approach to demonstrating early pathology in dystrophic muscle uses manganese enhancement MRI (MEMRI). This process relies on the uptake of manganese via calcium channel receptors (Hu et al., 2001). Increase in manganese enhancement has been suggested to correlate to calcium channel influx, and therefore demonstrate inotropic effects within the heart (Hu et al., 2001). In *mdx* mice, MEMRI was shown to be reduced compared to a disease model of sarcoglycanopathy, and was used as an outcome measure alongside functional cardiac assessment – though no significant difference was demonstrated between the treated and untreated groups in the study (Blain et al., 2013, Greally et al., 2013). MEMRI has been evaluated *in vivo* in skeletal *mdx* muscle as a measure of calcium influx. Loehr *et al.* demonstrated significant differences between disease and control groups in skeletal muscle, suggesting a significant correlation to function (Loehr et al., 2016). To date, this method has not been evaluated in humans, and carries a higher risk to other contrast agents as it is neurotoxic and has been shown to accumulate within the brain (Alaverdashvili et al., 2017).

2.4 Pathological hallmarks of muscular dystrophies - Fibrosis

The term 'fibrosis' refers to the replacement of normal tissue with collagen and other ECM components. Fibrosis is a secondary process of tissue replacement following irreparable tissue damage (Wynn and Ramalingam, 2012). Collagen is a structural protein involved in the fibrotic response. Collagen is detectable within healthy organs in relatively high concentrations ranging from 1-20nmol/g (Neuman and Logan, 1950). Fibrosis is a prominent histological feature of human muscle affected by muscular dystrophies and has been suggested to have value as a prognostic feature (Klingler et al., 2012, Desguerre et al., 2009).

2.4.1 Therapeutic avenues related to fibrosis

Anti-fibrotic therapies have advantages over mutation-specific putative therapies, as they can be given to any muscular dystrophy exhibiting significant fibrosis irrespective of gene mutation. Anti-fibrotics are commonly administered to patients with autoimmune diseases, and either have global immunosuppressive effects or target specific inflammatory pathways. Although in theory anti-fibrotics could be given to any muscular dystrophy exhibiting a fibrotic phenotype, studies exploring anti-fibrotics in muscular dystrophies have focussed on DMD as the most common and well described form of muscular dystrophy. Studies have also examined models of sarcoglycan-null mice and suggested these phenotypes may have a more fibrotic phenotype compared to the *mdx* mouse (Gibertini et al., 2014).

Studies using anti-fibrotics in *mdx* mice have aimed to reduce muscle pathology by reducing the pro-fibrotic molecule TGF-ß1 with mixed results (Andreetta et al., 2006, Gosselin et al., 2004, Gosselin and Williams, 2006, Huebner et al., 2008, Turgeman et al., 2008, Taniguti et al., 2011). Other anti-fibrotic compounds studied include: inhibition of PDGF (Ito et al., 2013, Huang et al., 2009), and phosphodiesterase-5 inhibitors (Adamo et al., 2010, Leung et al., 2014, Percival et al., 2012). Ciclosporin A (Kirschner et al., 2010), idebenone (Buyse et al., 2015), and eplerenone (Raman et al., 2015, Udelson et al., 2010) have been evaluated in human trials. The latter two agents providing significantly positive results in terms of respiratory function and cardiac function respectively (Buyse et al., 2015, Raman et al., 2015, Udelson et al., 2010).

Halofuginone is a potent anti-fibrotic that inhibits phosphorylation of Smad 3 and attenuates of gene expression of collagen-α1 in fibroblasts, this leads to a reduction in collagen deposition and reduction in fibrosis (McGaha et al., 2002, Barzilai-Tutsch et al., 2016). Inhibition of phosphorylation of Smad 3 promotes satellite cell survival, which is central to muscle renewal (McGaha et al., 2002,

Barzilai-Tutsch et al., 2016). Halofuginone is used in the treatment of inflammatory and autoimmune diseases (Cui et al., 2015b, Zion et al., 2009, Pines, 2014). Halofuginone has been trialled as an anti-fibrotic in the treatment of *mdx* mice with success *in vivo* (Turgeman et al., 2008, Huebner et al., 2008, Barzilai-Tutsch et al., 2016). Turgeman *et al*. administered halofuginone to mice from three weeks of age over a period of three months, demonstrating statistically significant improvements in measures of skeletal muscle function and laboratory measurements of fibrosis (Turgeman et al., 2008). Huebner *et al.* investigated halofuginone administered to mice above 30 weeks of age. There was a statistically significant reduction of skeletal muscle fibrosis following 10 weeks of treatment (Huebner et al., 2008). Beneficial effects were seen in skeletal muscle functional assessments, functional recovery post-exercise, and reduced susceptibility to exercise-induced injury (Huebner et al., 2008). A clinical trial evaluating halofuginone in the treatment of DMD was commenced in 2016 however the trial was halted for over a year due to a serious adverse event, it has since restarted (Clinical Trials.gov, 2016).

2.4.2 Non-contrast-enhanced imaging of fibrosis

MRI detection and quantification of fibrosis without contrast enhancement can be technically difficult, particularly in diseases with diffuse patterns of fibrosis, as found in muscular dystrophies. With non-contrast enhanced MRI, the aetiology of signal change is not always clear and may be due to inflammation, oedema or other disease processes.

A non-contrast enhanced MRI technique, ultrashort echo time (UTE), is based upon the very short T2 relaxation time of collagen in skeletal muscle in response to a radiofrequency excitation pulse. The technique involves suppression of the longer T2 values from water and fat, as these mask the shorter T2 values. This technique is a promising approach to fully non-invasively quantify fibrosis; i*n vitro* there was a strong positive correlation with collagen content (r=0.999 p=0.009) (Ericky et al., 2017). This technique has been piloted in skeletal muscle of healthy volunteers with positive preliminary results compared to collagen containing phantoms. It has not yet been investigated as an outcome measure or correlated with histology (Ericky et al., 2017). Ericky *et al.* highlight the importance of fat signal subtraction, as this will interfere with T2 values (Ericky et al., 2017). UTE is in its infancy and currently requires a long acquisition time. The variable and high volume of adipose replacement in skeletal muscle in muscular dystrophies could reduce the efficacy of this technique.

2.4.3 Contrast enhanced MRI of Fibrosis

Contrast agents distinguish between different tissues that appear magnetically similar, but are histologically distinct (Manus et al., 2012). An ideal contrast agent would be quickly excreted, highly tissue specific, and at as low a dose as possible to limit toxicity (van Zijl and Yadav, 2011).

One group of contrast agents are 'relaxation agents' which alter either T1 or T2 relaxation times of different tissues. Paramagnetic agents typically reduce relaxation time of T1 in water molecules of tissues where absorbed, providing a bright area termed a 'positive contrast'.

Gd-based contrast agents are considered to be paramagnetic (Hermann et al., 2008). Gd III complex with diethylenetriaminepentaacetic (DTPA) was first approved for use in clinical practice in 1988 (Hermann et al., 2008). Most Gd-based probes are charge neutral molecules that are readily excreted via the kidneys. In clinical practice, Gd-based agents are used with caution in the extremes of age (<1 year or >65 years old); this is because of the risk of reduced excretion due to impaired kidney function. Gd molecules are chelated in clinical contrast agents to reduce toxicity.

Non-specific Gd contrast agents are routinely used in cardiac magnetic resonance imaging (CMRI) to delineate fibrosis. The seven unpaired electrons of the Gd ion lead to a reduction in T1 relaxation times of the protons of nearby water molecules. Gd readily diffuses out of the capillaries into the extracellular space of the cardiac tissue but is unable to cross an undamaged healthy membrane. Both healthy and abnormal myocardial tissue accumulates contrast agent in the extracellular space. Contrast between healthy and remodelled tissue is due to a combination of altered kinetics and an increase in the volume of the extracellular space in unhealthy tissue (Weinmann et al., 1984, Moon et al., 2013). To determine the correct inversion time to null healthy myocardium, an inversion recovery sequence is performed. This sequence involves a series of images at different T1 values. The series of images can be chosen based upon which visually demonstrates nulled myocardium. LGE is dependent on fibrotic or damaged tissue having a slower efflux of contrast agent compared to the nulled myocardium. Images taken 10-15 minutes post-Gd administration allow comparison between healthy and remodelled tissues. Recognition of LGE is usually qualitative and dependent on a visually detectable difference in contrast in the myocardium. Diffusely fibrotic tissue, as found in muscular dystrophies, may be difficult to appreciate due to the minimal contrast between healthy and fibrotic tissues (Puntmann et al., 2016). In spite of this limitation, LGE can enable non-invasive, accurate detection of focal fibrosis within the heart (McCrohon et al., 2003). Animal studies correlating the extent of LGE in the heart to histological findings, found that LGE can

demonstrate the extent of fibrosis to a highly sensitive degree (Pop et al., 2013, Schelbert et al., 2010). The ability to perform LGE is therefore a major advantage of MRI over echocardiogram (Wong et al., 2013). Presence of LGE has been shown to be an adverse prognostic factor for dysfunction, arrhythmia and death in several conditions, including non-ischaemic cardiomyopathy (Wu et al., 2008b, Kuruvilla et al., 2014, O'Hanlon et al., 2010, Gulati et al., 2013, Pozo et al., 2016, Shin et al., 2016, Schelbert et al., 2015). LGE can demonstrate cardiac dysfunction in DMD before functional parameters have declined (Ashford et al., 2005).

Other than the previously mentioned drawback around diffuse fibrosis, quantification of LGE is a controversial topic. This is due to uncertainty around baseline measurement of remote myocardium; areas of myocardium not adjacent to the area of cardiac disease, which may be remodelled or affected due to altered cardiac dynamics. Attempts to standardise quantification recommended a cut off of >2 standard deviations from the mean signal intensity in healthy myocardium (Kramer et al., 2008); however, this is not widely accepted, with other studies using other cut offs for quantification. One study compared seven different methods, including visual interpretation. These methods yielded significantly different results (Flett et al., 2011). The most variability was seen with hypertrophic obstructive cardiomyopathy (HCM), which, of the diseases included, is the most similar to the dystrophic heart in terms of fibrosis (Flett et al., 2011). The authors posited that the most reliable method was the full width at half maximum method, which measures maximal signal intensity and includes all contiguous regions where signal is at least 50% of this (Amado et al., 2004, Flett et al., 2011). Controversy over this and other methods continues; several studies in muscular dystrophies use segmental LGE as a dichotomous variable (Giglio et al., 2014, Florian et al., 2014a, Florian et al., 2014c, Raman et al., 2015).

ECV is calculation of the extracellular compartment volume using T1 mapping to measure T1 relaxation times pre and post-Gd contrast within each voxel of the myocardium and the LV blood pool (aus dem Siepen et al., 2015). Intracellular compartments are dominated by myocyte mass while the extracellular compartment contains ECM and connective tissue. An increase in this extracellular compartment is likely to reflect an increase in interstitial fibrosis (Moon et al., 2013, Bull et al., 2013). Increase in ECV may be non-specific to fibrosis and could be influenced by the presence of oedema. Studies have, however, attempted to validate ECV histologically by looking at myocardial biopsies, these demonstrated significant correlations ranging from r=0.55-0.98 (Flett et al., 2010, Miller et al., 2013, White et al., 2013, Fontana et al., 2012). Increases in ECV may have a negative prognostic value in cardiac disease (Wong et al., 2012, Wong et al., 2013). ECV has been associated with earlier detection of fibrosis than LGE (Wong et al., 2012, Kellman et al., 2012, Schelbert et al., 2011, Tham et al., 2013). This technique has also been used as an outcome

measurement providing quantification of fibrosis (Moon et al., 2013, aus dem Siepen et al., 2015, Daniel et al., 2006, Kawel et al., 2012).

In ECV quantification, the difference between T1 values pre and post-contrast agent allows a measurement of the distribution volume of Gd. This allows calculation of the relaxation rate (R1), the reciprocal of T1, which is proportional to Gd concentration. Calculation of ECV requires equilibrium of the concentration of contrast agent between myocardium and the blood pool. Originally this was achieved by using a bolus of the contrast agent, followed by a slow infusion (Miller et al., 2013, Everett et al., 2016). Due to the increased duration of an infusion and subsequent acquisition, this has been replaced by a Gd bolus. Equilibrium between tissues is assumed 15-20 minutes after a bolus of contrast agent (Miller et al., 2013, Everett et al., 2016). T1 mapping values are obtained from a series of images at a number of inversion times following an inversion recovery imaging experiment, with cardiac gating used to enable acquisitions at identical time points within the cardiac cycle.

ECV is quantified by selecting a region of interest (ROI) and calculating the average T1 value within the ROI in both enhanced and native acquisitions. The difference in the reciprocal of these values (i.e.ΔR1) is divided by the difference in values of the blood pool to give the partition coefficient, which is then corrected for the patient haematocrit (Hct) to yield the ECV, as demonstrated in equation 1. The concentration of Gd within cardiac tissue is calculated using equation 2.

$$ECV = (1 - Hct) \times (\frac{\left(\frac{1}{T1_{myo\ post}}\right) - \left(\frac{1}{T1_{myo\ pre}}\right)}{\left(\frac{1}{T1_{post\ blood}}\right) - \left(\frac{1}{T1_{pre\ blood}}\right)}) \qquad (1)$$

$$R1_{Gd} = R1_{Pre-Gd} + k[Gd] \qquad (2)$$

Where k is the T1 relaxivity of Dotarem at 3T (Guerbet, France) (3.89mm^{-1}s^{-1}) (Vander Elst et al., 2013).

There is a wide range of values of ECV in healthy tissue. The highest values considered normal are in the range 0.23-0.27 (Sado et al., 2012, Banypersad et al., 2013, Radunski et al., 2014, Ugander et al., 2012, White et al., 2013, Florian et al., 2014b) (Table 1).

Several studies have reported a global ECV measurement, using a single or an averaged ROI value for the left ventricle (Sado et al., 2012, Ugander et al., 2012, Banypersad et al., 2013, Radunski et al., 2014). This approach may take account of the diffuse nature of fibrosis in these cohorts, but may give falsely normal results if there are areas of focal fibrosis surrounded by normal tissue, as seen in some conditions (i.e. acute MI).

Author	Disease	Mean control ECV values	Mean abnormal values	Significant correlations
(Sado et al., 2012)	Anderson-Fabry, DCM, HCM, MI, AS, Amy	0.253 ±0.035 Male 0.273 ±0.029 Female 0.233 ±0.029	DCM 0.25 ±0.004 HCM 0.291 ±0.005 AS 0.276 ±0.044 MI 0.585 ±0.076 Amy 0.466 ±0.076	DCM and Amy displayed significant correlation to EF. Control, DCM, and Amy correlated to LV mass.
(Ugander et al., 2012)	MI	0.27 ±0.081	0.36 ±0.022	EF
(Banypersad et al., 2013)	Amy	0.254	0.4	LV mass, EF,
(White et al., 2013)	DCM, HCM, MI, AS, Amy			High values (>0.4) correlate with histological values
(Radunski et al., 2014)	Myocarditis	0.25 (range 0.24-0.27)	0.31 (range 28-34)	
(Florian et al., 2014b)	BMD	0.24 ±0.005	0.29 ±0.0174	EF
(aus dem Siepen et al., 2015)	DCM	0.23 ±0.03	0.25 ±0.04 Early DCM, >0.27 ±0.04 established DCM	Weak correlation with EF
(Olivieri et al., 2017)	DMD	0.26 ± 0.33	0.279 ± 0.058	Native T1

Table 1. To show previous findings of reported ECV values in different diseases for reference. Values given as mean and standard deviation unless otherwise stated. Key: DCM, Dilated cardiomyopathy, HCM, hypertrophic obstructive cardiomyopathy, MI, myocardial infarction, AS, Aortic stenosis, Amy, Amyloidosis, EF, Ejection fraction, LV, left ventricle, LGE, Late gadolinium enhancement, BMD, Becker muscular dystrophy, DMD, Duchenne muscular dystrophy.

2.4.4 Molecule-specific contrast agents - Focus on EP3533

Gd-based contrast agents with an affinity to target molecules have also been developed but are not currently used in clinical practice (Amthor et al., 2004, Caravan et al., 2007, Caravan et al., 2013, Farrar et al., 2015, Fuchs et al., 2013, Helm et al., 2008, Huang et al., 2011, Polasek et al., 2012). EP3533 (EPIX pharmaceuticals, United States) is a collagen-specific contrast agent with potential for use as a biomarker of fibrosis in muscular dystrophies. EP3533 contains three Gd molecules with DTPA moieties bonded to a polypeptide with affinity for type one collagen (Caravan et al., 2007). EP3533 is a paramagnetic agent providing positive contrast with a molecular size of approximately 5kDa (Helm et al., 2008). Compared to standard Gd (DTPA), the relaxivity of EP3533 is five times higher per Gd atom. The high relaxivity is likely to be a result of the larger size of EP3533, which results in a longer correlation time (Caravan et al., 2007). The relaxivity rate of EP3533 in human plasma at 1.4T is 15.6mM^{-1}s^{-1} (Caravan et al., 2007). Similar relaxivity values of EP3533 were reported in another study (Helm et al., 2008).

Caravan *et al.* compared EP3612, an isomer of EP3533, identical with the exception of an inverted cysteine group (Caravan et al., 2007). Assuming the same number of equivalent binding sites between the two agents, EP3533 had a dissociation constant of 1.8μM ±1, compared to the ten times higher dissociation constant of EP3612. This was suggested to be due to the affinity of the molecule to collagen. EP3533 was calculated to have a half-life of 19 minutes ±2 in both fibrotic and control subjects (Fuchs et al., 2013). The biodistribution of EP3533 was assessed in four mice, fifteen minutes after administration.. EP3533 had a higher signal intensity compared to EP3612 in organs containing higher levels of collagen, i.e. liver, heart, and kidneys (Caravan et al., 2007). EP3533 has a slow tissue washout time; in the presence of fibrotic myocardium this may be more than three hours on average (Helm et al., 2008).

EP3533 has been used in murine models to identify areas of fibrosis post-MI (Helm et al., 2008), liver fibrosis (Fuchs et al., 2013), and pulmonary fibrosis (Caravan et al., 2013) (Table 2). *In vivo* studies have assessed the specificity of EP3533 to collagen compared to similar Gd-based contrast agents (Caravan et al., 2013, Polasek et al., 2012). EP3533 has also been used to accurately stage fibrotic disease (Fuchs et al., 2013), and to detect response to anti-fibrotic therapy (Farrar et al., 2015).

Helm *et al* (Helm et al., 2008) induced MI in eight mice by occluding the left anterior descending coronary artery for an hour. Six weeks after the induced MI, fibrosis would be expected to be fully formed (Ross et al., 2002). MRI scanning took place pre-MI, at 24 hours post-MI, and at six weeks post-MI. For comparison, a standard Gd (gadopentetate dimeglumine) contrast agent and EP3533 were

given intravenously. The results showed a significant difference in washout time of contrast agent in both the scar tissue and the normal myocardium. There was a strong correlation between circumferential extent of EP3533 at 40 minutes, and the levels of fibrosis as quantified by histology (R^2=0.97) (Helm et al., 2008).

Experiments using murine models of liver fibrosis compared EP3533, Gd (DTPA), and *ex vivo* quantification of collagen (Polasek et al., 2012). They found strong positive correlation between collagen as assessed by hydroxyproline quantification and Gd in liver tissues (R^2=0.74-0.77). The semi-quantitative 'Ishak score' and hydroxyproline quantification correlated well with the half-life of EP3533 in the liver; (R^2=0.64-0.81) the authors suggested that EP3533 could therefore be successfully used to quantify liver fibrosis (Polasek et al., 2012). A further study used EP3533 to successfully stage liver fibrosis using SNR post-contrast (Fuchs et al., 2013). The authors also compared this to other MRI techniques (apparent diffusion coefficient, T1 relaxation time, T2, magnetisation transfer ratio), finding only a weak correlation between them and levels of fibrosis and Ishak scoring (Fuchs et al., 2013). Assessment of fibrosis treatment response has been evaluated using EP3533 in murine models of bile duct ligation (Farrar et al., 2015).

Imaging of pulmonary fibrosis has also been investigated using EP3533 and a model of pulmonary fibrosis (Johnson et al., 2013). Caravan *et al.* found that lung signal increased significantly in the mice using EP3533, compared to those imaged with EP3612 and a control group (p<0.0001) (Caravan et al., 2013). Good correlation was also seen between Gd levels in the lungs and hydroxyproline quantification (R^2=0.90) (Caravan et al., 2013).

Author	Disease model	Field strength (T)	Dose (μmol/kg)
(Helm et al., 2008)	Myocardial Infarction	4.7	25
(Polasek et al., 2012)	Liver Fibrosis	4.7	20
(Fuchs et al., 2013)	Liver Fibrosis	4.7	10
(Caravan et al., 2013)	Pulmonary fibrosis	4.7	10
(Farrar et al., 2015)	Bile duct ligation	1.5	10
(Polasek et al., 2017a)	Pancreatic cancer	4.7	10

Table 2. Summary of publications assessing the use of EP3533 in detection of fibrosis in various disease models.

2.5 Pathological hallmarks of muscular dystrophies - Adipocyte replacement of muscle

Fat replacement of muscle is considered an end-stage pathology of muscular dystrophies. The exact mechanism is unclear (Wagatsuma, 2007). Several studies have found that skeletal muscle tissue has adipose precursor cells and these can differentiate into full adipocytes *in vitro* (Sato et al., 1996, Hausman and Poulos, 2004). Abnormalities in serum lipid and skeletal muscle lipid metabolism have been reported in muscular dystrophies (Srivastava et al., 2017, Nishio et al., 1990), though it is unclear whether this is due to phospholipid layer breakdown of skeletal muscle, corticosteroid administration, or a pro-adipogenic factor.

2.5.1 Imaging of adipocyte replacement of muscle

Dixon FF measurement was first described in 1984. It exploits the chemical shift difference between the water and main fat resonances. It consists of two MRI images of the same anatomy with in-phase and out of phase echo times, giving rise to images with constructive and destructive interference of fat and water respectively (Dixon, 1984). Off-resonance frequency effects mean that the water images are contaminated by fat and the converse is true. Several studies suggested that a third measurement would enable quantification of the value of off-resonance frequency effects, and therefore could give a more accurate quantification of the FF (Ma, 2008, Glover and Schneider, 1991). The Dixon technique is used widely in clinical practice, both in suppressing fat signals to provide clear anatomical information, and in quantification of fat contained within many soft tissues (Wokke et al., 2013, Hetterich et al., 2015, Homsi et al., 2015).

Skeletal muscle FF quantification has been used in several studies to correlate well with functional methods of assessment in both DMD and LGMDR9 cohorts (Willis et al., 2013, Wren et al., 2008, Fischmann et al., 2013). Changes in FF calculations over a one year period are sensitive enough to change for both LGMDR9 and DMD cohorts (Willis et al., 2013, Arpan et al., 2014). Several studies have supported quantitative FF measurement as an outcome measure in DMD and BMD (Akima et al., 2012, Barnard et al., 2018, Burakiewicz et al., 2017, Gaeta et al., 2012, Kim et al., 2013, Willcocks et al., 2016b, Wokke et al., 2013, Wokke et al., 2014b, Wren et al., 2008).

2.5.2 Focus on previous studies into Dixon fat fraction in LGMDR9

In 2013, Willis *et al*. published the largest natural history study investigating LGMDR9 (Willis et al., 2013). Four centres took part in the study: Newcastle University (UNEW), UK and University College

London, UK, The University of Copenhagen, Denmark, and the Institute of Myology, France. Willis *et al*. recruited 38 ambulant participants with the most common homozygous mutation in the *FKRP* gene (L276I). 32 out of 38 participants completed the one year follow up study, which involved both quantitative MRI scans and standardised functional assessments (Willis et al., 2013). The aim was to assess which outcome measures were able to monitor disease progression over one year.

The standardised physiotherapy assessments included myometry of the lower limbs (knee extension and flexion, hip adduction and abduction), timed tests (timed up and go, six minute walk test (6MWT), and 10 metre walk or run, chair rise, stair climb and descend), and spirometry testing (Willis et al., 2013). The authors used the semi-quantitative scale of muscle fat replacement on MRI published by Mercuri *et al.* to grade T1 weighted images (Mercuri et al., 2002, Willis et al., 2013), and compared the grade to calculation of the FF using the Dixon technique.

Patient demographics were recorded, including the nature of first motor symptoms, cardiac and respiratory involvement. Of the 38 recruited initially, the age range was 18-64 years. The most commonly reported first motor symptoms were difficulties in climbing stairs (28%), difficulty running (21.1%), myalgia (21.2%) falls (10.5%) and difficulties rising from a chair (10.5%). Serum CK activity was measured and ranged from 222units/L to 23,858units/L. Documented cardiac involvement was reported in 42% of patients; with the majority males (77%), mean age of onset was 44.4 years. Respiratory involvement was present in 33% of participants, as indicated by less than 75% of FVC predicted for height (Willis et al., 2014).

Willis *et al.* demonstrated that there was a significant increase in FF in nine of the fourteen muscle groups assessed over the twelve month period: biceps femoris long head (BFLH) (p=0.0004), ST (p=0.02), semimembranous (p=0.02), Sar (p=0.01), Gr (p=0.02), VL (p=0.03), RF (p=0.03), medial gastrocnemius (MG) (p=0.01) and the lateral gastrocnemius (LG) (p=0.01) (Willis et al., 2013). The most variable increase in FF for a muscle was in the ST. No statistically significant differences were seen in the myometry or the timed tests over the same period. Spirometry was the only functional test to show a significant difference over the year (p=0.001). Use of the Mercuri scale to grade T1 weighted images showed significant overlap between the middle grades (2a, 2b and 3), with comparatively low rates of inter-observer reliability (Willis et al., 2013).

The findings of the study provided support for the efficacy of quantitative MRI as an outcome measure in LGMDR9. Willis *et al.* demonstrated that over a one year period, calculation of the FF via MRI is able to detect and quantify disease progression, whereas the majority of functional assessments were unable to demonstrate a significant difference (Willis et al., 2013). The 6MWT, the most commonly used primary end point in therapeutic trials in muscular dystrophy, showed a marginal increase in

distance walked (baseline median 312m, 1 year follow up median 353m p=0.77) (Willis et al., 2013). This result suggested that this test may not be appropriately sensitive to disease progression and that there might be an element of participants learning how to better perform the task, rather than improvement in ability. The study identified several muscle groups which could be targeted for quantitative MRI in future trials: the MG, VL, Gr, and RF muscles. These muscles were chosen based on variability of involvement, ease of ROI placement, and rate of disease progression (Willis et al., 2013). The findings of this study have important implications for the design of prospective interventional trials into LGMDR9.

2.5.3 Cross sectional area and contractile cross sectional area

Longitudinal measurement of FF in muscle relates to increasing pathology caused by muscular dystrophy. Using MRI, cross sectional area (CSA) of muscle can be measured, and reflects trophicity of muscle tissue; in healthy individuals there is a relatively linear relationship between CSA and muscle strength (Maughan et al., 1983). Hypertrophy of dystrophic muscle fibres has been demonstrated on muscle biopsy, and increased CSA has been demonstrated in the triceps surae of individuals with DMD (Wokke et al., 2014b, Cros et al., 1989). A high degree of inter-muscle variation in FF and CSA suggests that these factors are distinct pathological processes (Wokke et al., 2014b).

The area of muscle not taken up by fat (i.e. 1-FF) can be multiplied by the total CSA, to calculate the remaining contractile cross sectional area (cCSA) of a muscle. cCSA has been shown to significantly correlate to functional measures of strength in muscular dystrophies (Lokken et al., 2016, Wokke et al., 2014b, Vohra et al., 2015). The non-uniform distribution of fat throughout muscle may be important and is not accounted for using cCSA. This method of demonstrating advancing disease pathology also fails to take into account fibrotic tissue, which may alter the dynamics of muscle contraction. Regardless of these factors, cCSA may be able to demonstrate disease progression by showing loss of healthy muscle tissue rather than increased pathology.

2.6 Pathological hallmarks of muscular dystrophies – Progressive muscular weakness

2.6.1 Musculo-skeletal functional assessments

Physiotherapy assessment is readily available in many centres, and if standardised with sufficient training, reliability tests show high levels of inter observer correlation (Connolly et al., 2015). Functional assessments are the most clinically meaningful to patients and are important in demonstration of efficacy of therapies in clinical trials. Functional assessment has the benefit of including whole muscle groups, rather than individual muscles which may demonstrate significant variability. Drawbacks of functional testing include a dependence on age and intellectual ability, as well as some subjectivity due to patient effort (Alfano et al., 2014). Functional assessments may lack the sensitivity to detect deterioration over shorter periods of time (Willis et al., 2013).

Manual muscle testing (MMT) using scales developed by the Medical Research Council has been used in clinical practice. MMT has been criticised as lacking sufficient objectivity to be an endpoint for clinical trials (Escolar et al., 2001). Studies have shown that MMT assessors who have reliability assessments regularly can demonstrate high levels of inter-observer correlation (Florence et al., 1984, Escolar et al., 2001). Quantitative muscle testing (QMT) using a strain gauge has also been used to test maximal voluntary isometric contraction. In contrast to MMT, QMT has a consistently higher inter-observer correlation of 0.93-0.99 (Escolar et al., 2001). Criticisms of QMT include cost of equipment, complexity of use and the need to keep assessing repeatability to ensure accurate results (Escolar et al., 2001).

The 6MWT is a standardised assessment that measures the distance a patient is able to walk uninterrupted over a six minute period on a flat surface (American Thoracic Society, 2002). A major strength of the 6MWT is that it assesses a clinically relevant function (McDonald et al., 2010). The 6MWT has been used to assess both adult and paediatric diseases (de Groot et al., 2011, Geiger et al., 2007, Kierkegaard and Tollbäck, 2007, Wraith et al., 2004). Results of the 6MWT have been seen to correlate in specific cohorts with oxygen consumption, aerobic fitness, exercise induced desaturations and lung function; as well as other variables such as age, height and weight (Li et al., 2005, Haass et al., 2000, Burr et al., 2011, Dogra et al., 2015, Chen et al., 2012). The 6MWT has been shown to be a reproducible, valid test in assessing function in DMD (Kempen et al., 2014). Studies have suggested a high test-retest reliability correlation, between 0.91-0.94 (McDonald et al., 2010, Li et al., 2005, Kempen et al., 2014). The 6MWT is not appropriate for children with severe learning difficulties or very young patients (McDonald et al., 2010). The 6MWT may be biased by multiple factors, including cardio-respiratory comorbidities, and motivation (Slaman et al., 2013).

The North Star Ambulatory Assessment (NSAA) is a validated functional assessment tool used in clinical practice to assess boys with DMD (Scott et al., 2012, Ricotti et al., 2015). The NSAA uses 17 domains to assess patients and can be performed in 10-15 minutes (Mayhew et al., 2013b). The score was developed as a disease specific scale for use in clinical practice with potential to detect meaningful deterioration in ability (Scott et al., 2012, Mayhew et al., 2013b). In contrast to other neuromuscular scales such as the Egen Klassification, the NSAA was designed for use in ambulant patients (Steffensen et al., 2001). With appropriate training, the NSAA has a high inter-observer reliability score of 0.99 (Mazzone et al., 2009). The NSAA can be criticised as it is not designed for non-ambulant patients. Similar to the 6MWT, the assessment would therefore not be expected to be sensitive to further deterioration in patients.

2.6.2 Cardiac functional assessment

In all neuromuscular diseases which affect the heart, regular cardiac surveillance is recommended (Bushby et al., 2010b, Romfh and McNally, 2010, Ho et al., 2016). Therapeutic trials aimed at amelioration of cardiac dysfunction in neuromuscular disease have used echocardiographic and CMRI measurements as an outcome measure (Uhlir et al., 1997, Silversides et al., 2003, Ishikawa et al., 1999, Duboc et al., 2005, Duboc et al., 2007, Ogata et al., 2009, Raman et al., 2015, Witting et al., 2014, Leung et al., 2014). Petri *et al.* reported the longest follow up study of LV indices in a mixed muscular dystrophy cohort, demonstrating that over nine years, LVEF significantly fell by 1% per year in a BMD cohort (n=25), and 0.4% per year in LGMDR9 (n=28) (Petri et al., 2015). Cross-sectional measures of strain and torsion using cardiac tagging have been reported in a LGMDR9 cohort (n=10), finding that peak torsion (PT) was reduced and torsion to strain ratio (TSR) was significantly lower than controls (Hollingsworth et al., 2013b). To date, no studies have reported cardiac tagging values in BMD or longitudinal changes in a LGMDR9 cohort.

CMRI is more sensitive than echocardiogram, due to increased accuracy of functional measurement and the reliability of obtaining good quality images (Ashford et al., 2005, Mavrogeni et al., 2009, Brunklaus et al., 2015, Gardner et al., 2009, Raman et al., 2015). The slow progression of cardiac fibrosis in neuromuscular conditions requires sensitive outcome measures to detect change over short time periods. Routine CMRI to obtain cardiac indices, such as LVEF, typically involves acquisition of contiguous short axis slices to cover the left ventricle with a temporal resolution of 40ms with approximately 25 cardiac phases (Walsh and Hundley, 2007). CMRI uses retrospective vectorcardiogram (VCG) gating to allow for the continuous movement of the heart during the cardiac

cycle, and to allocate acquisitions to a predefined number of cardiac phases. To reduce respiratory artefact, the majority of CMRI is performed during patient breath-holding. Significant processing time is required during CMRI acquisitions with a typical resolution of 1.85mm x 1.54mm (reconstructed to 1.37 x 1.37mm), and a field of view (FOV) of approximately 350 x 315mm in 12-14 slices. For the patient, during a typical assessment this involves repeated periods of breath holding (BH) for up to 10 seconds each (Fratz et al., 2013).

Reducing scan times is important in imaging of patients with neuromuscular diseases. Scoliosis and respiratory muscle weakness make it difficult for patients to remain supine for long periods and maintain breath-holds (Hull et al., 2012). Additionally, for children and those with learning difficulties, conventional CMRI can be uncomfortable, distressing and may require anaesthesia to produce sufficiently good quality images. Successful reduction in scan times may reduce burden on patients, free up scanner time, and potentially have financial implications. Any method that reduces acquisition times must however, maintain the quality of the image compared to conventional acquisition, and give reproducible results free of significant artefacts (Lin et al., 2016).

2.6.3 Focus on reducing acquisition times for cardiac magnetic resonance imaging functional indices via accelerated imaging

The time taken for MRI acquisition relies on several factors. In processing terms, the acquisition is complete once sufficient samples of the raw signal are collected to fulfil the Nyquist criterion (Lustig et al., 2008). The Nyquist criterion states that the only way to perfectly reproduce an image from an analogue signal is to sample at more than twice the maximum frequency of the signal. In practice, once the FOV and resolution of the desired MRI acquisition is chosen, then an equivalently sized matrix of raw (k-space) data has to be collected (Hollingsworth, 2015).

Parallel imaging uses multiple surface coil elements to under-sample the k-space matrix in a regular way. The multiple receiver coils enable quicker acquisition; each of these coils is most sensitive to the nearby tissue, allowing spatially dependent sensitivity to be used (Hollingsworth, 2015). As it is only the magnitude of the MR signal not the phase that is important for cine imaging, partial Fourier imaging can be used to omit nearly half of the k space by taking advantage of conjugate symmetry of magnitude images in k-space (Hollingsworth, 2015), at the cost of a reduction in SNR (Hollingsworth, 2015, McGibney et al., 1993, Bydder and Robson, 2005). Compressed sensing approaches are based upon the large amount of similarities in images through the cardiac phases, permitting a reduction in the amount of acquired k-space (Tsao and Kozerke, 2012). The acquisitions can be transformed into

sparse domains, allowing a reduction in the volume of data to be collected whilst maintaining image fidelity. Additionally, some investigators have reduced the amount of data that they need to collect by guide-point modelling techniques. Rather than collecting contiguous slices of the heart, a limited number of non-contiguous slices and views are collected, and an "average" heart model is applied based on defining a few key points on the endocardial and epicardial boundaries (Young et al., 2000, Young et al., 2011). These approaches have been combined with other acceleration techniques, such as compressed sensing (Vincenti et al., 2014). With any under sampling method, loss of fidelity compared to the conventional image can occur. If blending of information throughout the cardiac phases is present, this might result in reducing the end diastolic volume or increasing the end systolic volume, which would lead to inaccurate measurement of cardiac indices.

Several different approaches have been explored to reduce CMRI acquisition times. The majority of studies have not established clinical validity, focussing on image quality metrics (particularly the root mean square error between conventional and accelerated images) rather than the effect on functional indices (Hollingsworth, 2015). In clinical trials, longitudinal changes in cardiac indices are important. Studies are lacking which assess how much bias and variability may be introduced using accelerated imaging techniques. Studies evaluate the presence of artefacts and preservation of LV function; these require definition of the epicardial and endocardial boundaries. The majority of studies utilise the balanced turbo field echo (TFE) sequence (a sequence with mixed T1/T2 weighted contrast). This leads to bright blood, mid-grey myocardium and bright epicardial adipose tissue. Although this produces clear endo- and epicardial boundaries in most of the cardiac phases, basal images and boundaries at systole may be difficult to identify. It is used because it is the most efficient sequence for collecting high SNR images per unit time. If the reconstruction of under-sampled data transfers too much information between cardiac phases, this can lead to loss of boundary definition with subsequent inaccuracies in the segmentation of the left ventricle, leading to inaccurate LV indices.

2.6.4 Cardiac tagging

Measures of strain and torsion using cardiac tagging have been reported in a LGMDR9 cohort (n=10), finding that PT was reduced and TSR was significantly lower than controls (Hollingsworth et al., 2013b). To date, no studies have reported cardiac tagging values in BMD or longitudinal changes in a LGMDR9 cohort. Cardiac strain is a useful measure of myocyte movement. Strain is defined as a relative change in a defined linear dimension of the heart, compared to end diastole (Taylor et al., 2015). Measurement of myocardial strain has been shown to be a sensitive measure of cardiac dysfunction,

and may be more sensitive than measurement of regional wall thickening in detection of regional cardiac dysfunction (Gotte et al., 2001). Cardiac tissues have a complicated architecture, with sub-epicardial fibres running obliquely in a spiral at 75°. Sub-endocardial musculature fibres run in the opposite orientation to the sub-epicardial at -70°, mid-wall fibres run circumferentially (MacGowan et al., 1997). Shortening of these fibres in various planes enables contraction of the heart; however, dysfunction due to fibrosis often increases measurements of torsion.

Cardiac tagging is a technique first described by Zerhouni *et al*. in 1988 (Zerhouni et al., 1988), with subsequent refinements (Axel and Dougherty, 1989, Osman et al., 1999, Osman et al., 2001, Abd-Elmoniem et al., 2008, Basha et al., 2009). Cardiac tagging works by the application of radiofrequency pulses to cancel signal from the diastolic myocardium, leaving a localised grid pattern of areas of nuclei excitation. Distortion of the grid pattern as the heart undergoes systole allows calculation of torsion and circumferential strain (Hollingsworth et al., 2013b).

Cardiac tagging techniques have been used in muscular dystrophies. Use of cardiac tagging has been investigated in DMD (Hagenbuch et al., 2010b, Raman et al., 2015, Hor et al., 2009). Patterns of abnormal torsion have been found to be evident before global measures of dysfunction, such as decline in LVEF or fractional shortening (Hor et al., 2009, Hagenbuch et al., 2010a, Ashford et al., 2005, Rosales et al., 2011). Hollingsworth *et al*. investigated a cohort of patients with LGMDR9, demonstrating that peak cardiac torsion was significantly lower than healthy controls, with selective preservation of some strains. The findings showed the unusual pattern of impaired torsion and preserved circumferential strain, which is not reflected in studies reporting cardiac tagging in other cardiac disease (MacGowan et al., 1997, Hollingsworth et al., 2013b).

2.7 Conclusions

As putative therapies for muscular dystrophies move toward clinical testing, there is a need for minimally invasive, sensitive outcome measures related to muscle pathology. Outcome measures based upon earlier stages of disease pathology may have a greater likelihood of being sensitive to disease progression over shorter periods but are less clinically relevant. This chapter highlights promising ways to monitor disease progression, including collagen-specific contrast agents, extra cellular volume, longitudinal Dixon FF calculation and cardiac tagging. Improvement in the speed of acquisition of CMRI would be beneficial as a study outcome measure reducing study burden. This thesis will evaluate some of these methods, comparing against traditional ways of demonstrating disease progression.

Chapter 3: Methods

To fully explore the topic of this thesis, investigation of novel methods of using quantitative MRI in assessing the pathology of muscular dystrophies, it was necessary to perform both animal and clinical experiments. Methods are therefore described in two sections:

- Section 1: Animal (basic science) methods
- Section 2: Clinical methods

3.1 Section 1: Animal assessments

3.1.1 Ethics

All animal experiments described conform to directive 2010/63/EU of the European parliament and under the auspices of the terms of the animals (scientific procedures) act 1986, authorized by the Home Secretary, Home Office, UK. All animal experiments were carried out under Project Licence 70/8538, and personal licence I8E4D5AEF approved by the Home Office.

3.1.2 Animal anaesthesia

Animals were anaesthetised using isoflurane 5% in 0.5L/min of oxygen. Prior to cannulation of the tail vein, anaesthetic was maintained at 1-1.5% isoflurane in 0.5L/min of oxygen. Heart rate, ECG, respiratory rate and core body temperature were monitored throughout all procedures.

3.2 Overview of EP3533 experiments (Chapter 4)

3.2.1 Pilot study of EP3533

One 48 week old *mdx* mouse and an age-matched control (BL10) were scanned. The aim was to optimise the imaging protocol and assess timing of greatest signal change within skeletal muscle. The timing of maximal signal increase could then be used as timing for subsequent experiments.

The animals were individually anaesthetised and cannulated. Following initial scouting images and shimming, both mice underwent pre-contrast baseline imaging and subsequent bolus of 20µmol/kg of EP3533 administered. This dose was chosen based on previous studies using EP3533 (Helm et al., 2008). Post-contrast agent, continuous repeated scanning was performed over two hours. The mice were scanned using T1 weighted 3d gradient echo (GRE). MRI analysis was performed using hand-drawn ROI in skeletal muscle.

3.2.2 Cross sectional assessment of EP3533

Nine *mdx* and five BL10 mice were age-matched to approximately 40 weeks of age. Animals were anaesthetised, monitored and underwent tail vein cannulation. For each mouse, two scans were performed a week apart. In the first week the contrast agent was with standard gadolinium agent (SGd), with EP3533 used in the second week. To incorporate both skeletal and cardiac muscle acquisitions into the same scan, the mouse was first positioned with the lower limbs at the level of the centre of the radiofrequency coil. This position was marked to ensure repeatability of positioning. Once skeletal muscle baseline acquisitions were completed, the mouse was repositioned with the level of the heart at the centre of the radiofrequency coil. Baseline cardiac images were obtained, then contrast administered with post-contrast acquisition until completion at sixty minutes. After this time the mouse was repositioned back to the original marked position for skeletal muscle imaging (Figure 3).
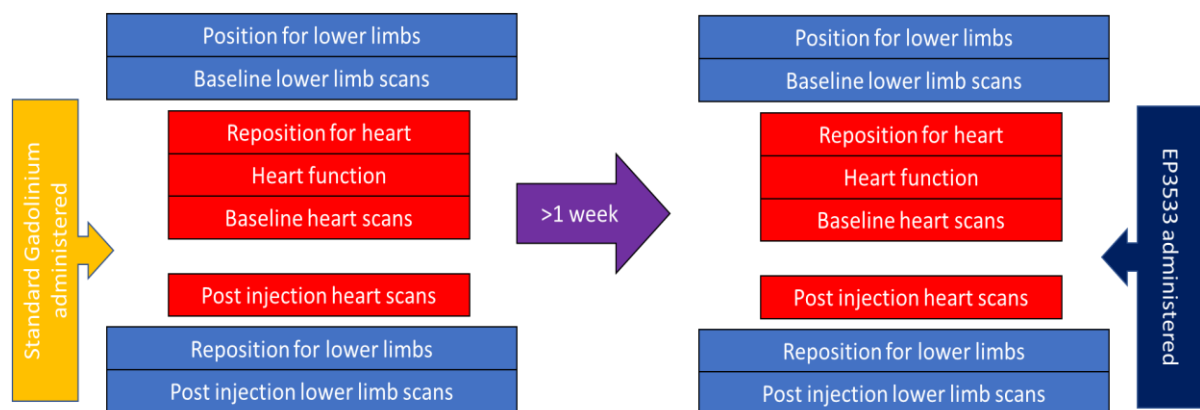
Figure
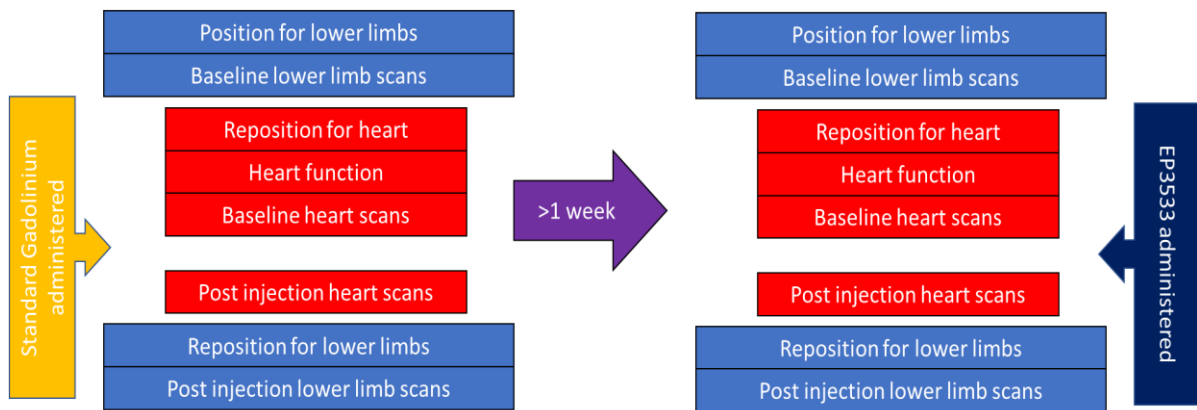
Figure 3. Depiction of the imaging protocol and how the mice were repositioned during the scan to place heart or skeletal muscle within the centre of the radiofrequency field. This figure demonstrates how the different contrasts were over a week apart to ensure no contamination of gadolinium (Gd) during the second scan.

3.2.3 Longitudinal assessment of EP3533 as an outcome measure

Four groups of age-matched (16 ±3 weeks) *mdx* and BL10 mice were obtained. The first group, referred to as 'treated *mdx*' (n=8), were treated for twelve weeks with halofuginone (Sigma-Aldrich, 2018) 7.5ug three times per week via intraperitoneal (IP) injection based on a previous study (Turgeman et al., 2008). A control group of mice, 'treated BL10' (n=3), received the same treatment as the first group. A second group, 'untreated *mdx*' (n=13), were begun on a course of 3 weekly IP injections over twelve weeks of 150μl of dimethyl sulfoxide (DMSO) (5%) and saline (0.9%) (vehicle). A corresponding group of control mice, 'untreated BL10' (n=5), received vehicle only. Halofuginone was reconstituted as a stock solution in saline (0.9%) and DMSO (5%). For long term administration Halofuginone was aliquoted into separate tubes and frozen at
-20°C.

All IP injections were administered by an animal technician with appropriate training. Daily welfare checks and weekly weight documentation were completed. No side effects or adverse events relating to the drug were noted in any of the four groups of mice.

Due to the high degree of correlation between EP3533 and histology seen in skeletal muscle in initial experiments as well as the clinical relevance of skeletal muscle in human muscular dystrophy, it was decided to limit the scans to skeletal muscle. Both treated mice groups (treated *mdx* and treated BL10) and the untreated *mdx* mice were imaged at baseline, then recovered to commence a 12-week course of either halofuginone or vehicle administration. Following this, all mice underwent two and four limb strength assessments, then were imaged within a week and finally humanely killed. As little variation is expected on imaging in BL10 mice, the only BL10 mice that were imaged at baseline were the treated BL10. Vehicle treated mice were imaged when they reached the same age as the mice receiving halofuginone.

Following administration of 20μmol/kg of EP3533, mice underwent T1 weighted GRE imaging in a 1:2 ratio with gradient echo multi-slice inversion-recovery Look-Locker (gemsIR-LL), continuing until seventy minutes post-contrast when the final gemsIR-LL was performed. The muscles to be analysed included hamstrings (HMS), QUADS, GCN, and TA.

3.3 MRI protocol

Magnetic resonance scanning was performed on a 7-Tesla micro-imaging system (Varian; Agilent Technologies, Santa Clara, United States) equipped with a 12cm micro-imaging gradient insert (maximum gradient, 40mT/m). Pre and post-contrast timings differed between sections.

3.3.1 Skeletal muscle protocol

The skeletal muscle imaging protocol for both upper and lower legs involved a T1 mapping sequence using a gemsIR-LL with 1 slice of 1mm thickness selected through lower leg muscles with the following parameters: repetition time (TR) inversion = 5s, 10 inversion times (from 0.1 to 5s), TR/echo time (TE) = 9.68/4.86ms, echo train length (ETL) = 4, flip angle (FA) = 4°, FOV 30 x 30mm, matrix = 128 x 128. This sequence was alternated with a series of T1 weighted GRE acquired pre and post-contrast enhancement with TR/TE = 9.46/4.75ms, FA = 20°, FOV = 30 x 30 x 30mm, matrix 128 x 128 x 128, band width = 20KHz.

For the lower leg muscles, mice were positioned with the upper border of the FOV beginning at the lower border of the knee. For the upper leg (only performed in section 3), mice were positioned with the centre of the knee joint as close as possible to the centre of the radiofrequency coil. Four slices were used to obtain the gemsIR-LL, two positioned above (+0.6mm, 1.2mm) and two below the knee joint (-0.6mm, -1.2mm). This enabled homogeneity in positioning for analysis.

3.3.2 Cardiac protocol

Only the second experiment looking at cross sectional measurement of fibrosis included cardiac imaging. Following initial scouting images and shimming, baseline cardiac acquisitions were obtained. Following power calibration, four transverse images were acquired as a pilot from which single slice sagittal and coronal acquisitions were obtained at the level of the mitral valve and the apex of the heart planes. A short-axis stack of slices was acquired covering the whole heart using a spoiled gradient-echo cine sequence with parameters as follows: TR=5ms, TE=1.42ms, FA = 15°, FOV 30mm × 30mm, data matrix 128 × 128, 1 mm slice thickness, maximum of 12 slices depending on heart size, 4 averages. Images were gated to the R wave of the heart cycles to coincide with ventricular contraction with a cine delay of 15ms. Following morphological imaging, a quantitative T1 map dataset was then acquired using a gated-gemsIR-LL with 3 axial slices of 1mm thickness through the mid-point of the

left ventricle with the following parameters: TR inversion = 5s, 10 inversion times (from 0.1 to 5s), TR/TE = 9.68/4.86ms, ETL = 4, FA = 4°, FOV 30mm × 30mm, Matrix = 128 × 128. Finally, gated-baseline T1 weighted GRE images were acquired with identical parameters to the skeletal muscle acquisition. Using anaesthetic titration median heart rate was kept closely to 400 beats per minute (bpm) throughout the scans.

After cine imaging and baseline images were taken, contrast was administered. A continuous series of T1 weighted GRE scans was acquired in succession, then a single gated gemsIR-LL as close to 40 minutes as possible. Immediately after this a continuous series of T1 weighted GRE scans was performed until approximately 60-65 minutes post-contrast, when the mouse was repositioned for skeletal muscle imaging.

3.4 Skeletal muscle: analysis and ROI selection

All scans were analysed using 'Aedes software' (Niskanen). Creation of T1 maps was performed by pixel-wise fitting of the lower limb datasets to equation [3]. Where $s(T_{IR})$ is the pixel intensity in the image collected at inversion time T_{IR} and S_o is the equilibrium signal intensity. Gated T1 maps were created using the same method, but with T_{IR} adjusted for gating by recording of the contemporaneous heart rate and inputting the inversion times manually prior to fitting and ROI drawing.

$$s(T_{IR}) = s_0(1 - 2e^{\frac{T_{IR}}{T_1}}) \tag{3}$$

Lower leg muscle ROI were selected by hand based on previous MRI-based murine studies (Zhang et al., 2008) (Figure 4). For section 3, which included upper leg muscles, ROI selection in the thigh has not previously been reported, selection was therefore based upon anatomical position (Charles et al., 2016). The anterior compartment of the thigh corresponded to the dissection of the QUADS muscles, with the posterior compartment corresponding to the dissection of the hamstring muscles. Muscles were located using the T1 weighted GRE, and then approximated on the same position as the T1 map (Figure 5). These are referred to throughout this chapter as HMS and QUADS.
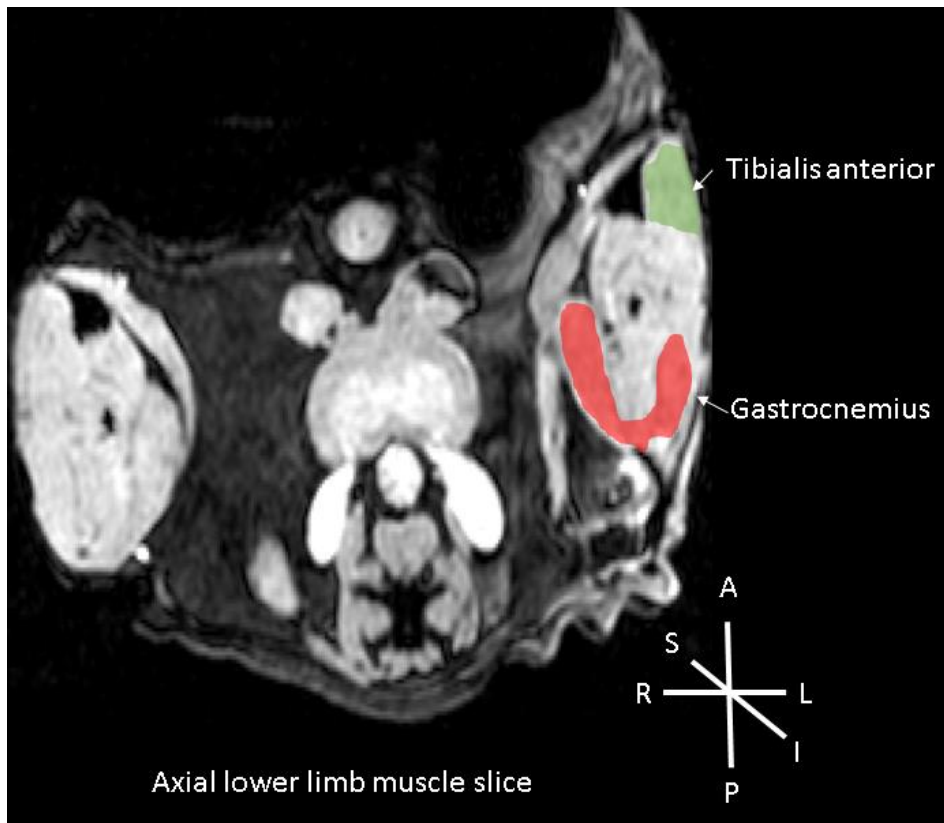
Figure 1. T1 weighted image to demonstrate the selection of regions of interest within the lower limb mouse muscles. Key: green, tibialis anterior (TA), red, gastrocnemius (GCN), P, posterior, A, anterior, L, left, R, right, S, superior, I, inferior.
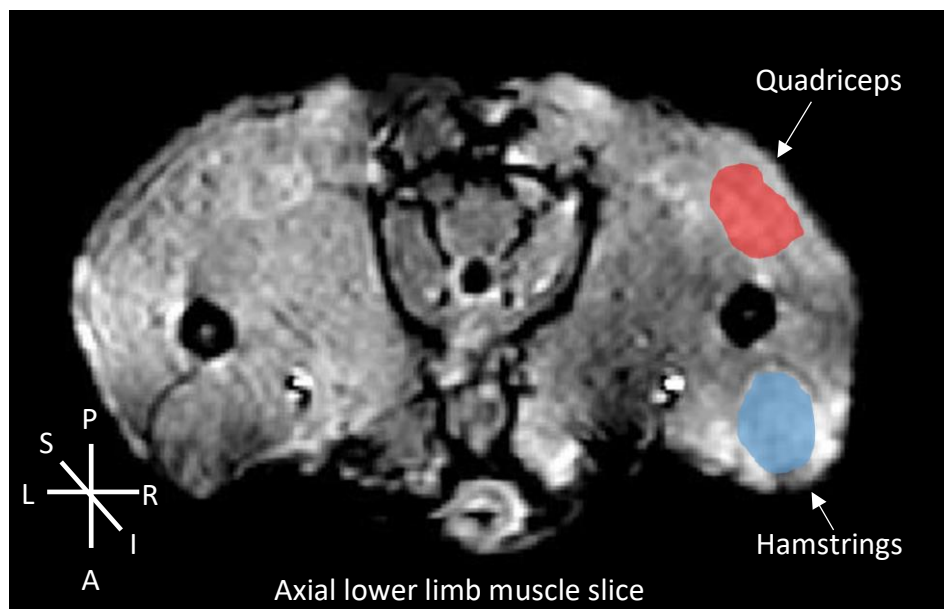
Figure 5. T1 weighted image to demonstrate the selection of regions of interest within the lower limb mouse muscles. Key: blue, Hamstrings (HMS), red, Quadriceps (QUADS), P, posterior, A, anterior, L, left, R, right, S, superior, I, inferior.

3.4.1 Cardiac muscle: MRI analysis and ROI selection

Images were zero-filled to a matrix size of 256x256 (Schneider et al., 2006). Scans were analysed using 'Segment v1.8' (Medviso, Lund, Sweden) (E. Heiberg, 2010). For cine imaging ROI segmentation of the left ventricle and right ventricle was performed by hand, with measurement of LVM, LVEF and right ventricular ejection fraction (RVEF).

ROIs were selected from a mid-cavity slice in the axial plane by hand using Aedes software (Niskanen), ROI included the complete slice of the myocardium in axial view (Figure 6).
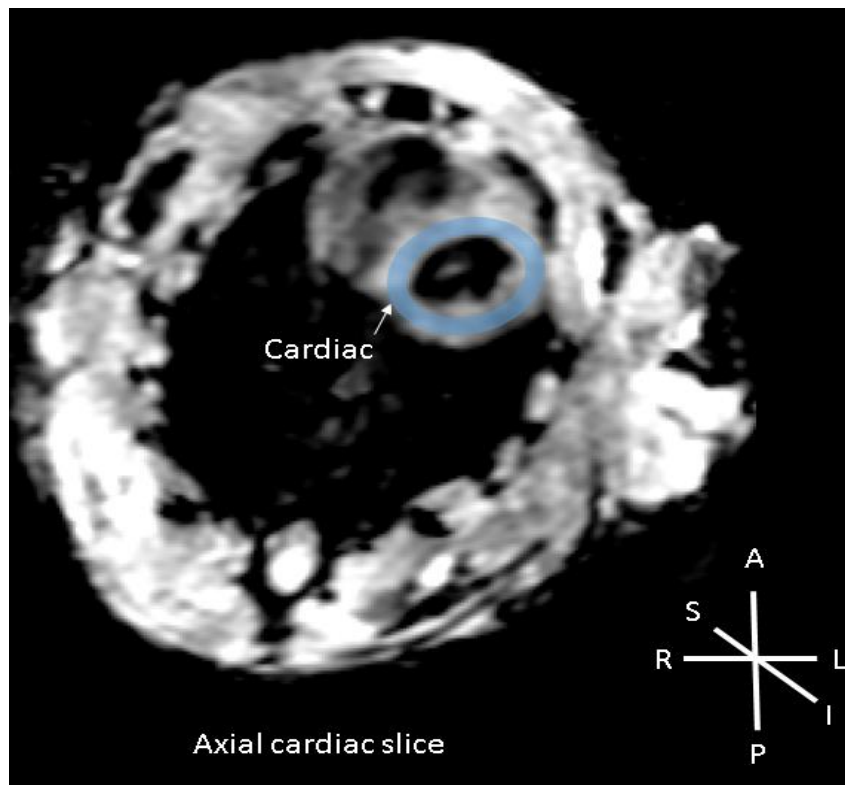
Figure 6. Gated T1 weighted image to demonstrate the selection of ROI within the cardiac muscle in axial view. Key: blue, cardiac ROI, P, posterior, A, anterior, L, left, R, right, S, superior, I, inferior.

For the purposes of calculating SNR, noise was obtained as the value of signal of air next to the animal. Change in SNR was calculated using the equation [4]:

$$Change\ in\ SNR\ (\%) = ((SNR_{post} - SNR_{Pre})/SNR_{Pre}) \times 100 \qquad (4)$$

3.5 *Ex vivo* quantification of fibrosis

Mice were humanely killed, with organs harvested (Section 2: the heart, both TA, and GCN muscles, section 3: both TA, both GCN, HMS and QUADS muscles). Samples were snap frozen in liquid nitrogen cooled isopentane and stored at −80°C. The left-sided muscles were collected for quantification of fibrosis markers via hydroxyproline, while right-sided muscles were obtained for histological analysis. In all muscles cryosections were cut 8µm thick. To ensure more coverage of the muscle to detect focal fibrosis, sections were spaced 200µm apart.

Cryosections were stained with Masson's trichrome (MT) (section 2 and 3), Haematoxylin and eosin (H&E) (section 2 and 3), sirius red (section 2), and for collagen 1 (immunofluorescence, section 3).

Cryosections were stained with MT using the HT15 staining kit (Sigma-Aldrich, UK). Slides were air dried then placed within Bouin's solution at room temperature overnight and washed in tap water. The slides were then stained in Weigert's haematoxylin for five minutes, then washed with distilled water for five minutes, and they were then placed in Beibrich scarlet acid fuchsin before being rinsed again. Slides were then placed in working phosphotungstic/phosphomolybdic acid solution for five minutes. Finally slides were placed in Aniline blue and acetic acid (1%) for five and two minutes respectively. Slides were dehydrated using increasing alcohol concentrations, cleared in histoclear and mounted using DPX mountant.

Percentage of fibrosis was quantified by hand using ROI analysis of the slides stained with MT. Imaging software (Fiji 64 bit) was used to calculate the area of fibrosis as a percentage of the total area of the muscle. This is referred to as MT quantification.

Tissue sections were incubated with formalin for ten minutes, then washed with water, five minutes of incubation with hematoxylin, then washed again in water. Slides were placed within Eosin for 30 seconds prior to ethanol dehydration and mounting in DPX.

Slides were fixed in a 3:1 solution of paraformaldehyde (PFA) (4%) and 90% alcohol for 45 seconds, then rinsed with water. Haematoxylin was added for 15 minutes, then rinsed with water for ten minutes prior to incubation of the slides for 15 minutes in direct red (0.1%) in 1% picric acid. Slides were dehydrated in 99% alcohol for one minute, then mounted in DPX mountant.

A rabbit anti-collagen 1 antibody was used (Novus biologicals, 2018). Slides were air dried at room temperature, then fixed in methanol for 10 minutes before being washed twice in phosphate buffered saline (PBS). Sections were identified and drawn around using an immunohistochemistry barrier pen. Slides were blocked using PBS with Tween 20 (PBST) in 1% bovine serum albumin (BSA), for 30

minutes, at room temperature. The primary antibody (1 in 250) in 1% PBST (0.1%) was added to the slides overnight at 4°C. The slides were washed three times for five minutes in PBS then incubated in (1:500) secondary antibody (anti-rabbit raised in donkey) (Li-Cor, United States) for one hour in the dark. The slides were then washed three times further in PBS in the dark. The slides had 4',6-Diamidine-2'-phenylindole dihydrochloride (DAPI) added with a cover slip.

3.5.1 Hydroxyproline assay

The hydroxyproline assay was performed for *ex vivo* quantification of fibrosis for direct comparison with MRI acquisitions. The hydroxyproline assay method was modified from the skeletal muscle specific standard operating procedure available from the TREAT-NMD website (Carlson, 2014). Individual muscles were weighed before being hydrolysed in 5N hydrochloric acid, at 110°C for 18 hours, and at a concentration of 10mg of muscle per ml. All samples were performed in triplicate, a 50μL sample of the hydrolysate was diluted to a volume of 2.3ml with distilled water and neutralised with (0.1N) potassium hydroxide. Sodium borate buffer 0.5ml (pH 8.7) was added with 2ml of 0.2N chloramine-T dissolved in distilled water, with sodium citrate buffer, and 2-methoxyethanol solution, this was then incubated for 25 minutes.

Sodium thiosulfate (3.6N) 1.2ml was added to the solution. To remove contaminating impurities, 2.5ml of toluene and 1.5g of potassium chloride was added to each of the tubes. The contents were mixed thoroughly, and then centrifuged at 400g; the toluene was then removed and discarded. The remaining solution was heated at 100°C for 30 min, and the final reaction product was removed by adding a further 2.5mls of toluene, appropriately mixed and then centrifuged at 400g. 1.5mls of the toluene phase was removed into separate containers, with 0.6mls of Ehrlich's reagent added to each, and incubated at room temperature for 30 minutes. Spectroscopy at 560nm was used to compare hydroxyproline standards (0μg, 0.75μg, 1.5μg, 3μg, and 6μg) to the experimental samples. Regression analysis was performed using the trend line from the hydroxyproline standards, with values divided by the weight of the muscle from the hydrolysate (0.5mg) to give the value of hydroxyproline content in μg/mg (Graham et al., 2010, Carlson, 2014).

3.6 Pharmacokinetics sampling

To confirm serum levels of halofuginone, pharmacokinetics (PK) was performed by a private company in four halofuginone-naive *mdx* mice of similar ages to the experimental groups, using liquid chromatography – mass spectrometry/mass spectrometry (LC-MS/MS). Venesection of the saphenous vein was performed using a needle and capillary tubes after IP administration of halofuginone. To keep within UK Home Office guidance for volume of venesection per mouse, the samples were taken from four mice at different time points (UK Home Office, 2018). The first sample was 150µl, and the second was 150µl from a terminal cardiac sample. The timings were as follows: mouse one 5 and 15 minutes, mouse two 30 minutes and 1 hour, mouse three 2 and 4 hours, mouse four 8 and 24 hours. These were stored as serum in lithium-heparin bottles and stored at -80°C prior to transport.

LC-MS/MS allowed quantification against a calibration curve from 0.5-1000ng/ml. A stock solution of halofuginone in DMSO (5%) and saline (0.9%) was provided at a concentration of 10mM as well as serum from a halofuginone naive *mdx* mouse. Quality control samples (3, 30 and 700 ng/mL) and mouse samples were mixed with organic solvent (methanol) containing a mixture of three generic internal standards. Samples were treated at a ratio of 3:1 solvent to sample. Following protein precipitation, samples were then centrifuged (30 minutes at 5000g). The resulting supernatant was diluted with double distilled water at a ratio of 2:1 parts of supernatant in a 96-well plate. The plate was sealed, vortex mixed and analysed by LC-MS/MS with incurred samples quantified from the calibration line.

3.7 Functional assessment of grip strength

Prior to the final scan, grip strength was assessed using a grip strength apparatus (BioSeb, Chaville, France), with both fore-limb assessment (referred to as two limb assessment) and all four limbs assessed. These were tested using a 'T' shaped bar attachment, and an 8cm x 8cm grid respectively (Figure 7). The test relies on the tendency of mice to grip a bar or grid if pulled by the tail with nothing else to hold on to. Mice were placed upon the apparatus and pulled gently backwards by the tail. Mice had three attempts with at least a one minute rest between assessments. To ensure homogeneity of the test, the same examiner performed each test. Mice were assessed on one occasion in the same temperature controlled, quiet environment. The weight and the maximal recorded value from the three attempts was used to calculate the normalised force (force/body weight) (Tinsley et al., 2014).

Figure 7. Photo of grip strength testing using the grid attachment to measure four limb strength, two limb strength was measured using a metal bar attachment shaped like the letter 'T'.

3.8 Section 2: clinical methods

To explore how MRI can be used to show disease progression in muscular dystrophies, two cohorts were examined: a group of participants with BMD, and a group with LGMDR9. For comparison in the ECV and the accelerated imaging studies (Chapters 6 and 7), 10 age-matched healthy control participants were recruited. To provide six year longitudinal cardiac and skeletal muscle data, participants were recruited that had taken part in a previous LGMDR9 natural history study performed by Willis *et al.* from June 2009 (Willis et al., 2013).

3.8.1 Ethical approval

All clinical studies complied with the declaration of Helsinki, and were run in line with the principles of 'Good clinical practice'. For the LGMDR9 six year follow up study (Chapter 5), local ethical approval was sought for each site. For the UK based sites (UNEW and University of central London (UCL)), ethical approval was sought from national research ethics service committee South Central Oxford C (Ref 15/SC/0037). Approval was granted for the LGMDR9 study in the UK in January 2015.

For the BMD cohort a separate ethical approval was required. This was granted by the National Research ethics service committee Newcastle and North Tyneside 2 (Ref 12/NE/0070) as an amendment to an existing approval in December 2014.

3.8.2 Recruitment

Participants were recruited from participants of the original LGMDR9 study by Willis *et al.* (Willis et al., 2013). Willis *et al.* recruited from local patient databases with the following inclusion and exclusion criteria: all participants must be homozygous for the c.286C>A Leu276I *FKRP* mutation, ambulant without support for more than 50m, not requiring ventilator support, able to lie supine, and have no contraindications to MRI. In the original study, validation testing of the physiotherapy assessments was performed at four weeks and six months after the first assessment. Thirty-eight participants were recruited. Due to several reasons, such as pregnancy and comorbidities during the study period, 32/38 participant data sets were complete (Willis et al., 2013).

Participants with BMD were selected with the following inclusion and exclusion criteria: a genetically confirmed diagnosis of BMD (in frame mutation within the *DMD* gene), ability to lie supine, with no MRI contraindications. The age-matched control group was male without cardiac conditions.

After informed consent was obtained, each participant underwent a brief medical history and physical examination, including routine observations (i.e. heart rate, blood pressure, respiratory rate, oxygen saturation and temperature); this was to ensure they could safely undergo the study procedures.

3.9 MRI protocols

Acquisitions consisted of four distinct sections:

- Skeletal muscle protocol and analysis
- Conventional and accelerated cine imaging for cardiac indices
- Cardiac tagging
- Imaging pre and post-Gd administration

3.9.1 Skeletal muscle protocol and analysis

There were some minor differences in protocol details between sites, all scans were performed on 3T scanners (Philips Achieva, Siemens TIM Trio) using surface coil arrays. Three point Dixon images were acquired using a spoiled gradient echo sequence, UNEW and UCL used 2D TR/TE =100/3.45,4.6,5.75ms, FA of 10 degrees, 10 slices of 10mm slice thickness with a 5mm gap. Paris used 3D TR/TE 10/2,0.75,3.95,5.15ms, with a FA of 3 degrees, 64 slices of 5mm thickness. Copenhagen used a similar TR/TE but with 3D 36 slices per acquisition, and 2 point Dixon with correction for homogeneity of B_0.

To ensure consistency between sites of positioning, acquisitions in the legs were positioned with the patella anterior and the calf images centred by locating the broadest region of the calf and recording the distance from the lower border of the patella. Positioning of the thigh images was ensured by locating the superior border of the patella and acquiring one third between this and the anterior superior iliac spine. A matrix of 160x160 interpolated to 256x256, FOV 200x200mm was used, with each leg imaged separately. Separate fat and water images were obtained and quantitative FF maps were produced by expressing the fat signal as a percentage of the total signal per voxel. The Paris site was able to scan both left and right legs at the same resolution using FOV 448x244mm.

To further ensure homogeneity of acquisition across sites, phantom images with known fat water content were quantified and healthy volunteer images were taken in each site. These were then compared by a MRI physicist at the UNEW site.

In contrast to the original study, skeletal muscles were not graded using the Mercuri scale, because such semi-quantitative scales have been long superseded by the less subjective, more reliable measures such as the Dixon technique. Skeletal MRS was not repeated due to the findings of the original study, which suggested that although there was a change in metabolites in LGMDR9 muscle detected, this was less significant compared to other muscular dystrophies. Unpublished data suggested that the scope for these values to change over time was limited. Taken together with the long acquisition time for MRS, it was decided to not include these in the final protocol.

Both functional assessment data and MRI were anonymised and assigned unique patient identifiers prior to secure electronic transfer to UNEW for analysis. Information from all four sites was collated electronically onto a master sheet.

MRI acquisitions were all analysed at UNEW. Once assigned the unique identifier code for each participant, these were analysed in batches by hand drawn ROI using imaging software 'Image J' (Abràmoff et al., 2004). Two observers drew ROIs separately around the selected muscle groups (Figures 8 and 9) at a single level. The images were separated into fat and water fractions; the fat percentage of a voxel was calculated as a percentage of total signal per voxel. Data from the left and right legs was combined by averaging, as were the results from the two analysts.

Mean FF and muscle CSA were calculated using the ROIs. c-CSA was calculated by multiplying the CSA by one minus FF; this represents the muscle content of the ROI.

During movement muscles rarely function in isolation, therefore composite FFs were calculated as area-weighted averages. Composite muscle groups were all muscles of the thigh, all muscles of the calves, the QUADS (RF, VL, vastus medialis (VM)), HMS (SM, ST, biceps femoris short head (BFSH), BFLH), triceps surae (LG, MG, Sol).

Figure 8. MRI acquisitions to demonstrate imaging of the left thigh using the Dixon technique. Both images were taken at six year follow up. A is a water separated image, B is a fat separated image.
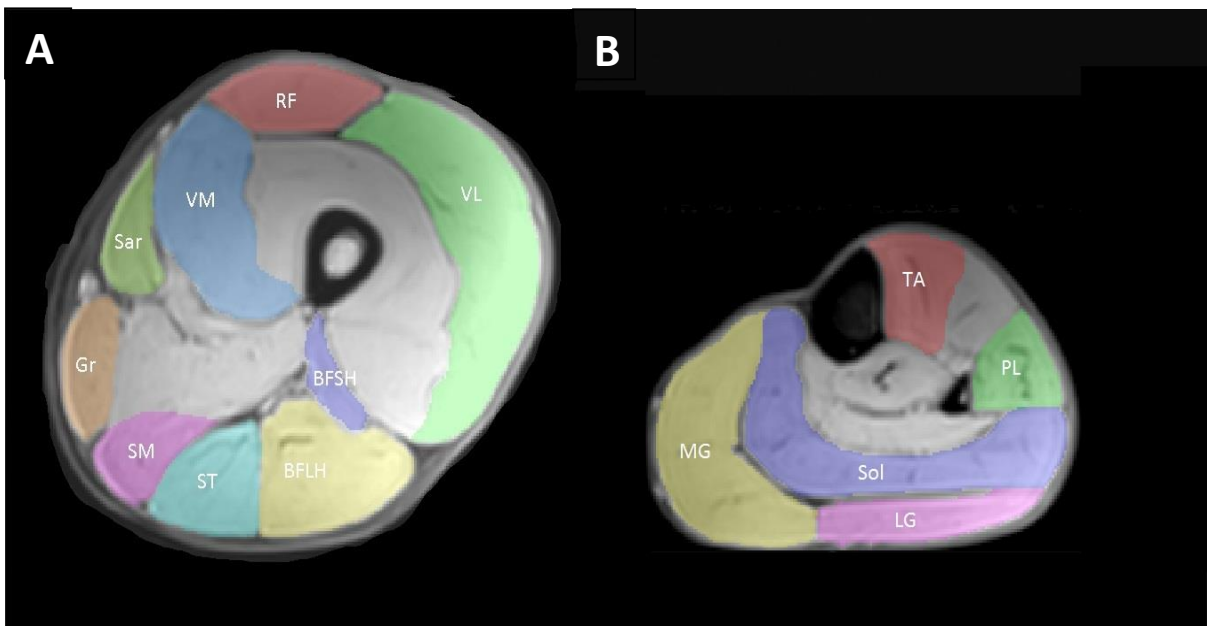
Figure 9. Examples of ROI selection from baseline water separated images. Image A left thigh, image B left calf.
Key: RF, rectus femoris, VL, vastus lateralis, VM, vastus medialis, Sar, Sartorius, Gr, Gracilis, SM, semimembranosus, ST, semitendinosus, BFLH, biceps femoris long head, BFSH, biceps femoris short head, TA, tibialis anterior, PL, peroneus longus, Sol, Soleus, MG, medial gastrocnemius, LG, lateral gastrocnemius.

3.9.2 Conventional and accelerated cine imaging for cardiac indices

During breath-holding, steady-state free precession images were acquired in the short axis plane with a FOV of 350x315mm, FA 40°, slice thickness 8mm, 0mm gap, cardiac cine 25 phases, with 14 slices. Resolution of 1.85 x 1.54mm, zero-filled to 1.37mm, temporal duration 40ms per phase, dependent on heart rate.

For comparison the protocol acquires cardiac cine data using two techniques:

1) Standard conventional protocol with contiguous slice coverage,
2) Accelerated protocol with contiguous slice coverage

In all cases, two chamber and four chamber long axis views were acquired using parameters as described below. The accelerated protocols utilise enhanced gradient mode to reduce TR by 20% and TE by 24%, making use of a higher SENSE factor 2.1 on the 16 channel coil, and higher turbo acceleration factor 23 compared with the previous 17. Due to reduced TR, the TFE shot length is similar for the two acquisitions: 61ms (TR x turbo factor – 23 x 2.65 = 61ms) for the accelerated sequence and 58.5ms (17 x 3.44 = 58.5ms) for conventional images. The short and long axis acquisitions were made sequentially, using the parameters as outlined (Table 3).

To compare inter-rater reliability, two appropriately trained observers reviewed a sample of the accelerated images (n=10) for the five cardiac indices studied. Images were reviewed independently and results were compared using Bland Altman analysis.

To qualitatively analyse the images, observers were asked to rate a sample (n=8) of the accelerated images in terms of quality based on a five point scoring system (Table 4).

Axis	Parameter	Conventional stack	Accelerated stack
Short axis	TR/TE/Turbo factor	3.3ms/1.7ms/17	2.7ms/1.3ms/23
	SENSE acceleration factor	1.5	2.1
	Partial Fourier factor (%)	37.5	37.5
	Phase acquisition factor (%)	55	55
	Slices per breath-hold	2	4
	Number of breath-holds	7	4
	Duration of breath-hold†	7 x 10.3s	3 x 10.3s, 1 x 5s
Long axis	TR/TE/Turbo factor	3.3ms/1.7ms/17	2.7ms/1.3ms/23
	SENSE acceleration factor	1.5	2.1
	Partial Fourier factor (%)	37.5	37.5
	Phase acquisition factor (%)	55	55
	Slices per breath-hold	1	1
	Number of breath-holds	1	1
	Duration of breath-hold†	1 x 5s	1 x 2.6s

Table 3. A table to show the short-axis parameters of the three techniques of acquisition. The same partial Fourier factor and phase acquisition factor is used in all acquisitions (0.625/55% respectively). Slice thickness was the same in all three techniques (8mm).
Key: TR, repetition time, TE, echo time, SENSE, SENSitivity Encoding.
† at 70 bpm

Score	Description
1	Image quality in conventional is considerably better than that of accelerated
2	Image quality in conventional is marginally better than that of accelerated
3	No obvious difference between the image quality in conventional and accelerated
4	Image quality in accelerated is marginally better than that of conventional
5	Image quality in accelerated is considerably better than that of conventional

Table 4. Five point qualitative rating scale of image quality.

3.9.3 Cardiac tagging

Tagged short-axis images were obtained during the same scan session. Short axis slices of 10 mm thickness were prescribed centred at the mid-ventricle, with a spacing of 12mm. The apical and basal slices themselves were avoided due to the risk of the grid moving out of the heart during the cardiac cycle. Calculation of cardiac tagging indices involved acquisition of tagged images at identical position to the slices used in cine imaging. A TFE sequence with acceleration factor 9 was used TR/TE/FA/number of excitations 4.9/3.1/108/1, SENSitivity Encoding (SENSE) factor 2, FOV 350×350mm, voxel size 1.37 × 1.37mm, orthogonal complementary spatial modulation of magnetisation (CSPAMM) grid with tag spacing of 7mm. Reconstruction was possible using view sharing, 15–27 time frames per cardiac cycle. Breath-holds were requested of participants to reduce potential respiratory artefact (Lumens et al., 2006).

3.9.4 Imaging pre and post-gadolinium administration

Pre-contrast T1 map acquisition for ECV calculation used a modified Look Locker (MOLLI) sequence (TR/TE/TI/FA = 2.1ms/0.95ms/350ms/20°, FOV 300x300, resolution 2 x 2mm zero-filled to 1.17mm^2) to acquire at a fixed diastolic cardiac phase using a 5s(3s)3s inversion scheme. This was followed by an injection of 0.2mmol/kg Gd contrast agent, Dotarem (Guerbet, France). A LGE short-axis stack and orthogonal long-axis planes were acquired using 3D Phase Sensitive Inversion Recovery (PSIR) sequence 10 minutes post-Gd. Enhanced post-contrast T1 map acquisition was made at 15 minutes post-administration using a 4s(1s)3s(1s)2s inversion scheme. Pre- and post- contrast T1 mapping acquisitions were at three short-axis locations (apical, mid-cavity, and basal) during separate breath-holds (duration 12s), then reconstructed using custom software.

3.9.5 Cardiac magnetic resonance imaging analysis

Five cardiac indices were obtained from the accelerated and conventional images: LVEF, LVM, left ventricular stroke volume (LVSV), left ventricular end diastolic volume (LVEDV), and left ventricular end systolic volume (LVESV). Cardiac indices were obtained from the cine images using ViewForum workstation (Philips). End-systole and end-diastole were defined with endocardial and epicardial boundaries manually traced as described previously (Jones et al., 2010). Five cardiac indices were calculated: LVEF, LVSV, LVM, LVEDV, and LVESV. WMA were identified by an experienced observer looking for asymmetrical LV wall contraction.

All tagging data was analysed using the 'Cardiac Image Modelling package' (University of Auckland), as described in detail previously (Hollingsworth et al., 2013b). In line with previous analyses (Lumens et al., 2006) we calculated PT at systole, peak whole wall circumferential strain (PWWS), and peak endocardial circumferential strain (PECS). The relationship between torsion and strain was estimated using torsion to shortening ratio (TSR = PT/PECS), a constant among age-matched healthy subjects, but which increases with healthy ageing (Lumens et al., 2006, Hollingsworth et al., 2012).

ECV is quantified by selecting a ROI and calculating the average T1 values within the ROI in both enhanced and native acquisitions. The difference in the reciprocal of these values (i.e. the relaxation rate) is divided by the difference in values of the blood pool to give the partition coefficient; this is demonstrated in equation 1. Correction for Hct is achieved by multiplication of one minus the serum values (L/L). The concentration of Gd within cardiac tissue is calculated using equation 2.

Mean T1 values were obtained from the MOLLI images using manually-defined ROI within the LV wall using ImageJ (Abràmoff et al., 2004) (Figure 10). Each slice (basal, mid, apical) was divided into four

segments modified from the American Heart Association topographical segments (Cerqueira et al., 2002): the insertion point of the right ventricular wall into the left ventricle was the border of the septal and ventricular regions. These were divided to give anterior, posterior, anterior septal, posterior septal segments (Figure 11). ECV values are referred to: segmentally, regionally (either: basal, mid-cavity or apical), or globally, which is the mean of all segments in all slices. Other studies refer to 'global ECV' measurement but include only one slice that is analogous to the 'regional' values in this study (Sado et al., 2012, Ugander et al., 2012, Banypersad et al., 2013, Radunski et al., 2014).

LGE was confirmed by an experienced observer from the PSIR images with segmental location recorded. ROIs were defined on the intraventricular lumen on the pre- and post-contrast images to obtain blood pool values, while avoiding papillary muscles and LV trabeculae.
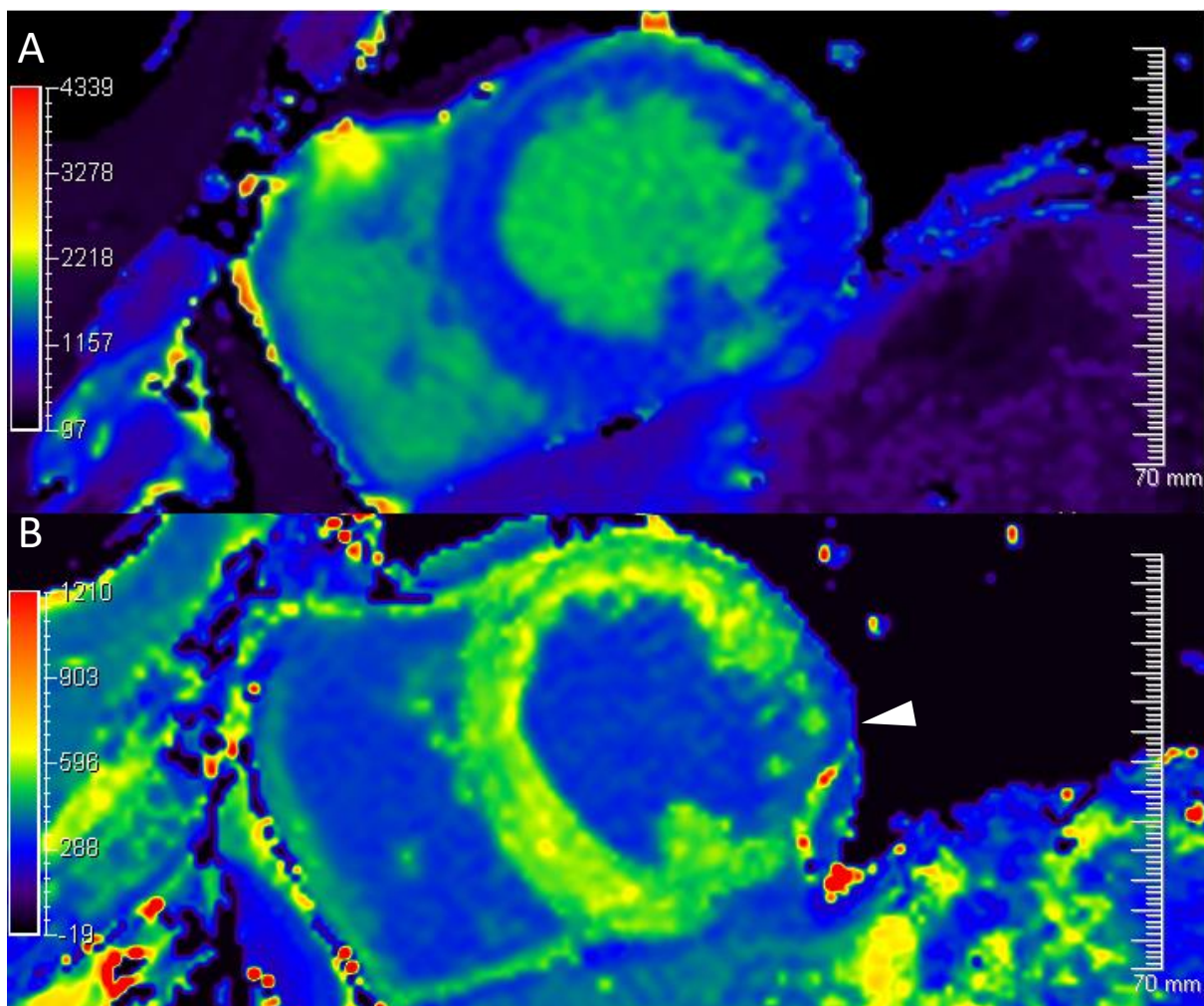
Figure 10. An example of T1 maps. The upper image (A) shows pre-contrast enhancement, the lower image (B) shows post contrast enhancement. Images were taken from the same point in the cardiac cycle. Intensity map has been applied to provide an intensity scale as seen to the left of the image. The lower image demonstrates the reduction in uptake in areas of fibrotic tissue (demonstrated by the white arrow).
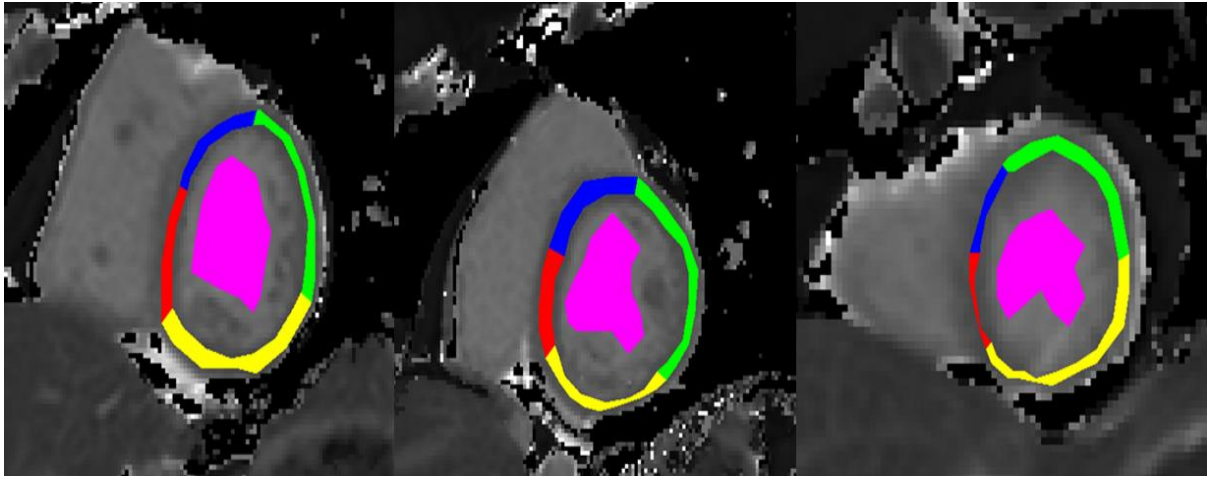
Figure 11. Region of interest (ROI) selection and labelling on a pre-contrast T1 map for extracellular volume (ECV) calculation. The blood pool ROI avoids papillary muscles. 'Regional' ECV values are taken from a single slice. Left – Basal region, centre mid-cavity region, right apical region. Global ECV values are taken from all slices and all segments combined.

Key: Blue, septal anterior, red, septal posterior, green, anterior, yellow, posterior.

3.10 Physical assessments

The physical function tests were set out in a manual with recording sheets. Teleconferencing enabled standardised training of the physiotherapists across the four sites. All assessors were familiar with the equipment and tests as set out in the manual.

Specialist physiotherapists administered tests in a specific order to reduce variability between assessors. The order of the testing was: ten metre walk or run (10MWR), spirometry (with hand-held device), myometry (hand held assessment of the dominant side), range of ankle movement, timed up and go, stair climb, stair descent, chair rise, the NSAA, and finally the 6MWT. If participants were unable to complete a test due to being non-ambulant, they were graded as unable and the reason recorded.

3.10.1 Standardised functional testing

The timed tests included a 10MWR in a quiet corridor, with a course pre-measured using a measuring tape. Grades indicating how well the participants performed and time taken to complete the course were recorded. Similar grading and timing were performed for all the other timed tests. The stair climb, and descent were performed on a set of steps, and the height of each step was standardised across the four sites at 15cm. Chair rise and timed up and go tests were performed using a chair of a standardised 47cm height with arm rests. In the chair rise, the participant was asked to get from a

sitting to standing position with their arms by their sides. The timed up and go test involved the participants starting in the standing position, then being timed in walking 3 meters from and then back to the chair, with the timer stopped once the participant was re-seated. Grades were assigned for all of these assessments (with the exception of the timed up and go test) based on the grading scale on the physiotherapy data entry forms. The NSAA is a 17 point assessment tool grading ability to perform multiple domains, including jumping, climbing a single step, and running as well as timed tests. Domains are graded from 0-2 then totalled out of 34; a higher score implies more functional ability. The NSAA has been validated for use as a clinical trial outcome measure for DMD (Mazzone et al., 2010, Mazzone et al., 2009). The 6MWT involves the participants walking for six minutes around a 25m course marked out with cones on either end. Two assessors are required, both with stop watches. One walks closely behind the participant for safety purposes; the second counts how many times the course is completed. The final distance is calculated using the number of completed laps added to the number of metres the participant had completed on the final lap. Full descriptions of these functional assessments are detailed in the physiotherapy manual (Appendix A).

3.11 Statistical analysis

Statistical analysis was performed using SPSS v23 and Microsoft Excel. All data was checked for normality using the Shapiro-Wilk test. In Chapter 4, where data is normally distributed, results are presented as mean and standard deviation unless otherwise indicated, with significance tested via two tailed paired Student t-test. Where data is non-normally distributed median and range are used, with statistical significance calculated using the Wilcoxon signed test. Throughout assessment of correlation, strength and significance was performed using Pearson correlation.

For timed tests a participant may be unable to perform a functional assessment. For the purposes of obtaining statistical significance this is recorded as a time greater than all others measured, to permit ranking in non-parametric statistical tests: in this case 10,000 seconds. Statistical significance was taken to be $p < 0.05$.

For longitudinal data it is possible to calculate the standardised response mean (SRM) by taking the average of the paired difference over the follow up, and dividing by the standard deviation of the differences. SRM facilitates comparison between different outcome measures with a high SRM (>0.8) implying a high level of responsiveness to changes in value (Cohen, 1988).

Chapter 4: Quantification of fibrosis using the novel gadolinium-based contrast agent EP3533

4.1 Summary

Fibrosis is a pathological process in muscular dystrophies. Increased levels of fibrosis in skeletal and cardiac muscle have been associated with a worse prognosis in DMD. Anti-fibrotic medications are being evaluated for amelioration of DMD. To date, MRI has not been used successfully to image fibrosis within skeletal muscle as an outcome measure. EP3533 is a novel Gd-based contrast agent using a complex peptide with an affinity to collagen 1. EP3533 has been used successfully to quantify fibrosis in pre-clinical trials of several disease models.

This chapter is a description of experiments on age-matched 40 week old *mdx* and BL10 mice, using EP3533 to detect and quantify fibrosis within skeletal and cardiac muscle. Correlation between *ex vivo* measures of fibrosis and R1 change is compared following both EP3533 and non-collagen specific SGd agent. T1 mapping was used to quantify changes in R1 over time in areas of interest. R1 change using EP3533 was significantly higher in the *mdx* than the BL10 mouse group (cardiac muscle p=0.02, GCN p=0.04, TA p=0.04). A strong correlation was demonstrated between change in R1 and histological quantification of fibrosis in muscle (GCN r=0.83 p=0.0001, TA r=0.73 p=0.01, cardiac muscle r=0.73 p=0.02). There were no significant correlations between *ex vivo* quantification and the use of standard gadolinium. No differences were seen in LVEF however RVEF was significantly lower in the *mdx* group, and correlated with *ex vivo* quantification change (MT r=-0.70 p=0.01, hydroxyproline assay r=-0.72 p=0.008,) and R1 change (r=-0.83 p=0.006).

EP3533 was further assessed as an outcome measure in quantifying the difference in R1 change between treated and untreated *mdx* mice following a 12 week treatment of an anti-fibrotic. Four age-matched mouse groups (treated *mdx*, untreated *mdx*, treated BL10 and untreated BL10) were scanned at baseline using T1 mapping looking at skeletal muscle (TA, GCN, QUADS, HMS). Treated groups were administered IP halofuginone three times a week for 12 weeks. Control groups received vehicle injections via the same route. All mice underwent grip strength testing (two and four limb assessment) prior to a second scan with EP3533; they were then killed for *ex vivo* quantification of fibrosis. R1 change was significantly different from baseline to follow up scan in three out of four muscles (GCN p=0.04, HMS p=0.009, and TA p=0.01) in the untreated *mdx* group only. In terms of absolute R1 change at follow up, there were no significant differences between the treated and untreated *mdx* groups (P=NS). Treated *mdx* mice had significantly less fibrosis than untreated *mdx* mice in all four muscles.

Correlation of R1 change was significant but less strong than in the first experiment, and varied between the two methods of *ex vivo* quantification. EP3533-induced R1 change correlated significantly but weakly to the functional assessment of grip strength (two r=-0.33 p=0.004, four r=-0.32 p=0.06).

In conclusion, EP3533 was used successfully to detect and quantify fibrosis in skeletal muscle and cardiac muscle, and detected differences between *mdx* and BL10 mice. SGd was unable to demonstrate the same difference. EP3533 was unable to detect change in response to treatment in absolute numbers, but did detect changes in values over the period of follow up, this may be in part due to variation in R1 change at baseline. EP3533-induced R1 change correlated significantly to a measure of right ventricular heart function and grip strength. Further studies in humans will eventually be required to confirm these findings of EP3533 as an outcome measure in DMD.

4.2 Results

The development of this technique involved three separate experiments. The first (Section 1) was to find the optimal time for skeletal muscle imaging; the second (Section 2) was to assess the efficacy of EP3533 *in vivo*, and the final stage (Section 3) explored the use of EP3533 as an outcome measure following anti-fibrotic treatment.

4.2.1 Section 1 – Pilot study of EP3533 in skeletal muscle

Both the *mdx* and BL10 mouse survived the anaesthetic and were killed post-procedure. All muscle groups had increased SNR at 5 minutes, which may be due to interference from Gd enhancement in blood vessels. Levels of SNR in the *mdx* mouse reached a plateau at 60-90 minutes, and did not return to pre-contrast levels by the end of the scanning period (120 minutes). The BL10 mouse showed an initial peak in SNR at 5 minutes, and then plateaued at a much lower level from approximately 10 minutes onwards (Figure 12). Differences between *mdx* and BL10 mouse muscles in signal were demonstrated most clearly in the TA muscles (Figure 13).

The mice tolerated injection with EP3533 contrast agent and the prolonged scanning procedure. The greatest change in SNR was in the *mdx* mouse at 60-90 minutes. Due to this the optimal time to measure R1 change in lower limb skeletal muscle was taken as 70 minutes.
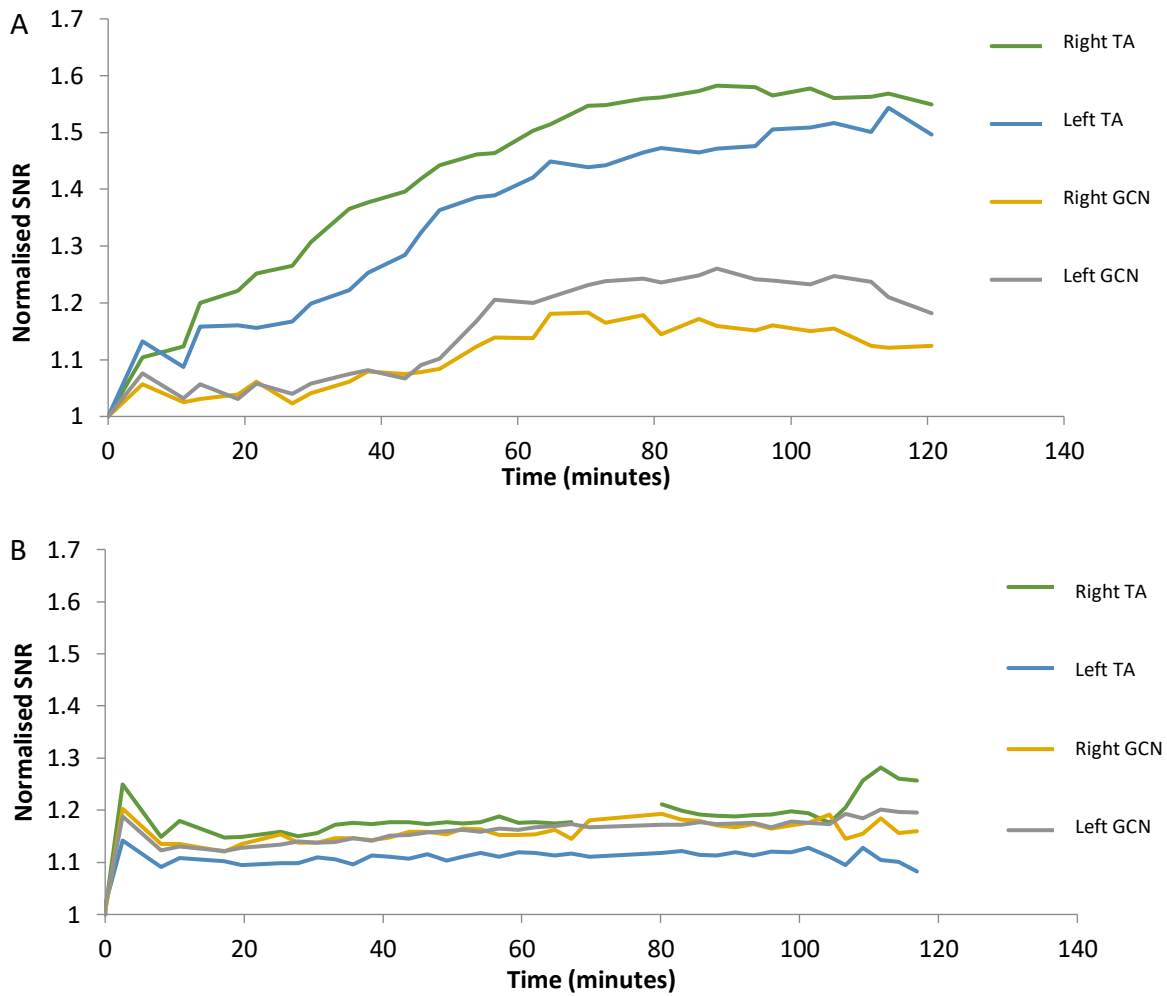
Figure 12. A line graph to display the dynamic changes in signal to noise ratio (SNR) in the mdx mouse (A) and the BL10 mouse (B). All lines are lower in the BL10 mouse compared to the mdx muscles at the same time point suggesting that contrast enhancement was higher in certain mdx muscles compared to the BL10 mouse at these times. Note that the SNR increase is at a plateau from approximately 60 minutes onwards in the mdx mouse. In (B) from 60-65 minutes an artefact was present in the right TA muscle these points were therefore excluded.
Key: TA, tibialis anterior, GCN, gastrocnemius, SNR, signal to noise ratio.
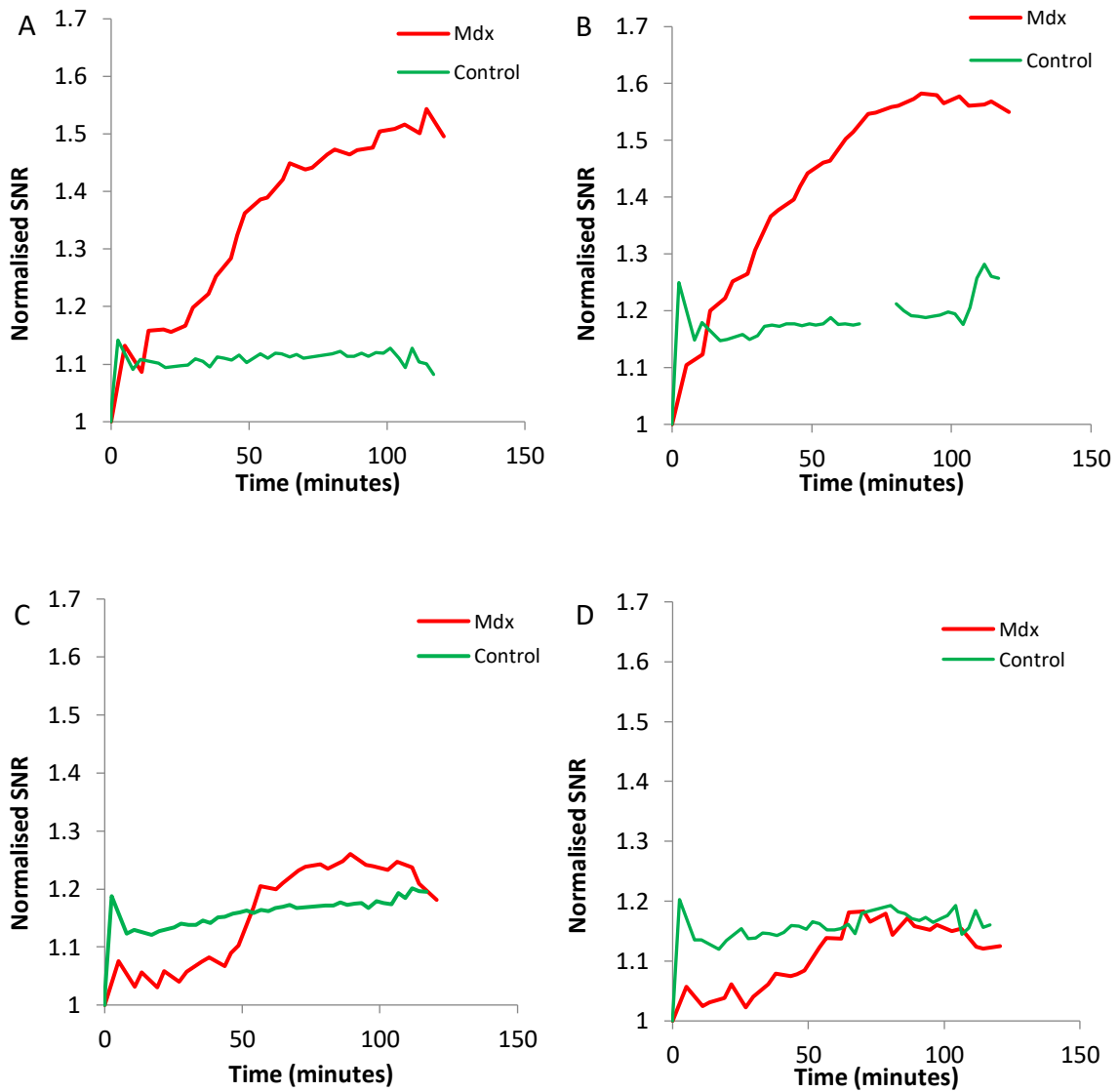
Figure 13. Comparison of signal to noise ratio (SNR) change in individual muscles between mdx and BL10 mice. The mdx tibialis anterior (TA) demonstrated the greatest SNR change compared to the BL10 TA. (A) Left TA, (B) Right TA, (C) Left gastrocnemius (GCN), (D) Right GCN.

Key: SNR, signal to noise ratio, TA, Tibialis anterior, GCN, gastrocnemius.

4.2.2 Section 2 - Evaluation of the utility of EP3533 in assessing fibrosis within cardiac and skeletal muscle

One *mdx* mouse died during the scanning process, most likely due to the stress of the anaesthetic. This mouse was therefore excluded from the MRI analysis and dissection. All other mice (BL10 n=5, *mdx* n=8) survived both scans and were included in the analysis.

Post-contrast using continuous gated-T1w-GRE acquisitions it was possible to show dynamic change of signal in cardiac tissue over a one hour period. The peak change in SNR in the *mdx* using EP3533 was at 40 minutes, with a smaller peak at 15-20 minutes (Figure 14). SGd scanning also demonstrated a small peak at 15 minutes; however after this the difference with BL10 mice was minimal.
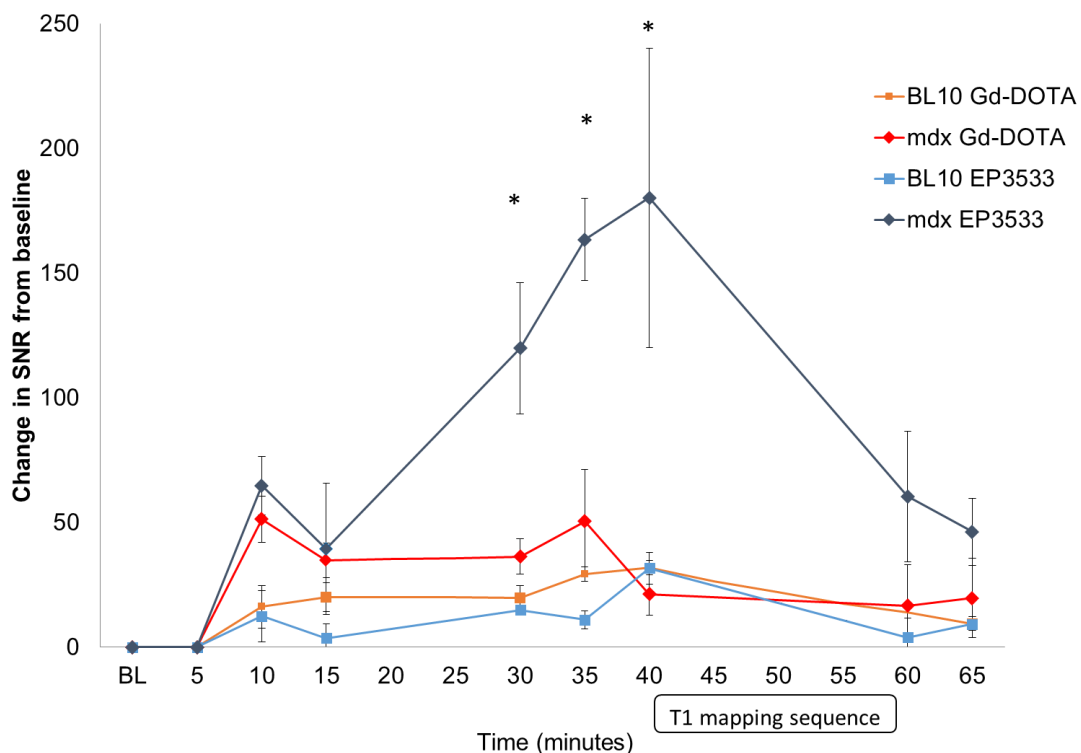
Figure 14. Line graph to show the results of the dynamic cardiac study. There is an increase in signal in the mdx mice during the scan using EP3533 at 10-15 minutes and again at 40 minutes. Each line represents the averaged values. All measurements are from ROI measurement of the left ventricle of T1 values from axial slice at the approximate middle of the ventricle during diastole. Due to the nature of cardiac gating measurement times are approximate; no measurements were taken from 40 minutes to 60 minutes due to T1 mapping acquisition, as highlighted in the grey rectangle.
Key: blue lines, EP3533, red lines, scans with standard gadolinium (SGd).
* - significant difference (p<0.001) between EP3533 scan and Gd-DOTA.

Four mice (2 BL10, 2 *mdx*) were excluded from analysis with the T1 mapping data due to movement artefact. The remaining images (3 BL10, 6 *mdx*) were deemed of sufficient quality (Figure 15).
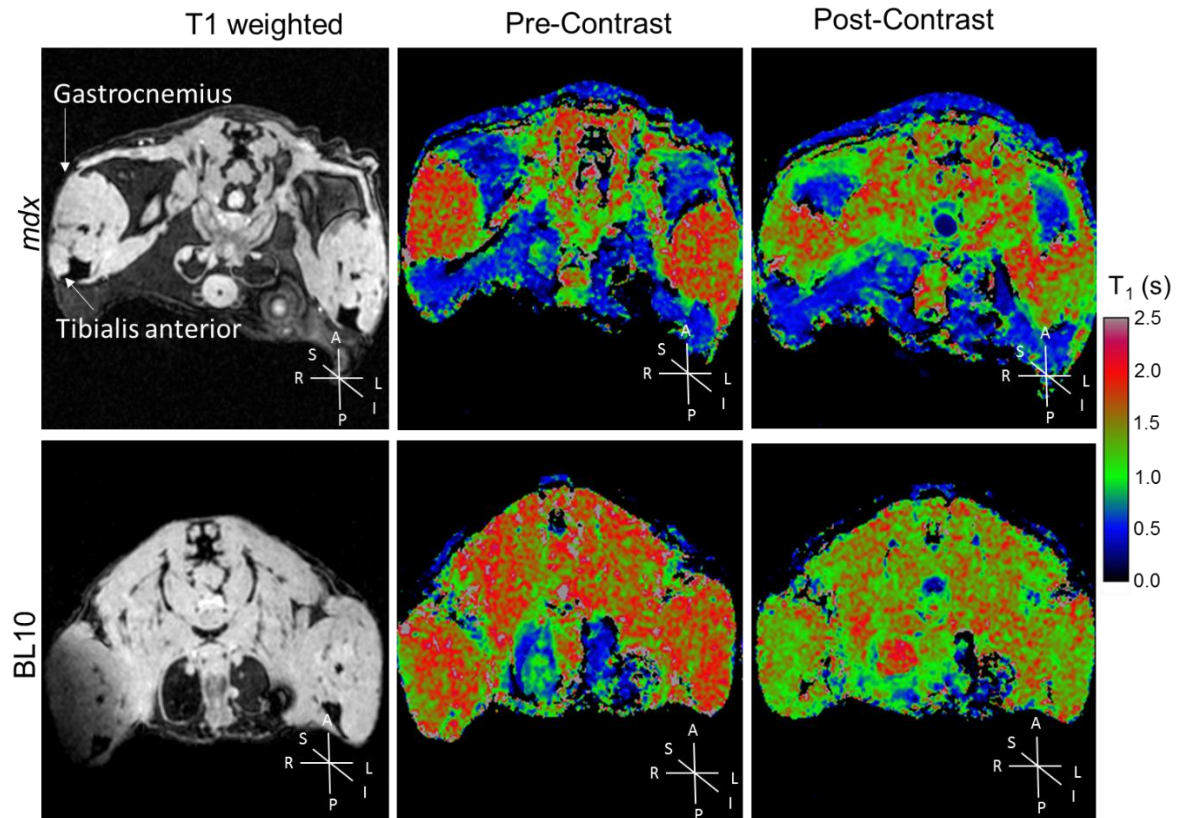
Figure 15. Examples of T1 maps acquired pre and post-administration of EP3533 contrast (Murphy et al., 2018). Upper row shows lower limb muscles in an mdx mouse, while the lower row shows images at a similar location in a BL10 mouse. Contrast binding in muscle reduces the tissue T1 in the mdx mouse in the post-contrast scan (right), compared to the pre-contrast scan (centre). Non-homogenous signal increase is demonstrated as an increase in green in mdx lower limb muscles in the post-contrast images. These images demonstrate the change in T1 post contrast in the mdx mouse, which is evident in the tibialis anterior (TA) and gastrocnemius (GCN), but less obvious in the BL10 mouse where it is more homogenous in colour.
Key: P, posterior, A, anterior, L, left, R, right, S, superior, I, inferior.

Change in R1 following EP3533 was higher in the muscle of *mdx* mice compared to BL10 mice, with significant differences in all three muscles (cardiac p=0.02, GCN p=0.04, TA p=0.04) (Figure 16Figure 16).
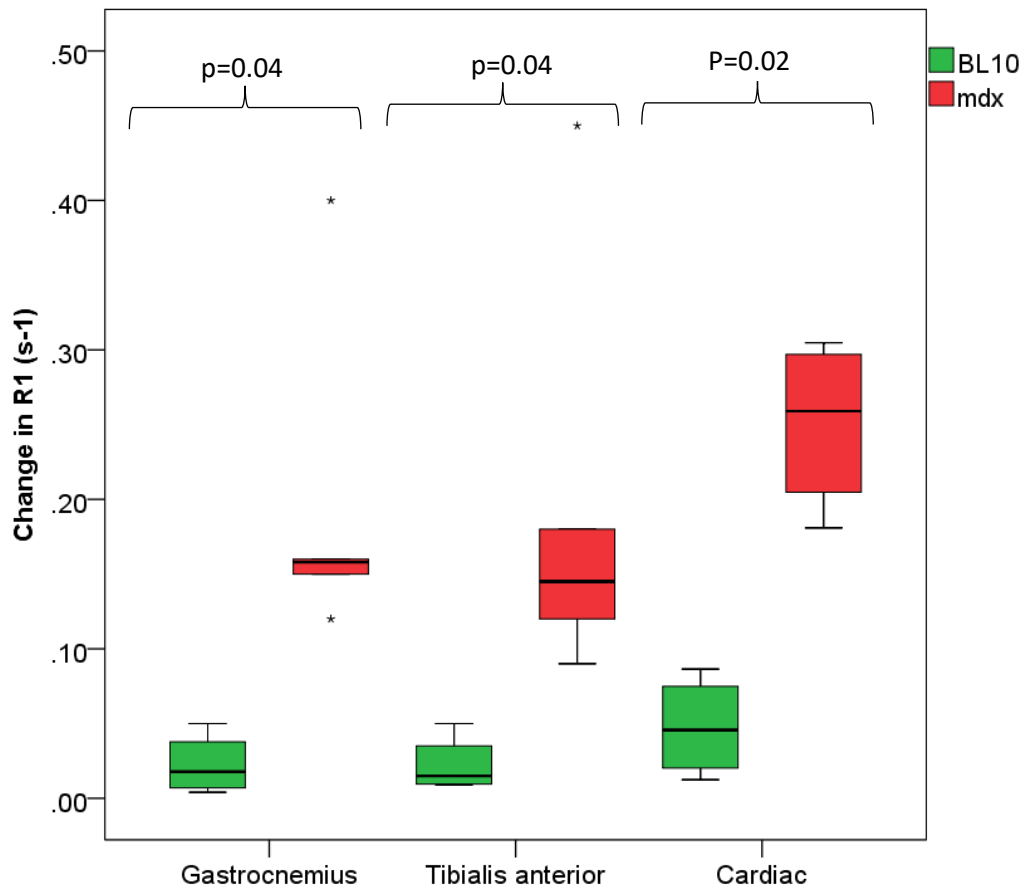
Figure 16. Box plot showing R1 change between BL10 and *mdx* mice using EP3533 broken down by muscle (Murphy et al., 2018). Cardiac muscle had the greatest change in R1 from baseline scan. All three muscles demonstrated a significant difference compared to BL10. Asterisks demonstrate outliers greater than three times the interquartile range (IQR). Key: green, BL10, red, *mdx,* GCN, gastrocnemius, TA, tibialis anterior.

Quantification of fibrosis was performed using two methods: MT and hydroxyproline assay. To identify other disease features, sirius red and H&E staining was also performed (Figure 17). Taking all measurements from muscles into account, MT quantification and hydroxyproline correlated to a highly significant degree (r=0.64, p<0.001) suggesting a level of correlation between the two methods of *ex vivo* quantification.

BL10 mice had significantly lower mean quantities of fibrosis when quantified with both MT (BL10 heart 0.5% ±0.4 vs *mdx* 6.1% ±2, p<0.001, BL10 GCN 2.4% ±0.9 vs *mdx* 15.2% ±3.99, p<0.001, BL10 TA 1.3% ±0.8 vs *mdx* 10% ±3, p<0.001) and hydroxyproline quantification (BL10 heart 2.8μg/mg ±1.5 vs

mdx 5.2µg/mg ±1.9 p=0.04, BL10 GCN 1.8µg/mg ±0.4 vs *mdx* 3.9µg/mg ±1.1 p=0.002, BL10 TA 3.5µg/mg ±1.4 vs *mdx* 5.3µg/mg ±1.1 p=0.04) (Figures 17 and 18).
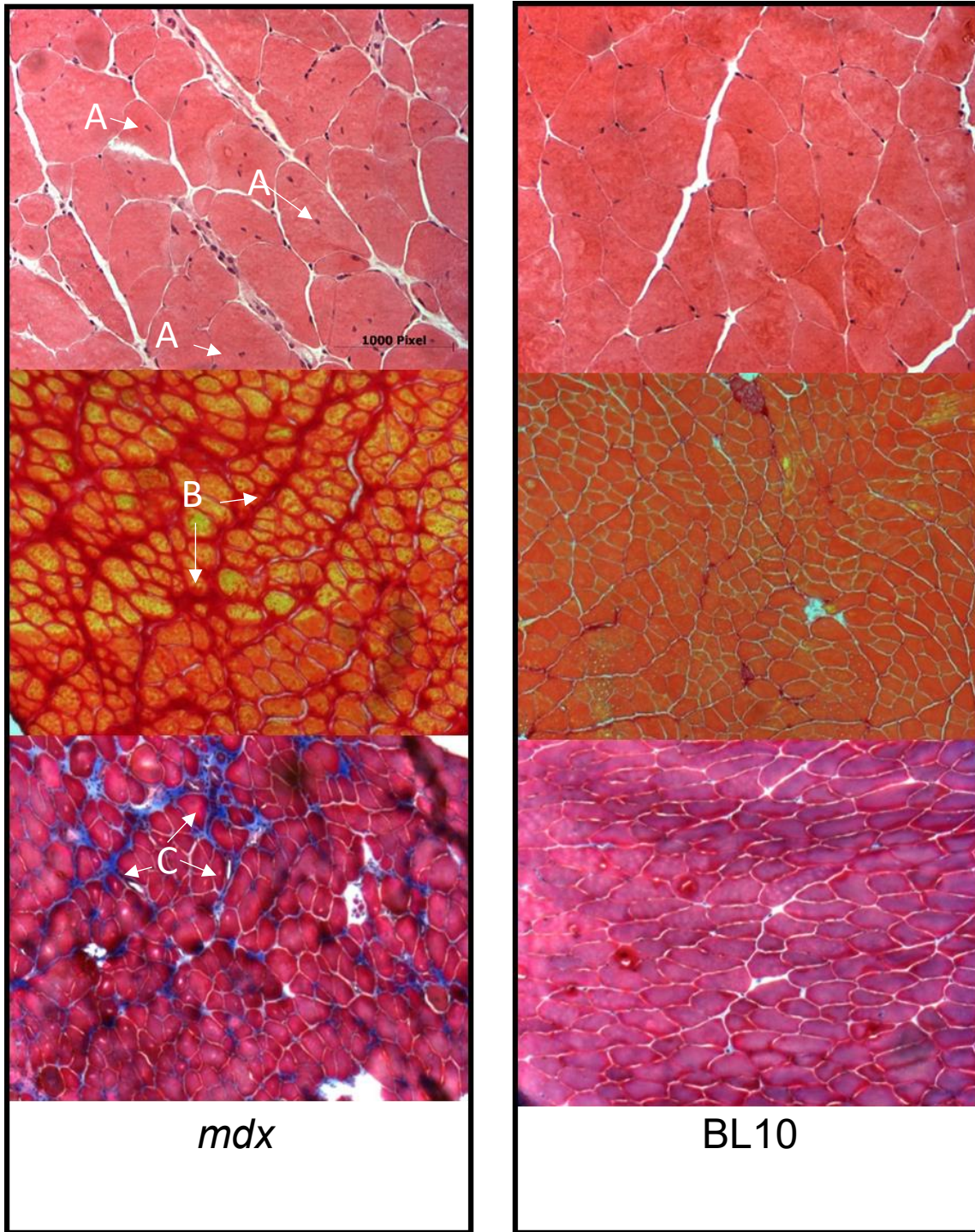
Figure 2. Examples of transverse sections from gastrocnemius (GCN) muscles. Top row: Haematoxylin and eosin (H&E) staining – *mdx* **section shows centrally located nuclei (marked as 'A') and evidence of extracellular fibrosis, with regenerated myocytes. Middle row: Sirius red stain – fibrosis is shown as areas of dark red (marked as 'B'). Bottom row: Masson's trichrome (MT) staining – fibrosis is shown as dark blue (marked as 'C') or larger focal areas appear as white regions. MT staining shows evidence of diffuse fibrosis in the extracellular space throughout, with focal fibrosis in some regions of muscle. Magnification of H&E stain is intentionally shown as higher to highlight the dystrophic features - x20 magnification, MT and Sirius red stains are shown as x10 magnification to demonstrate the extent of extracellular fibrosis (x10 magnification).**
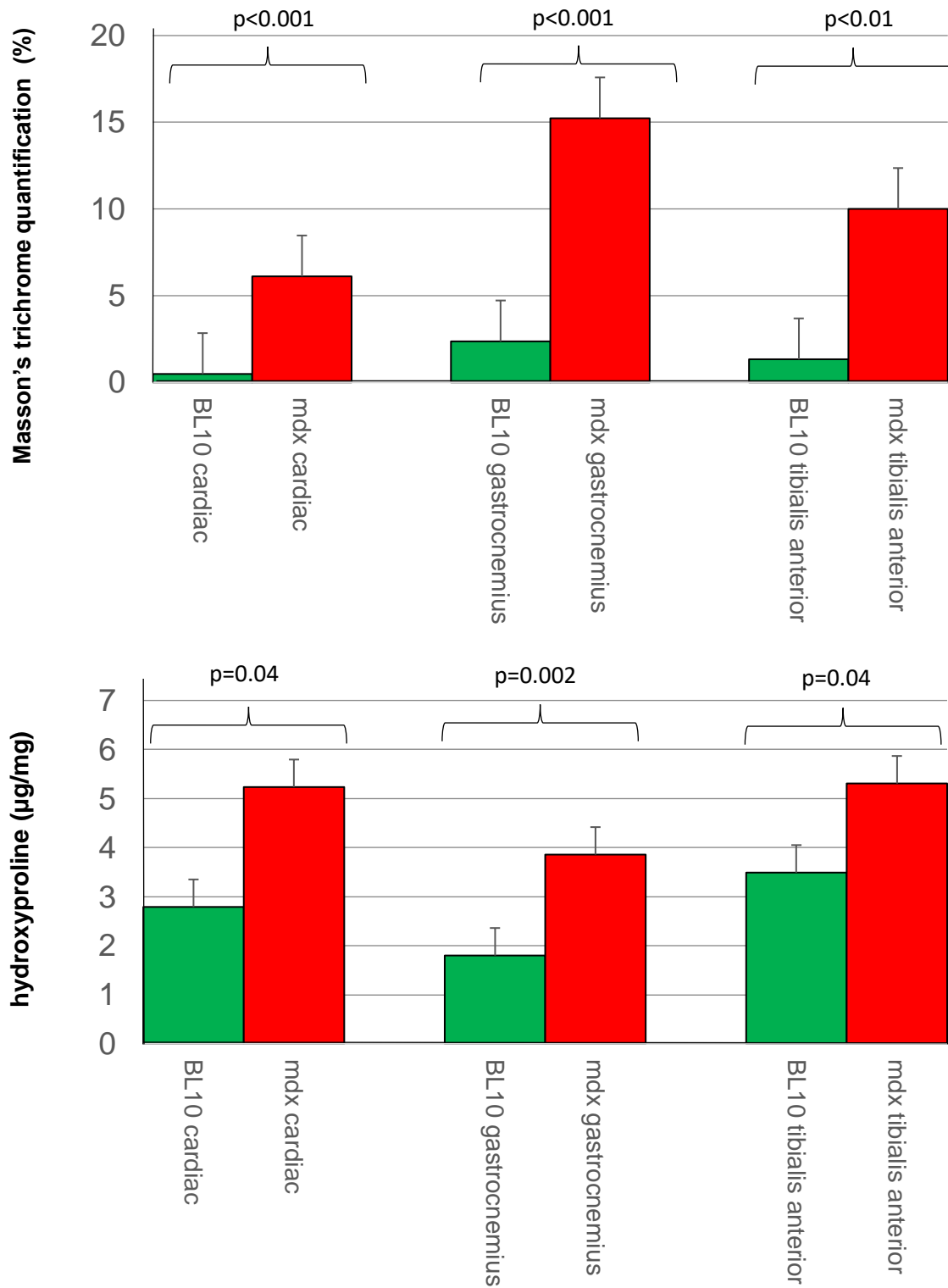
Figure 18. Bar charts to show *ex vivo* mean quantification of fibrosis in BL10 and *mdx* mice: top - Masson's trichrome (MT), bottom - hydroxyproline assay. Both methods of quantification showed significant differences (p<0.05) between BL10 and *mdx* values in all types of muscle.
Key: green, BL10, red, *mdx*, MT, Masson's trichome.
Error bars display standard error.

Change in R1 obtained during scans with EP3533 showed several strong and significant correlations (Table 5). The strongest correlation was seen between hydroxyproline and change in R1 using EP3533 in the GCN muscle (r=0.83, p=0.001).

Method of quantification	Change in R1 GCN	Change in R1 TA	Change in R1 cardiac
Masson's trichrome	0.60 p=0.04*	0.62 p=0.03*	0.76 p=0.01*
Hydroxyproline assay	0.83 p=0.001*	0.73 p=0.01*	0.73 p=0.02*

Table 5. A table to demonstrate the calculated Pearson correlation of EP3533-induced R1 change and the two methods of ex vivo quantification. In all three muscles change in R1 and ex vivo measures correlated to a significant degree.
* - p value < 0.05

For measurement of cardiac function one *mdx* mouse had significant respiratory artefact during the cine scanning and was excluded from the analysis. RVEF was the only measure of cardiac function that was significantly higher in BL10 (59.9% ±11.3) compared to *mdx* mice (31.1% ±9.1) (p=0.01). Other parameters, LVEF and LVM, were not significantly different between *mdx* and BL10 mice (Figure 19). Heart rate was maintained between 300-400 bpm in both mouse groups.
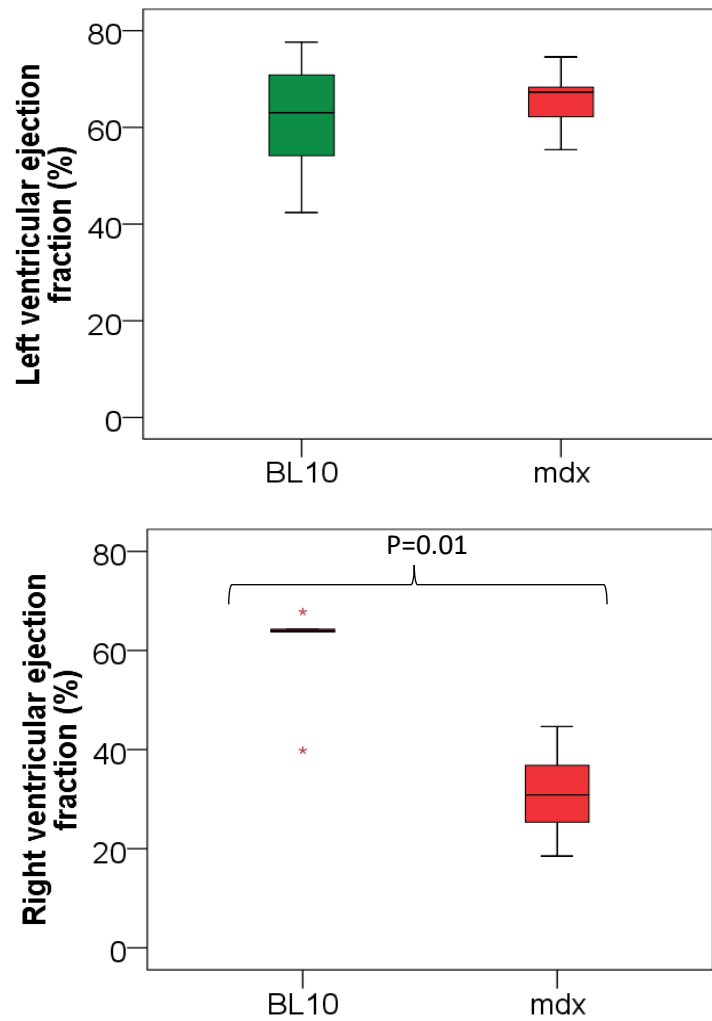
Figure 19. Comparison between cardiac indices in left and right ventricular function in mdx and BL10 mice; no significant differences were seen between BL10 and mdx mice except in right ventricular ejection fraction (RVEF) (p=0.04). Asterisks demonstrate outliers greater than three times the interquartile range (IQR). Right ventricular mass and left ventricular mass were not significantly different between BL10 and mdx mice (p=NS)

RVEF correlated inversely to a significant degree with MT quantification (r=-0.70, p=0.01) and hydroxyproline assay values (r=-0.72 p=0.008). Concentration of EP3533 as calculated using T1 mapping correlated strongly to RVEF (r=-0.83 p=0.006) (Figure 20). LVEF and LVM did not significantly correlate to either of the *ex vivo* methods of fibrosis quantification. These findings demonstrate a significant relationship between increases in fibrosis, R1 change using EP3533 and cardiac dysfunction.
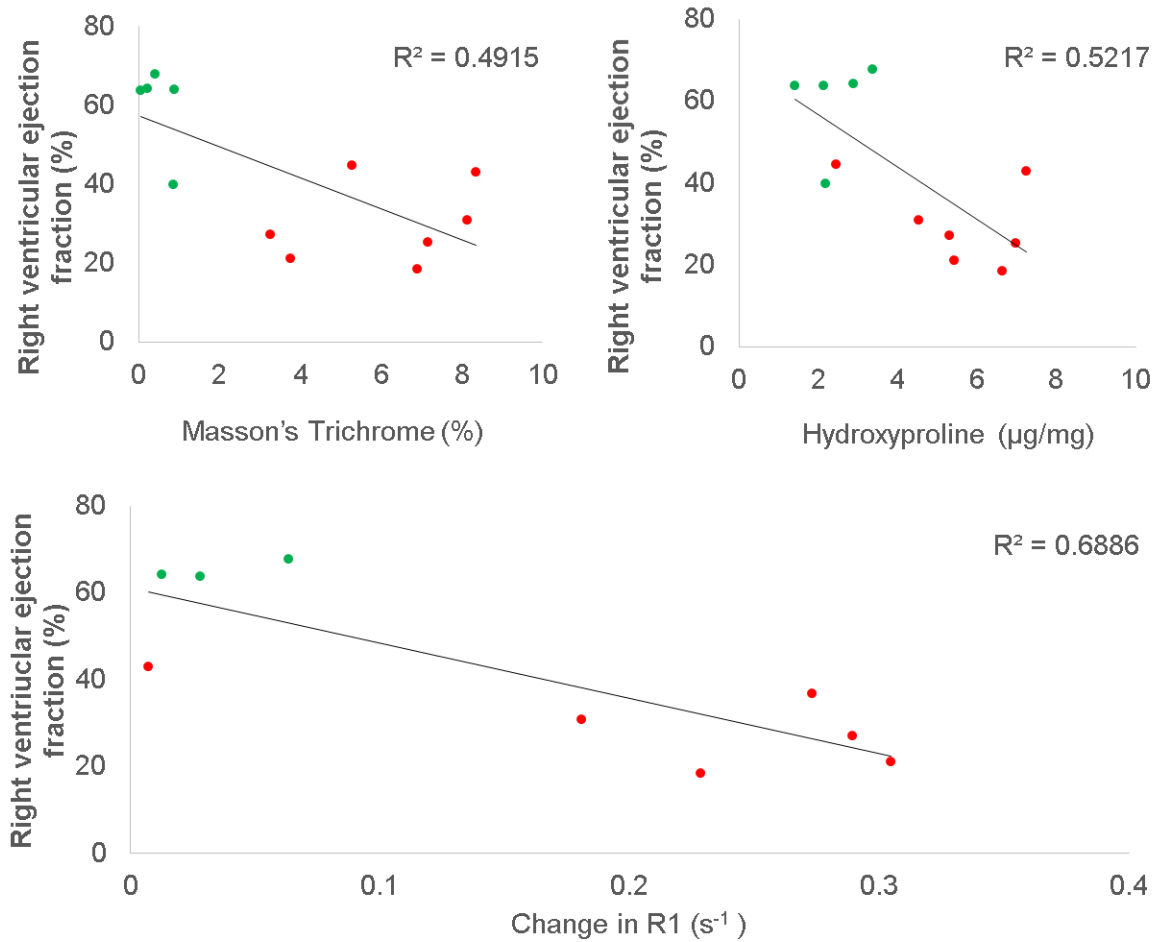
Figure 20. Top row - correlation of right ventricular ejection fraction (RVEF) to ex vivo measures of fibrosis quantification (Masson's Trichome (MT) and hydroxyproline assay). Bottom row – correlation of RVEF to EP3533 derived R1 change in the heart. These graphs demonstrate the strong, significant correlation between RVEF and change in R1 (p=0.006), as well as the degree of correlation between ex vivo measures and change in R1. None of the other cardiac indices correlated significantly to change in R1 (p=NS).
Key: green, BL10, red, mdx, RVEF, right ventricular ejection fraction, MT, Masson's trichrome.

4.2.3 Section 3 - Evaluation of EP3533 in monitoring disease progression in response to anti-fibrotic treatment

The final section of this chapter aims to evaluate whether EP3533 is sensitive enough to detect disease progression in skeletal muscle of *mdx* mice following administration of an established anti-fibrotic (Halofuginone).

All mice (*mdx* n=21, BL10 n=6) tolerated the halofuginone, vehicle and EP3533 administration with no side effects attributed to the drug and no significant weight difference was seen between treated and untreated groups. There were no significant differences between BL10 mouse groups in terms of weight, functional assessment, *ex vivo* measures of fibrosis or baseline and follow up R1 change; the BL10 groups were therefore considered together for comparison with *mdx* mouse groups.

4.2.3.1 Pharmacokinetics

Pharmacokinetic results demonstrated that halofuginone was detectable in serum at six of the eight time points (5 minutes, 15 minutes, 30 minutes, 1 hour, 2 hours, 4 hours, 8 hours and 24 hours). The concentration range was from 2.85-21.2ng/ml with the highest peak at 5 minutes post-administration (Figure 21). Area under the curve analysis was 913.68ng/ml/min.
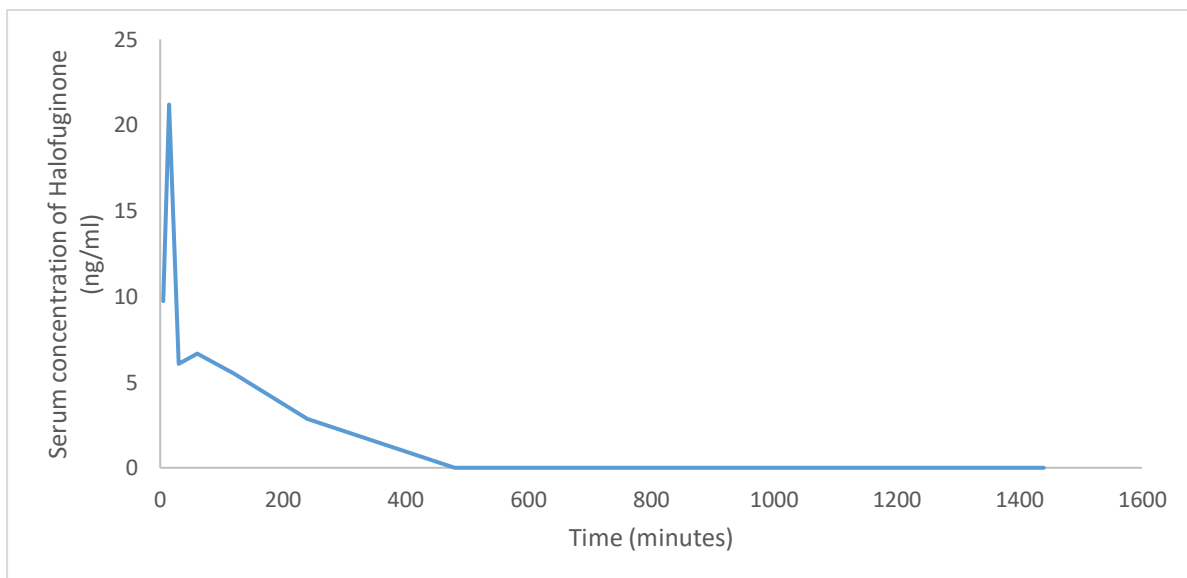
Figure 21. A line graph demonstrating the change in serum halofuginone post - intraperitoneal (IP) administration of 7.5ug (n=4). To allow inclusion of all time points, time is measured in minutes. The last five data points are at 1, 2, 4, 8 and 24 hours respectively.

4.2.3.2 Inter-observer data

Inter-observer consistency was assessed using Bland-Altman analysis of five randomly chosen scans. The observers had a mean difference in R1 change of $0.005s^{-1}$ (Figure 22). The 95% limits of agreement (LOA) were $0.05s^{-1}$, therefore no fixed bias was present. Four of the seven data points outside of the 95% LOA were from where the two observers disagreed on the positioning of all four muscles at 40 minutes in one mouse. These findings suggest an overall good, non-biased agreement between observers using this technique.
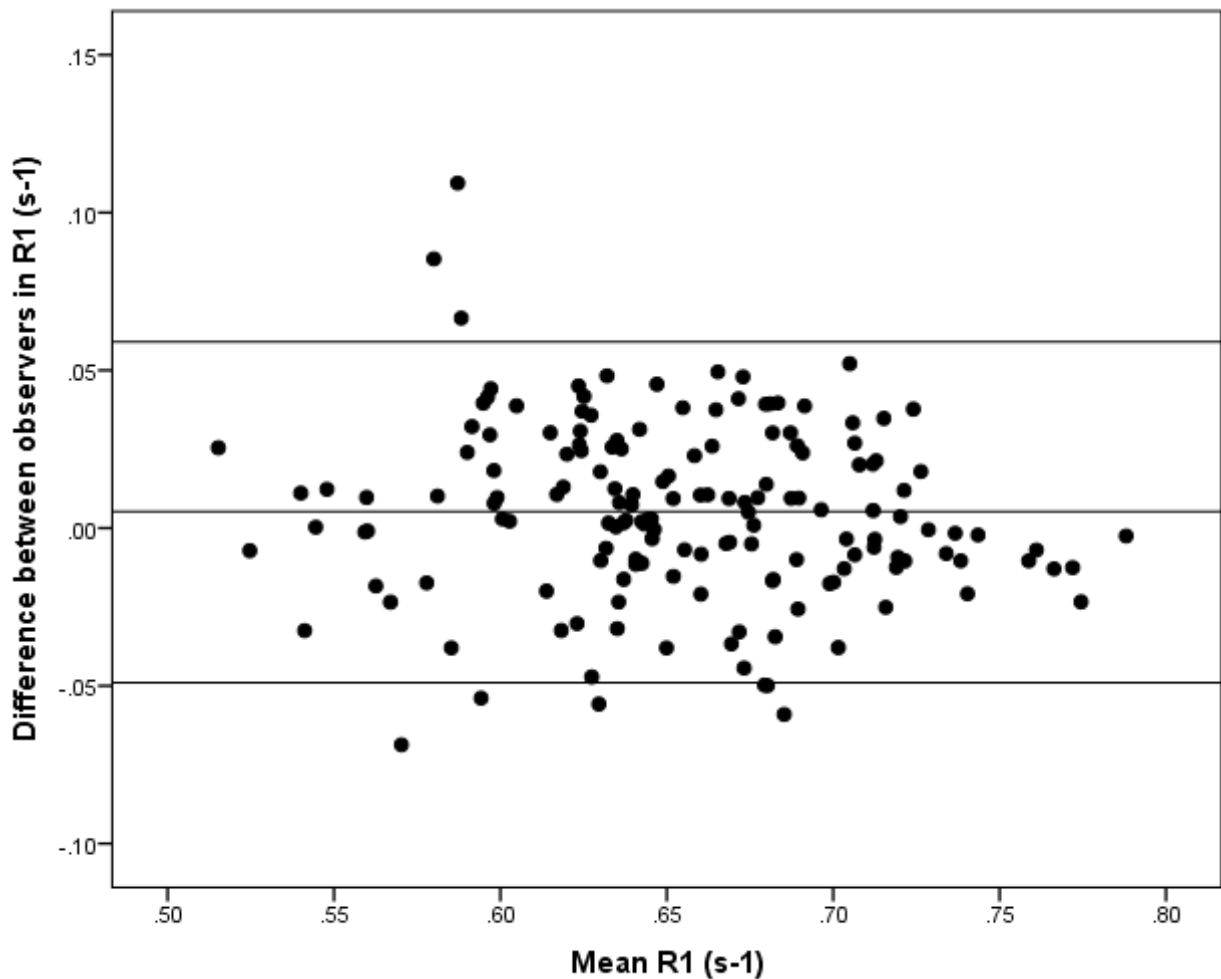
Figure 22. A Bland-Altman plot to show the mean inter-observer differences in ROI analysis between two observers. Two observers calculated R1 change in all muscles of five mdx mice chosen at random and included all time points (0-70 minutes) during the pre-treatment scan. Horizontal lines from top to bottom denote +1.96 standard deviation, the mean difference, and -1.96 standard deviation.

4.2.3.3 Functional assessment

All mice tolerated the grip strength testing with no signs of discomfort. Both treated groups had significantly lower starting weight than their respective control groups (*mdx* p=0.02, BL10 p=0.02).

Comparison of absolute force values demonstrated a significantly lower force in the two limb assessment (treated mouse group 1.3mN versus untreated *mdx* group 0.8mN, p=0.002). Treated *mdx* mice were not significantly different to BL10 mice (p=0.32); however untreated *mdx* were significantly lower than BL10 (p=0.035). No significant differences were seen when comparing the two BL10 groups, or comparing all BL10 to all *mdx* mice. Four limb assessment was not significantly different in any of the mouse groups, except for untreated *mdx* compared to BL10 (p=0.048).

Normalising force to weight, in the *mdx* cohort as a whole, there were no significant differences in the two or four limb assessments compared to the BL10 groups (p=0.85, p=0.72 respectively). The grip assessments were not significantly different between the treated and untreated BL10 groups (p=0.69) (Table 6).

Two and four limb assessments demonstrated significantly larger value of weight normalised-force in the treated *mdx* compared to the untreated *mdx* (two limb p<0.001, four limb p=0.049) (Table 6). No significant differences were seen between the *mdx* treated group and the 'all BL10' group (two p=0.08, four p=0.52) (Table 6). The untreated *mdx* were significantly lower than the 'all BL10' group in the two limb assessment only (two p=0.04, four p=0.17). These findings lend support to the efficacy of the treatment and suggest that the treated *mdx* groups were able to generate similar force to the BL10 groups. Furthermore the treated *mdx* group could generate significantly greater than the untreated *mdx* groups (p=0.002).

Group	Mean two limb weight normalised-force (mN/g)	Mean four limb weight normalised-force (mN/g)
All *mdx*	27.9 ±11.4	49.4 ±8.6
All BL10	28.7 ±7.5	50.7 ±8.1
mdx untreated	21.5 ±6.8	46.4 ±5.5
mdx treated	37.0 ±10.6	53.7 ±10.7
BL10 untreated	29.6 ±9.7	45.9 ±5.9
BL10 treated	27.2 ±2.1	58.5 ±3.6

Table 6. The table summarises the differences in force assessment between the four mouse groups. In the two limb assessment significantly lower force was demonstrated in the untreated compared to the treated mdx group (p=0.002). Significant differences were seen between the untreated mdx group and the BL10 group as a whole in both two (p<0.001) and four limb assessments (p=0.049). No difference was seen between the treated mdx and the BL10 groups. These findings suggest that the treated mdx were able to generate more force which suggests that the treatment may have been efficacious.

4.2.3.4 Dynamic measurement of R1 change in skeletal muscle

Gd-based contrast agents reduce the relaxation time (denoted as T1) in target tissue. Relaxivity rate, (denoted as R1) is the reciprocal of T1. The difference in R1 from baseline is calculated at ten minute intervals as a dynamic measurement of the tissue change in response to the contrast agent (Figures

23 to 25). In the pre-treatment scans the R1 change of the TA was significantly higher in the *mdx* groups than BL10, at all time points with the exception of 10 and 70 minutes (Table 7). In the GCN and the QUADS R1 change was only significantly higher in the *mdx* group at the 60 and 70 minute time points. At post-treatment scan, all muscles at 40, 50 and 60 minutes had significantly higher R1 change in the *mdx* groups (Table 7).

In the pre-treatment scan, no significant differences were demonstrated between the *mdx* groups at any time points in any muscles, with the exception of the TA at 50 minutes (untreated *mdx* $0.09s^{-1}$ ±0.06 versus treated *mdx* $0.15s^{-1}$ ±0.05 p=0.04), and in the HMS at 70 minutes (untreated *mdx* $0.08s^{-1}$ ±0.05 versus treated *mdx* $0.12s^{-1}$ ±0.03 p=0.04) (Figure 23).

In the post-treatment scan, there were no significant differences between the untreated and treated BL10 groups in any of the muscles at any of the time points (Table 7). Post-treatment R1 change in the untreated *mdx* groups demonstrated significantly higher values compared to the treated *mdx* in the HMS at 10-40 minutes and in the GCN at 20 minutes (Tables 8 to 9 and Figure 24). These findings suggest a degree of variability and dependence on the timing of R1 measurement, 70 minutes was retained as the point for correlation and comparison as this had been used in the previous experiments (Sections 1 and 2). There was a lack of significant difference in the absolute value using the magnitude of R1 change alone in treated versus untreated *mdx* mouse groups. The following section will assess whether the degree of R1 change demonstrates a significant difference between the groups when comparing the pre-treatment scan to the post-treatment scan.

In the halofuginone experiment, mean values of R1 change at follow up scan in the untreated *mdx* group (0.11-$0.16s^{-1}$) were similar to the skeletal *mdx* muscle results seen in section 2 (skeletal muscle R1 change 0.14-$0.15s^{-1}$). The similarity in values between separate experiments suggests that EP3533 R1 change measurement is consistent.

	10	20	30	40	50	60	70
mdx TA	0.08 ±0.04	0.10 ±0.05*	0.11 ±0.05*	0.12 ±0.05*	0.11 ±0.06*	0.11 ±0.05*	0.11 ±0.05
BL10 TA	0.08 ±0.03	0.10 ±0.02	0.11 ±0.01	0.12 ±0.01	0.11 ±0.01	0.11 ±0.02	0.11 ±0.06
mdx GCN	0.07 ±0.03	0.08 ±0.04	0.10 ±0.04	0.09 ±0.04	0.09 ±0.04	0.10 ±0.04*	0.09 ±0.04*
BL10 GCN	0.03 ±0.05	0.03 ±0.05	0.04 ±0.06	0.05 ±0.05	0.04 ±0.06	0.04 ±0.05	0.01 ±0.004
mdx HMS	0.07 ±0.03*	0.08 ±0.03*	0.09 ±0.04*	0.10 ±0.04*	0.10 ±0.04*	0.11 ±0.04*	0.10 ±0.05
BL10 HMS	0.02 ±0.01	0.02 ±0.00	0.001 ±0.05	0.02 ±0.04	0.01 ±0.04	0.03 ±0.04	0.07 ±0.02
mdx QUADS	0.06 ±0.04	0.07 ±0.05	0.08 ±0.06	0.08 ±0.06	0.09 ±0.07	0.09 ±0.12*	0.08 ±0.00*
BL10 QUADS	0.03 ±0.04	0.03 ±0.05	0.03 ±0.06	0.04 ±0.06	0.03 ±0.07	0.001 ±0.12	0.01 ±0.001

Table 7. Comparing dynamic R1 change in mdx and BL10 groups at pre-treatment scan. All measurements were significantly higher in the mdx group at 60 minutes, only the gastrocnemius (GCN) and the quadriceps (QUADS) were significantly higher at 70 minutes.

*p value <0.05 compared to contemporaneous control group.

Key: TA, Tibialis anterior, GCN, Gastrocnemius, HMS, Hamstrings, QUADS, Quadriceps.

	10	20	30	40	50	60	70
mdx TA	0.09 ±0.04	0.12 ±0.05	0.14 ±0.05*	0.15 ±0.04*	0.15 ±0.05*	0.14 ±0.06*	0.15 ±0.04*
BL10 TA	0.06 ±0.06	0.09 ±0.08	0.09 ±0.07	0.10 ±0.08	0.08 ±0.08	0.07 ±0.01	0.08 ±0.05
mdx GCN	0.07 ±0.03*	0.09 ±0.04*	0.10 ±0.04*	0.10 ±0.04*	0.11 ±0.05*	0.10 ±0.05*	0.12 ±0.04*
BL10 GCN	0.03 ±0.03	0.03 ±0.04	0.04 ±0.04	0.05 ±0.04	0.04 ±0.05	0.04 ±0.05	0.03 ±0.04
mdx HMS	0.08 ±0.04	0.10 ±0.04	0.12 ±0.05	0.12 ±0.05*	0.12 ±0.05*	0.12 ±0.04*	0.12 ±0.05*
BL10 HMS	0.06 ±0.04	0.06 ±0.06	0.08 ±0.06	0.06 ±0.06	0.06 ±0.06	0.06 ±0.06	0.05 ±0.05
mdx QUADS	0.05 ±0.03	0.06 ±0.04	0.07 ±0.04	0.08 ±0.04*	0.08 ±0.04*	0.09 ±0.05*	0.10 ±0.06
BL10 QUADS	0.04 ±0.04	0.05 ±0.04	0.05 ±0.05	0.04 ±0.05	0.03 ±0.05	0.04 ±0.06	0.05 ±0.06

Table 8. Comparing dynamic mean R1 change in mdx and BL10 groups at post-treatment scan. There were significant differences between BL10 and mdx mouse groups at 70 minutes during the post-treatment scan in the tibialis anterior (TA), gastrocnemius (GCN) and the hamstrings (HMS).

*p value <0.05 compared to contemporaneous control group.

Key: TA, Tibialis anterior, GCN, Gastrocnemius, HMS, Hamstrings, QUADS, Quadriceps.

	10	20	30	40	50	60	70
Untreated TA	0.09 ±0.04	0.13 ±0.05	0.15 ±0.05	0.15 ±0.05	0.15 ±0.06	0.15 ±0.06	0.16 ±0.05
Treated TA	0.08 ±0.04	0.10 ±0.05	0.13 ±0.03	0.14 ±0.03	0.14 ±0.05	0.13 ±0.05	0.15 ±0.04
Untreated GCN	0.07 ±0.03	0.10 ±0.03	0.11 ±0.04	0.12 ±0.05	0.12 ±0.05	0.12 ±0.05	0.13 ±0.03
Treated GCN	0.05 ±0.03	0.07 ±0.04*	0.08 ±0.04	0.09 ±0.04	0.09 ±0.05	0.08 ±0.05	0.10 ±0.04
Untreated HMS	0.08 ±0.04	0.11 ±0.03	0.13 ±0.04	0.14 ±0.05	0.13 ±0.05	0.13 ±0.05	0.13 ±0.04
Treated HMS	0.05 ±0.03*	0.07 ±0.04*	0.09 ±0.04*	0.09 ±0.04*	0.10 ±0.04	0.10 ±0.04	0.10 ±0.05
Untreated QUADS	0.06 ±0.03	0.07 ±0.04	0.08 ±0.04	0.08 ±0.04	0.09 ±0.04	0.11 ±0.05	0.11 ±0.06
Treated QUADS	0.03 ±0.04	0.04 ±0.04	0.05 ±0.04	0.07 ±0.04	0.06 ±0.04	0.07 ±0.04	0.08 ±0.05

Table 9. Comparing dynamic R1 change in treated and untreated mdx groups at post-treatment scan. No significant differences were demonstrated between the untreated and treated mdx groups in terms of absolute R1 change value values at 60 or 70 minutes.

*p value <0.05 compared to untreated contemporaneous mdx group.

Key: TA, Tibialis anterior, GCN, Gastrocnemius, HMS, Hamstrings, QUADS, Quadriceps.
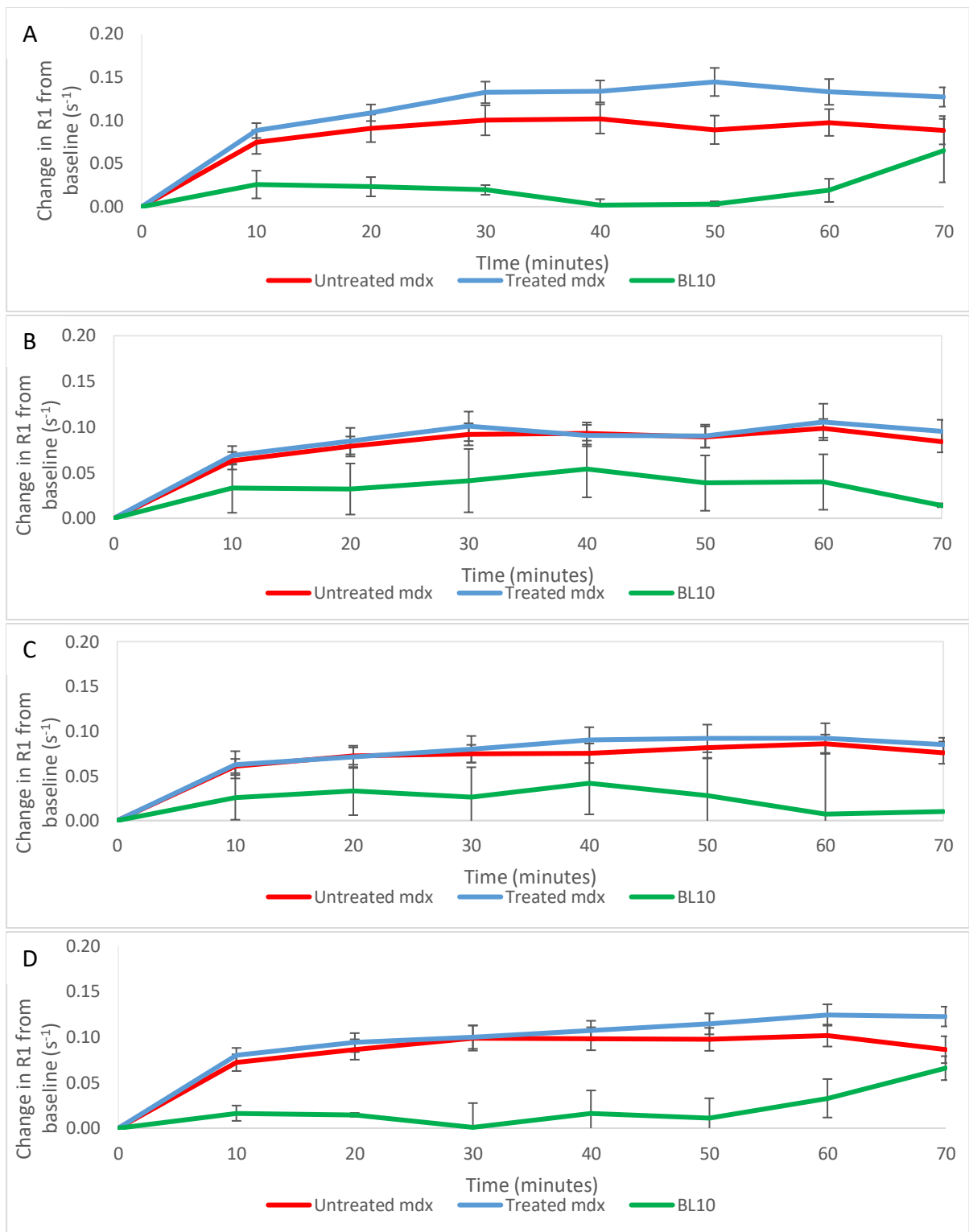
Figure 23. Dynamic R1 change over the period of the pre-treatment acquisition, each graph represents a different muscle: (A) Tibialis anterior (TA), (B) Gastrocnemius (GCN), (C) Hamstrings (HMS), (D) Quadriceps muscles (QUADS). Lines represent mean values of R1 change. Error bars display standard error for the groups at baseline. Untreated mdx (n=13), treated mdx (n=8), BL10 (n=3). One image was not analysable in the BL10 group at 70 minutes, at this time therefore n=2. These graphs demonstrate the variability of R1 change from baseline in individual muscles. There was minimal difference between the two mdx groups over the period of scanning suggesting that at baseline scan there were no significant differences prior to treatment. It is possible to detect a difference between BL10 and mdx mice at this age although this is only significant at certain time points and is variable.
Key: red, untreated mdx, blue, treated mdx, green, BL10.
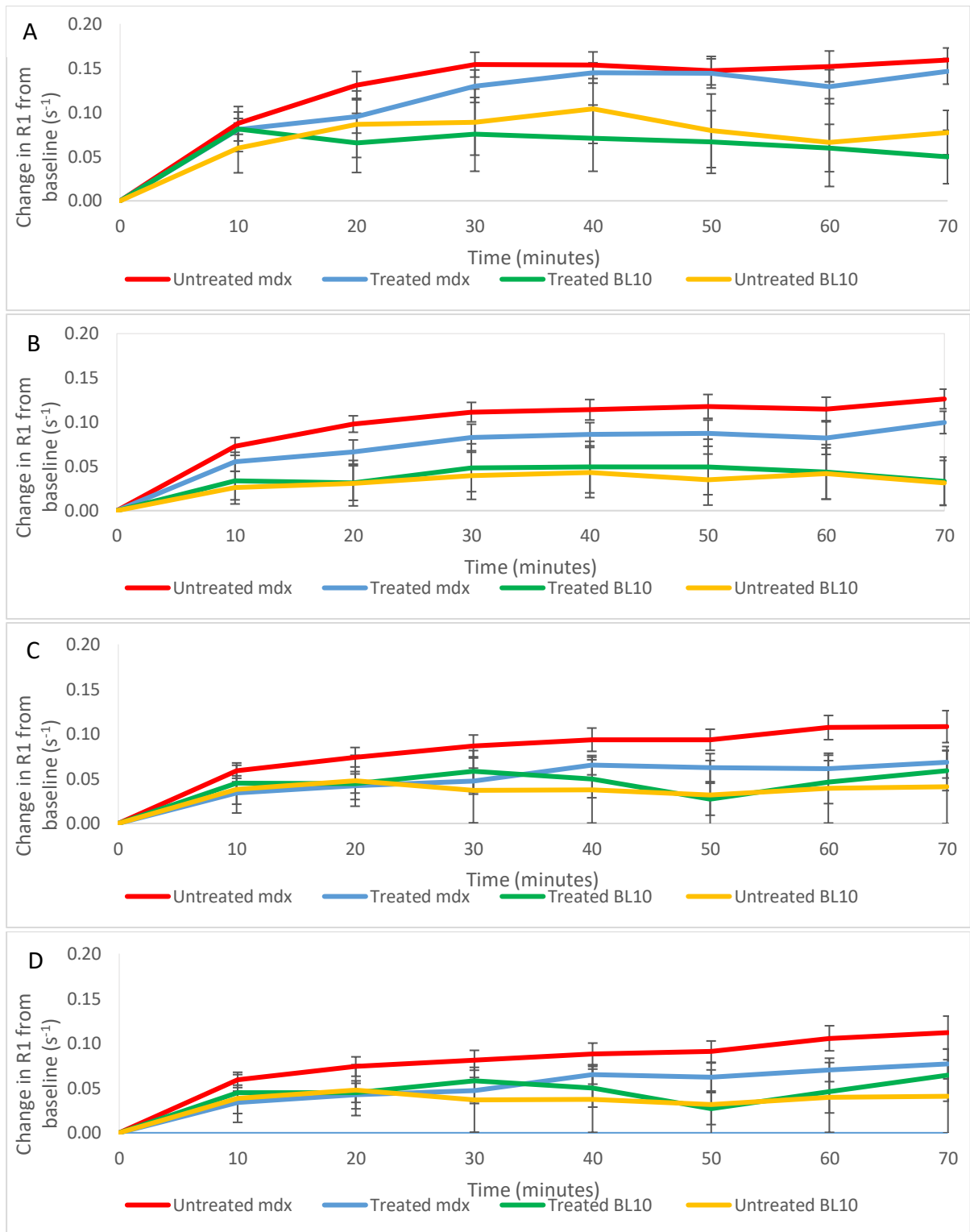
Figure 24. Dynamic R1 change over the period of the post-treatment acquisition, each graph represents a different muscle: (A) Tibialis anterior (TA), (B) Gastrocnemius (GCN), (C) Hamstrings (HMS), (D) Quadriceps muscles (QUADS). Lines represent mean values of R1 change. Error bars display standard error for the groups at follow up. Untreated mdx (n=13), treated mdx (n=8), Treated BL10 (n=3), Untreated BL10 (n=5). The proximal slices in one of the treated mdx was not analysed in the due to an artefact therefore QUADS and HMS are based upon one fewer subject (n=12). There were no significant differences in R1 change at 70 minutes comparing the two mdx groups. There were significant differences between the BL10 groups and the mdx groups in three out of four muscles.
Key: red, untreated mdx, blue, treated mdx, green, BL10.

4.2.3.5 Comparison of R1 values at 70 minutes between pre-treatment and post-treatment scans

Comparison of the R1 change from pre-treatment to post-treatment scan at 70 minutes, in the three groups with paired longitudinal data, (*mdx* treated, *mdx* untreated, and BL10 groups) demonstrated significant increases in R1 values at 70 minutes in the untreated *mdx* group (GCN p=0.04, HMS p=0.009, and TA p=0.01). The QUADS in this group did not demonstrate a significant change (p=0.20). There were no significant differences comparing pre-treatment to post-treatment scan values for any of the muscles in either of the other two groups (Table 10).

Comparing R1 values of treated *mdx* and BL10 groups together demonstrated significantly higher values in the former group at post-treatment in the TA p=0.006, and the GCN p=0.009.

It is possible to calculate the SRM value for the different muscles at 70 minutes; the TA had the highest SRM (0.56), then GCN (0.48), with the QUADS and HMS demonstrating the lowest SRM value (both 0.36).

Group	Muscle	Mean R1 change at 70 minutes pre-treatment (s^{-1})	R1 change at 70 minutes post-treatment (s^{-1})	P value
Untreated *mdx* (n=13)	TA	0.09 ±0.06	0.16 ±0.05	0.01*
	GCN	0.08 ±0.04	0.13 ±0.04	0.04*
	HMS	0.08 ±0.05	0.13 ±0.04	0.009*
	QUADS	0.08 ±0.04	0.11 ±0.07	0.20
Treated *mdx* (n=8)	TA	0.13 ±0.03	0.15 ±0.04	0.33
	GCN	0.10 ±0.04	0.10 ±0.04	0.79
	HMS†	0.12 ±0.04	0.10 ±0.05	0.23
	QUADS†	0.08 ±0.02	0.08 ±0.05	0.70
BL10 treated (n=3)	TA	0.07 ±0.06	0.05 ±0.05	0.88
	GCN	0.01 ±0.00	0.03 ±0.05	0.69
	HMS	0.07 ±0.02	0.07 ±0.02	0.50
	QUADS	0.10 ±0.00	0.07 ±0.05	0.36
BL10 untreated (n=5)	TA˜	N/A	0.08 ±0.05	N/A
	GCN	N/A	0.03 ±0.04	N/A
	HMS	N/A	0.05 ±0.06	N/A
	QUADS	N/A	0.04 ±0.07	N/A

Table 10. Comparison of R1 changes at 70 minutes at pre-treatment and post-treatment. In the untreated mdx group the tibialis anterior (TA), gastrocnemius (GCN) and hamstrings (HMS) all demonstrated a significant difference from pre-treatment to post-treatment scan. This was not evident in the treated mdx group.
*p value<0.05 compared to pre-treatment R1 change
†Linear artefact through proximal slices in two mice, HMS and quads not analysed (n=6).
˜One image removed due to image artefact at 70 minutes (n=4)
Key: TA, Tibialis anterior, GCN, Gastrocnemius, HMS, Hamstrings, QUADS, Quadriceps, N/A, not applicable.

4.2.3.6 *Ex vivo* measures of fibrosis

Histological analysis demonstrated the diffuse nature of the fibrotic changes in *mdx* mouse muscle and comparative differences between groups (Figures 25 and 26). All treated *mdx* muscles demonstrated significantly lower mean levels of fibrosis compared to untreated, using hydroxyproline assay (Figure Figure 27). Comparing treated to untreated *mdx,* MT quantification was significantly lower in three of the four muscles, except for the QUADS (p=0.06) (Figure 27). These results suggest that the levels of fibrosis were lower in the majority of muscles in treated *mdx* groups.

BL10 muscles had significantly lower levels of fibrosis compared to untreated *mdx* using both methods of quantification. Hydroxyproline quantification suggested that only the HMS had significantly lower levels of fibrosis in BL10 compared to treated *mdx* (p=0.01). In contrast, MT quantification suggested that the treated *mdx* group had significantly higher levels of fibrosis in the GCN (p=0.001), QUADS (p=0.001), and the TA (p=0.003) (Figure 27).

Pearson correlation between hydroxyproline and MT quantification was significant (r=0.57, p<0.001). suggesting a significant correlation between the two methods of *ex vivo* quantification.

4.2.3.7 Correlation of EP3533 to *ex vivo* measures of fibrosis

R1 change at 70 minutes in all muscles at post-treatment scan correlated significantly with Masson's trichrome (Table 11). R1 change at post-treatment correlated in three out of four muscles with hydroxyproline. The strongest correlations to *ex vivo* measures of fibrosis were in the GCN muscle (Table 11).

Method of quantification	Change in R1 TA	Change in R1 GCN	Change in R1 HMS	Change in R1 QUADS
Masson's trichrome	0.84**	0.80**	0.59*	0.59*
Hydroxyproline assay	0.58*	0.59*	0.41*	0.24

Table 11. Table to show Pearson correlation R values between R1 change at post-treatment scan and *ex vivo* measures of fibrosis.
* - P value is less than 0.05, ** - P value <0.001.
Key: TA, Tibialis anterior, GCN, Gastrocnemius, HMS, Hamstrings, QUADS, Quadriceps.
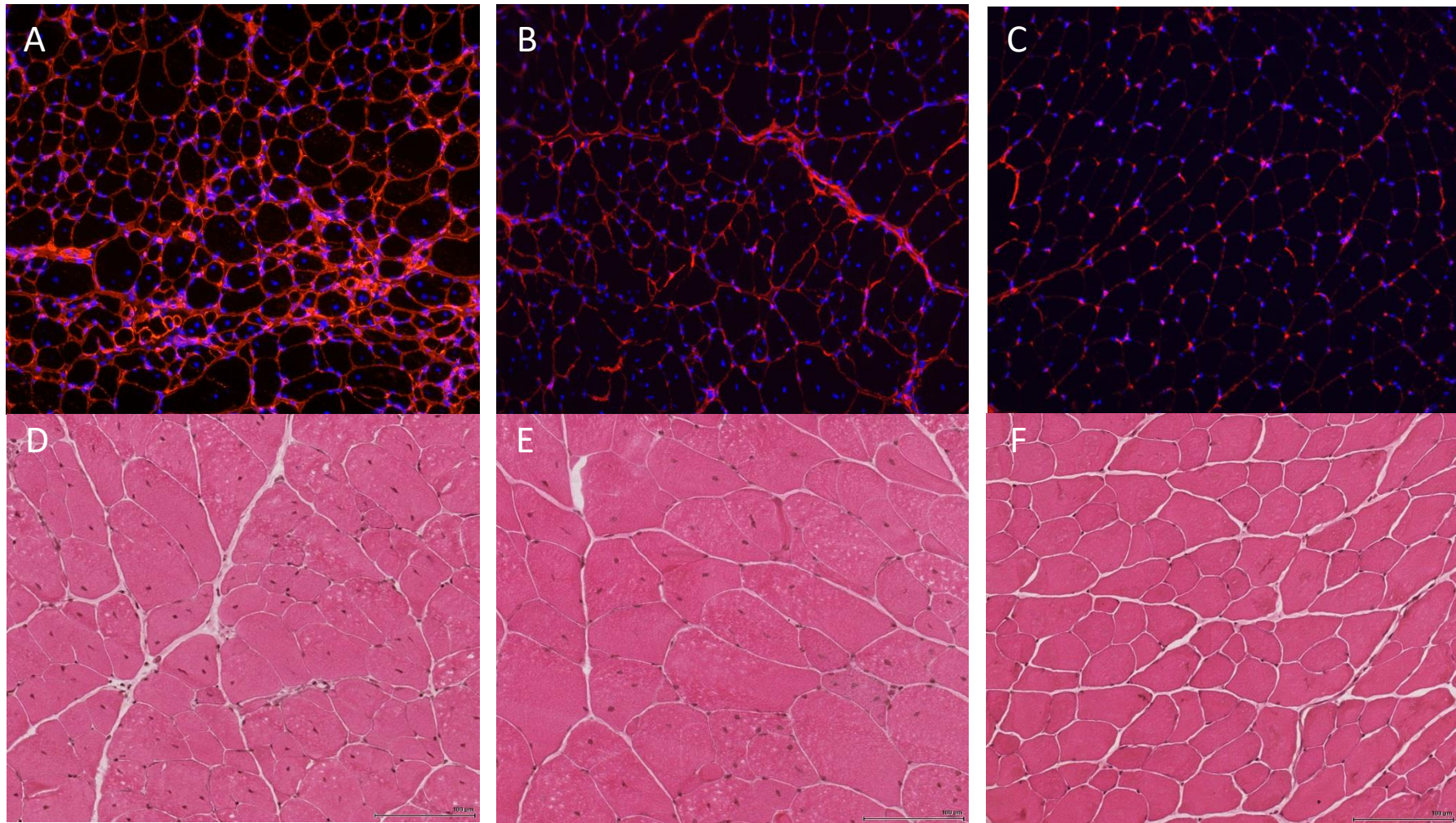
Figure 25. Examples of transverse sections from gastrocnemius (GCN) muscles. Top row: collagen 1 immunofluorescent staining with DAPI, areas of red are areas with collagen 1, nuclei are highlighted as blue using DAPI. Magnification x10. A) *mdx* **untreated with large highlighted collagen-rich regions. B) Treated** *mdx* **mice demonstrating focal areas of fibrosis and areas of endomysial collagen 1. C) BL10 group limited fibrosis evident, nuclei are peripherally located. Bottom row - H&E Staining. D)** *mdx* **untreated areas of fibrosis in white with varying myocyte size and centrally located nuclei. E) Treated** *mdx* **– fewer areas of fibrosis, though with similar variation in myocyte size and centrally located nuclei. F) BL10 group with regularly sized myocytes and peripheral nuclei.**
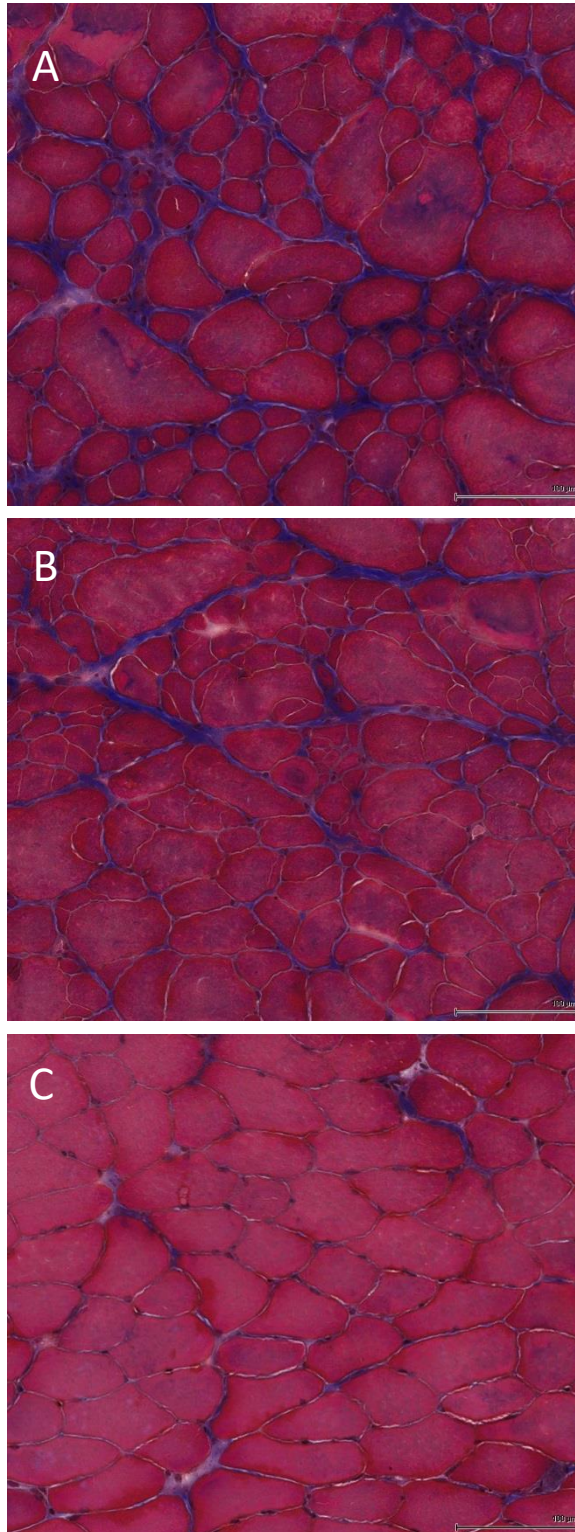
Figure 26. Masson's trichrome (MT) staining *x*20 magnification – fibrosis is dark blue. A) *mdx* treated shows diffuse fibrosis in the extracellular space throughout. B) treated *mdx* fewer areas of blue staining. C) BL10 group demonstrating small amounts of blue staining.
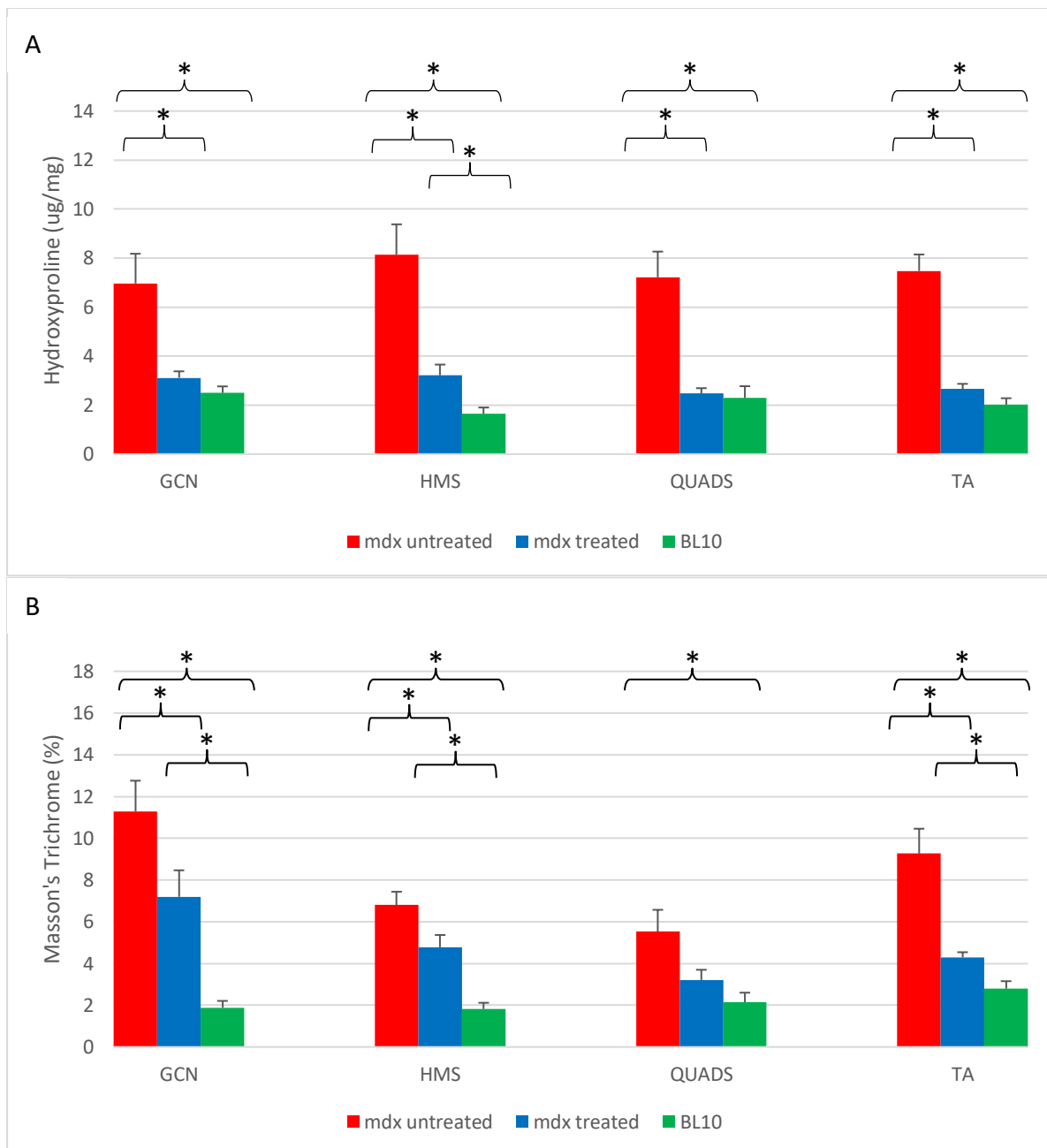
Figure 27. Bar charts to show the differences in *ex vivo* quantification of fibrosis within muscle between treated *mdx*, untreated *mdx* and BL10 groups. A) hydroxyproline quantification, B) MT quantification. Significant differences are seen between the all muscles of the untreated mdx mice and the BL10 group using bother measures of fibrosis. Using Masson's trichrome (MT) quantification, all muscles were significantly lower in the treated *mdx* group compared to the untreated. Hydroxyproline quantification identified 3/4 of these muscles as significantly lower in the treated *mdx* group. Error bars represent standard error.
* p value <0.05
Key: GCN, Gastrocnemius, HMS, Hamstrings, QUADS, Quadriceps, TA, Tibialis anterior.

4.2.3.8 Correlation of EP3533 to functional assessment

None of the two or four limb force assessments significantly correlated to the change in R1 values at follow up, in either the individual muscles or all muscles grouped together (p=NS). Considering all muscles together, the change in R1 values from baseline to follow up scan correlated significantly, albeit weakly, to two limb assessment (two r=-0.33 p=0.004, four r=-0.32 p=0.06) (Figure 28). The correlation here may suggest there is an association between R1 change at post treatment and muscle function, the lack of a strong correlation may be due to the other compounding factors that influence muscle function.
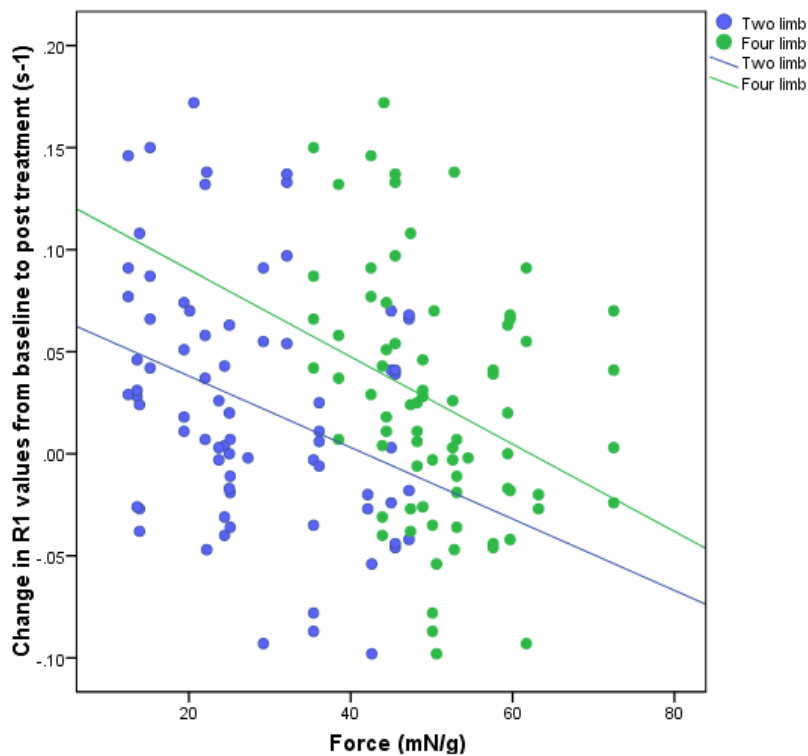
Figure 28. Scatter graph of the relationship of force assessment using two and four limbs to the change in R1 value from pre-treatment to post treatment. Demonstrating the weak correlation between the two types of assessment and change in R1.

Chapter 5: Results of quantitative MRI in the assessment of long term changes in skeletal muscle in limb girdle muscular dystrophy type R9

5.1 Summary

The LGMD are a group of heterogeneous neuromuscular diseases, LGMDR9 is a subtype with a slowly progressive and variable phenotype. Few natural history studies have investigated this cohort. With the development of several promising putative therapies, there is a real need to develop and validate outcome measures for clinical trials. A previous study performed by Willis *et al.* in 2010 followed up a group of 34 participants over a twelve month period (Willis et al., 2013). They compared MRI measures (i.e. Dixon technique FF calculation) to standardised functional assessments (i.e. 6MWT, timed up and go). Willis *et al.* found that quantitative MRI using FF calculation was able to detect a significant change in 9 of the 14 muscle groups studied. Both semi-quantitative MRI grading of conventional T1-weighted imaging using the Mercuri scale and functional muscle assessments were unable to demonstrate significant changes over the same period (Willis et al., 2013).

For this study, participants were recruited six years after their participation in the original study to undergo calculation of the FF of upper and lower leg skeletal muscles and standardised functional assessments. The aim was to compare these outcome measures and investigate whether they were able to detect a significant change over this time period.

Participants were recruited from the four original sites, in Newcastle upon Tyne, Paris, Copenhagen and London. A three point Dixon acquisition was used to calculate the FF in fourteen muscle groups of the upper and lower legs for each subject. Participants underwent the following standardised functional assessments: myometry of the lower limbs (knee extension and flexion, hip adduction and abduction), timed tests (timed up and go, 6MWT, and 10MWR, chair rise, stair ascend and descend), and spirometry testing.

A total of 23/34 participants from the original study were available and recruited into the six year follow-up study. All fourteen muscles and selected composite groups demonstrated a significant increase in fat content over the six year period. Of the timed tests all functional assessments and FVC demonstrated a significant decline over six years. Of all the myometry measurements only hip adduction significantly declined over the period of follow up. Significant correlations were seen in 18/20 muscles at six years with the 6MWT test and the 10MWR.

The results of this study suggests that FF measurement using the Dixon technique is sensitive to changes over a six year period in all skeletal muscles. Use of the Dixon technique has several advantages over standardised functional assessments and can provide useful interim measures of disease progression which is not currently possible with functional assessment. The results of this study support FF calculation in LGMDR9 clinical trials as a primary outcome measure alongside functional assessments. The results suggest the most appropriate target muscles for analysis are the VL, Gr, Sar, and the MG and LG. The 10MWR, 6MWT and spirometry are the selected as the most appropriate functional measures that could be used as outcome measures in a therapeutic trial over a six year period.

5.2 Results

5.2.1 Recruitment

Of the 38 participants in the baseline study, 23 participated in the six year follow up reassessment; the recruitment rate was overall therefore 60.5% across the four sites. The following reasons were given for not taking part in the six year follow up: subject was deceased (n=1), contraindication to MRI (implantable cardioverter defibrillator (ICD)) (n=2), undergoing treatment for a comorbidity (n=2), uncontactable (n=2) or declined to participate for various personal reasons (such as difficulties in travel) (n=8). Recruitment in all four sites took place from June 2015 to February 2017. All 23 participants completed both the skeletal muscle MRI and the functional assessments. Fourteen muscle groups were assessed, 9 in the proximal leg and 5 in the distal leg. Identification of the borders of the muscle groups was more difficult in those with higher percentages of fat replacement.

At baseline assessment the median age of the participants (n=23) was 39.1 years (interquartile range (IQR) 27.4-50.6). Median length of follow-up was 6.1 years (IQR 5.8 to 6.1). In the original study by Willis *et al.*, participants were required to be ambulant with an ability to walk over 50m (Willis et al., 2013, Willis et al., 2014): by six years, six participants were non-ambulant. At baseline, no participants received NIV, by six years five participants required NIV overnight. Seven participants received cardio-active medication at baseline and this had increased to thirteen six years later.

5.2.2 Inter-observer consistency

Inter-observer consistency of ROI analysis was assessed using the Bland-Altman analysis (Figure 29). The observers reported a mean difference in FF of 0.05%. The muscle with the widest 95% LOA between observers was the BFSH at 10.46% (Table 12). ROI analysis of this muscle was difficult because of the small size and irregular shape.
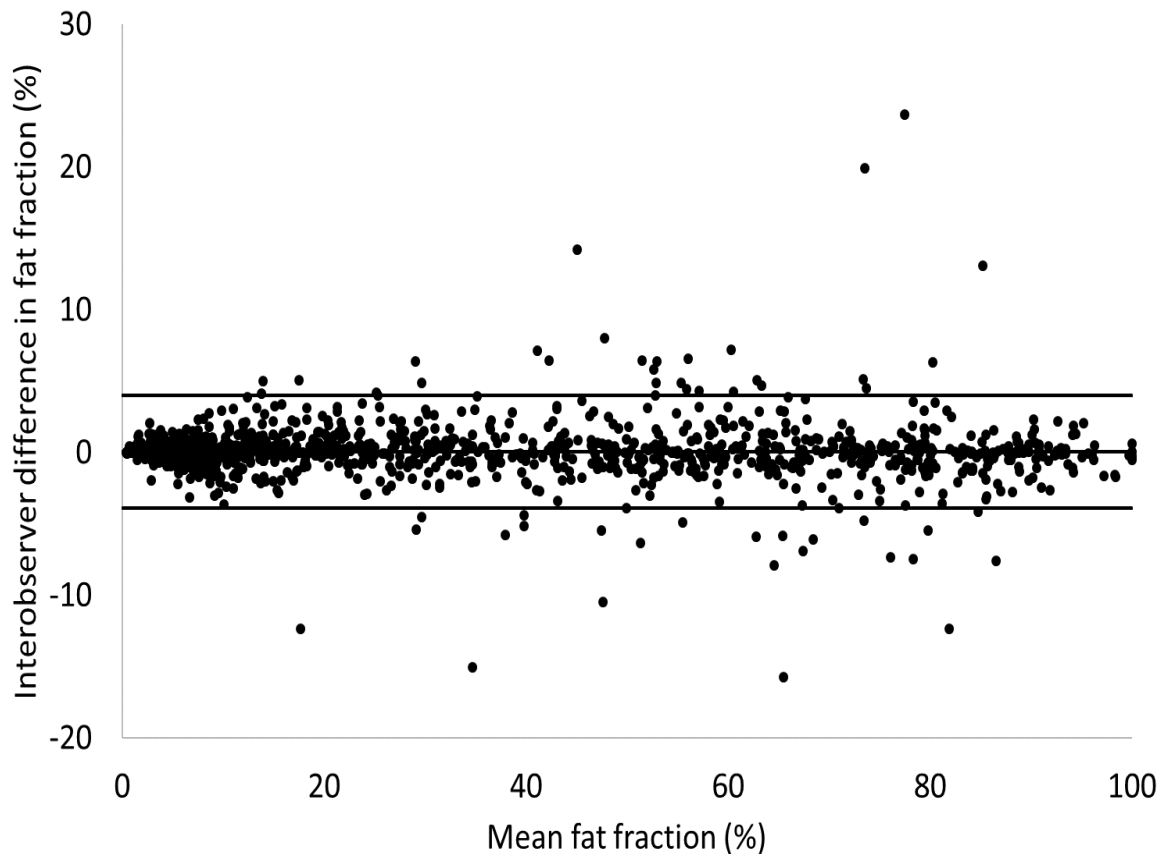
Figure 29. A Bland-Altman plot to show the mean inter-observer differences in ROI analysis between two observers. This includes all measurements of all participants' muscles in both left and right legs. Horizontal lines from top to bottom denote +1.96 standard deviation, the mean difference, and -1.96 standard deviation. 95% limits of agreement (LOA) were -3.92 and 4.02. Eight of the furthest outliers were from inter-observer differences in values for the rectus femoris (RF) in two of the participants. This was due to the difficulties in identifying the borders due to large amounts of peripheral fat in the muscle.

Muscle	Bias (%)	95% Limit of Agreement (%)
Biceps femoris short head	0.11	10.46
Gracilis	-0.03	4.44
Rectus femoris	0.28	3.75
Vastus medialis	0.45	3.37
Sartorius	0.09	3.23
Semitendinosus	0.34	3.21
Lateral gastrocnemius	-0.18	3.11
Medial gastrocnemius	-0.53	3.07
Semimembranosus	0.09	3.04
Vastus lateralis	0.14	2.28
Biceps femoris long head	0.05	2.25
Peroneus longus	0.04	1.83
Tibialis anterior	-0.84	1.24
Soleus	-0.03	1.12

Table 12. Comparing inter observer differences between muscles in terms of bias and 95% limits of agreement (LOA) for fat fraction (FF) between observers in individual muscles. Data presented as bias (mean difference) and LOA (1.96 times the standard deviation of the differences between observers). The widest LOA were between different observers regarding the BFSH, which was difficult to identify due to the shape of the muscle. The gracilis (Gr) and rectus femoris (RF) muscles had the next widest LOA at 4.44 and 3.75 respectively.

5.2.3 Functional assessments

All of the timed assessments of patients demonstrated a significant change over six years (Table 13). Of the myometry assessments, only measurement of the hip adduction decreased significantly over the period of follow up (median baseline 6.1kg, median six years 4.2kg, p=0.02). FVC measured in both positions significantly declined over six years (Table 13).

Functional assessment	Median baseline (range)	Median six years (range)	P value	SRM
Forced vital capacity sitting (%)†	77 (55-94)	64 (31-86)	0.001*	-1.29
Forced vital capacity lying (%)$	70 (36-90)	54 (21-84)	0.002*	-1.06
Hip flexion (kg)	7.7 (0-36.8)	6.4 (0-24.3)	0.13	-0.35
Hip adduction (kg)	6.1 (0.7-26.7)	4.2 (0-23.9)	0.02*	-0.59
Hip abduction (kg)	8.3 (0.6-25.0)	7.2 (2.2-25.3)	0.76	-0.01
Knee extension (kg)	11.1 (2.0-40.3)	12.0 (1.5-39.1)	0.15	-0.26
Knee flexion (kg)	8.4 (0.9-30.0)	4.8 (0-37.9)	0.21	-0.12
Ankle dorsiflexion (kg)	14.7 (2.5-38.6)	13.9 (2.4-26.3)	0.07	-0.42
Six-minute walk (meters)	391 (67-625)	286 (0-750)	0.001*	-0.85
Timed up and go velocity (ms^{-1})‡	0.5 (0-1.7)	0.3 (0-1.6)	0.007*	-0.48
Ten-meter walk or run velocity (ms^{-1})‡	1.2 (0.5-4.4)	0.8 (0-3.9)	<0.001*	-1.02
Stair ascent velocity (steps/s^{-1})‡	0.7 (0-4.4)	0.4 (0-3.0)	0.001*	-0.46
Stair descent velocity (steps/s^{-1})‡	1.2 (0-4.4)	0.4 (0-3.3)	0.008*	-0.47
Chair rise (s)~ ‡	2.6 (0.3 to ∞)	9.8 (0.5 to ∞)	0.001*	N/A

Table 13. The median change in functional assessments over the follow up of six years (n=23). The only myometry measurement that was significantly reduced over the follow up period was hip adduction. Both measures of FVC, all timed tests significantly changed over the follow up period.
P values calculated using Wilcoxon non-parametric rank signed test. * P value <0.05. SRM – standardised response mean.
† Paired values available in 17 participants
~ Participants unable to perform the chair rise were given a value of 10,000 (effectively infinity) for the purposes of the Wilcoxon non-parametric rank signed test.
$ Paired values available in 16 participants
‡ Paired values available in 22 participants

Several of the functional tests (timed up and go, 10MWR, stair ascend and stair descend, 6MWT test) require ambulation for the test to take place. Ability for the participants to complete timed assessments is measured in duration to complete the test. Participants are also assigned a grade depending on their use of compensatory mechanisms. The grading is from '1 - unable', to '6 - with no support or normal function'. While the grading scale is not weighted to allow direct statistical comparisons, it does take account of compensatory mechanisms that may be employed by a participant to maintain their speed in the face of increased weakness. The participants at six years showed a significant reduction in all timed assessment grades except for the stair ascend (p=0.06) (Table 14).

Test	Number increased grade	Number decreased grade	Unchanged grade	P value~
Ten metre walk or run (%)	2 (8.7)	14 (60.9)	7 (30.4)	0.006*
Chair rise (%)	0 (0)	14 (60.9)	9 (39.1)	0.001*
Stair ascend (%)	5 (21.7)	11 (47.8)	7 (30.4)	0.06
Stair descend (%)	4 (17.4)	9 (39.1)	10 (43.5)	0.01*

Table 14. To show the change in grading of the timed tests over six years: Ten metre walk or run (10MWR), chair rise, stair ascend and stair descend. The majority of participants decreased their grade suggesting that more participants were using compensatory mechanisms or were unable than at baseline.
*p value <0.05.
~ Calculated using Wilcoxon non-parametric signed test.

The 6MWT demonstrated a significant reduction in distance from median baseline of 391 metres (67 to 625) to 286 metres (0 to 750) at six years (p=0.001) (Table 13). Four participants improved from their first assessment at baseline by a mean increase of 68.8 metres ±50.3 at six years (Figure 30). These four subjects were from different sites and showed a FF increase of at least 1% in the majority of the 20 muscle groups and composite groups studied (15/20 groups for 1 patient, 19/20 groups for 2 patients and all groups for 1 patient). No significant differences between those that improved were seen in terms of age (improved 37.7 years (24.1 to 68.9) versus declined 47.5 years (14.1 to 70.5), p=0.49). Median fat content was lower in all muscles at baseline and six year follow up in the participants that improved on the 6MWT, however this didn't reach significance and there was significant overlap. There were no significant differences in the rate of fatty transformation in this group as detected by MRI over the six years.
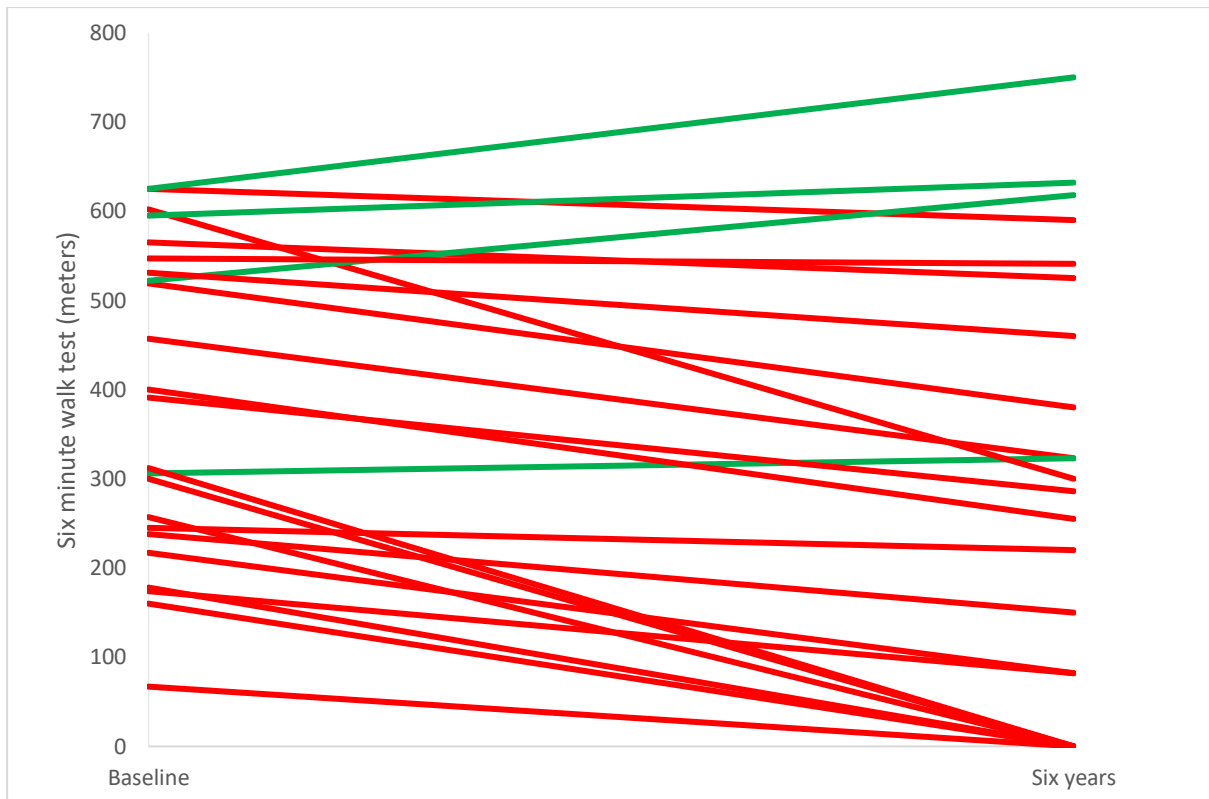
Figure 30. The line chart shows the individual participant scores on the six minute walk test (6MWT). As demonstrated here, four participants improved over the four years. No obvious cut off for loss of ambulation is noted, although half of those walking under 300m at baseline were non ambulant at six years. Red lines – participants that declined from baseline to year six. Green lines – participants that improved from baseline to year six.

Data from the baseline NSAA was available only from Newcastle site participants (n=10). Participants had a significantly higher mean total score of 20 ± 11 at baseline and 10 ± 11 at six year follow up (p=0.04). Individual loss of NSAA score is shown in Figure 31.
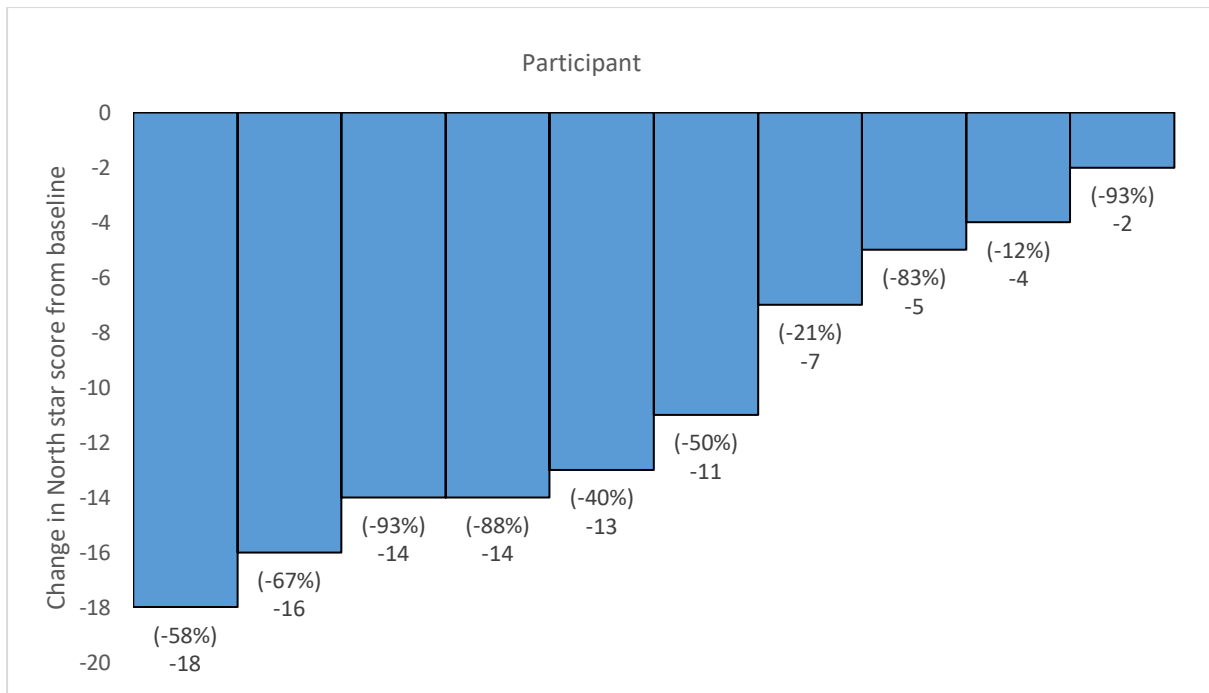
Figure 31. Waterfall plot of loss in North star ambulatory assessment (NSAA) scores. All participants had decline in score over six years, a greater number of points were available to lose in those who were more functional at baseline. Each blue bar is an individual assessed over the six year follow up period, values are obtained by taking the total score at baseline from the total score at follow up. Numbers in brackets are the percentage of loss of points from baseline.

5.2.4 Quantitative Dixon fat fraction

Over the six years, all 14 muscle groups demonstrated a significant increase in percentage of fat replacement (Table 15 and Figure 32). The highest median percentage of fat replacement at baseline was in the BFLH at 69.4%, increasing to 78.6% at six years. The TA muscle was least affected at baseline, median 5.2% and at follow-up, median 7.1%. The TA also had the smallest median change over the six year period (Table 15). The inter-observer variability in FF demonstrated in the BFLH, ST and SM muscles may be caused by high levels of fat replacement at follow-up, making recognition of ROI borders difficult. The BFSH had the widest LOA of any of the muscles (Table 12), this is likely due to the small size of the muscle in the transverse plane. The RF muscle had one of the next widest LOA and had difficult to define borders when replaced by fat (Figure 33). The values of the RF muscle from two participants were excluded from analysis due to the high levels of discrepancy between observers in ROI placement.

Following analysis of the FF results, a post-hoc group of potential 'target muscles' for use in future clinical trials was identified. These muscles demonstrate significant change at one year (Sol was excluded as the change was not significant over this time period (Willis et al., 2013)), allowing an interim analysis, and demonstrate disease progression with the highest SRM. They are reported as an

additional composite group using area-weighted FF averaging (Table 15). The averaged target muscle group consisted of the VL, Gr, Sar, MG and LG.

Muscle group	Median baseline (range), %	Median six years (range), %	P value	SRM
Rectus femoris†	10.8 (0.9-81.9)	19.9 (0.4-92.2)	<0.001*	0.90
Vastus medialis	21.0 (1.1-86.6)	44.4 (2.5-87.9)	<0.001*	0.83
Vastus lateralis	13.7 (1.5-65.2)	36.1 (2.8-81.7)	<0.001*	0.92
Sartorius	20.9 (1.7-89.8)	34.2 (5.4-88.3)	<0.001*	0.98
Gracilis	18.4 (3.7-81.0)	32.4 (4.5-90.2)	<0.001*	1.04
Biceps femoris long head	69.4 (2.2-97.7)	78.6 (4.8-100)	0.001*	0.81
Biceps femoris short head	21.3 (3.2-94.5)	32.5 (4.6-84.3)	0.002*	0.53
Semitendinosus	35.6 (2.1-100)	69.6 (4.1-100)	<0.001*	0.83
Semimembranosus	25.7 (0.5-95.1)	53.4 (4.6-99.2)	<0.001*	0.90
Tibialis anterior	5.2 (0.9-25.3)	7.1 (1.1-27.1)	0.002*	0.67
Peroneus longus	15.8 (3.0-46.2)	18.0 (4.6-65.2)	0.001*	0.88
Soleus	7.5 (1.8-67.4)	16.7 (3.1-70.1)	<0.001*	1.17
Lateral gastrocnemius	19.4 (0.9-76.1)	35.8 (3.1-75.2)	<0.001*	0.91
Medial gastrocnemius	19.9 (1.1-91.8)	48.0 (2.8-84.2)	<0.001*	0.95
Averaged thigh†	30.8 (2.1-76.2)	47.3 (4.2-82.1)	<0.001*	1.20
Averaged lower leg	15.4 (1.6-56.1)	26.8 (3.4-55.5)	<0.001*	1.28
Averaged quadriceps†	23.0 (1.3-67.6)	40.4 (2.6-79.8)	<0.001*	1.05
Averaged hamstrings	45.0 (2.8-97.8)	60.4 (4.7-98.7)	<0.001*	0.93
Averaged triceps surae	16.7 (1.4-74.2)	30.3 (3.3-72.6)	<0.001*	1.25
Averaged target muscles	21.5 (1.8-70.8)	43.8 (3.6-76.9)	<0.001*	1.23

Table 15. Median muscle fat fractions (FF) at baseline and six-year follow up. All muscles and composite muscle measures of FF were significantly increased over the six years. The measures with the strongest standardised response mean (SRM) were the averaged lower leg, triceps surae, and target muscles.
P values calculated using Wilcoxon non-parametric rank signed test.
* P value<0.05. SRM – standardised response mean.
† Due to difficulties in ROI placement in the rectus femoris (RF) muscle the FFs for two of the participants were excluded for this muscle group (n=21). As the RF measures are excluded from two participants it is not possible to create composite measures (thigh and quadriceps (QUADS)) involving this muscle for these participants. The thigh and QUADS measures are based on 21 participants.
Key: SRM, standardised response mean.
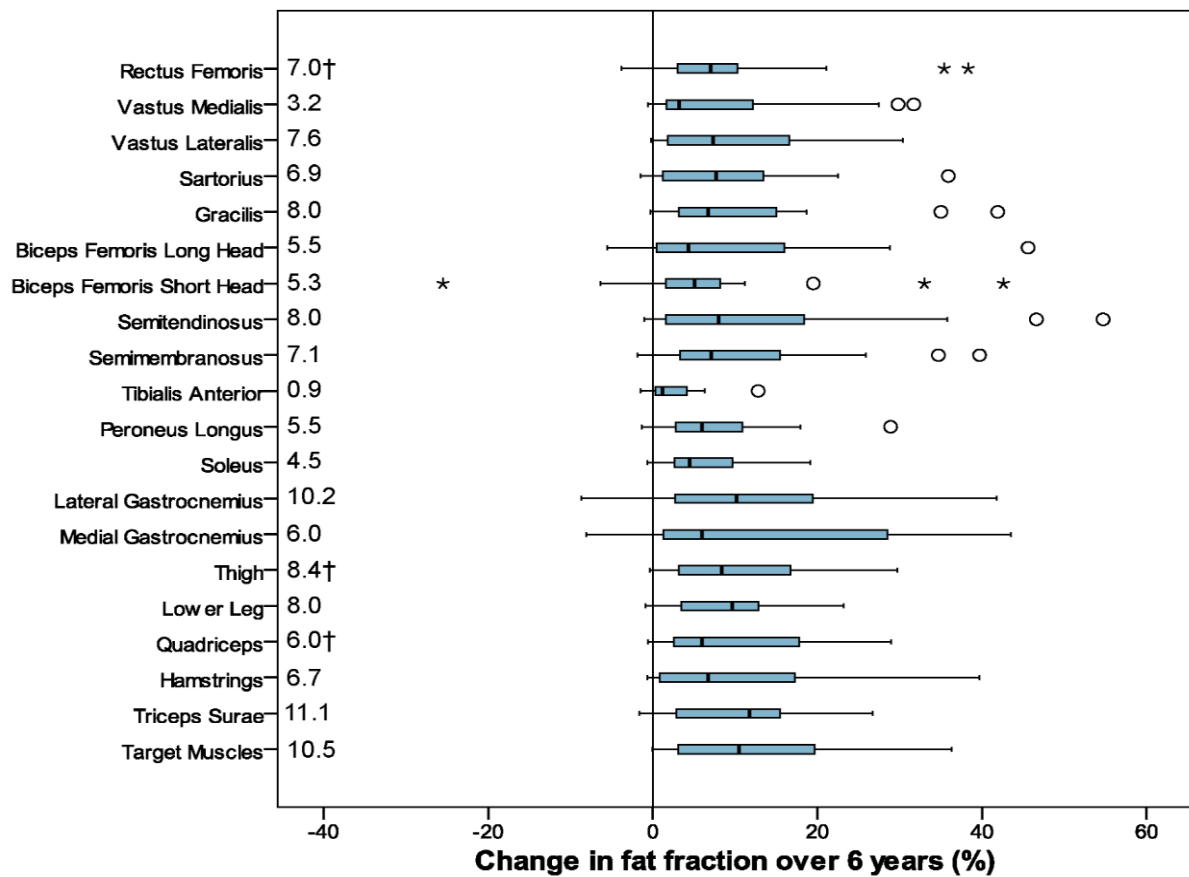
Figure 32. Box plot showing the change in fat percentage from baseline to six years. This demonstrates that the muscles with the largest median change were the triceps surae, target muscles and the lateral gastrocnemius (GCN). The blue bars show the interquartile range (IQR) and the median. The lines show the range of the data. Outliers that are one to three times the IQR are marked as circles. Outliers greater than three times the IQR from the median are shown as individual asterisks. The median change is shown for each muscle group on the left side.

†Due to difficulties in region of interest (ROI) placement in the rectus femoris (RF) muscle the fat fractions (FF) for two of the participants were excluded for this muscle group, and no composite results calculated where appropriate (n=21).

Baseline

Six years
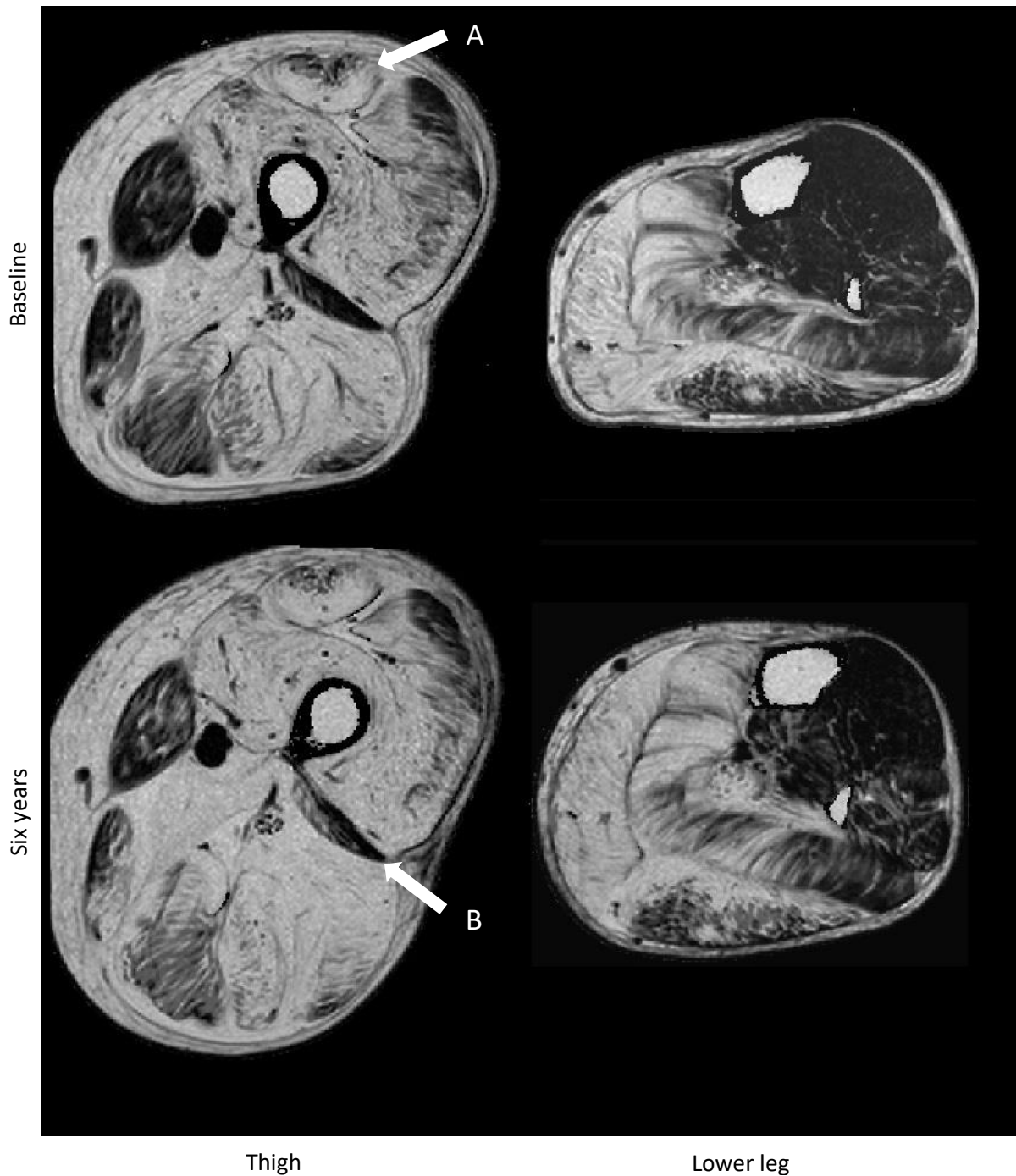
Thigh

Lower leg

Figure 33. Images showing the change in fat replacement over six years. Fat fraction (FF) maps acquired from the left thigh and lower leg at baseline and six-year follow up. Progression of fat replacement was visible in almost all muscles, with changes most noticeable in the muscles relatively spared at baseline, such as the sartorius (Sar) (in this participant FF increased from 21.3% to 34.2%) and the Gracilis (Gr) (increased from 40.3% to 58.7%) muscles. As indicated by the white arrow (A), fat replacement began at the borders of the rectus femoris (RF) muscle at both baseline and six years, which caused difficulties in ROI placement. In this participant, the FF was 78.9% at baseline increasing to 81.9% at six years. The shape and size of the biceps femoris short head (BFSH) muscle also caused difficulties in ROI placement as demonstrated by the white arrow (B).

5.2.5 Cross sectional area and contractile cross sectional area

The CSA and cCSA results are presented in Table 16Table . The CSA did not significantly decline in any of the muscles over the period of the study. The cCSA was significantly decreased in 8 of the 14 individual muscles and in all of the averaged muscle groupings (Table 16).

Muscle group	CSA baseline (mm^2)	CSA six years (mm^2)	c-CSA baseline (mm^2)	c-CSA six years (mm^2)	P value	c-CSA SRM
Rectus femoris†	343	344	260	232	0.009*	-0.51
Vastus medialis	720	932	428	389	0.11	-0.15
Vastus lateralis	1639	1517	1195	1025	0.003*	-0.62
Sartorius	402	425	346	231	0.06	-0.41
Gracilis	344	309	168	154	0.003*	-0.64
Biceps femoris long head	1012	911	316	145	0.02*	-0.49
Biceps femoris short head	153	157	110	81	0.63	-0.16
Semitendinosus	687	679	316	206	0.002*	-0.71
Semimembranosus	685	671	410	301	0.04*	-0.37
Tibialis anterior	568	569	536	537	0.67	-0.20
Peroneus longus	578	546	464	436	0.09	-0.29
Soleus	1803	1635	1512	1430	0.09	-0.35
Lateral gastrocnemius	553	523	435	317	0.04*	-0.39
Medial gastrocnemius	1243	993	879	516	0.02*	-0.53
Averaged thigh†	6024	6071	3288	3087	0.006*	-0.55
Averaged lower leg	4263	4264	3637	3365	0.01*	-0.52
Averaged quadriceps†	3078	3103	2017	1577	0.01*	-0.44
Averaged hamstrings	2322	2347	1101	842	0.007*	-0.63
Averaged triceps surae	3272	3113	2834	2469	0.009*	-0.53
Averaged targeted muscles	4211	3803	2745	2248	0.005*	-0.67

Table 16. Median cross-sectional area (CSA) and contractile cross sectional area (c-CSA) at baseline and at six year follow up. All p values quoted refer to c-CSA. There are no significant changes in CSA between baseline and six years. C-CSA are shown to be significantly different over the period of follow up in fewer of the muscles than fat fraction (FF) alone. The standardised response means (SRM) are highest in the semitendinosus, though not has high as using FF alone (Table 13). Key: SRM, Standardised response mean, CSA, cross sectional area, c-CSA, contractile cross sectional area.
*Denotes a p value <0.05.
† Due to difficulties in ROI placement in the rectus femoris (RF) muscle the FFs for two of the participants were excluded for this muscle group (n=21)

5.2.6 Correlation between MRI and functional assessments

The median increase in FF per year from this study and the 12-month Willis *et al.* study is given in Table 17 (Willis et al., 2013), together with a correlation between the FF change over 12 months and six years: correlation indicates where the short-term measurement may be predictive of long-term change. The 10MWR velocity and the 6MWT had several significant negative correlations with the FF of most muscle groups at baseline and six years. These were particularly strong in the composite muscle groups (such as the thigh, HMS and QUADS) (Tables 18 to 19). Changes in FF and the 10MWR velocity across six years correlated significantly only in the Sol muscle. Changes in FF and the 6MWT across six years correlated significantly in the Sol, rectus femoris (RF) and less strongly in some of the composite muscle groups: the thigh, QUADS, and triceps surae.

The analysis of individuals who had muscle groups with less than 20% fat replacement at baseline, and then progressed by less than 20% over six years, showed that there were 5 individuals for whom this was true for all 13 muscle groups and 1 further individual for whom this was true for 11/13 groups. This group of 6 subjects was significantly younger than the other 17 participants (median 23.5 years vs 43.0 years, p<0.001).

Muscle group	Annual median change in FF over six years (%) (n=23)	Annual median change in FF Willis *et al.* (%) (n=32)	Correlation of change in FF over one year compared to calculated rate of annual increase in FF over six years (n=20)
Lateral gastrocnemius	1.7	1.4	NS
Semitendinosus	1.3	1.6	0.51*
Gracilis	1.3	1.6	NS
Vastus lateralis	1.3	0.5	0.41*
Sartorius	1.2	1.2	NS
Semimembranosus	1.2	1.8	NS
Rectus femoris	1.1†	0.8	NS
Medial gastrocnemius	1.0	1.4	0.63*
Biceps femoris long head	0.9	1.9	NS
Biceps femoris short head	0.9	1.2	NS
Peroneus longus	0.9	0.1	0.45*
Soleus	0.8	0.3	0.50*
Vastus medialis	0.5	0.6	0.46*
Tibialis anterior	0.2	-0.1	NS

Table 17. Rate of annual median fat fraction (FF) increase derived from the six year data (i.e. total fat fraction increase over six years divided by number of years) compared to the 12 month data presented in Willis *et al* (Willis et al., 2013). The change in FF over one year and six years were correlated – Pearson coefficients for significant correlations are given. Significant correlation is only seen in the semitendinosus, vastus lateralis, peroneus longus, soleus (sol) and the vastus medialis. Annual median change is similar in the majority of muscle groups, but short term measurement may reduce the accuracy of detection of change (as seen in the biceps femoris long head or the lateral gastrocnemius (GCN))
* p value < 0.05,
† Due to difficulties in ROI placement in the rectus femoris (RF) muscle the FF for two of the participants were excluded for this muscle group (n=21).
Key: NS, not significant, FF, Fat fraction

Muscle group	Correlation between FF and 6MWT at baseline	Correlation between FF and 6MWT at six years	Correlation of increase in FF with change in 6MWT over six years
Lateral gastrocnemius	-0.60*	-0.59*	NS
Semitendinosus	-0.81**	-0.67**	NS
Gracilis	-0.68**	-0.74**	NS
Vastus lateralis	-0.79**	-0.73**	NS
Sartorius	-0.67**	-0.66**	NS
Semimembranosus	-0.86**	-0.75**	NS
Rectus femoris†	-0.70**	-0.80**	-0.53*
Medial gastrocnemius	-0.58*	-0.57*	NS
Biceps femoris long head	-0.69**	-0.63*	NS
Biceps femoris short head	-0.60*	-0.69**	NS
Peroneus longus	-0.45*	NS	NS
Soleus	-0.49*	-0.56*	-0.60*
Vastus medialis	-0.76**	-0.73**	NS
Tibialis anterior	-0.47*	NS	NS
Averaged thigh†	-0.88**	-0.91**	-0.47*
Averaged lower leg	-0.61*	-0.59*	NS
Averaged quadriceps†	-0.85**	-0.87**	-0.46*
Averaged hamstrings	-0.81**	-0.71**	NS
Averaged triceps surae	-0.56*	-0.58*	-0.45*
Averaged target muscles	-0.75**	-0.75**	NS

Table 18. The correlation between the fat fraction (FF) and 6MWT is shown: at baseline, at six years, and between the change in FF and change in 6MWT across the six years. Pearson coefficients for significant correlations are given. The most significant group correlations are found in the averaged thigh, hamstrings (HMS) and quadriceps (QUADS).
*p value < 0.05, **p value < 0.001
† Due to difficulties in ROI placement in the rectus femoris (RF) muscle the FF for two of the participants were excluded for this muscle group (n=21).
Key: NS, not significant, FF, Fat fraction, 6MWT, six minute walk test,

Muscle group	Correlation between FF and 10MWR velocity at baseline~	Correlation between FF and 10MWR velocity at six years	Correlation of increase in FF with change in 10MWR velocity over six years~
Lateral gastrocnemius	-0.62*	-0.64*	NS
Semitendinosus	-0.76**	-0.77**	NS
Gracilis	-0.63*	-0.74**	NS
Vastus lateralis	-0.70**	-0.71**	NS
Sartorius	-0.61*	-0.67**	NS
Semimembranosus	-0.76**	-0.77**	NS
Rectus femoris†	-0.63*	-0.75**	NS
Medial gastrocnemius	-0.59*	-0.65*	NS
Biceps femoris long head	-0.78**	-0.76**	NS
Biceps femoris short head	-0.61*	-0.74**	NS
Peroneus longus	NS	NS	NS
Soleus	-0.49*	-0.52*	-0.52*
Vastus medialis	-0.69**	-0.68**	NS
Tibialis anterior	NS	NS	NS
Averaged thigh†	-0.83**	-0.90**	NS
Averaged lower leg	-0.60*	-0.62*	NS
Averaged quadriceps†	-0.76**	-0.80**	NS
Averaged hamstrings	-0.80**	-0.80**	NS
Averaged triceps surae	-0.58*	-0.62*	NS
Averaged target muscles	-0.71**	-0.77**	NS

Table 19. The correlation between the fat fraction (FF) and ten meter walk or run (10MWR) is shown: at baseline, at six years and between the change in FF and change in 10MWR across the six years. Pearson coefficients for significant correlations are given. Similar to the 10MWR, the most significant group correlations are found in the averaged thigh, hamstrings (HMS) and quadriceps (QUADS).
*p value < 0.05, **p < 0.001.
† Due to difficulties in ROI placement in the rectus femoris (RF) muscle the FF for two of the participants were excluded for this muscle group (n=21).
~ Results of the 10MWR test not available for one participant at baseline (n=22).
Key: NS, not significant, FF, fat fraction, 10MWR, 10 metre walk or run test.

5.2.7 Subgroup analyses

Male participants (n=10) had a median age of 48.0 years (range 14.1 to 70.5), females (n=13) who participated had a similar median age, but a narrower range of ages (47.2 years range 24.1 to 65.2) (p=0.61). Weight was not significantly different between gender groups. The male cohort had a significantly higher median percentage of fat in the Sol and the VM (Table 20). Change in median percentage over the six year follow up period was similar between genders, with the exception of the LG (female 15.9% range 0.1 to 41.8, versus male 3.3% range -8.7 to 19.4, p=0.02) and TA (female 3.1% range -2.8 to 12.8, versus male 0.3% range -1.5 to 4.1, p=0.04). In these two muscles the female fat percentage rose at a significantly higher rate than the males, this was in spite of no significant differences in these muscles at baseline or follow up.

Muscle	Male baseline	Female baseline	P value	Male six years	Female six years	P value
Vastus medialis	68.4 (1.1-86.6)	20.7 (2.7-92.2)	0.01*	77.5 (4.3-70.8)	23.8 (4.3-70.8)	0.03*
Soleus	21.3 (1.8-67.4)	6.0 (3.3-19.4)	0.01*	27.5 (4.0-70.1)	8.6 (3.1-81.9)	0.01*

Table 20. Male and female cohorts fat content at baseline and six year follow up. In these two muscles more fat replacement was evident at baseline and six year follow up.
P values calculated using Wilcoxon non-parametric rank signed test.
*p value <0.05. Muscles not included within the table were not significantly different between genders.

No significant differences were demonstrated between genders using myometry at either baseline, or at six year follow up. The only timed assessment that was significantly different between genders was the 10MWR. The velocity was significantly smaller median in the male cohort (0.0ms^{-1} range 0.0 to 2.1, versus female 1.0ms^{-1} range 0.0 to 4.0, p=0.02).

Of the 6 participants that had become non-ambulant, all were male, with a median age of 58.5 years (27.9 to 70.5) compared to the ambulant group 44.7 years (14.1 to 65.2) (p=0.11). The non-ambulant cohort median weight was significantly higher at final follow up compared to ambulant participants (non-ambulant 93.3kg range 59.0 to 111.8, versus ambulant 69kg range 53.6 to 82.4, p=0.02).

In non-ambulant participants, FF was significantly higher in three muscle groups at baseline and at six years: these were the Sol, RF and VM (Table 21). The rate of increase in fat percentage was not statistically different in any of the muscles between the two groups over the six years.

Muscle	Ambulant (baseline)	Non-ambulant (baseline)	P value	Ambulant (six years)	Non-ambulant (six years)	P value
Rectus femoris	6.9 (0.9-81.9)	43.4 (21.4-78.9)	0.03*	13.7 (0.4-92.2)	64.3 (4.4-81.9)	0.03*
Vastus medialis	18.7 (1.1-86.6)	74.3 (10.6-79.2)	0.001*	23.8 (2.5-87.9)	79.8 (19.7-84.1)	0.005*
Soleus	6.1 (1.8-67.4)	30.3 (7.0-43.1)	0.03*	8.6 (3.1-70.1)	41.1 (21.4-78.9)	0.008*

Table 211. Muscles that demonstrated a significant difference between ambulant and non-ambulant at baseline and 6 year follow up. Participants that were non-ambulant at follow up had significantly higher fat content at baseline and 6 year follow up in the rectus femoris (RF), vastus medialis and the soleus (sol).

P values calculated using Wilcoxon non-parametric rank signed test.

*p value <0.05. Muscles not included within the table were not significantly different between ambulant and non-ambulant groups.

No significant differences were demonstrated between the non-ambulant and ambulant cohorts in any of the muscle groups using myometry.

Age significantly correlated to the percentage FF in four muscles. The muscles included: BFLH (r=0.57, p=0.005), BFSH (r=0.65, p=0.001), the ST (r=0.62, p=0.002), SM (r=0.54, p=0.008). The only functional test that inversely correlated weakly to age was the 6MWT (r=-0.43, p=0.04). No significant correlations were demonstrated between age and spirometry, other timed tests or myometry.

Chapter 6: Use of cardiac extracellular volume measurement as a biomarker of fibrosis in limb girdle and Becker muscular dystrophies

6.1 Summary

This study pilots ECV quantification in LGMDR9 and BMD. Progressive cardiac fibrosis in muscular dystrophies is a cause of morbidity and mortality mostly through LV dysfunction and increased risk of arrhythmias. Increased ECV measured with post-Gd MRI has been investigated as a biomarker of myocardial fibrosis (Table 1).

Gd-enhanced MRI examination was performed in participants with LGMDR9 (n=6), BMD (n=7) and controls (n=10). T1 maps were taken before and 10 minutes after Gd injection. ROI analysis and Hct correction allowed ECV value calculation.

In BMD and LGMDR9 cohorts, of 20 segments with ECV of ≥0.28 15 were in the lateral wall. ECV correlated to measures of cardiac function LVEF, WMA, and LGE. Higher ECV values were found in LGE-positive segments. ECV values of ≥0.28 were found in 5 participants without LGE-positive segments. Increased ECV correlated with reduced LVEF in LGMDR9 (r=-0.41, p=0.047) and BMD cohorts (r=-0.45, p=0.02). Unlike the BMD group, LGMDR9 participants had significantly different torsion and strain values compared to controls (PT LGMDR9 3.3 ±1.1, versus control 6.2 ±1.8, p=0.004). In the LGMDR9 cohort increased ECV correlated with reduced strain and torsion in the basal region PT (r=-0.51 p=0.01). Apical ECV values correlated with measures of strain (PWWS r=0.58 p=0.003) and inversely to torsion, PT r=-0.50 p=0.01). Regional and global ECV values were significantly higher in participants with evidence of global cardiac dysfunction.

ECV correlated with measures of cardiac dysfunction: LVEF, LGE, WMA, and abnormal cardiac tagging values. ECV may be abnormal where other measures are normal. ECV has potential to quantify diffuse fibrosis for use in clinical practice or therapeutic trials.

6.2 Results

Mean age of LGMDR9 participants was 51.0 years ±15.6 and the BMD cohort had a median age of 45.0 years ±13.1 (Table 22). Mean age of the controls was 45.5 years ±14.2 which was not significantly different from the disease cohort (p=0.77). NIV was required by 83.3% (n=5) LGMDR9 participants. Angiotensin converting enzyme inhibitors and beta blockers were prescribed to 83.3% (n=5) LGMDR9 participants and 57.1% (n=4) BMD participants suggesting more severe cardiac involvement in the LGMDR9 group (Table 22).

ECV was analysable in 269/276 segments with 7 segments unanalysable due to artefact. No significant correlations were evident between ECV and age in any of the groups.

Characteristic	LGMD (n=6)	BMD (n=7)	Controls (n=10)
Age (years)	51.0 ±15.6	45.0 ±13.1	45.5 ±14.2
Number of segments analysed (%)$	67 (93.1)	83 (98.9)	119 (99.2)
Number of males (%)	4 (66.7)	7 (100.0)	10 (100.0)
Weight (kg)‡	93.3 (59.8-111.8)	81.7 (56.7-181.0)	76.7 (66.2-114.6)
Body surface area (m^2)	1.91 ±0.19	2.01 ±0.26	2.02 ±0.21
Systolic blood pressure (mmHg)	133.4 ±11.5	126.1 ±19.4	122.4 ±10.7
Diastolic blood pressure (mmHg)	85.0 ±8.7*	73.0 ±14.2	68.7 ±10.9
Heart rate (bpm)	84.3 ±15.9	73.9 ±7.1	70.3 ±16.1
Haematocrit (L/L)	0.42 ±0.04	0.42 ±0.02	0.44 ±0.02
Number receiving cardio-active medication (%)	5 (83.3)	4 (57.1)	0 (0)
Number with late gadolinium enhancement (%)	1 (16.7)	1 (14.3)	0 (0)
Number with wall motion abnormality (%)	4 (66.7)	1 (14.3)	0 (0)
LVEF (%)	43.0 ±5.8*	51.0 ±7.7*	69.5 ±7.2
LVSV (ml)	39.3 ±13.4*	43.2 ±10.8*	80.5 ±10.4
LVSV/BSA (ml/m^2)	19.3 ±4.9*	22.4 ±4.6*	41.3 ±5.1
LVM (g)	119.0 ±34.6	117.4 ±15.9	139.9 ±30.5
LVM/BSA (ml/m^2)	54.8 ±13.2*	62.0 ±11.4	71.2 ±12.5
LVEDV (ml)‡	72.1 (58.9-151.2)	81.8 (66.6-133.0)*	113.8 (87.7-151.4)
LVEDV/BSA (ml/m^2)	36.1 (29.6-62.9)*	41.4 (34.9-66.6)*	57.3 (50.8-74.1)
LVESV (ml)‡	41.6 (28.3-93.6)	34.6 (30.2-70.5)	31.6 (17.9-56.3)
LVESV/BSA (ml/m^2)	22.6 (14.2-39.9)	20.8 (16.5-69.8)	17.3 (9.0-27.5)
Peak torsion (°)	3.3 ±1.1*	6.1 ±1.2	6.2 ±1.8~
Peak whole wall strain (%)	15.4 ±3.4*	16.1 ±3.2	18.2 ±2.7†
Peak endocardial strain (%)	21.2 ±3.4*	21.1 ±3.2	24.3 ±3.0†
Torsion to strain ratio (rad/%)‡	0.31 (0.14-0.38)*	0.46 (0.38-0.97)	0.45 (0.28-0.75)
Global ECV (-)‡	0.24 ±0.02	0.24 ±0.02	0.23 ±0.02
Regional ECV – Basal (-)‡	0.24 (0.23-0.31)*	0.23 (0.19-0.35)	0.23 (0.18-0.27)
Regional ECV – Mid cavity (-)‡	0.24 (0.20-0.30)	0.22 (0.20-0.30)	0.23 (0.18-0.27)
Regional ECV – Apical (-)‡	0.24 (0.21-0.32)	0.24 (0.21-0.35)*	0.23 (0.19-0.26)

Table 22. Comparison of cardiac characteristics between the disease and control groups. Left ventricular ejection fraction (LVEF), and all cardiac indices corrected for BSA were significantly different in the disease groups compared to controls. Left ventricular stroke volume (LVSV) are significantly lower in the disease groups compared to the control group. Cardiac tagging data is significantly different in the LGMDR9 group only. Data is represented as mean ±standard deviation unless otherwise stipulated.

*Significant difference between cohort and controls, p value <0.05.

†(n=9) Due to a parallel imaging artefact the results from one participant was unanalysable and therefore excluded.

~(n=8) Due to tracking difficulties in one participant it was not possible to get torsion values.

$ Excluding all segments where image quality was insufficient due to artefact (in total n=7).

‡ non-normally distributed – Mann Whitney U test used to calculate significance. Data is presented as median and range.

Key: LVEF, left ventricular ejection fraction, LVSV, left ventricular stroke volume, LVEDV, left ventricular end diastolic volume, LVESV, left ventricular end systolic volume, ECV, extracellular volume.

6.2.1 Measures of cardiac dysfunction

To demonstrate cardiac dysfunction detectable via traditional means within the disease cohorts the scans were assessed for signs of LGE and WMA. Two participants had sub-endocardial LGE; one from each disease cohort. 4/6 of the LGMDR9 and 1/7 from the BMD cohorts had WMA with LVEF significantly lower in those with WMA (43.1% ±7.4) compared to those without WMA (50.2% ±6.9, p<0.001) and controls (69.5% ±7.2, p=<0.001) suggesting that the WMA seen were pathological and reducing cardiac function.

Overall mean LVEF was significantly higher in the control group (69.5% ±7.2) compared to LGMDR9 (43.0% ±5.8, p<0.001) and BMD cohorts (51.0% ±7.7, p<0.001). LVSV/BSA was significantly lower in both disease groups (LGMDR9 p<0.001, BMD p<0.001), which was contributed to by a significant reduction in LVEDV/BSA (LGMDR9 p<0.001, BMD p=0.03) with no significant difference in LVESV (Table 22). The reduction in LVEDV may be secondary to an increase in fibrosis leading to restriction of the left ventricle's ability to expand during diastole. These measures of cardiac indices suggest that there was sufficient cardiac dysfunction within the disease groups to significantly reduce average cardiac function overall.

Cardiac tagging revealed that the LGMDR9 cohort had significantly lower PT (p=0.004), PECS (p=0.04), PWWS (p=0.03), and TSR (p= 0.04) than controls (Table 22). In spite of the reduced LVEF in the BMD group, the BMD and control cohorts were not significantly different in strain or torsion.

The LGMDR9 group had a significant, strong correlation between reduced LVEF and reduced PT (r=0.93 p<0.001). Correlation was seen between reduced LVEF of this cohort and reduced TSR (r=0.65 p<0.001), PWWS (r=0.52 p<0.001) and PECS (r=0.72 p<0.001). The correlations demonstrated between cardiac tagging indices may be evidence of the different mechanism of cardiac dysfunction in LGMDR9 with subepicardial dysfunction seen, in contrast to dystrophinopathies and normal aging. No significant correlations were observed between LVEF and cardiac tagging in BMD or control groups.

6.2.2 ECV correlation to measures of cardiac dysfunction

The highest ECV segmental value in the controls was 0.27 (2/119 segments). In both disease cohorts the highest segmental ECVs (0.28-0.35) were in the basal posterior (BP) segments which correspond to the most common areas of LGE. ECV was ≥0.28 in 20 segments, 15/20 of these were lateral wall segments the remainder were in the septal wall (5/20). In spite of the cardiac pathology seen within the LGMDR9 cohort of the participants with ECV values ≥0.28 the majority (6/7) were BMD

participants. There were no significant differences in global ECV between controls and either cohort which may reflect the regional nature of the fibrosis with normal areas reducing the global average. The highest median regional ECV values were in apical regions of both LGMDR9 (0.25 (0.23-0.30)) and BMD groups (0.26 (0.22-0.28) compared to control (0.23 (0.19-0.26)). The LGMDR9 cohort had significantly higher median basal ECV values (0.23 (0.22-0.29)) than controls (0.22 (0.20-0.26), $p=0.04$). Assuming that higher ECV values correspond to more fibrosis, this suggests that the basal regions were more likely to be affected in the LGMDR9 and BMD groups.

Reduced LVEF significantly correlated to increased basal ECV in BMD ($r=-0.45$ $p=0.02$) and LGMDR9 ($r=-0.41$ $p=0.047$). In the BMD cohort reduced LVEF also correlated significantly to increased ECV in the apical ($r=-0.42$ $p=0.03$) and mid-cavity regions ($r=-0.61$ $p=0.001$). These findings may suggest that there is a significant link between reduction in overall function and rises in ECV.

In the BMD participant with evidence of LGE 7/12 segments were affected these segments corresponded to higher ECV values (0.26-0.35) (Figure 34). This participant had a low LVEF of 36%. In the LGMDR9 participant with LGE positive segments, 5/11 segments were LGE positive which corresponded to modest ECV values (0.24-0.27) LVEF in this participant was also found to be low (46.2%). These are mixed results with the LGMDR9 participant having ECV values in the LGE positive segments which were similar to corresponding segments in controls. In the participant with LGMDR9 the ECV values of LGE negative segments did not exceed values of LGE positive segments. This may suggest that although ECV didn't increase to the same degree as seen in the participant with BMD, ECV did proportionally rise in the LGE positive areas compared to surrounding LGE negative segments.

Segment	ECV value	Evidence of LGE
BA	0.30	Y
BP	0.35	Y
BSA	0.23	N
BSP	0.22	N
MCA	0.26	Y
MCP	0.30	Y
MCSA	0.24	N
MCSP	0.22	N
AA	0.31	Y
AP	0.29	Y
ASA	0.26	Y
ASP	0.26	N
Mean	0.27	N/A
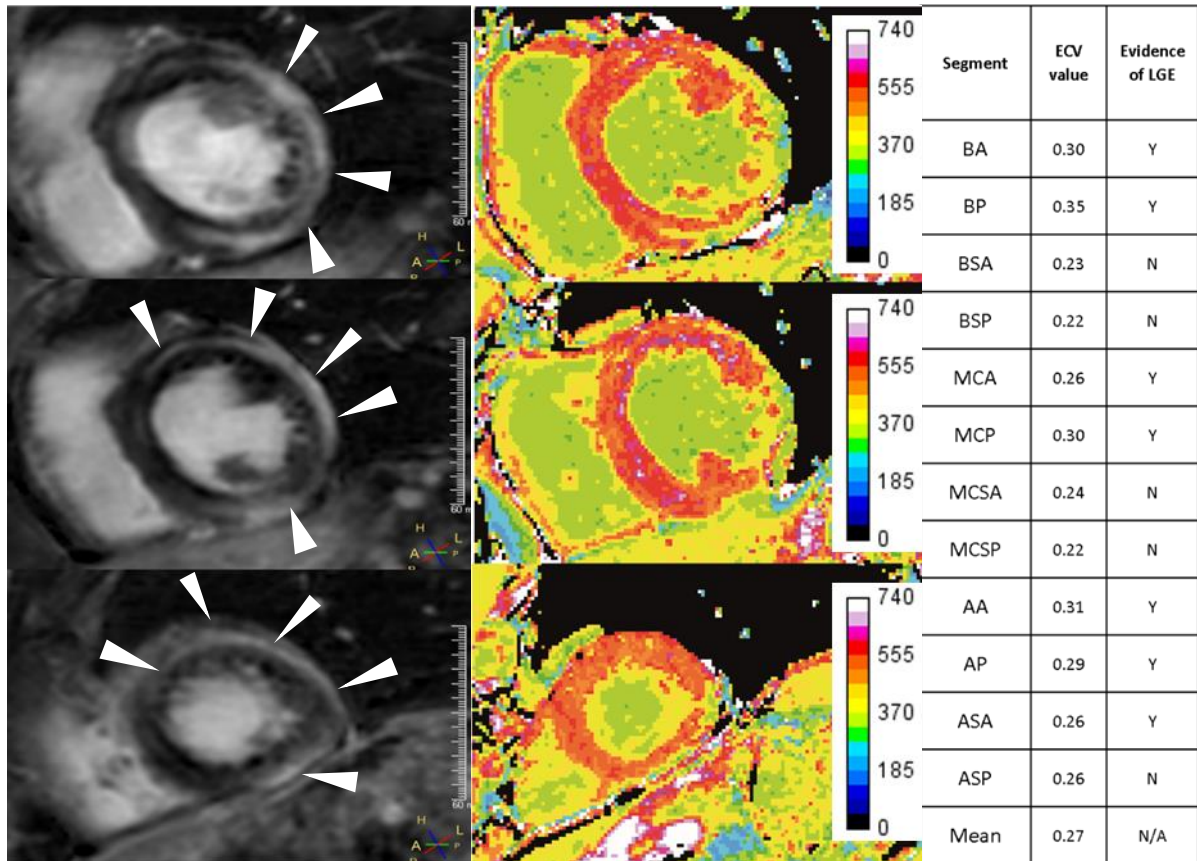
Figure 34. To compare the values of extracellular volume (ECV) segments in regions with late gadolinium enhancement (LGE) in a participant with Becker muscular dystrophy (BMD). Left – 3D phase sensitive inversion recovery (PSIR) sequence 10 minutes post-gadolinium (Gd) injection, from top to bottom basal, mid cavity and apical slices. Middle – Corresponding post-contrast T1 map slices with colour scale of values of T1 relaxation time (in ms). Right – table with ECV values in corresponding segments. These images suggest that in the presence of late gadolinium enhancement (LGE) ECV has a corresponding rise in the same segment.

Key: BP, Basal anterior, BA, Basal anterior, BSA, Basal septal anterior, BSP, Basal septal posterior, MCSA, Mid cavity septal anterior, MCSP, Mid cavity septal posterior, MCP, Mid cavity posterior, MCA, Mid cavity anterior, AA, Apical anterior, AP, Apical posterior, ASA, Apical septal anterior, ASP, Anterior septal posterior.

There was a significant difference between ECV basal regional values in the five participants with a WMA (0.26 (0.21-0.32)) compared to the eight without (0.24 (0.21-0.32) p=0.04) which may suggest that WMA are more common in those with basal fibrosis. No significant differences were demonstrated between ECV values in apical or mid-cavity regions, stratifying by WMA.

In the LGMDR9 cohort there were significant correlations between regional ECV values and cardiac tagging indices; including increasing basal regional ECV values correlating to both lower TSR (r=-0.42 p=0.04) and lower PT (r=-0.51 p=0.01). Increased apical values correlated to both increased strain (PWWS r=0.58 p=0.003, PECS r=0.56 p=0.04) and decreased torsion (TSR r=-0.637 p=0.03, PT r=-0.50 p=0.01). As suggested earlier, cardiac tagging indices may be sensitive to cardiac dysfunction in LGMDR9, the fact that ECV also correlates significantly to these measures suggests it is reflecting cardiac dysfunction. BMD regional ECV values did not correlate significantly to cardiac tagging indices which were not significantly different from control values.

6.2.3 ECV and cardiac dysfunction

To further assess ECV in detection of cardiac dysfunction, participants were compared by creating two groups. The first group had clinically diagnosed cardiac dysfunction defined as an LVEF<55% or evidence of LGE, (n=7) (LGMDR9 n=5, BMD n=2). The second group were all disease group participants without cardiac dysfunction and all controls were grouped together. Segmental, regional and global ECV values were significantly higher in those with cardiac dysfunction (Figure 35). Significant increases were seen comparing ECV segmental values between these two groups in: the basal anterior (BA), BP and mid cavity posterior (MCP) segments (Figure 36). These findings strongly suggest that ECV increases in participants with clinically defined cardiac dysfunction. It may also follow that cardiac dysfunction and reduced function occurs due to these segments being less able to move due to increased fibrosis.

Using these results it is possible to suggest ways to increase power in future therapeutic studies. Although all cardiac segments could be included using ECV calculation, a therapeutic trial should consider use of basal segments for an outcome measure; this is due to the higher frequency of high ECV values in this region. Using a power analysis, a minimum of 63 participants would be required to appropriately power a therapeutic trial using basal region ECV values as an outcome measure in LGMDR9 and BMD.
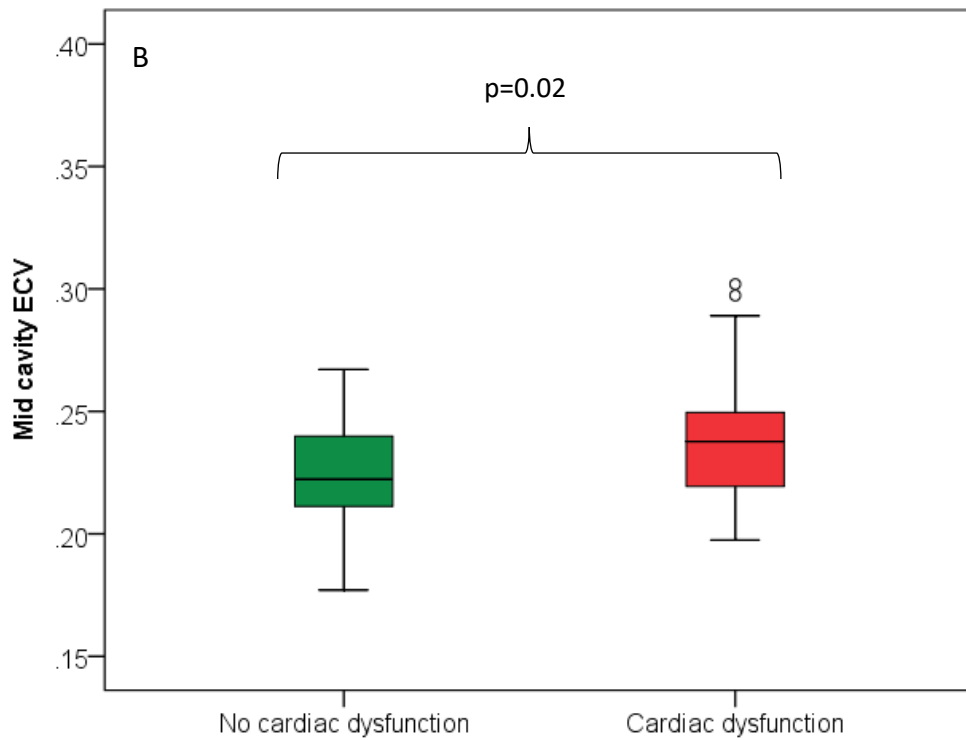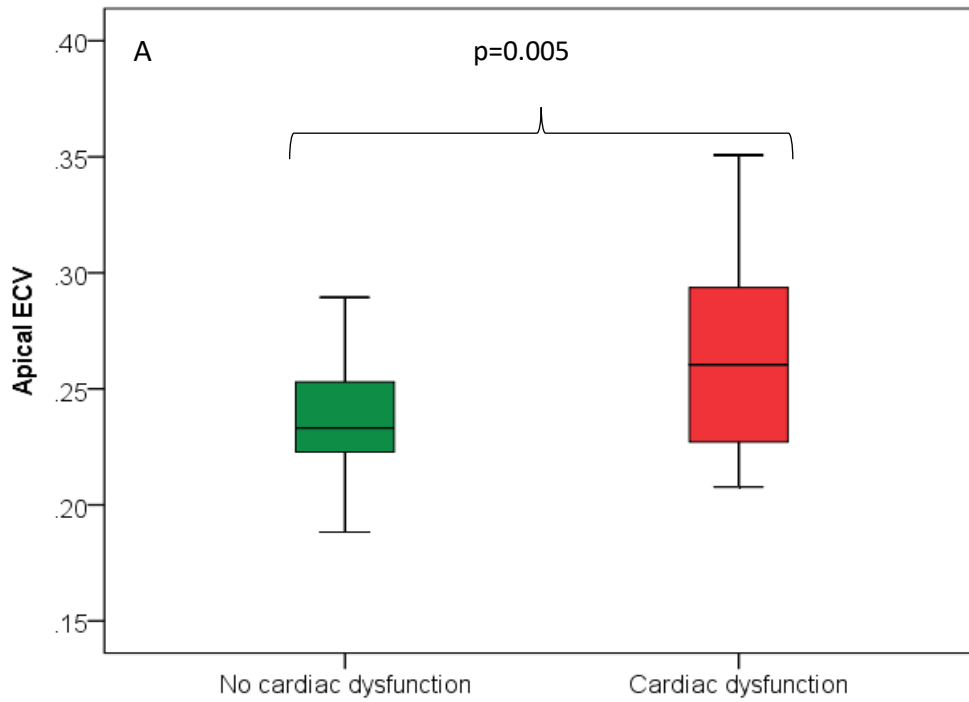
Figure 35. Part 1: Box plots to compare between extracellular volume (ECV) with and without cardiac dysfunction (as defined as an left ventricular ejection fraction (LVEF) <55% or evidence of late gadolinium enhancement (LGE)). The most highly significant increase in ECV was the global measure. Overall ECV was significantly higher in the cardiac dysfunction group, providing evidence of sensitivity. P values calculated using Mann-Whitney U test.
Key: A) Apical ECV, B) Mid cavity ECV, C) Basal ECV, D) Global ECV.
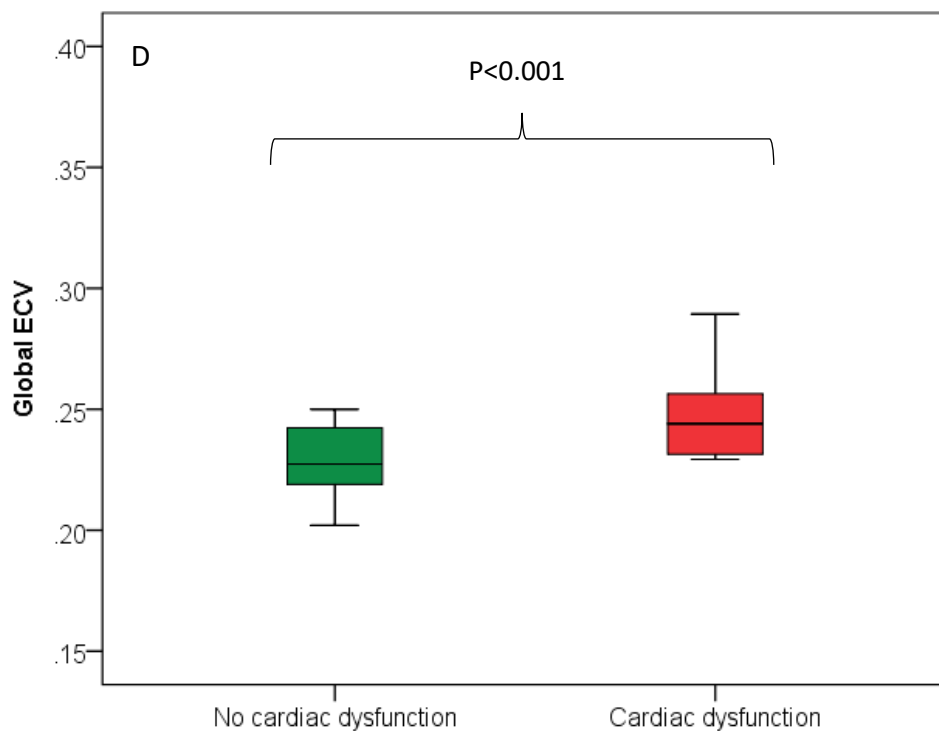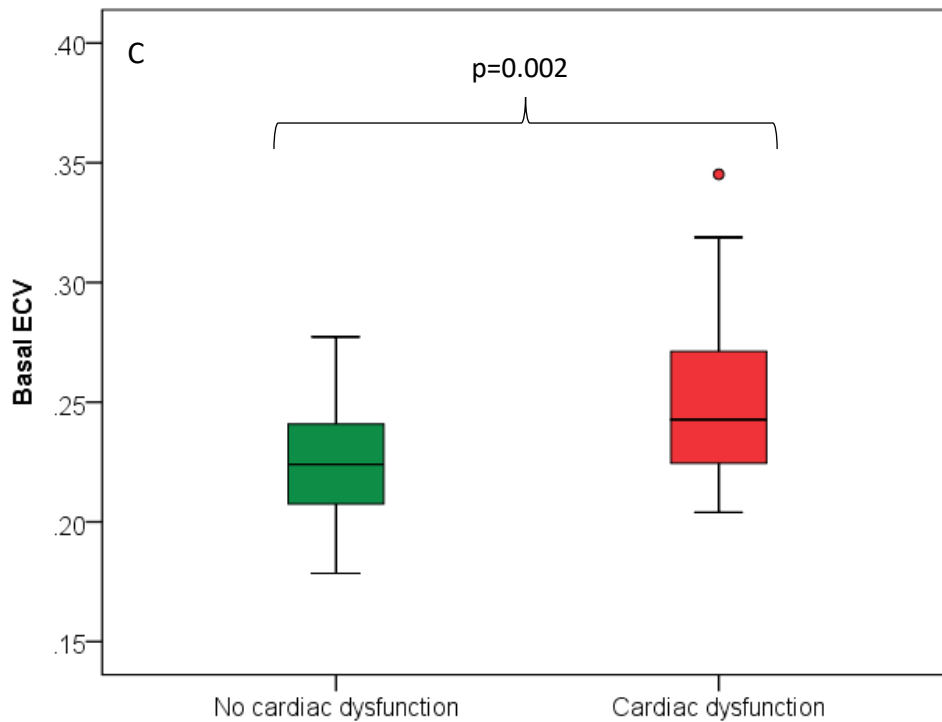
Figure 35. Part 2: Box plots to compare between extracellular volume (ECV) with and without cardiac dysfunction (as defined as an left ventricular ejection fraction (LVEF) <55% or evidence of late gadolinium enhancement (LGE)). The most highly significant increase in ECV was the global measure. Overall ECV was significantly higher in the cardiac dysfunction group, providing evidence of sensitivity. P values calculated using Mann-Whitney U test.
Key: A) Apical ECV, B) Mid cavity ECV, C) Basal ECV, D) Global ECV.
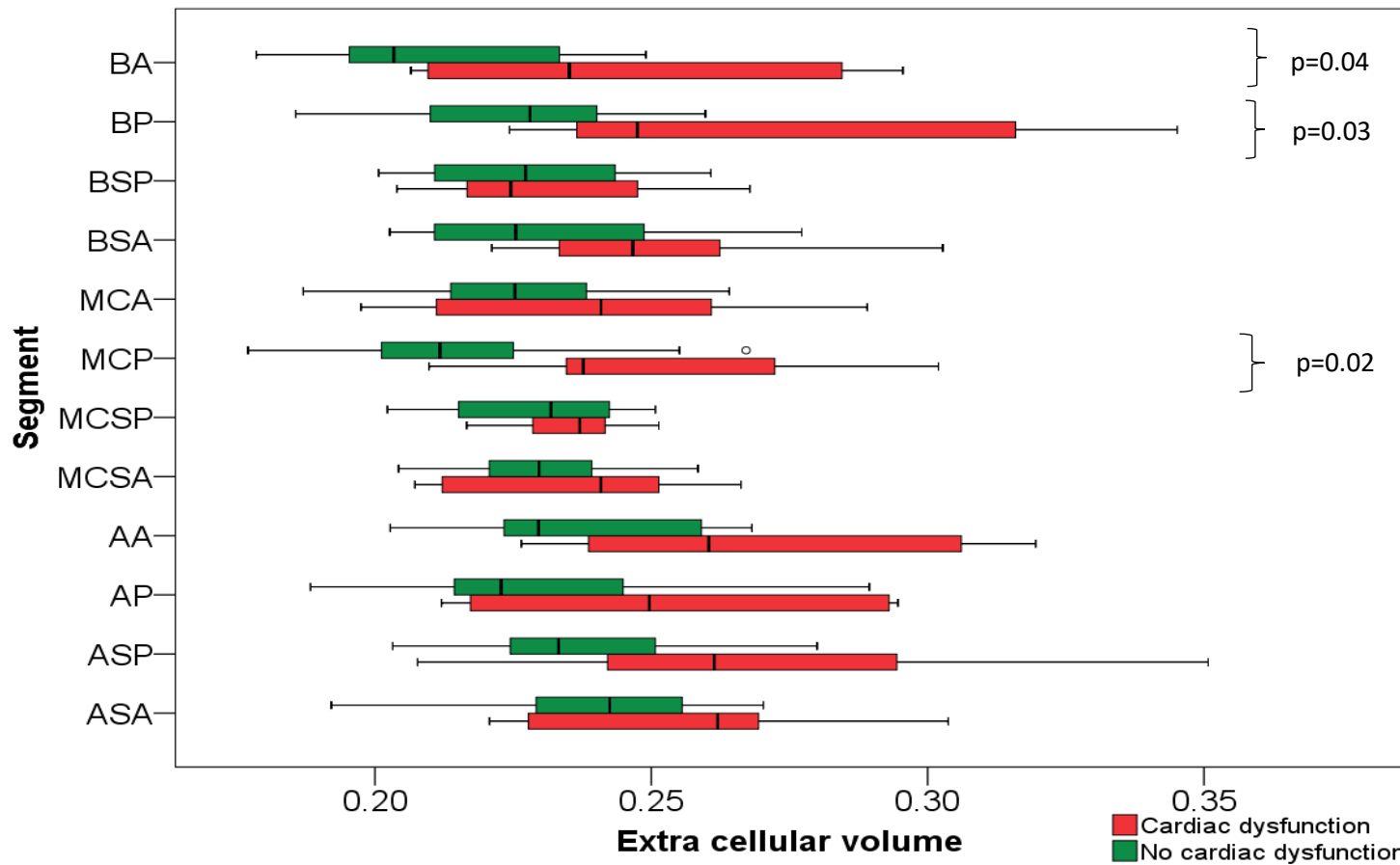
Figure 36. Comparing segmental extracellular volume (ECV) values in participants with cardiac dysfunction (n=7) (reduced left ventricular ejection fraction (LVEF) <55%, or late gadolinium enhancement (LGE) to those without combined with the control cohort (n=16). Only three segments had significantly higher ECV values in the group with cardiac dysfunction, these were the basal anterior (BA), basal posterior (BP) and the mid-cavity posterior (MCP) segments. These significantly higher ECV values here may relate to the fact that cardiac dysfunction is seen when these are affected due to restriction of movement, secondary to fibrosis.

Key: BP, Basal anterior, BA, Basal anterior, BSA, Basal septal anterior, BSP, Basal septal posterior, MCSA, Mid cavity septal anterior, MCSP, Mid cavity septal posterior, MCP, Mid cavity posterior, MCA, Mid cavity anterior, AA, Apical anterior, AP, Apical posterior, ASA, Apical septal anterior, ASP, Anterior septal posterior.

Chapter 7: The quantification of left ventricular indices in muscular dystrophy cohorts: Evaluation of accelerated imaging

7.1 Summary

CMRI provides highly versatile, detailed information about myocardial function and anatomy. CMRI-generated functional indices are widely used in clinical practice and as an outcome measure in therapeutic trials. Neuromuscular cohorts pose challenges to CMRI assessments due to discomfort in lying supine for long periods, scoliosis, and cardiorespiratory compromise. There are clear advantages to reducing acquisition times required for cardiac functional indices.

In spite of the common usage of functional cardiac indices as outcome measures for therapeutic trials, few studies have investigated cardiac outcome measures in neuromuscular disease. Long term follow up of cardiac indices in LGMDR9 has not been investigated using CMRI. It is therefore not clear whether CMRI is an effective tool to monitor long term changes in cardiac indices in this cohort.

An aim of this chapter is to explore whether accelerated imaging can be used to reduce acquisition times whilst maintaining image fidelity and obtaining accurate cardiac indices. This chapter will also assess the use of CMRI as an outcome measure in LGMDR9, assessing change in LV indices and cardiac tagging over a five year period.

Three groups of age-matched participants were recruited to undergo CMRI assessment: LGMDR9 (n=8), BMD (n=7) and healthy volunteers (n=10). Participants from the LGMDR9 group had undergone CMRI assessment five years prior to this recruitment as part of their participation in an LGMDR9 natural history study (Hollingsworth et al., 2013b). Participants were scanned supine within a 3T Philips Achieva scanner (Best, NL), a 16-channel torso XL coil (Philips, Best, NL) and VCG gating (Philips VCG). The protocol included conventional and accelerated cine imaging, and cardiac tagging. Cine imaging was performed during BH, with steady-state free precession in the short axis plane, cardiac cine 25 phases, with 14 slices. Two and four chamber long axis views were also collected using both conventional and accelerated cine. The following cardiac indices were obtained using segmentation software: LVEF, LVSV, LVEDV, LVESV and LVM. Cardiac tagging indices obtained included: PT, PECS, PWWS, and TSR. Two observers separately reviewed 8 images rating image quality and generating cardiac indices for comparison.

Bland Altman analysis of the accelerated versus conventional imaging demonstrated no significant bias in any of the cardiac indices with 95% LOA for LVEF at 5.9%. A high degree of inter-observer

agreement was found with no significant bias between ratings of cardiac indices. Both observers scored the accelerated images on average as either 'no difference appreciated in quality' or 'marginally improved image quality' compared to conventional images. Follow up of cardiac indices and measures of strain and torsion in the LGMDR9 group demonstrated no significant differences over the five year period.

The accelerated method had comparable 95% LOA to other published accelerated approaches, and had high inter-observer reproducibility. The technique does however lead to a 95% LOA in LVEF of 5.9%, which in a clinical context is a potentially significant degree of uncertainty with values of greater than 55% being considered normal. Therefore, although accelerated imaging yields images of a visually equivalent quality, variation between measurements of cardiac indices may not be clinically acceptable. The results of the five year follow up portion of this study suggest that CMRI generated cardiac indices and cardiac tagging may be insufficiently sensitive to detect change in the LGMDR9 cohort over a five year time period. Limitations of the studies are the small sample size and the confounding factor of cardioactive medication administration.

7.2 Results

7.2.1 Recruitment

Accelerated and conventional CMRI acquisition was performed on three groups of participants: LGMDR9 (n=8), BMD (n=7), and healthy volunteers (n=10). For the LGMDR9 five year follow up, cardiac tagging was not available in two participants due to artefact (n=6). Breakdown of the demographics of participants is given in 'Table 23'.

7.2.2 Comparing accelerated and conventional imaging

To compare accelerated and conventional imaging, the three disease groups were considered together. Mean LVEF was statistically significantly lower measured from the accelerated imaging (54.4% ±13.8), compared to the conventional (56.0% ±13.5) (p=0.01). Mean values for other cardiac indices LVSV, LVM, LVEDV and LVESV were not significantly different between the two techniques.

Bland Altman analysis of the different cardiac indices demonstrated that the 95% LOA for LVEF were 5.9%, with a positive bias of 1.6%. LOA and bias for LVSV, LVEDV, LVESV and LVM are given in 'Table 24' and 'Figures 37 to 41' demonstrate the relationship between the two methods. No significant bias was demonstrated between the two imaging techniques for any of the cardiac indices, as all LOA straddle zero.

Characteristic	LGMDR9 (n=8)	BMD (n=7)	Control (n=10)
Age (years)	54.5 ±15.0	45.0 ±13.1	45.5 ±14.2
Number of males (%)	6 (66.7)	7 (100)	10 (100)
Systolic blood pressure (mmHg)	133.4 ±11.5	126.1 ±19.4	122.4 ±10.7
Diastolic blood pressure (mmHg)	85.0 ±8.7	73.0 ±14.2	68.7 ±10.9
Heart rate (bpm)	84.3 ±15.9	73.9 ±7.1	70.3 ±16.1
Receiving cardio-active medication≠	5 (83.3)	4 (57.1)	0 (0)
Left ventricular ejection fraction (%)~	43.4 ±6.3*	51.0 ±7.7*	69.5 ±7.2
Left ventricular stroke volume (ml)~	38.8 ±11.7*	43.2 ±10.8*	80.5 ±10.4
Left ventricular mass (g)~	112.3 ±35.0	117.4 ±15.9	139.9 ±30.5
Left ventricular end diastolic volume median (ml) (range) ~	72.1 (58.9-151.2)	81.8 (66.6-133.0)*	113.8 (87.7-151.4)
Left ventricular end systolic volume median (ml) (range)~	41.6 (28.3-93.6)	34.6 (30.2-70.5)	31.6 (17.9-56.3)
Peak torsion (°)	3.3 ±1.3$*	6.1 ±1.2†	6.2 ±1.8‡
Torsion to strain ratio (rad/%) median (range)	0.31 (0.14-0.38)$*	0.46 (0.38-0.97)†	0.45 (0.28-0.75)‡
Peak whole wall strain (%)	14.9 ±2.3$	16.1 ±3.2†	18.2 ±2.7†
Peak endocardial strain (%)	20.6 ±3.5$	21.1 ±3.2†	24.3 ±3.0†

Table 23. Demographics of the three groups comparing accelerated and conventional acquisitions. Values reported as mean and standard deviation unless otherwise stipulated. Demonstrating the significant differences between the disease groups and the control group in terms of ejection fraction (EF) and stroke volume (SV). The LGMDR9 had significantly different values for cardiac tagging indices.
*p<0.05 significant difference between group and controls.
† Due to a parallel imaging artefact the results from one participant was unanalysable and therefore excluded.
~ Calculated using conventional imaging
$ Due to a parallel imaging artefact the results from two participants was unanalysable and therefore excluded.
‡ Torsion values were not obtainable in two participants due to a parallel imaging artefact and a tracking difficulty in one other participant.
≠ Cardioactive medication is defined as either monotherapy or combination therapy with: beta blockers, angiotensin converting enzyme inhibitors, or angiotensin receptor blockers.

Comparison	(n)	LVEF (%)	LVSV (mls)	LVEDV (mls)	LVESV (mls)	LVM (g)
Inter-observer	n=8	0.4, 0.8	0.4, 0.8	0.04, 0.4	0.4, 0.9	3.2, 9.7
Conventional vs accelerated	n=25	1.6, 5.9	2.5, 13.1	2.2, 17.3	-1.6, 11.4	-3.3, 17.3

Table 24. Summary of results from Bland Altman analysis with values presented as: bias, 95% limits of agreement (LOA). Although the 95% LOA were small between observers, the calculation of cardiac indices (i.e. ejection fraction (EF)) using the accelerated imaging technique led to wide 95% LOA.
Key: LVEF, left ventricular ejection fraction, LVSV, left ventricular stroke volume, LVEDV, left ventricular diastolic volume, LVESV, left ventricular end systolic volume, LVM, left ventricular mass.
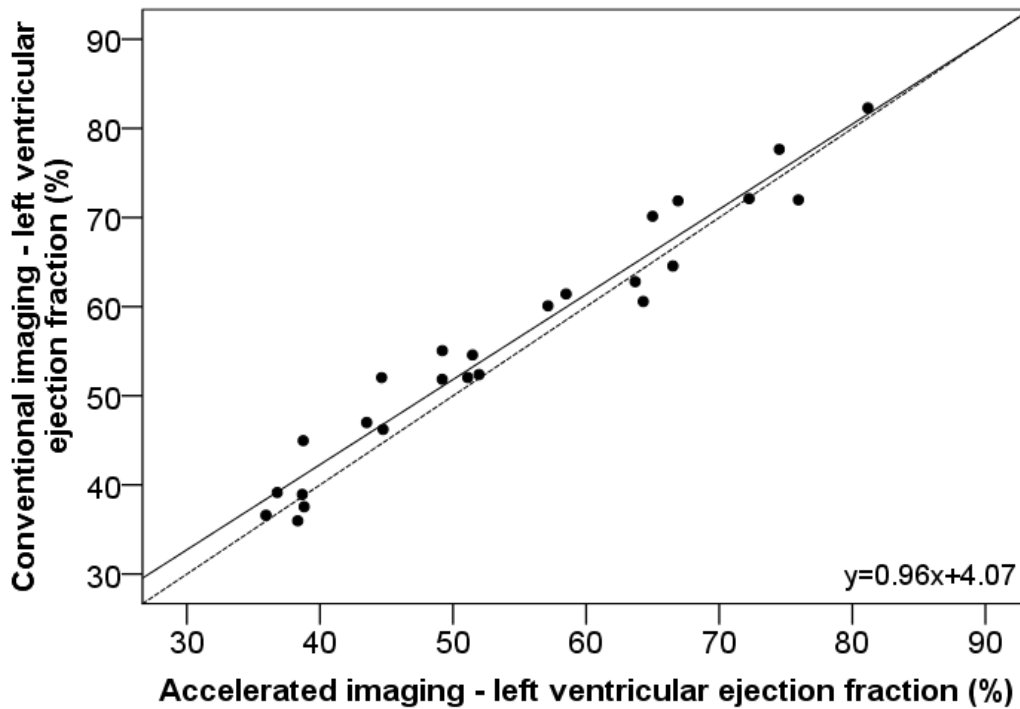
Figure 37. Left ventricular ejection fraction (LVEF) using accelerated and conventional imaging. This demonstrates the close relationship of the two methods of measurement, with minimal differences comparing on a individual basis. Key: Solid line, line of best fit, Dotted line, line of equality (y=x).
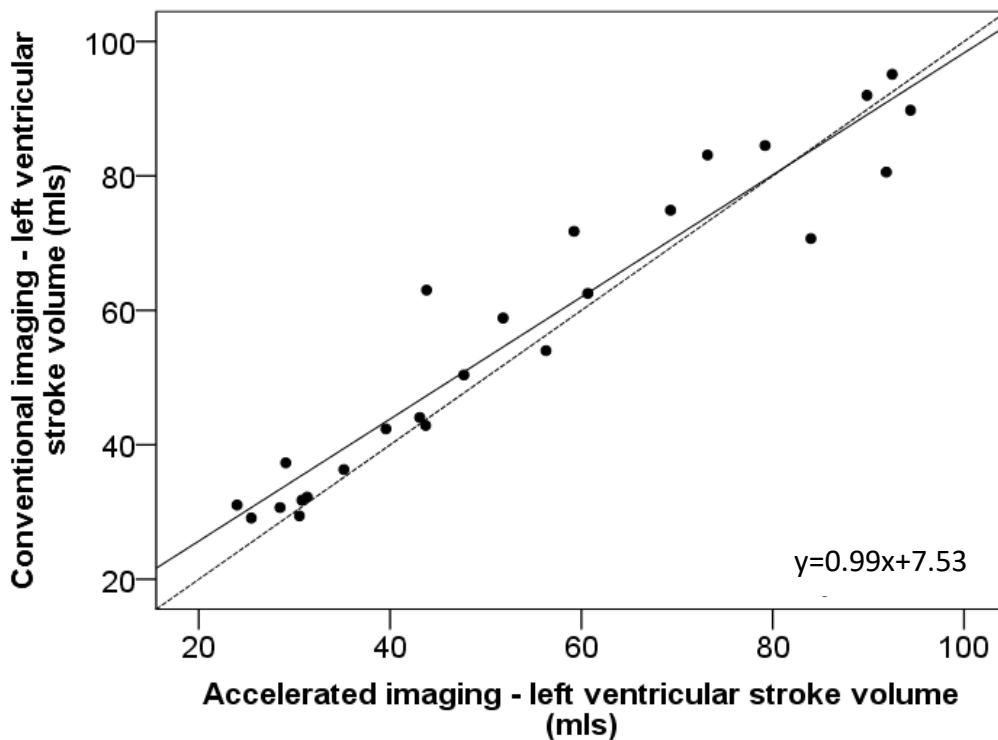
Figure 38. Left ventricular stroke volume (LVSV) using accelerated and conventional imaging. This demonstrates the close relationship of the two methods of measurement, higher values had more discrepancy between the two methods. Key: Solid line, line of best fit, Dotted line, line of equality (y=x).
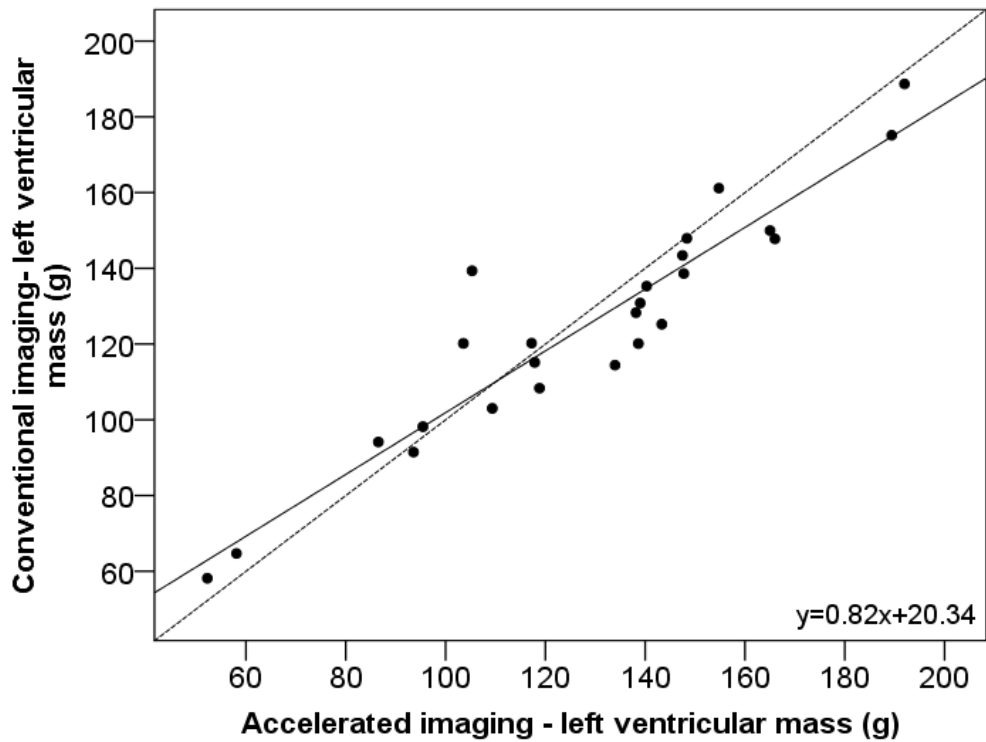
Figure 39. Left ventricular mass (LVM) using accelerated and conventional imaging. This demonstrates the close relationship of the two methods of measurement, varibility between the two methods of measurement was greatest in the middle values (100-150g)
Key: Solid line, line of best fit, Dotted line, line of equality (y=x).
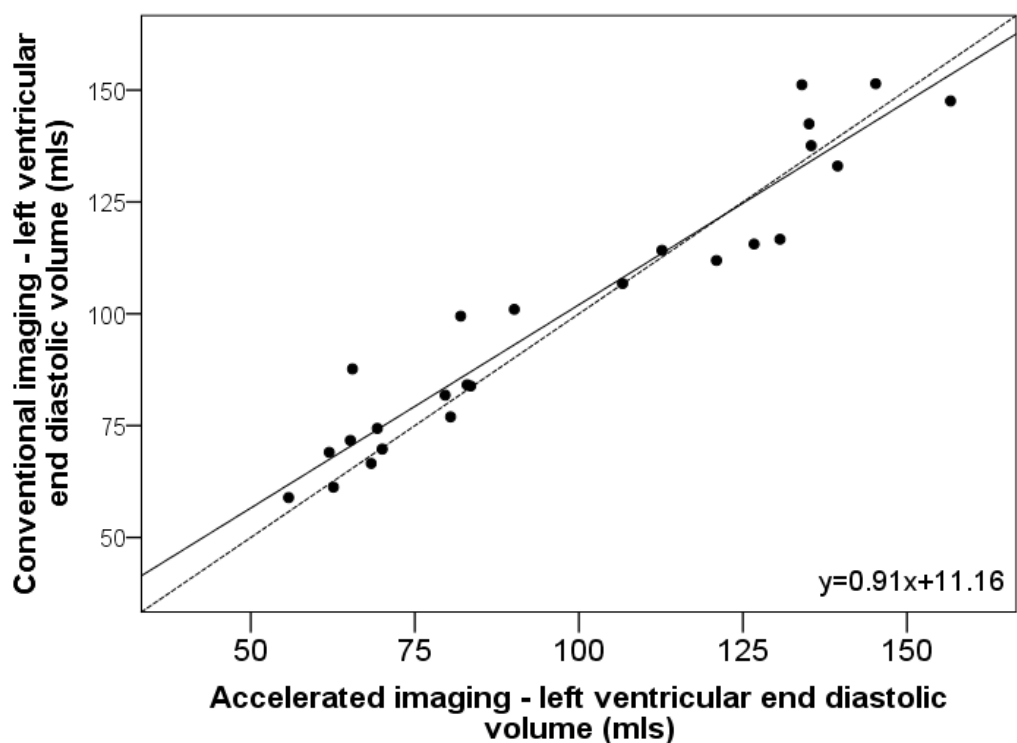
Figure 40. Left ventricular end diastolic volume (LVEDV) using accelerated and conventional imaging. This demonstrates the close relationship of the two methods of measurement, greater varibility between the two methods was seen at higher values.
Key: Solid line, line of best fit, Dotted line, line of equality (y=x).
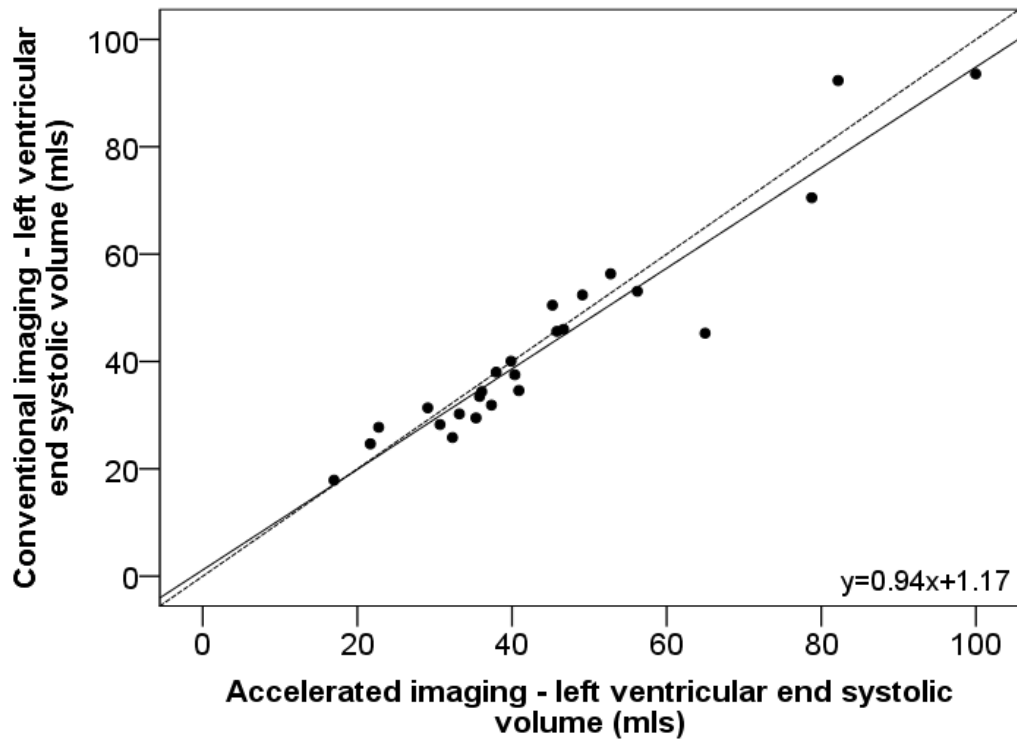
Figure 41. Left ventricular end systolic (LVESV) volume using accelerated and conventional imaging. This demonstrates the close relationship of the two methods of measurement, with minimal differences comparing on a individual basis. Key: Solid line, line of best fit, Dotted line, line of equality (y=x).

7.2.3 Inter-observer analysis

Image quality of both imaging techniques was acceptable for analysis for all of the conventional and accelerated scans (Figure 42). Qualitative analysis with the five point scoring system (Table 4) with a higher score demonstrating better image fidelity, showed that the accelerated images were rated as 3.8 and 4.1 by observer one and two respectively. This suggests that quality in accelerated images has no obvious difference or is marginally better than conventional imaging.
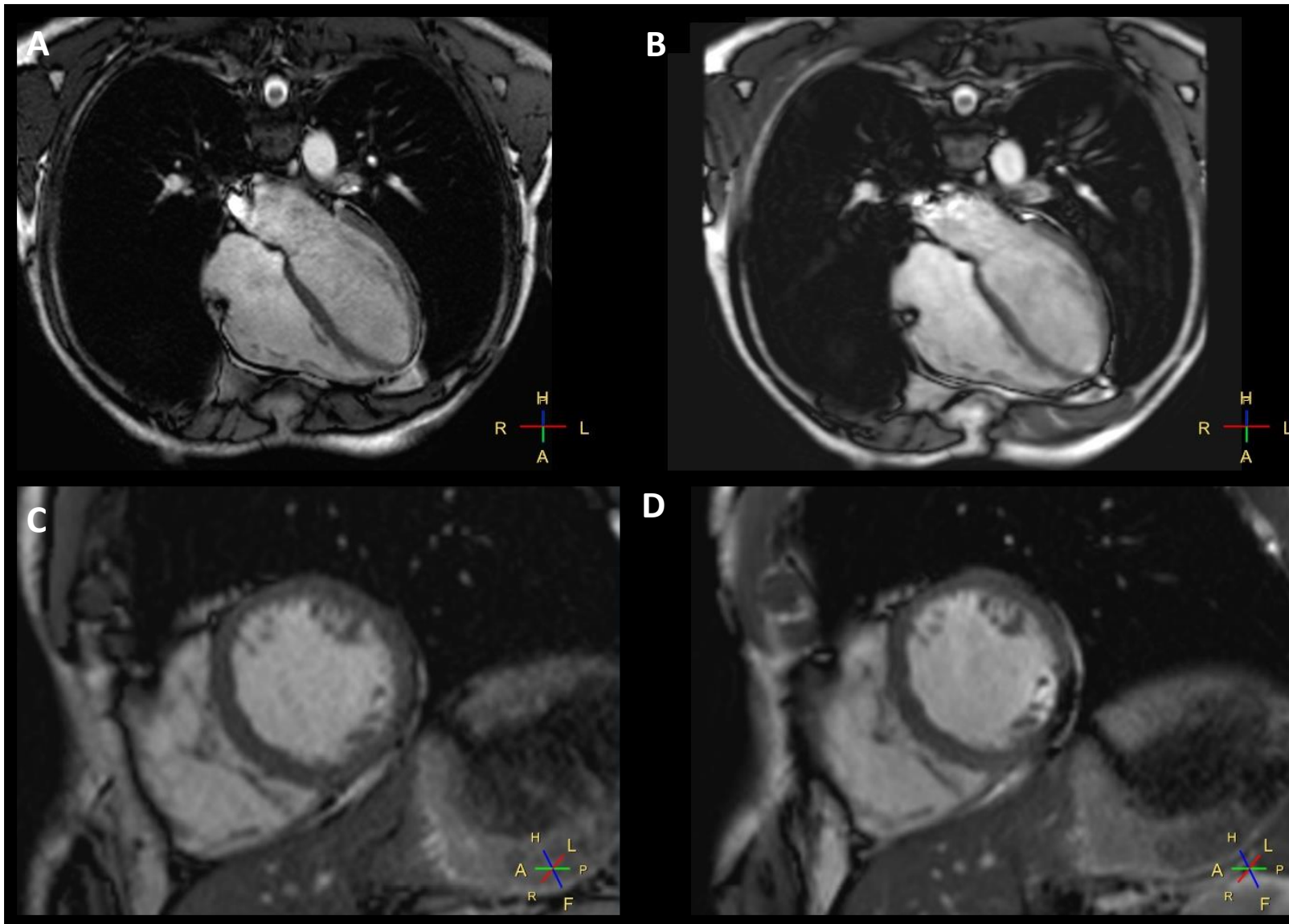
Figure 42. Example of 2 chamber long axis view (top row) and mid-ventricular short axis views (bottom row) at approximated points in the cardiac cycle. This is a demonstration of the close image fidelity.
A and C – accelerated images, B and D – conventional images.
Key: H, head, F, feet, L, left, R, right, A, anterior, P, posterior.

Bland Altman analysis of the cardiac indices showed narrow 95% LOA in all cardiac indices (Table 24). No significant inter-observer bias was demonstrated, with all 95% LOA bracketing zero.

7.2.4 Comparison of results with previous studies

Previous work in obtaining cardiac indices using accelerated sensing or free breathing (FB) techniques have been summarised in 'Table 25'. The inter-observer 95% LOA in all cardiac values in this study were very narrow compared to other studies (Table 25). 95% LOA in the current study for LVEF were narrower (5.9%) than Vincenti *et al.* (8.6%) and Jaroni *et al.* (9.5%), but similar to Kido *et al*. (5.2%) (Vincenti et al., 2014, Jaroni et al., 2013, Kido et al., 2016). LOA for LVEF were similar to those reported in FB approaches adopted by Liu *et al.* (6.4%), Usman *et al.* 2015 (7.0%) and 2017 (6.2%) (Liu et al., 2017, Usman et al., 2015, Usman et al., 2017).

Study (year)	Mode	Method summary	Cohort (n)	LVEF	LVSV	LVEDV	LVESV	LVM	Breath holds	NAcc/sl
Current inter-observer	BH	3.0T, SENSE, PF	LGMDR9 (8) BMD (7)	0.4, 0.8	0.4, 0.8	0.04, 0.4	0.4, 0.9	3.2, 9.7	3 x 10s, 1 x 5s	2.0x, 2.5s
Current conventional vs accelerated	BH	3.0T, SENSE, PF	LGMDR9 (8) BMD (7) Controls (10)	1.6, 5.9	2.5, 13.1	2.2, 17.3	-1.6, 11.4	-3.3, 17.3	3 x 10s, 1 x 5s	2.0x, 2.5s
(Hudsmith et al., 2005) interobserver	BH	1.5T, view sharing, PF	Controls (12)	1.6, 4.4	NG	0.4, 4.2	NG	5.8, 10.2	7 x 10.3s	1.0x, 5s
(Greil et al., 2008)	BH	1.5T, SENSE, BLAST	Controls (17)	0.5, 6.5	4.0, 8.0	5.0, 9.0	1.0, 11.0	-0.9, 7	2 x 15s	5.0x, 0.5s
(Vincenti et al., 2014)	BH	1.5T, SENSE, PF, GPM	Controls (12) LV involvement (21)	1.6, 8.6	8.7, 25.6	9.9, 20.4	2.0, 23.4	-2.5, 19.2	1 x 14s	5.2x, 2s
(Jaroni et al., 2013)	BH	1.5T, BLAST	Myocarditis (18) cardiomyopathy (22) MI (15)	4.5, 9.5	NG	NG	-4.0, 19.0	NG	1 x 3.8s, 1 x 5.5s	7.5x, 1.8s
(Kido et al., 2016)	BH	3.0T, SENSE PF	Coronary artery disease (44) other cardiac conditions (21) controls (16)	0.4, 5.2	1.1, 11.6	1.3, 15.9	0.2, 10.1	1.0, 12.3	1 x 24s	3.0x, 3s
(Usman et al., 2015)	FB	1.5T, SENSE	Controls (8) patients (3)	1.3, 7.0	2.2, 12	1.3, 8.5	-1.0, 8.5	NG	FB duration 2 min	0.5x, 9s
(Usman et al., 2017)	FB	1.5T, SENSE	Controls (8) patients (3)	-2.0, 6.2	-1.0, 10.4	2.7, 8.3	3.7, 7.3	NG	FB duration 5 min	0.9x, 5.5s
(Liu et al., 2017)	FB	3.0T, SENSE CIRCUS	Controls (8)	1.4, 6.4	NG	2.6, 3.3	-0.8, 7.5	NG	FB duration 2.5 min	0.9x, 4.7s

Table 25. Summary of results from current study and previous publications using compressed sensing or free breathing (FB). All figures for cardiac indices are reported as: mean difference, 95% limits of agreement (LOA). Comparison of the current study results ejection fraction results are similar in terms of the degree of LOA to other compressed sensing techniques.
Key: MI, myocardial infarction, BMD, Becker muscular dystrophy, LGMDR9, limb girdle muscular dystrophy type R9, LVEF, left ventricular ejection fraction, LVSV, left ventricular stroke volume, LVEDV, Left ventricular end diastolic volume, LVESV, left ventricular ends systolic volume, LVM, left ventricular mass, SENSE, PF, partial Fourier, LV, left ventricular, NAcc/sl, Net acceleration per slice, NG, not given, FB, free breathing, BH, breath holding, SENSE, Sensitivity encoding, CIRCUS, circular cartesian undersampling, GPM, guide point modelling, BLAST, Broad-use Linear Acquisition Speed-up Technique.

7.2.5 Five year follow up of cardiac dysfunction

8 participants from the LGMDR9 group had undergone measurement of cardiac indices over the five year period. 2 participants did not have baseline cardiac tagging; therefore averages for tagging indices are based upon 6 participants.

Characteristic	Baseline (n=8)	Five years (n=8)	P value
Age (years)	47.7 ±15.2	53.5 ±15.4	N/A
Number of males (%)	6 (75)	6 (75)	N/A
Systolic blood pressure (mmHg)	134.6 ±13.4	133.4 ±11.5	0.76
Diastolic blood pressure (mmHg)	83.6 ±9.9	85.0 ±8.7	0.54
Heart rate (bpm)	73.8 ±13.6	84.3 ±15.9	0.09
Receiving cardio-active medication	5 (62.5)	7 (87.5)	N/A
Left ventricular ejection fraction (%)	45.6 ±5.7	43.4 ±6.3	0.48
Left ventricular stroke volume (ml)	46.9 ±12.6	38.8 ±11.7	0.21
Left ventricular mass (g)	121.2 ±41.4	112.3 ±35.0	0.65
Left ventricular end diastolic volume (ml)	106.0 ±38.0	93.3 ±38.6	0.52
Left ventricular end systolic volume (ml)	59.2 ±26.0	54.5 ±27.3	0.73
Peak torsion (°)†	3.6 ±0.8	3.3 ±1.3	0.60
Torsion to strain ratio (rad/%)†	0.3 ±0.1	0.3 ±0.0	0.58
Peak whole wall strain (%)†	15.8 ±2.6	14.9 ±2.3	0.53
Peak endocardial strain (%)†	20.7 ±3.2	20.6 ±3.5	0.96

Table 26. Summary of participant demographics over five years
† n=6 as two participants did not have baseline cardiac tagging measurements.

None of the cardiac indices derived from cine imaging declined significantly over the five year period (Table 26 and Figures 43-44). Measures of strain and torsion did not decrease significantly. LVEF strongly correlated to a significant degree to PT (r=0.81, p=0.01 at follow up). PT and TSR demonstrated individual variation (Figure 45).

The only participant not to receive cardio-active medication over the five year follow up had an LVEF of 45.0% at five year follow up, which had not changed from baseline measurement. Cardiac indices such as LVM, LVSV, LVEDV, and LVESV were not different from other participants over the five years.
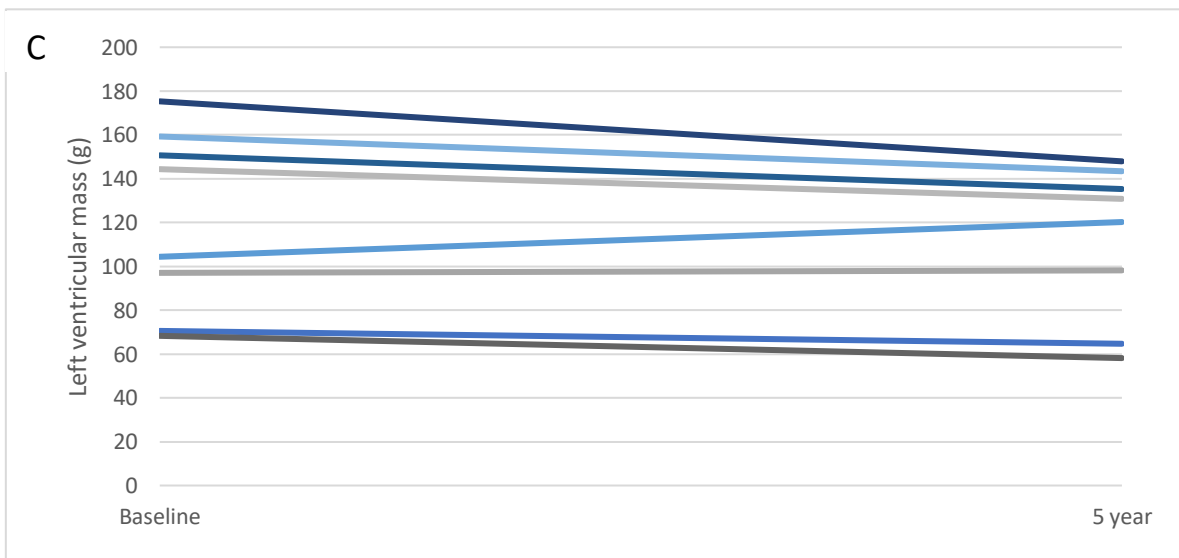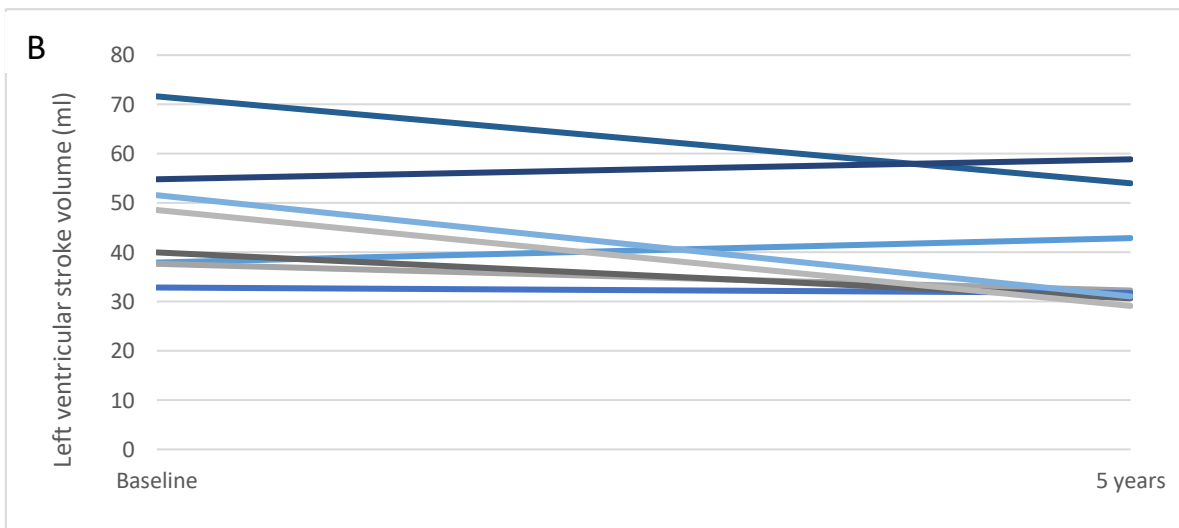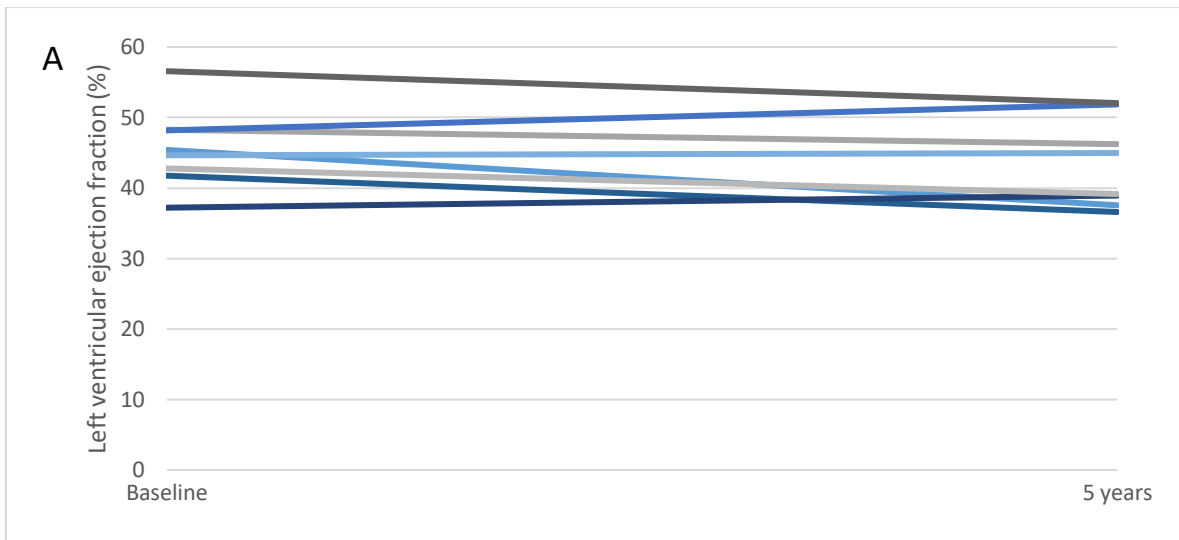
Figure 43. Line graphs to show individual trajectories in cardiac indices over five year follow up: A) Left ventricular ejection fraction (LVEF), B) left ventricular stroke volume (LVSV), C) left ventricular mass (LVM). No significant differences in any of the cardiac indices over the five years. This may be due to small sample size or due to the confounding factor of cardioactive treatment.
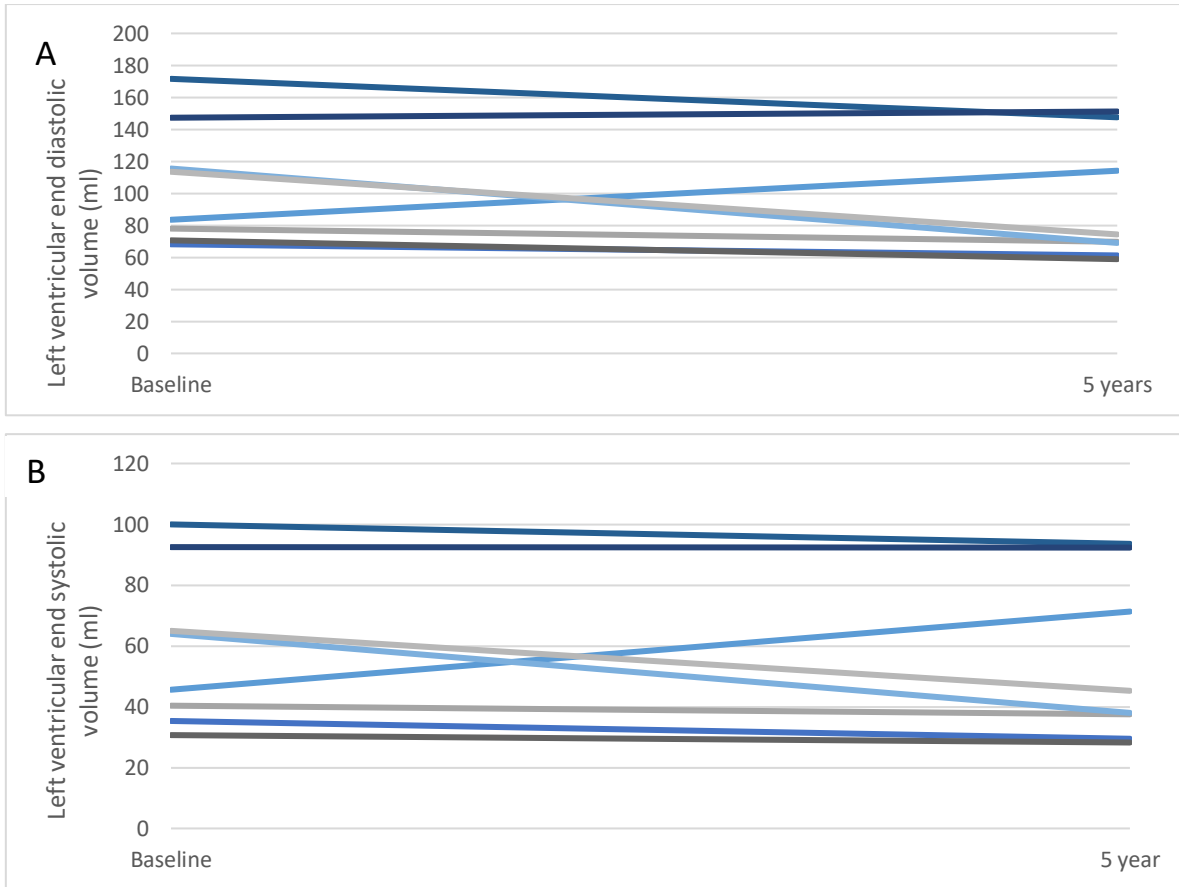
Figure 44. Line graphs to show individual trajectories in cardiac indices over five year follow up: A) Left ventricular end diastolic volume (LVEDV), B) left ventricular end systolic volume (LVESV). No significant differences were demonstrated in any of the cardiac indices over the five years, this may be due to small sample size or due to the confounding factor of cardioactive treatment.
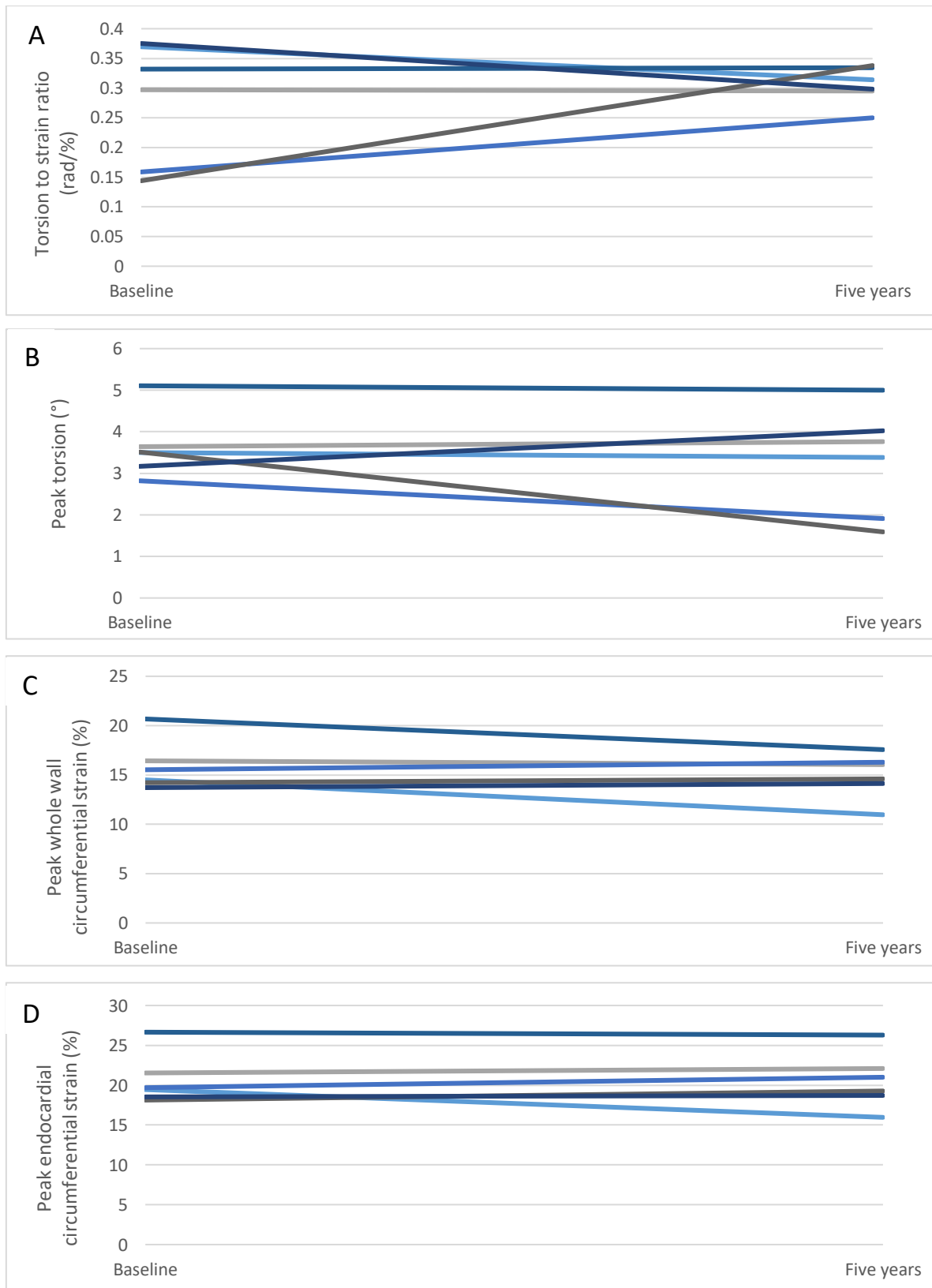
Figure 45. Line graphs to show individual trajectories in cardiac tagging indices over five year follow up: A) Torsion to strain ratio (TSR), B) Peak torsion (PT), C) Peak whole wall circumferential strain (PWWS), D) Peak endocardial circumferential strain (PECS). No significant differences were demonstrated in any of the cardiac indices over time, this may be due to insensitivity as an outcome measure, small sample size, or confounding factors such as cardioactive treatment.

Chapter 8: Discussion

8.1 Discussion

The work contained in this thesis has advanced the knowledge of how quantitative MRI can be used to examine different aspects of the pathology of muscular dystrophies. This thesis has expanded upon existing knowledge by applying the established quantitative measures of Dixon FF, ECV and cardiac tagging to muscular dystrophy cohorts over an extended period. A novel method of quantifying dystrophic muscle fibrosis *in vivo* was also investigated, as well as exploring acceleration of acquisition of cardiac indices. For outcome measures of early-stage pathology in muscular dystrophies (i.e. fibrosis, fatty transformation) to be utilised in future therapeutic trials, they must be compared to existing functional assessments. A particular focus of this work has been comparing existing outcome measures and demonstrating where new techniques are more sensitive to disease progression.

8.2 Quantification of fibrosis - Use of EP3533-enhanced magnetic resonance imaging to quantify fibrosis

EP3533 has been utilised to accurately stage fibrotic disease in several non-muscle studies (Helm et al., 2008, Caravan et al., 2013, Fuchs et al., 2013, Polasek et al., 2012). Experiments described in Chapter 4 are the first to use this agent for the quantification of fibrosis in skeletal muscle, and to take this further to assess EP3533 as an outcome measure after deployment of therapy. Although a promising therapeutic avenue, clinical trials of anti-fibrotics in muscular dystrophies have had mixed results (Buyse et al., 2015, Kirschner et al., 2010, Raman et al., 2015, Udelson et al., 2010). A reliable, sensitive, and non-invasive outcome measure which can directly quantify fibrosis within skeletal muscle has great potential to fully assess therapeutic response in both animal experiments and ideally human clinical trials. In muscular dystrophies, native T1 and T2 weighted scans demonstrate increases in signal intensity in areas of disease activity without use of contrast enhancement, though this largely reflects oedema and fat replacement, and distinction between these and fibrosis is not readily possible and currently unreliable (McCully et al., 1992, McIntosh et al., 1998, Dunn and Zaim-Wadghiri, 1999). In this study, no significant differences were detected between *mdx* and BL10 groups using pre-contrast (baseline) R1 values in any of the muscles (p=NS). However EP3533 was able to demonstrate significant differences between *mdx* and BL10 groups,

which correlated strongly with fibrosis, as opposed to other disease processes. The specificity of EP3533 to collagen would be a particular strength when evaluating an anti-fibrotic treatment.

8.2.1 EP3533 and quantification of fibrosis in muscle

In Chapter 4 the degree of correlation of EP3533-based R1 change to histological measures of fibrosis was lower than some of the results seen in previous studies using EP3533 (Fuchs *et al.* r=0.89, p=NG), (Caravan *et al.* SNR to hydroxyproline r=0.72, p=NG). Previous studies showed strong linear correlation between signal change using EP3533 and *ex vivo* measures of fibrosis (Helm et al., 2008, Caravan et al., 2013, Farrar et al., 2015, Fuchs et al., 2013, Polasek et al., 2012). In both experiments in Chapter 4 measuring fibrosis via *ex vivo* quantification, the strongest correlation was seen between *ex vivo* measures and R1 change in the GCN muscle (Chapter 4 - Section 2 r=0.83 p=0.001, Section 3 r=0.84 p<0.001). Although GCN showed the strongest correlation it did not have the greatest level of fibrosis in *ex vivo* quantification. This may be explained by ROI positioning or slightly higher blood flow to this muscle during the scan.

Previous studies have compared their findings using EP3533 using an isomer of EP3533 which does not display the same degree of affinity to collagen (EP3612) (Helm et al., 2008, Polasek et al., 2017b). Gd-DOTA was selected as a control in the second of the experiments in Chapter 4 as it is currently used to prognosticate and delineate fibrosis in clinical practice thereby giving the experiment greater external validity (Kim et al., 2000, Wu et al., 2008a). Unlike EP3533, Gd-DOTA was unable to show any significant differences in R1 change between *mdx* and control groups, or any significant correlation to *ex vivo* measures of fibrosis (p=NS); EP3533 can quantify fibrosis where the probe currently used in clinical practice cannot. Non-specific gadolinium probes are extracellular and only taken up into muscle fibres when muscle damage has occurred (Amthor et al., 2004). A non-specific gadolinium probe has been investigated before in dystrophic human skeletal muscle with only the TA showing significant enhancement post-exercise (Garrood et al., 2009). A control probe would ideally be structurally similar to EP3533 to prove the signal change demonstrated is due to the affinity of EP3533 to fibrosis. If the probes are not structurally similar then bias is introduced. Comparing to a non-structurally similar probe means that a change in signal intensity may be due to delayed washout time of the peptide-based probe rather than true affinity to a target molecule. The contrast probe EP3612 would be better a control to prove the signal change demonstrated was due to affinity to fibrosis however this was not available for use in these experiments.

8.2.2 Fibrosis in *mdx* mice

Prior studies have identified that the most fibrotic muscle in *mdx* mice is the diaphragm, however it is not possible to accurately image this muscle quantitatively due to its size and shape (van Putten et al., 2012, Carlson, 2014, Turgeman et al., 2008). *Ex vivo* measurements of fibrosis in all three experiments confirmed a significant difference between all muscles in the older BL10 and untreated *mdx* mice. Taking all measurements of the extent of fibrosis from muscles into account, MT quantification and hydroxyproline correlated to a significant degree (Chapter 4 - Section 2 r=0.64 p=0.00004, section 3 r=0.57 p<0.001). An exact correlation is not expected, as Masson's trichrome averages cross sections of muscle, and may exclude focal fibrosis. The levels of fibrosis seen in these experiments were comparable to values reported by others (Pistilli et al., 2011, Graham et al., 2010, Cohn et al., 2007), although *mdx* mice can vary widely in subject age and disease severity. Other studies using MT to assess fibrosis have suggested results similar to our findings in cardiac fibrosis; values range from 0-2% in BL10 and 5-8% in *mdx* mice (Cohn et al., 2007, Au et al., 2011). The hydroxyproline assay has been criticised for insufficient specificity, sensitivity, reproducibility and accuracy (Caetano et al., 2016). The hydroxyproline assay is time consuming and involves a multi-step laborious method through which errors can occur (Ignat'eva et al., 2007, Caetano et al., 2016). In both section 2 and 3, quantification of fibrosis through MT staining was shown to correlate significantly and strongly with the amount of hydroxyproline in cardiac, GCN and TA muscles in 40 week old mice (Table 5). In the halofuginone experiment, R1 change at post-treatment scan demonstrated weak correlation to hydroxyproline quantification, this was however statistically significant in three out of the four muscles (Table 10). Issues with the hydroxyproline assay may have led to a weaker correlation with R1 change in the third experiment. More accurate, and less laborious, methods of fibrosis quantification should be considered in the future, such as computer-assisted histomorphometric analysis (Perini et al., 2015, Caetano et al., 2016) or image intensity analysis of Western blot (Taylor et al., 2013, Huebner et al., 2008).

8.2.3 R1 change following EP3533 administration

Timing of R1 change was selected based upon the results of the dynamic SNR change in cardiac muscle with the greatest change in EP3533 seen at forty minutes (Figure 14). The timing of this increase correlated well with previous cardiac-related EP3533 experiments (Caravan et al., 2007). No previous studies have investigated EP3533 in skeletal muscle therefore the timing of measurements of R1 change was taken as the point of signal plateau in the pilot experiment at seventy minutes (Figures 12 and 13).

Comparing the findings of Chapter 4 to other previous studies in terms of the magnitude of R1 change demonstrates that the difference in R1 value from pre-treatment to post-treatment scans was smaller than was reported in studies using EP3533 in other disease models (Fuchs et al., 2013, Polasek et al., 2012). Suggesting there may be a linear relationship between the amount of fibrosis in tissue and the degree of EP3533-R1 change. In order for a contrast agent to exhibit visually observable contrast, it is estimated that a change in relaxation time of at least $0.5s^{-1}$ is required (Caravan, 2006). EP3533 did not demonstrate this degree of change in the *mdx* mouse in these experiments so the difference was not visually evident. A greater change in R1 may have been seen in older mice although these were not selected as previous studies using younger mice had shown a more significant treatment effect (Turgeman et al., 2008).

Considering the potential for use of EP3533 in clinical trials, humans exhibit a greater degree of fibrosis and this may lead to an increase in R1 change which may be more readily visualised (Pessina et al., 2014a). While gadolinium-based contrast probes are widely used in clinical practice, to date no peptide-enhanced gadolinium probes have been licenced by either the European Medicines Agency or the Food and Drug Administration in the United States. Gadolinium-based probes are associated with complications such as local tissue toxicity and nephrogenic systemic fibrosis. Studies have also shown accumulation of gadolinium in the brain (Neeley et al., 2016). The European Medicines Agency have approved the use of certain non-specific gadolinium agents at the lowest possible dose to provide enhancement and when unenhanced scans could not be used instead (European Medicines Agency, 2018). Due to the delays in washout time and potential for gadolinium toxicity in different tissues, targeted gadolinium agents will need extensive preclinical and subsequent clinical studies to demonstrate their safety profile prior to use in humans. In muscular dystrophies there are no specific contraindications to gadolinium enhancement, there are issues limiting MRI use in this cohort such as scoliosis and reduced respiratory reserve on lying supine.

8.2.4 Validity of the halofuginone experiment

Previous murine studies have established the efficacy of halofuginone in reducing fibrosis in *mdx* mice, with clinical trials of halofuginone ongoing (Clinical Trials.gov, 2018c, Huebner et al., 2008, Turgeman et al., 2008). Turgeman *et al.* demonstrated a reduction in collagen as shown by quantification of sirius red staining, the number of central nuclei, and areas of degeneration in treated mice; suggesting less muscle fibre damage (Turgeman et al., 2008). Turgeman *et al.* also

suggested that there was enhanced motor coordination, balance and cardiac muscle function seen in treated mice, suggesting significant reduction in muscle injury (Turgeman et al., 2008). Huebner *et al.* used two treatment lengths of up to 10 weeks in *mdx* mice of an advanced age (32-36 weeks) (Huebner et al., 2008). Both studies suggested that there was a significant reduction of collagen in the halofuginone receiving groups (Huebner et al., 2008, Turgeman et al., 2008). The efficacy of halofuginone in reducing fibrosis and improving function was reflected in the halofuginone experiment in Chapter 4, with significant differences in *ex vivo* measures of fibrosis in the majority of muscles, and a significant difference between untreated and treated *mdx* mice (Figure 27).

One of the most important aspects of the halofuginone experiment was the PK study; these were performed to provide evidence that halofuginone dose was sufficient to produce a change in fibrosis as expected. The results suggest that the halofuginone administered via the IP route was at detectable levels similar or higher than reported in other studies (Stecklair et al., 2001, de Jonge et al., 2006). The dose of halofuginone (7.5ug/kg) used in this study was selected based on the positive results of previous studies in skeletal muscle (Turgeman et al., 2008). To date, no studies of halofuginone treated *mdx* mice have published PK data. Previous murine studies looking at halofuginone have suggested that doses above 1.5mg/kg were toxic to mice, and that oral routes of administration may not have sufficient bioavailability for detectable serum levels of halofuginone (Stecklair et al., 2001). Stecklair *et al.* reported that mean peak concentration was 386ng/ml using a 1.5mg/kg dose (Stecklair et al., 2001). In this experiment, using a dose 200 times smaller, the peak PK was proportionally higher at 21.2ng/ml after 15 minutes (for comparison this would have been 1.93ng/ml reported by Stecklair *et al.,* assuming a linear dose to serum PK relationship). Taking into account the lower administered dose, the area under the curve for this experiment was proportionally almost ten times higher, at 913.68ng/ml/min compared to 99.37ng/ml/min (Stecklair et al., 2001). Serum PK levels of halofuginone were not detectable after 8 hours (Figure 21), which is longer than the 3 hours reported by Stecklair *et al.* (Stecklair et al., 2001). Although not the remit of this study, organ PK studies would give more definitive evidence of the concentration of halofuginone in tissue, and are therefore likely to have the previously described effect (Turgeman et al., 2008, Huebner et al., 2008). The significant differences in muscle fibrosis on *ex vivo* quantification between treated and untreated *mdx* mice provides further evidence of efficacy of the halofuginone administered in this experiment.

8.2.5 Use of EP3533 to measure longitudinal disease progression

Currently the only validated way to quantify fibrosis in human skeletal muscle is via muscle biopsy (Sardone et al., 2018). Muscle biopsy is invasive, risks sampling error and includes the risk of a general anaesthetic in patients with reduced respiratory function. EP3533, by contrast, is able to measure change in skeletal muscle fibrosis over time in a relatively non-invasive manner. Previous studies have focussed on whether EP3533 can stage or quantify progression of induced disease (Caravan et al., 2013, Fuchs et al., 2013). Farrar *et al.* looked at response to Rapamycin post-bile duct ligation, their findings suggested that EP3533 was able to distinguish between treated and untreated groups (p<0.001) (Farrar et al., 2015). In contrast to the halofuginone experiment, they found that the magnitude of EP3533-induced signal change was significantly different between these groups. Magnitude of R1 change was not significantly different between the treated and untreated *mdx* groups (Tables 8 to 9); however the difference between R1 change in the pre-treatment to post-treatment scan was significantly different (Table 10). As seen in humans with muscular dystrophy, *mdx* mice demonstrate individual variation in fibrosis. This may explain why it was the *change* in R1 value from pre-treatment to post-treatment which demonstrated a significant difference between the treated and untreated groups (Spurney et al., 2009, Grounds et al., 2008).

Automated segmentation of skeletal muscle boundaries has been attempted in computerised tomography (van Vugt et al., 2017), but there are no software programs currently validated for use in MRI. Difficulties in automated ROI imaging are due, in part, to the small degree of difference in signal between muscles and their surrounding fascia. Automated cardiac analysis is possible due to the signal difference between the intraventricular blood and cardiac tissue (Huang et al., 2018). In the EP3533 studies, ROIs were drawn by hand using software programs. This can introduce a small degree of subjectivity to muscle analysis, particularly when comparing highly fat replaced muscles or small muscles in cross section. In the halofuginone experiment, inter-muscular and inter-observer variation was seen in R1 change at all time points. ROI analysis was more difficult in the quadriceps and the hamstrings, as these are composite muscle groups with the external borders less defined. ROIs of composite muscle groups include fascia and blood supplies, which may also have contributed to variability within the results. Difficulties in drawing ROIs to encompass these muscles may have led to a less significant correlation to MT and hydroxyproline quantification (Table 11), compared to the GCN and TA muscles.

Efforts to standardise preclinical trials using *mdx* mice have suggested several standardised methods of assessing treatment response. Spurney *et al.* compared several potential treatment outcome measures in female *mdx* mice, first comparing *mdx* to control, then assessing the degree

of change required to reach statistical significance of various outcome measures. The results suggested several measures demonstrated unacceptable variability or were insufficiently sensitive to disease change. In the Halofuginone experiment, EP3533-enhanced R1 change was assessed for responsiveness with the TA and GCN, giving mid-range SRM values (0.56, 0.48 respectively). The SRM was lower in the HMS and quadriceps (both 0.36). This suggests that there is a reasonable level of responsiveness to change in value in response to treatment, in at least two of the muscles, using this method.

8.2.6 Correlation of EP3533-enhanced R1 change to functional measures

MRI-based studies have suggested that there are no significant differences between *mdx* and BL10 mice in LV indices (LVEF and LVM) even at two years of age (Cohn et al., 2007). Opposing studies using echocardiogram have suggested that LV indices (LVM and fractional shortening) can be significantly different in *mdx* mice as early as 42 weeks of age (Quinlan et al., 2004). These differences could be due to many factors, such as amount of exercise, and heterogeneity of *mdx* mice. Right ventricular dysfunction in *mdx* mice has been reported by Quinlan *et al.,* who reported that *mdx* mice had increased right ventricular fibrosis and that progression of fibrosis was similar to the left ventricle (Quinlan et al., 2004). A study looking at the effect of beta blockers on *mdx* heart function showed that there was no difference between control and *mdx* groups in LV indices at 24 weeks, but that right ventricular ejection fraction was significantly lower in the latter group (Blain et al., 2013). Our results showed that RVEF was the only cardiac functional measure significantly lower in the *mdx* mouse and that the RVEF correlated inversely to a significant degree with both *ex vivo* measures of fibrosis (MT quantification r=-0.70, p=0.01, hydroxyproline assay r=-0.72 p=0.008 (Figures 19 and 20). Further to this, EP3533-derived R1 change correlated strongly to RVEF (r=-0.83 p=0.006). Measurement of the R1 change is based upon ROI selection within the left ventricle, as the size and shape of the right ventricle make this impracticable. The strength of the correlation between R1 change and RVEF lends support to the possibility of a proportional increase in fibrosis between left and right ventricles in *mdx* mice, as suggested by Quinlan *et al* (Quinlan et al., 2004). It was unclear why LVEF was not significantly different in spite of the EP3533-derived signal increase, suggesting an increase in fibrosis; this may be due to compensatory mechanisms. Alternatively, right ventricular dysfunction may be disproportionally affected by the increase in fibrosis of the diaphragm affecting venous return to the heart and increase right ventricular afterload due to hypoxia-induced pulmonary arteriolar vasoconstriction.

In murine experiments several standardised assessments have been developed to measure motor function and strength in a reliable way (Tinsley et al., 2014, Spurney et al., 2009, Treat NMD, 2016). Existing experimental measures of force may be subjective, and musculature is significantly different from humans in terms of mechanism of movement; external validity may be reduced due to different compensatory mechanisms employed by both species (Hu et al., 2017). Previous studies looking at halofuginone in *mdx* mice have suggested that there were significant improvements in functional assessment, including exercise endurance and exercise-induced damage repair (Huebner et al., 2008, Turgeman et al., 2008). In Chapter 4, skeletal muscle function was assessed using two and four limb myometery (grip strength testing) (Table 6). Grip strength tests are most akin to quantitative muscle assessment in humans (McDonald et al., 2013). Grip assessments have shown significant differences between control and *mdx* mice (Spurney et al., 2009). In the results of Chapter 4, the weight-adjusted two limb assessment results correlated more significantly to R1 change (r=-0.33 p=0.004), and demonstrated a significant difference between untreated and treated *mdx* groups (Figure 28). The four limb assessment was unable to demonstrate a significant difference between the untreated *mdx* and the BL10 groups. In contrast to these results, Huebner *et al.* did not report a significant difference between halofuginone treated *mdx* mice and controls in grip assessment (Huebner et al., 2008). This difference may be due to the smaller group sizes used by Huebner *et al.* (n=5) (Huebner et al., 2008). As with functional outcome measures in humans, other factors such as cognition, stress and motivation can be confounding variables (Grounds et al., 2008). In humans with DMD, quantitative MRI such as Dixon FF measurement has been shown to have high levels of correlation to the 6MWT (r=-0.65, p<0.001), as well as other functional assessments (Fischer et al., 2016, Wokke et al., 2014b, Willcocks et al., 2016a, Willcocks et al., 2017). The correlations seen in this experiment were lower than that of Dixon FF in humans. Any future evaluation of efficacy of EP3533-induced R1 change in clinical trials should therefore be compared with Dixon FF and other MRI measures such as cCSA (Fischer et al., 2016, Akima et al., 2012). The four limb assessment was expected to correlate more strongly than the two limb to MRI measures of fibrosis, as it included the hind muscles in the assessment. The weak correlation seen here may be due to the assessment taking into account strength from other muscles not selected as regions of interest. The two limb assessment was only able to assess forelimb skeletal muscle, and was therefore only an indirect measure of fibrosis in hind limb skeletal muscle. The relatively weak correlation between function and EP3533-induced R1 change may be due to the non-linear development of fibrosis throughout muscle, as seen in other human and murine studies (Vohra et al., 2017, Arpan et al., 2012, Gutpell et al., 2015).

8.2.7 Conclusions: EP3533-induced R1 change as an outcome measure in muscle of *mdx* mice

The experiments performed in Chapter 4 have been the first to examine use of EP3533 in muscle of *mdx* mice. The results support several conclusions: firstly, that EP3533-induced R1 change at 70 minutes can be used to reliably detect differences between older age-matched *mdx* and control mice in the TA, GCN, hamstrings and the heart. Secondly, that EP3533-induced R1 change correlated to a significant degree with *ex vivo* measures of fibrosis in the same muscles. Finally, there was a significant overall correlation between EP3533-induced R1 change in both measures of heart and skeletal muscle function.

Less clear was whether EP3533 can be used to successfully quantify disease progression over time. Absolute R1 change values were not significantly different between groups at either pre-treatment or post-treatment. Comparison of the difference in R1 change at 70 minutes from baseline to follow up scan did show significant increases in the untreated *mdx*, which were not evident in the treated *mdx* group.

There is therefore potential for EP3533 to be used as an outcome measure for clinical trials, though little is known of the safety profile of peptide-based gadolinium agents. Further preclinical studies are required to provide safety data findings used to inform a future application for registration of potential human trials before this agent can be used as an outcome measure or in clinical practice.

8.2.8 Limitations of EP3533-induced R1 change as an outcome measure in muscle of *mdx* mice

As with all animal studies, there are questions over the detailed translation of findings to the clinical disease, which relies on imperfect animal models. A serious flaw in the *mdx* mouse is the absence of one of the hallmarks of muscular dystrophies, fatty transformation of skeletal muscles. It is not possible to ascertain how other measures of disease progression, such as FF, relate to EP3533-induced R1 change; which is particularly important in light of the high levels of fatty transformation in human dystrophic muscle. Compared to other animal models that have investigated EP3533, there are relatively small amounts of fibrosis present in skeletal *mdx* mouse muscle. The mild phenotype of *mdx* mice may have contributed to a relatively small treatment effect and reduced the significance of our findings; larger scale murine or other animal model studies with treatment over prolonged periods may be required. Humans with DMD have larger volumes of collagen and may be more likely to have proportionally higher signal using this probe. Alongside FF

measurement, using EP3533 as an outcome measure could provide significant and sensitive insight into disease progression.

Little is known about the potential safety profile of EP3533, this needs to be explored extensively prior to registration for human trials and subsequent licencing application.

8.3 Quantification of adipose tissue - quantitative MRI in skeletal muscle in limb girdle muscular dystrophy type R9

Whilst EP3533 has shown promise in quantification of fibrosis in skeletal and cardiac muscle, it is important to consider that this is only on aspect of the pathology of muscular dystrophy. In humans, adipose replacement of skeletal muscle is an important aspect of pathology in muscular dystrophies. Non-invasive imaging of muscle fat replacement has been shown to correlate to disease progression and functional assessments in conditions such as the LGMD (Willis et al., 2014, Willis et al., 2013, Diaz-Manera et al., 2018), DMD (Schmidt et al., 2018, Ricotti et al., 2016) and BMD (Fischer et al., 2016).

Research into LGMDR9 has been increasing, with several putative therapies showing promise in ameliorating LGMDR9 *in vivo* and *in vitro* (Qiao et al., 2014, Stevens et al., 2013, Richard et al., 2016, Svahn et al., 2015). Due to the likelihood of upcoming human trials of various promising agents, a European neuromuscular centre workshop addressed the trial readiness of LGMDR9 (Richard et al., 2016), highlighting the need for a large scale longitudinal study, with an array of outcome measures (Richard et al., 2016). The results of the study detailed represent the longest multicentre natural history study of LGMDR9 to date. The results have several important findings which are relevant to developing outcome measures for clinical trials into treatments for LGMDR9. These results provide support for the Dixon technique as an early outcome measure to show effects on disease progression. The results also identified the standardised physical outcome measures which significantly changed over a six year period.

8.3.1 Dixon fat fraction and quantitative MRI in skeletal muscle in LGMDR9

The Dixon technique has been established as a sensitive measure of skeletal muscle disease progression in muscular dystrophies (Fischmann et al., 2013, Ricotti et al., 2016, Wren et al., 2008, Gaur et al., 2016, Hollingsworth et al., 2013a, Willcocks et al., 2016b, Willis et al., 2013, Fischer et al., 2016). In a slowly progressive condition such as LGMDR9, a highly sensitive outcome measure is required for clinical trials, unless the effect size of an intervention is very high. Functional measures may not significantly change except over prohibitively long periods. In Chapter 5, the use of FF calculation demonstrated that over six years, all muscle groups significantly increased in percentage of fat replacement (Table 15). Comparing individual muscles, the TA (median 7.1%) was relatively spared, with the most fat infiltrated muscle being BFLH (median 78.6%) (Table 15). The median fat replacement per year was greatest in the lateral GCN (1.7%), ST (1.3%), Gr (1.3%) and

VL (1.3%) muscles (Table 15). The highest composite muscle changes over six years were in the triceps surae (12.5%). Comparable rates of fat replacement were seen in several muscles, including TA (Willis *et al.* -0.1%, six year follow up 0.2%) and lateral GCN (Willis *et al.* 1.4%, six year follow up 1.7%) (Table 17).

The Dixon technique for FF calculation had a high degree of inter-rater reliability, as shown by Bland Altman analysis (Figure 29). Wide range of fat replacement was demonstrated in several muscles and muscle groups; this may be a sign of variable involvement between participants, or due to ROI placement because of difficulty in identification of the borders of the muscle, in those heavily fat replaced (Figure 32 and Table 12).

To increase the power and reliability of the Dixon technique as a biomarker, muscles can be selected for analysis over the follow up period. Such muscles need to be easy to identify, with high levels of interrater reliability. Muscles also need to be progressively affected from baseline to follow up, and it is important to consider the variability of involvement of the muscle between participants. Following a database lock therapeutic trials plan to release interim results during a long term trial after a year or more of follow up. Such publications may be used to justify further studies into a treatment. Ideally any selected muscle should demonstrate a significant change over a short period. Willis *et al.* identified nine muscles demonstrating significant change over one year; four were suggested to be appropriate targets for analysis (Willis et al., 2013). The muscles selected were, proximally, the RF, VL, Gr, and, distally, the medial GCN. Over a six year period, the RF was not appropriate as this muscle had the most outliers, which may be due to difficulties in ROI placement. SRM values were above 0.8 in all muscles, with the exception of the BFSH (0.53), and the TA (0.67). There were several highly significant p values coupled with high SRM values, which suggests that to maximise power the following muscles should be targeted for analysis: the VL (0.92), Gr (1.04), and Sar (0.98). In the lower leg both of the gastrocnemii muscles should be included (lateral 0.91, medial 0.95). Other thigh muscles, including the BFLH, ST and SM, were not suitable in spite of high SRM values (0.81, 0.83, and 0.90 respectively). These muscles showed high fat fractions at baseline; therefore it is likely that therapeutic effects would be reduced. High levels of fat content at baseline increased difficulty and reliability of ROI placement (Figure 33). The VM, BFSH, and remaining calf muscles (PL, Sol, and TA) were less suitable endpoints due to the lack of significant difference at one year, thereby excluding interim analysis. Other composite muscle groups such as the averaged thigh (1.20), averaged lower leg (1.28) and averaged triceps surae (1.25) had high SRM values, similar to the value of the target muscle group (1.23). Therefore, these composite measures may also have utility as a powerful outcome measure.

Lokken *et al.* suggested that in LGMDR9, a lower cCSA is found compared to controls, but with preserved ratio between the cCSA and force (Lokken et al., 2016). Chapter 5 did not aim to evaluate this relationship, and is unable to, due to the physical function tests which were based on those done six years previously to allow for long term comparison. For each muscle group the SRM for the cCSA was smaller, with a less significant p value than the FF, which may indicate that variability in the CSA within the group outweighed the smaller changes in FF (Table 16). cCSA has been previously shown to correlate to measures of strength in muscular dystrophies (Lokken et al., 2016, Wokke et al., 2014b); however our results suggest that cCSA is a less sensitive endpoint than FF quantification in the LGMDR9 cohort.

8.3.2 Functional outcome measures in LGMDR9 over six years

Compared to functional assessment, MRI is criticised as not being as clinically relevant to the patient. If MRI results were used in isolation as an outcome measure, there is a risk that improvements may not necessarily benefit the patient in terms of desirable functional ability or measures of health. The European Medicines Agency has stipulated that therapeutic trials into neuromuscular diseases include measurements of movement that affect quality of life (Richard et al., 2016). For quantitative MRI to be accepted as a primary outcome measure, it is important for the measurements to provide an extra dimension that isn't provided by other cheaper, quicker tests. The advantage of using FF progression as an outcome measure is that it is more sensitive to slowly progressive disease changes, as seen in LGMDR9 (Richard et al., 2016, Willis et al., 2013). The results of this thesis and that of Willis *et al.* suggested that the Dixon technique can reliably detect changes in leg muscles over one and six years in LGMDR9. None of the skeletal muscle functional assessments demonstrated a significant difference over one year (Willis et al., 2013). Over six years all of the timed muscle function tests demonstrated disease progression (Table 13). Of the hand-held myometry tests, only hip adduction significantly declined. The 6MWT and the 10MWR assessments had high SRMs (-0.85 and -1.02 respectively); other timed assessments had lower SRM values <0.5. Two participants improved their speed for the 10MWR assessment over six years, though both had a reduction in their 6MWT distance. Willis *et al.* found that in one year, the median 6MWT distance improved from 312m to 353m – possibly due to learning effects, patient motivation or motor strategy adaptations (Hamilton and Haennel, 2000, Guyatt et al., 1985, Wu et al., 2003, Willis et al., 2013, Alfano et al., 2014). Over six years, the 6MWT distance significantly declined; six participants became non-ambulant. All timed functional assessments demonstrated a significant decline but only the 6MWT and the 10MWR velocity had SRM values of >0.5 (Table 13).

Four participants improved their distance (mean increase 68.8m ±50.3). These participants demonstrated FF increase of at least 1% in the majority of the 20 muscle groups and of the composite groups studied (15/20 groups for 1 participant, 19/20 groups for 2 participants and all groups for 1 participant). This shows that quantitative MRI can demonstrate disease progression in individuals where a physical function test cannot. Looking at the increase in FF of the two participants that improved in their 10MWR test velocity, one had >1% increase in all muscles, and the other had only one muscle with >1% increase. The differences in the FF increase and between the results of the two functional tests (6MWT and the 10MWR) may further highlight the participant dependent factors of the functional tests, i.e. effort or fatigue. In contrast to DMD studies (McDonald et al., 2013), there was no clear cut-off in distance walked at baseline, which could predict non-ambulation in the LGMDR9 cohort at six years (Figure 30). This is likely due to the variability in rate of progression of weakness.

The only myometry measurement which demonstrated a significant decline over six years was hip adduction. In DMD, myometry measurements may be predictive of decline, though they are not always significant even over two years (McDonald et al., 2013). The timed tests lack the sensitivity to detect the slowly progressive weakness of LGMDR9 over one year (Willis et al., 2013).

Forced vital capacity (FVC) was the only functional assessment significantly reduced over both one and six-year time periods (Table 13) (Willis et al., 2013). The annual median FVC decline in the sitting position was -2.6% annually, with -1.9% median annual decline when in the supine position. This is less than reported elsewhere, which is perhaps explained by the differing cohort ages (Poppe et al., 2003, Willis et al., 2013). Respiratory muscle involvement was only indirectly linked to skeletal muscle involvement, but as a comorbidity may have led to a reduction in functional assessments.

As a potential clinical trial outcome measure, the 6MWT and the 10MWR were the only functional timed assessments relating to skeletal muscle, demonstrating a significant difference over six years which included all participants at baseline. The 6MWT, 10MWR, chair rise, stair ascend, and stair descend tests are important to include as outcome measures in future trials investigating LGMDR9 cohorts. These tests were also graded to show whether participants were relying on compensatory methods to assist with the test. In all assessments except the stair ascend, the grading had significantly decreased over six years, implying an increase in compensatory measures to perform the test (Table 14). Such tests of leg function rely on ambulation; upper limb measures and multi-domain tools may be able to show disease progression after this point (Mazzone et al., 2009, Mayhew et al., 2013a).

The NSAA demonstrated a significant reduction in total score over six years (p=0.04). As only ten participants underwent NSAA, this precludes definitive conclusions or more detailed analysis. The results of the ten participants who underwent the NSAA did demonstrate wide differences in loss of function over six years. This variability may have been due to the heterogeneity of disease progression, or merely to higher losses recorded in those with more function at baseline; i.e. more function to lose (Figure 31).

8.3.3 Subgroup analyses

Gender differences in affected muscles have been identified in the LGMDR9 cohort. Willis *et al.* reported that the Gr was more preserved in males, though there was more fat replacement in the VM compared to females (Willis et al., 2014). At six years the VM continued to have a significantly higher percentage of fat content (Table 20). Timed assessments and myometry results were similar between genders, with females only performing significantly better on the 10MWR (p=0.02). The 6MWT results were not significantly different between genders. Due to the small numbers in each group, our results may lend evidence to gender difference, particularly in fat replacement of the VM; however definitive conclusions cannot be drawn. The overall effect of such gender differences on functional assessments is also not certain. Based on previous studies and results of this PhD future clinical trials should not stratify according to gender but a larger scale clinical trial would confirm whether gender differences exist (Willis et al., 2014, Willis et al., 2013).

Non-ambulant patients (n=6) were not significantly different in terms of age, but did have significantly increased fat replacement at both baseline and follow up in the Sol, RF, and VM (Table 21) - three of the most important muscles for walking. It is unclear whether this was causative of loss of ambulation; there was a significant overlap in terms of FF in the muscles of non-ambulant and ambulant participants. One participant had a higher fat fraction in all three muscles than the highest FF of the non-ambulant participants, yet remained ambulant. The increase in fat replacement in these muscles may merely be an effect of the reduced use of these muscles as the patient became less ambulant. However it is important to consider the significant heterogeneity between individuals in this condition, co-morbidities may be a factor in reduced ambulation, with reduced respiratory or cardiovascular drive reducing individual walking abilities (Siciliano et al., 2015). Other compensatory mechanisms such as changes in gait, may be employed by individuals to aid ambulation. Alternatively other muscles may compensate for weakness in the more affected

muscles, heterogeneity in individual muscle weakness can be controlled for using composite muscle measures.

Age correlated significantly with the four hamstring muscles, though not strongly; the 6MWT was the only functional assessment which correlated significantly (p=0.04). The lack of strong, significant correlations suggests that the loss of function may be independent to age and, as seen in other studies, there is heterogeneity in terms of phenotypic progression within participants with the same mutation (Harel et al., 2003, Rivas et al., 2014, Bourteel et al., 2007).

8.3.4 Correlation of fat fraction to functional assessments

Strong significant correlations were seen between the 10MWR, the 6MWT, and FF at both baseline and follow up (Tables 18 and 19). Change in FF over time did not correlate strongly to change in 6MWT or the 10MWR, which suggests a non-linear relationship. The lack of strong correlation to change in FF may be due to the existence of confounding factors such as co-morbidities and compensatory mechanisms. Other functional assessments did not demonstrate strong correlations with FF at baseline and follow up, which may be related to their insensitivity to disease progression, with the majority of assessments unable to demonstrate disease progression over this time period.

8.3.5 Conclusions

The results of Chapter 5 constitute the longest follow up into a LGMDR9 cohort to date, and suggest that FF calculation using the Dixon technique is sensitive to changes over a six year period in all muscle groups. Use of the Dixon technique has several advantages over standardised functional assessments, and can provide useful interim measures of disease progression – not currently possible with functional testing. The results of this study support FF calculation in LGMDR9 clinical trials as a primary outcome measure alongside functional assessments. The results suggested the most appropriate target muscles for analysis alongside composite muscle groups were the vastus lateralis, gracilis, sartorius, and the medial and lateral gastrocnemii. The results suggested that the 6MWT and the 10MWR were the most appropriate functional assessments over six years, and correlated reasonably strongly to FF in individual muscles. Measures of trophicity were unlikely to be useful as outcome measures in the LGMDR9 cohort, even over six years.

8.3.6 Limitations

It is important to acknowledge that these results may underestimate progression of the disease process; the most severely affected individuals were less likely to have returned at six years due to the difficulties in travel. Other limitations included the fact that only one slice was analysed in each subject at a predefined level. Multi-slice analysis could take account of heterogeneity in disease progression. While there were many possible correlations between FF calculations and functional measures, this work concentrates principally on the sensitivity of outcome measures to detect change over time. The studies performed only included participants with homozygous mutations, rather than the more severe form of the condition caused by compound heterozygous mutation. The results of this study is useful to inform clinical trials of LGMDR9 with a homozygous mutation and are not valid for the compound heterozygous cohort.

A drawback of quantitative FF analysis is that it is unable to identify the other main pathology of muscular dystrophies, namely fibrosis. The Dixon technique is able to sensitively and non-invasively detect disease progression; however it is possible that patients may have intra-subject variability in the percentage of fat replacement to fibrosis ratio. Potentially FF calculation could be used alongside contrast agents (i.e. EP3533) to allow quantification of both fibrosis and fat replacement. Although the development of use of contrast agents in this fashion is not expected for a long time due to the need for regulatory approval, use of these non-invasive biomarkers could be especially important in assessing anti-fibrotic therapeutic agents in clinical trials of muscular dystrophy.

8.4 Quantification of fibrosis - Use of extracellular volume in muscular dystrophies

The focus of the studies within this thesis have been quantification of fibrosis and adipose replacement of skeletal muscle. Although EP3533 was considered in mice to quantify overall cardiac fibrosis, comparing this to global measures of function and *ex vivo* measures, the focus was on the heart as a whole. In humans, cardiac dysfunction in muscular dystrophies can be insidious, with regional cardiac dysfunction and fibrosis difficult to detect. Chapter 6 aimed to assess how ECV could be used to quantify fibrosis and demonstrate cardiac dysfunction non-invasively within BMD and LGMDR9 cohorts, comparing this to traditional measures of cardiac pathology.

ECV has been investigated as a biomarker in both muscular dystrophy and other conditions causing dilated cardiomyopathy (Florian et al., 2014b, aus dem Siepen et al., 2015, White et al., 2013, Olivieri et al., 2017). This study is the first to investigate use of ECV in a LGMD cohort and to report use of cardiac tagging in BMD. The cardiac phenotype of BMD and LGMDR9 shows slowly progressive regional and global cardiac dysfunction. The slow progression requires a quantifiable, sensitive, and non-invasive biomarker for interventional trials and clinical practice. ECV may be useful in predicting regional cardiac dysfunction, though no large longitudinal studies have been undertaken to date. Florian *et al.* performed ECV quantification on two patients with BMD, finding no difference in ECV values over a short follow up of one year (Florian et al., 2014b). The findings of Chapter 6 suggest that ECV may provide quantification on disease progression and regional changes which are not evident with other measures of cardiac dysfunction. Further to this, cardiac studies often consider BMD and LGMDR9 together due to their similar cardiac phenotype (Sveen et al., 2008a, Petri et al., 2015). Differences in torsion and strain measurements between these groups highlight potential mechanistic differences in cardiac dysfunction that may be relevant for future therapy development.

8.4.1 ECV in quantification of segmental fibrosis

Comparing ECV in individuals with cardiac dysfunction to those without demonstrated that ECV was significantly higher in all regions, and globally (Figures 35 and 36). The findings of Chapter 6 were similar to these, with higher average ECV values in lateral segments. A study of a BMD cohort by Florian *et al.* reported that ECV measures were highest in lateral wall segments, ranging from 0.26-0.35 in those with cardiac dysfunction (Florian et al., 2014b). Soslow *et al.* found high ECV values in lateral wall and anterior segments in a DMD cohort (Soslow et al., 2016). The magnitude

of our average regional ECV was lower than these studies, possibly due to the cohorts studied previously being more severely affected (Soslow et al., 2016, Florian et al., 2014b).

8.4.2 Relationship between extracellular volume to late gadolinium enhancement and wall motion abnormalities

Presence of late gadolinium enhancement (LGE) is a negative prognostic factor in muscular dystrophies (Florian et al., 2014a, Hor et al., 2013). Myocardial fibrosis develops diffusely in early-stage disease, potentially lacking the required visible contrast for LGE recognition. Generally, studies have shown a positive correlation between higher ECV values and LGE-positive regions (Collins et al., 2015, Flett et al., 2010, Ugander et al., 2012). Two participants in our study were LGE-positive with corresponding high ECV values (Figure 34). The highest ECV values were found in the basal posterior, basal anterior and the mid-cavity posterior regions. In BMD, the most common LGE-positive areas were the basal region and lateral walls (Florian et al., 2016, Yilmaz et al., 2008, Becker et al., 2016). These LGE-positive areas map to higher ECV values seen in our study in participants with cardiac dysfunction.

Other studies suggest ECV may be raised in LGE-negative segments, suggesting advancing disease progression not detectable by LGE (Florian et al., 2014b, Soslow et al., 2016, Hong et al., 2015). In 5 participants without LGE, there were 22 segments with ECV values ≥0.28 with a corresponding reduced LVEF (<55%).

WMAs are associated with focal fibrosis, restricting regional movement (Cicala et al., 2007). In the general population, WMAs are associated with increased risk of morbidity, and may be present with normal global function (i.e. LVEF) (Cicala et al., 2007). In this study, 5 participants had WMA with a significantly reduced LVEF (43.1% ±7.4), compared to both of those without (50.2% ±6.9, p<0.001). Participants with WMA had a significantly higher basal ECV (0.26 range 0.21 to 0.32), compared to those without (0.24 range 0.21-0.32) (p=0.04). None of those with WMA had LGE-positive segments, suggesting that WMAs may be associated with diffuse rather than focal fibrosis. Four participants without WMA had ECV ≥0.28 in 7 segments. ECV may be able to demonstrate areas of diffuse fibrosis not yet causing WMAs.

8.4.3 Correlation of ECV to measures of cardiac dysfunction

LVEF is the most commonly used measurement of global cardiac function in clinical practice, and as an outcome measure in clinical trials (Florea et al., 2016, Duboc et al., 2005, Bushby et al., 2010b). We observed significant correlation between reduced LVEF and increased ECV in our disease groups. Other studies have observed this in BMD and DCM (aus dem Siepen et al., 2015, Florian et al., 2014b). In 2/6 of the participants with LGMDR9 and an LVEF >55%, 3/24 segments had ECV values ≥0.28. Higher segmental ECV values were found in segments in spite of a normal global function.

Cardiac tagging provides sensitive quantification of regional cardiac dysfunction in muscular dystrophies (Hollingsworth et al., 2013b, Hor et al., 2009). The complicated nature of cardiac muscular architecture means that the tissues contract in multiple planes, allowing compensation for loss of contractility in layers of muscle fibre. Studies have used cardiac tagging with the most common pattern of dysfunction increased PT with reduction in PECS (Hollingsworth et al., 2012, Van Der Toorn et al., 2002, Young et al., 1994). By contrast, Hollingsworth *et al.* demonstrated lowered PT in a LGMDR9 cohort compared to controls (Hollingsworth et al., 2013b). The reduction in PT reflects epicardial dysfunction leading to abnormal transmission of mechanical forces from endocardium to epicardium (Hollingsworth et al., 2013b). Chapter 6 demonstrated significant differences between LGMDR9 and control groups in all measures of strain and torsion (Table 22). Reduced PT correlated strongly with reduced LVEF in the LGMDR9 cohort, suggesting this reduction in PT is directly linked with systolic performance. As demonstrated by Hollingsworth *et al.*, these results suggest that the sub-epicardium is affected in the LGMDR9 cohort (Hollingsworth et al., 2013b). These findings are consistent with Rosales *et al.* who found in a LGMDR9 cohort that LGE is most commonly identified in the epicardium and midwall (Rosales et al., 2011). Increased apical and basal ECV correlated with reduced torsion in both regions in this LGMDR9 cohort. Cardiac tagging is able to demonstrate cardiac dysfunction in the LGMDR9 cohort, with strong correlation to LVEF and ECV values.

To date, no previous studies have reported cardiac tagging in BMD cohorts. Studies of DMD cohorts have suggested that abnormalities of strain and torsion exist and may be present in those with normal LVEF (Hagenbuch et al., 2010a, Hor et al., 2009). In the BMD group, no significant correlations were demonstrated between measures of strain and torsion, ECV values or LVEF. Furthermore, there were no significant differences between control and BMD cohorts in PT, PWWS or PECS (Table 22). However, several indicators of cardiac dysfunction (i.e. reduced LVEF, WMA, and LGE-positivity) were present within the BMD cohort. The differences between the strain and

torsion in BMD and LGMDR9 cohorts suggest that the mechanism of cardiac dysfunction differs between these groups.

8.4.4 ECV in detecting cardiac dysfunction

For the purposes of this thesis, cardiac dysfunction was defined as LVEF <55%, or presence of LGE. Comparison of ECV values between groups demonstrated that global and regional values were significantly higher in the group with cardiac dysfunction (Figures 35 to 36). Segmental analysis revealed that basal posterior, basal anterior and mid-cavity posterior segments were significantly higher in those with cardiac dysfunction. Florian *et al.* suggested that basal segments were significantly higher in those with cardiac dysfunction, defined as being LGE-positive (Florian et al., 2014b). These results suggest a clear increase in ECV values in participants with cardiac dysfunction, providing further evidence of correlation between ECV and disease progression.

8.4.5 Conclusions

The findings of Chapter 6 support ECV as a measure in the assessment of cardiac disease in LGMDR9 and BMD cohorts, alongside traditional measures. ECV was most frequently higher in the basal region. Measures of PT, TSR, PWWS and PECS correlate to cardiac measures in the LGMDR9 cohort, but may have limited utility in the BMD cohort. ECV correlated well with traditional measures of cardiac dysfunction such as LVEF, LGE, and WMA. Additionally, ECV shows high values in segments of participants that would otherwise be considered normal by traditional measures. Alongside other measures, ECV is a potentially useful tool in quantification of fibrosis in muscular dystrophy. Although ECV will not replace traditional measures of global cardiac function, our findings suggest that there is potential for delineation of regional cardiac wall dysfunction.

8.4.6 Limitations

As an initial study of ECV measurement in LGMDR9 and BMD participants requiring intravenous gadolinium administration, the number of participants was small, precluding definitive conclusions, but suggesting further lines of inquiry. Another limitation was the lack of longitudinal data on how ECV varies in the natural history of these diseases, or in response to therapy. Whilst ECV has been shown to correlate histologically to cardiac fibrosis (Flett et al., 2010, Miller et al., 2013, White et

al., 2013, Fontana et al., 2012), potentially ECV may be increased by oedema and inflammation as seen in muscular dystrophies, which may vary over time. ECV therefore should not be used in isolation, but should be used alongside other measures of cardiac dysfunction such as: LGE, cardiac indices calculation, and cardiac tagging.

8.5 Quantification of function - Evaluation of accelerated imaging in quantification of left ventricular indices in the muscular dystrophy cohorts

This thesis has presented a number of studies into how MRI can be used to quantify different aspects of the pathology of muscular dystrophies. It is important to consider the individuals with the conditions and the burden that is placed upon them whilst undergoing these investigations. Due to their difficulties in lying supine and poor respiratory function there are clear reasons for reduction of acquisition times.

Accelerated imaging is one of a number of techniques that have the potential to speed up MRI acquisition and reduce scan burden on participants. The accelerated approach described within Chapter 7 was successful in providing high quality images (Figure 42), which for the purposes of generating cardiac indices demonstrated no significant bias compared to conventional cine imaging. The accelerated method had comparable 95% LOA to other published approaches using forms of compressed sensing (Tables 24 and 25), and was highly reproducible between observers (Table 24). The results of this study provided evidence for this approach in obtaining cardiac indices with high levels of image fidelity and potential to speed up acquisition by a net factor of two. Chapter 7 is the first to report longitudinal data on torsion and strain in a LGMDR9 cohort. The results of the five year follow up portion of this study suggest that CMRI generated cardiac indices and cardiac tagging may be insufficiently sensitive to detect change over this time period, although the small sample size and the confounding factor of the effects of cardio-active medications precludes any definitive conclusions. There were no significant differences detected between the LGMDR9 and BMD cohorts in terms of LVEF or age (Table 23).

8.5.1 Accelerated versus conventional imaging

Using Bland Altman analysis to compare accelerated to conventional images, none of the parameters demonstrated significant or consistent bias. In contrast to this, consistent bias was reported in LVEDV by Vincenti *et al.*; their method underestimating measurement by 9.9mls (Vincenti et al., 2014). Although the lack of significant bias may be considered to be in support of our approach, consistent bias can be corrected prior to reporting, which is not the case with our results.

Bland Altman analysis is unable to indicate whether LOA are clinically significant for a particular test; the clinical significance is dictated by the wider context. For CMRI, arguably the most important measure of function is LVEF. Studies investigating cardiac disease have used

measurements of global function, such as LVEF and fractional shortening, alongside presence of LGE and measurements of cardiac strain, as primary and secondary outcome measures in assessing response to treatments (Duboc et al., 2005, Duboc et al., 2007, Raman et al., 2015, Witting et al., 2014, Leung et al., 2014). In clinical practice the most commonly used measure of function is LVEF. In muscular dystrophies, LVEF has been shown to be most predictive of increased mortality alongside the presence of LGE (Tandon et al., 2015). It is therefore important for any technique aiming to improve the speed of acquisition of cardiac indices using CMRI to be as accurate as possible in reporting LVEF. 95% LOA between the two approaches for LVEF was 5.9%; clinically this may be considered a significant degree of error. Patients could therefore be under or over estimated by 5.9% using the accelerated approach. Comparing accelerated CMRI against echocardiogram in the measurement of LVEF has been suggested to have much wider LOA (95% LOA 12.3%) compared to CMRI (Bellenger et al., 2000). Echocardiogram has several advantages over accelerated CMRI, and in the event of an equivocal result a CMRI would be organised to confirm findings. If this also risked over or underestimating LVEF by 5.9%, it would be introducing further uncertainty as to the validity of the test. Studies looking at investigation of the variability of LVEF have estimated beat to beat variability to be as high as 5.8% (Wood et al., 2014). As it is not possible to take the conventional and accelerated acquisitions simultaneously the LOA found when comparing these methods could be wholly or partially due to natural variation which may be more profound in disease states (Wood et al., 2014).

These findings should be considered, too, in the context of other acceleration approaches, including compressed sensing, as shown in 'Table 25'. One of the most recently published articles into this field, Kido *et al.,* used a comparable net acceleration of three (Kido et al., 2016). Kido *et al.* reported bias and LOA for their technique (LVEF 5.2%) which were similar to our study. The other cardiac indices reportedly had similar or slightly narrower LOA (Table 25). Other compressed sensing approaches using k-t Broad-use Linear Acquisition Speed-up Technique (BLAST) and guide-point modelling had wider LOA in cardiac indices, which is likely to reflect the higher net acceleration 5.2-7.5-fold increase (Vincenti et al., 2014, Jaroni et al., 2013).

An alternative approach to reducing subject burden is to not require breath holding during acquisition. Free breathing techniques incorporate motion correction algorithms to allow high quality image acquisition without breath-holding. To date, there have been three studies attempting to clinically validate the use of this technique in obtaining cardiac indices (Usman et al., 2015, Usman et al., 2017, Liu et al., 2017). The results of Chapter 7 provided narrower LOA for LVEF; however wider LOA were present when comparing other cardiac indices such as LVEDV and LVM (Table 25). Free breathing techniques are considered less efficient, with data discarded as a result

of the breathing motion. When combined with compressed sensing, this technique has been able to acquire the full series of short axis slices in approximately two minutes without breath holding. Therefore, free breathing may have an advantage over accelerated imaging as described in this study, but with comparable 95% LOA (Usman et al., 2015, Usman et al., 2017).

Comparison of the results of Chapter 7 with other studies using similar degrees of net acceleration (two fold) showed similar negligible bias between observers (this study: LVEF mean difference 0.4, LOA 0.8 versus Mann *et al.*: mean difference 0.2% LOA 0.8) (Louis et al., 2016). Overall, using compressed sensing with parallel imaging, as described in both of these studies, at net acceleration of two leads to a high degree of agreement between observers (Louis et al., 2016).

8.5.2 Cardiac indices and tagging in LGMDR9 over a five year follow up period

Follow up of CMRI in the LGMDR9 group did not show any significant changes in any of the cardiac indices over the five years (Figures 43 and 44). Sveen *et al.* reported that in their group cardiomyopathy was present in 29% of those with LGMDR9; previously this figure has been reported to be between 10-55%, with a preponderance toward men with the condition (Sveen et al., 2008b, Poppe et al., 2004). At the beginning of our study, 6/8 participants were receiving cardioactive treatments; over the five years this increased to 7/8. This suggests that cardiomyopathy was more prevalent within our group than that found in other studies. Petri *et al.* published the longest follow up study of individuals, with LGMDR9 cohort reporting results from echocardiogram over a nine year period. Over the nine year period, Petri *et al.* reported an annual decline in LVEF of 0.4%, which was statistically significant (p=0.03). This is in line with our results, which had a lower baseline (45.6% versus 59% (Petri et al., 2015)) but declined at a similar rate of 0.44% annually (43.4% after five years, 55% after nine years (Petri et al., 2015)). The reason for lack of a significant change over the five year period could be due to the test being insensitive to small changes over five years, compared to nine years in Petri *et al.* (Petri et al., 2015). More likely, the reason for no significant difference being detected is the small sample size.

Hollingsworth *et al.* (2013) investigated measures of strain and torsion in a LGMDR9 cohort, demonstrating significant decrease in peak torsion compared to controls (3.9° ±1.3), with torsion to strain ratio significantly lower (0.31rad/% ±0.1) (Hollingsworth et al., 2013b). In Chapter 7, over a five year period these measures were not significantly different (Figure 45). The reasons for this may be that these changes were non-progressive or too slowly progressive to detect with these measures. Another reason could be that the study number here was too small to show a significant

change over the five year period. Hollingsworth *et al.* suggested that these measures correlated to LVEF (r=0.93, P<0.001) (Hollingsworth et al., 2013b), which was also seen in this study with LVEF correlating strongly to PT (r=0.81, p=0.01).

None of the cardiac indices demonstrated significant changes over five years, which may be in part explained by using cardio-active treatments. Treatments such as angiotensin converting enzyme inhibitors, beta blockers and angiotensin receptor antagonists reduce afterload, and have been shown to induce ventricular remodelling (Khalil et al., 2001, Yusuf et al., 1992). These medications are recommended in the treatment of dilated cardiomyopathy and cardiac manifestations of muscular dystrophy (Feingold et al., 2017). Duboc *et al.* used angiotensin converting enzyme inhibitors in prophylactic treatment of DMD, finding that these can increase or stabilise LVEF over time (Duboc et al., 2007). As all but one of our participants were receiving cardioactive treatment by the end of the five year follow up, it is likely that these medications had a similar effect of increasing or stabilising the measures of cardiac function. Based on the results of this study, CMRI functional measures and cardiac tagging measures are unlikely to be a useful outcome measure for cardiac disease over a five year time period in this cohort. Potentially, a larger sample, a longer follow up period, or exclusion of participants taking cardioactive medications may have led to significant results.

8.5.3 Conclusions

The technique of accelerated imaging described here demonstrated that it is possible to reduce the time for acquisition and produce images with comparable image fidelity. The technique does lead to a 5.9% limit of agreement in LVEF, which for clinical work may not be acceptable. In the context of other imaging modalities and other approaches to speed up CMRI acquisition, this method was similar in terms of bias and width of the 95% LOA. The accelerated imaging approach may have a role in reducing patient burden during MRI scans in clinical practice, and may potentially be of use in clinical trials detecting disease progression of other neuromuscular conditions. Other techniques, such as free-breathing acquisitions, may provide an alternative way of reducing patient burden during CMRI.

In contrast to DMD, cardiac indices and cardiac tagging measures did not significantly change over a five year period in a LGMDR9 cohort, and may therefore be insensitive to disease progression (Hagenbuch et al., 2010a).

Chapter 9: Conclusions

9.1 Conclusions

This thesis examined how MRI techniques can be applied to quantify aspects of pathology and disease progression in muscular dystrophies. Each chapter looked at how MRI could be used to examine different hallmarks of disease progression. The findings demonstrated that quantitative MRI can be used to show progression of early muscle pathology such as fat replacement, and fibrosis. The most promising method of demonstrating disease progression in humans with muscular dystrophies was using Dixon FF calculation to quantify fat replacement of muscle in LGMDR9. In animal models of muscular dystrophy, imaging of fibrosis with EP3533 also showed promise in demonstrating disease progression. ECV was explored in two types of muscular dystrophy and its' use may show some benefits over conventional outcome measures.

EP3533-enhanced R1 change was shown to be: significantly higher in dystrophic muscles compared to in controls, correlating significantly to functional measures and *ex vivo* quantification of fibrosis. The widely clinically used gadolinium-based probe was unable to demonstrate any difference between disease and control groups. EP3533-enhanced R1 change was able to show response to an anti-fibrotic treatment, relying on the difference in R1 change from baseline to follow up, rather than absolute R1 values. The degree of R1 change was less than seen in other studies probably due to the mild phenotype of *mdx* mice. Human studies of EP3533 will eventually be required to confirm utility of this contrast agent in quantifying fibrosis in muscular dystrophies; more animal studies are required to confirm the safety profile of this contrast agent prior to registration with the relevant regulatory body (i.e. Food and Drug Administration or the European Medicines Agency).

The Dixon FF calculation is well established in imaging of muscular dystrophies, however the knowledge gained here in terms of how this applies to LGMDR9, can now be used to inform power calculations in future clinical trials. FF calculation over a six year time period can be used alongside functional assessments to show disease change and allows for interim analyses.

Regarding cardiac muscle fibrosis, ECV was explored in LGMDR9 and BMD cohorts for the first time. There were significantly higher values for ECV regionally and globally, which was evident in patients with demonstrable cardiac dysfunction and in some without. This suggested that ECV may be able to provide information on areas of regional cardiac dysfunction not evident using other measures i.e. global cardiac function and late gadolinium enhancement. ECV should be examined longitudinally to explore whether it can predict cardiac dysfunction in muscular dystrophies and therefore be used as an outcome measure.

The major challenge to therapeutic trials in muscular dystrophies and a recurrent theme of this thesis, is how difficult it is to demonstrate disease progression over short time periods. Functional assessments have been shown to be relatively insensitive to change. This was reflected in this thesis by the lack of significant difference in CMRI-generated measures of cardiac function and cardiac tagging indices in LGMDR9 over a five year period. The method of accelerating acquisition of cardiac indices demonstrated a lesser degree of variation compared to previous studies comparing echocardiography and a similar degree compared to other reported compressed sensing methods, with a qualitatively good image fidelity.

Quantification of fat replacement, and fibrosis in skeletal and cardiac muscle using MRI as described has been shown to have several advantages over other conventional measures of disease progression.

References

ABD-ELMONIEM, K. Z., STUBER, M. & PRINCE, J. L. 2008. Direct three-dimensional myocardial strain tensor quantification and tracking using zHARP. *Med Image Anal,* 12**,** 778-86.

ABRÀMOFF, M. D., MAGALHÃES, P. J. & RAM, S. J. 2004. Image processing with ImageJ. *Biophotonics international,* 11**,** 36-42.

ADAMO, C. M., DAI, D. F., PERCIVAL, J. M., MINAMI, E., WILLIS, M. S., PATRUCCO, E., FROEHNER, S. C. & BEAVO, J. A. 2010. Sildenafil reverses cardiac dysfunction in the mdx mouse model of Duchenne muscular dystrophy. *Proc Natl Acad Sci U S A,* 107**,** 19079-83.

AKIMA, H., LOTT, D., SENESAC, C., DEOL, J., GERMAIN, S., ARPAN, I., BENDIXEN, R., SWEENEY, H. L., WALTER, G. & VANDENBORNE, K. 2012. Relationships of thigh muscle contractile and non-contractile tissue with function, strength, and age in boys with Duchenne muscular dystrophy. *Neuromuscular Disorders,* 22**,** 16-25.

ALAVERDASHVILI, M., LAPOINTE, V., WHISHAW, I. Q. & CROSS, A. R. 2017. Manganese-Enhanced Magnetic Resonance Imaging and Studies of Rat Behavior: Transient Motor Deficit in Skilled Reaching, Rears, and Activity in Rats After a Single Dose of MnCl(2). *Magnetic Resonance Insights,* 10**,** 1178623X17706878.

ALFANO, L. N., LOWES, L. P., BERRY, K. M., YIN, H., DVORCHIK, I., FLANIGAN, K. M., CRIPE, L. & MENDELL, J. R. 2014. T.P.1: Pilot study evaluating motivation on the performance of timed walking in boys with Duchenne muscular dystrophy. *Neuromuscular Disorders,* 24**,** 860.

AMADO, L. C., GERBER, B. L., GUPTA, S. N., RETTMANN, D. W., SZARF, G., SCHOCK, R., NASIR, K., KRAITCHMAN, D. L. & LIMA, J. A. C. 2004. Accurate and objective infarct sizing by contrast-enhanced magnetic resonance imaging in a canine myocardial infarction model. *Journal of the American College of Cardiology,* 44**,** 2383-2389.

AMERICAN ACADEMY OF PEDIATRICS 2005. Cardiovascular health supervision for individuals affected by Duchenne or Becker muscular dystrophy. *Pediatrics,* 116**,** 1569-73.

AMERICAN THORACIC SOCIETY 2002. ATS statement: guidelines for the six-minute walk test. *Am J Respir Crit Care Med,* 166**,** 111-117.

AMTHOR, H., EGELHOF, T., MCKINNELL, I., LADD, M. E., JANSSEN, I., WEBER, J., SINN, H., SCHRENK, H. H., FORSTING, M., VOIT, T. & STRAUB, V. 2004. Albumin targeting of damaged muscle fibres in the mdx mouse can be monitored by MRI. *Neuromuscul Disord,* 14**,** 791-6.

ANAYA-SEGURA, M. A., GARCIA-MARTINEZ, F. A., MONTES-ALMANZA, L. A., DIAZ, B. G., AVILA-RAMIREZ, G., ALVAREZ-MAYA, I., CORAL-VAZQUEZ, R. M., MONDRAGON-TERAN, P., ESCOBAR-CEDILLO, R. E., GARCIA-CALDERON, N., VAZQUEZ-CARDENAS, N. A., GARCIA, S. & LOPEZ-HERNANDEZ, L. B. 2015. Non-Invasive Biomarkers for Duchenne Muscular Dystrophy and Carrier Detection. *Molecules,* 20**,** 11154-72.

ANDREETTA, F., BERNASCONI, P., BAGGI, F., FERRO, P., OLIVA, L., ARNOLDI, E., CORNELIO, F., MANTEGAZZA, R. & CONFALONIERI, P. 2006. Immunomodulation of TGF-beta 1 in mdx mouse inhibits connective tissue proliferation in diaphragm but increases inflammatory response: implications for antifibrotic therapy. *J Neuroimmunol,* 175**,** 77-86.

ANNERIET, M. H. & BRUCE, M. D. 2007. Diffusion Tensor MRI Assessment of Skeletal Muscle Architecture. *Current Medical Imaging Reviews,* 3**,** 152-160.

ANTHONY, K., CIRAK, S., TORELLI, S., TASCA, G., FENG, L., ARECHAVALA-GOMEZA, V., ARMAROLI, A., GUGLIERI, M., STRAATHOF, C. S., VERSCHUUREN, J. J., AARTSMA-RUS, A., HELDERMAN-VAN DEN ENDEN, P., BUSHBY, K., STRAUB, V., SEWRY, C., FERLINI, A., RICCI, E., MORGAN, J. E. & MUNTONI, F. 2011. Dystrophin quantification and clinical correlations in Becker muscular dystrophy: implications for clinical trials. *Brain,* 134**,** 3544-3556.

ARPAN, I., FORBES SEAN, C., LOTT DONOVAN, J., SENESAC CLAUDIA, R., DANIELS MICHAEL, J., TRIPLETT WILLIAM, T., DEOL JASJIT, K., SWEENEY, H. L., WALTER GLENN, A. & VANDENBORNE, K. 2012. T2 mapping provides multiple approaches for the characterization of muscle involvement in neuromuscular diseases: a cross‐sectional study of lower leg muscles in 5‐15‐year‐old boys with Duchenne muscular dystrophy. *NMR in Biomedicine,* 26**,** 320-328.

ARPAN, I., WILLCOCKS, R. J., FORBES, S. C., FINKEL, R. S., LOTT, D. J., ROONEY, W. D., TRIPLETT, W. T., SENESAC, C. R., DANIELS, M. J., BYRNE, B. J., FINANGER, E. L., RUSSMAN, B. S., WANG, D. J., TENNEKOON, G. I., WALTER, G. A., SWEENEY, H. L. & VANDENBORNE, K. 2014. Examination of effects of corticosteroids on skeletal muscles of boys with DMD using MRI and MRS. *Neurology,* 83**,** 974-80.

ASHFORD, M. W., JR., LIU, W., LIN, S. J., ABRASZEWSKI, P., CARUTHERS, S. D., CONNOLLY, A. M., YU, X. & WICKLINE, S. A. 2005. Occult cardiac contractile dysfunction in dystrophin-deficient children revealed by cardiac magnetic resonance strain imaging. *Circulation,* 112**,** 2462-7.

AU, C. G., BUTLER, T. L., SHERWOOD, M. C., EGAN, J. R., NORTH, K. N. & WINLAW, D. S. 2011. Increased connective tissue growth factor associated with cardiac fibrosis in the mdx mouse model of dystrophic cardiomyopathy. *International Journal of Experimental Pathology,* 92**,** 57-65.

AUS DEM SIEPEN, F., BUSS, S. J., MESSROGHLI, D., ANDRE, F., LOSSNITZER, D., SEITZ, S., KELLER, M., SCHNABEL, P. A., GIANNITSIS, E., KOROSOGLOU, G., KATUS, H. A. & STEEN, H. 2015. T1 mapping in dilated cardiomyopathy with cardiac magnetic resonance: quantification of diffuse myocardial fibrosis and comparison with endomyocardial biopsy. *European Heart Journal – Cardiovascular Imaging,* 16**,** 210-216.

AWANO, H., BLAESER, A., WU, B., LU, P., KERAMARIS-VRANTSIS, E. & LU, Q. 2015. Dystroglycanopathy muscles lacking functional glycosylation of alpha-dystroglycan retain regeneration capacity. *Neuromuscular Disorders,* 25**,** 474-484.

AXEL, L. & DOUGHERTY, L. 1989. MR imaging of motion with spatial modulation of magnetization. *Radiology,* 171**,** 841-5.

BANYPERSAD, S. M., SADO, D. M., FLETT, A. S., GIBBS, S. D., PINNEY, J. H., MAESTRINI, V., COX, A. T., FONTANA, M., WHELAN, C. J., WECHALEKAR, A. D., HAWKINS, P. N. & MOON, J. C. 2013. Quantification of myocardial extracellular volume fraction in systemic AL amyloidosis: an equilibrium contrast cardiovascular magnetic resonance study. *Circ Cardiovasc Imaging,* 6**,** 34-9.

BARNARD, A. M., WILLCOCKS, R. J., FINANGER, E. L., DANIELS, M. J., TRIPLETT, W. T., ROONEY, W. D., LOTT, D. J., FORBES, S. C., WANG, D. J., SENESAC, C. R., HARRINGTON, A. T., FINKEL, R. S., RUSSMAN, B. S., BYRNE, B. J., TENNEKOON, G. I., WALTER, G. A., SWEENEY, H. L. & VANDENBORNE, K. 2018. Skeletal muscle magnetic resonance biomarkers correlate with function and sentinel events in Duchenne muscular dystrophy. *PLoS One,* 13**,** e0194283.

BARP, A., BELLO, L., CAUMO, L., CAMPADELLO, P., SEMPLICINI, C., LAZZAROTTO, A., SORARÙ, G., CALORE, C., RAMPADO, A. & MOTTA, R. 2017. Muscle MRI and functional outcome measures in Becker muscular dystrophy. *Scientific reports,* 7**,** 16060.

BARP, A., BELLO, L., POLITANO, L., MELACINI, P., CALORE, C., POLO, A., VIANELLO, S., SORARU, G., SEMPLICINI, C., PANTIC, B., TAGLIA, A., PICILLO, E., MAGRI, F., GORNI, K., MESSINA, S., VITA, G. L., VITA, G., COMI, G. P., ERMANI, M., CALVO, V., ANGELINI, C., HOFFMAN, E. P. & PEGORARO, E. 2015. Genetic Modifiers of Duchenne Muscular Dystrophy and Dilated Cardiomyopathy. *PLoS One,* 10**,** e0141240.

BARZILAI-TUTSCH, H., BODANOVSKY, A., MAIMON, H., PINES, M. & HALEVY, O. 2016. Halofuginone promotes satellite cell activation and survival in muscular dystrophies. *Biochim Biophys Acta,* 1862**,** 1-11.

BASHA, T. A., IBRAHIM EL, S. H., WEISS, R. G. & OSMAN, N. F. 2009. Cine cardiac imaging using black-blood steady-state free precession (BB-SSFP) at 3T. *J Magn Reson Imaging,* 30**,** 94-103.

BASSETT, D. I. & CURRIE, P. D. 2003. The zebrafish as a model for muscular dystrophy and congenital myopathy. *Hum Mol Genet,* 12 Spec No 2**,** R265-70.

BECKER, P., KIENER, F. 1955. Eine neue X-Chromosomale Muskeldystrophie. *Arch Psychiatr Zschr Neurol. ,* 19**,** 427–448.

BECKER, S., FLORIAN, A., PATRASCU, A., RÖSCH, S., WALTENBERGER, J., SECHTEM, U., SCHWAB, M., SCHAEFFELER, E. & YILMAZ, A. 2016. Identification of cardiomyopathy associated circulating miRNA biomarkers in patients with muscular dystrophy using a complementary cardiovascular magnetic resonance and plasma profiling approach. *Journal of Cardiovascular Magnetic Resonance,* 18**,** 25.

BECKMANN, R., SCHEUERBRANDT, G. & ANTONIK, A. 1976. [Diagnosis of preclinical Duchenne's muscular dystrophy in the newborn using the CK screening test]. *Monatsschr Kinderheilkd,* 129**,** 658-9.

BEEDLE, A. M., NIENABER, P. M. & CAMPBELL, K. P. 2007. Fukutin-related protein associates with the sarcolemmal dystrophin-glycoprotein complex. *J Biol Chem,* 282**,** 16713-7.

BEEKMAN, C., JANSON, A. A., BAGHAT, A., VAN DEUTEKOM, J. C. & DATSON, N. A. 2018. Use of capillary Western immunoassay (Wes) for quantification of dystrophin levels in skeletal muscle of healthy controls and individuals with Becker and Duchenne muscular dystrophy. *PLoS One,* 13**,** e0195850.

BEEKMAN, C., SIPKENS, J. A., TESTERINK, J., GIANNAKOPOULOS, S., KREUGER, D., VAN DEUTEKOM, J. C., CAMPION, G. V., DE KIMPE, S. J. & LOURBAKOS, A. 2014. A sensitive, reproducible and objective immunofluorescence analysis method of dystrophin in individual fibers in samples from patients with duchenne muscular dystrophy. *PLoS One,* 9**,** e107494.

BELLENGER, N. G., MARCUS, N. J., DAVIES, C., YACOUB, M., BANNER, N. R. & PENNELL, D. J. 2000. Left ventricular function and mass after orthotopic heart transplantation: a comparison of cardiovascular magnetic resonance with echocardiography. *J Heart Lung Transplant,* 19**,** 444-52.

BIA, B. L., CASSIDY, P. J., YOUNG, M. E., RAFAEL, J. A., LEIGHTON, B., DAVIES, K. E., RADDA, G. K. & CLARKE, K. 1999. Decreased myocardial nNOS, increased iNOS and abnormal ECGs in mouse models of Duchenne muscular dystrophy. *J Mol Cell Cardiol,* 31**,** 1857-62.

BIRNKRANT, D. J., BUSHBY, K., BANN, C. M., ALMAN, B. A., APKON, S. D., BLACKWELL, A., CASE, L. E., CRIPE, L., HADJIYANNAKIS, S., OLSON, A. K., SHEEHAN, D. W., BOLEN, J., WEBER, D. R. & WARD, L. M. 2018a. Diagnosis and management of Duchenne muscular dystrophy, part 2: respiratory, cardiac, bone health, and orthopaedic management. *The Lancet Neurology,* 17**,** 347-361.

BIRNKRANT, D. J., BUSHBY, K., BANN, C. M., ALMAN, B. A., APKON, S. D., BLACKWELL, A., CASE, L. E., CRIPE, L., HADJIYANNAKIS, S., OLSON, A. K., SHEEHAN, D. W., BOLEN, J., WEBER, D. R. & WARD, L. M. 2018b. Diagnosis and management of Duchenne muscular dystrophy, part 2: respiratory, cardiac, bone health, and orthopaedic management. *Lancet Neurol*.

BIRNKRANT, D. J., BUSHBY, K., BANN, C. M., APKON, S. D., BLACKWELL, A., BRUMBAUGH, D., CASE, L. E., CLEMENS, P. R., HADJIYANNAKIS, S., PANDYA, S., STREET, N., TOMEZSKO, J., WAGNER, K. R., WARD, L. M. & WEBER, D. R. 2018c. Diagnosis and management of Duchenne muscular dystrophy, part 1: diagnosis, and neuromuscular, rehabilitation, endocrine, and gastrointestinal and nutritional management. *The Lancet Neurology,* 17**,** 251-267.

BIRNKRANT, D. J., BUSHBY, K., BANN, C. M., APKON, S. D., BLACKWELL, A., COLVIN, M. K., CRIPE, L., HERRON, A. R., KENNEDY, A., KINNETT, K., NAPRAWA, J., NORITZ, G., POYSKY, J., STREET, N., TROUT, C. J., WEBER, D. R. & WARD, L. M. 2018d. Diagnosis and management

of Duchenne muscular dystrophy, part 3: primary care, emergency management, psychosocial care, and transitions of care across the lifespan. *The Lancet Neurology,* 17**,** 445-455.

BLAIN, A., GREALLY, E., LAVAL, S., BLAMIRE, A., STRAUB, V. & MACGOWAN, G. A. 2013. Beta-blockers, left and right ventricular function, and in-vivo calcium influx in muscular dystrophy cardiomyopathy. *PLoS One,* 8**,** e57260.

BLATTER JOSHUA, A. & FINDER JONATHAN, D. 2013. Perioperative respiratory management of pediatric patients with neuromuscular disease. *Pediatric Anesthesia,* 23**,** 770-776.

BODOR, G. S., SURVANT, L., VOSS, E. M., SMITH, S., PORTERFIELD, D. & APPLE, F. S. 1997. Cardiac troponin T composition in normal and regenerating human skeletal muscle. *Clin Chem,* 43**,** 476-84.

BONNIAUD, P., MARGETTS, P. J., ASK, K., FLANDERS, K., GAULDIE, J. & KOLB, M. 2005. TGF-β and Smad3 Signaling Link Inflammation to Chronic Fibrogenesis. *The Journal of Immunology,* 175**,** 5390-5395.

BOROS, E., GALE, E. M. & CARAVAN, P. 2015. MR imaging probes: design and applications. *Dalton Trans,* 44**,** 4804-18.

BOURTEEL, H., STOJKOVIC, T., CUISSET, J. M., MAURAGE, C. A., LAFORET, P., RICHARD, P. & VERMERSCH, P. 2007. [Phenotypic aspects of FKRP-linked muscular dystrophy type 2I in a series of eleven patients]. *Rev Neurol (Paris),* 163**,** 189-96.

BROCKINGTON, M., YUVA, Y., PRANDINI, P., BROWN, S. C., TORELLI, S., BENSON, M. A., HERRMANN, R., ANDERSON, L. V., BASHIR, R., BURGUNDER, J. M., FALLET, S., ROMERO, N., FARDEAU, M., STRAUB, V., STOREY, G., POLLITT, C., RICHARD, I., SEWRY, C. A., BUSHBY, K., VOIT, T., BLAKE, D. J. & MUNTONI, F. 2001. Mutations in the fukutin-related protein gene (FKRP) identify limb girdle muscular dystrophy 2I as a milder allelic variant of congenital muscular dystrophy MDC1C. *Hum Mol Genet,* 10**,** 2851-9.

BROCKMANN, K., BECKER, P., SCHREIBER, G., NEUBERT, K., BRUNNER, E. & BONNEMANN, C. 2007. Sensitivity and specificity of qualitative muscle ultrasound in assessment of suspected neuromuscular disease in childhood. *Neuromuscul Disord,* 17**,** 517-23.

BRUNKLAUS, A., PARISH, E., MUNTONI, F., SCUPLAK, S., TUCKER, S. K., FENTON, M., HUGHES, M. L. & MANZUR, A. Y. 2015. The value of cardiac MRI versus echocardiography in the pre-operative assessment of patients with Duchenne muscular dystrophy. *Eur J Paediatr Neurol,* 19**,** 395-401.

BULL, S., WHITE, S. K., PIECHNIK, S. K., FLETT, A. S., FERREIRA, V. M., LOUDON, M., FRANCIS, J. M., KARAMITSOS, T. D., PRENDERGAST, B. D. & ROBSON, M. D. 2013. Human non-contrast T1 values and correlation with histology in diffuse fibrosis. *Heart***,** heartjnl-2012-303052.

BURAKIEWICZ, J., SINCLAIR, C. D. J., FISCHER, D., WALTER, G. A., KAN, H. E. & HOLLINGSWORTH, K. G. 2017. Quantifying fat replacement of muscle by quantitative MRI in muscular dystrophy. *Journal of Neurology,* 264**,** 2053-2067.

BURR, J. F., BREDIN, S. S., FAKTOR, M. D. & WARBURTON, D. E. 2011. The 6-minute walk test as a predictor of objectively measured aerobic fitness in healthy working-aged adults. *Phys Sportsmed,* 39**,** 133-9.

BUSHBY, K. & CONNOR, E. 2011. Clinical outcome measures for trials in Duchenne muscular dystrophy: report from International Working Group meetings. *Clinical investigation,* 1**,** 1217-1235.

BUSHBY, K., FINKEL, R., BIRNKRANT, D. J., CASE, L. E., CLEMENS, P. R., CRIPE, L., KAUL, A., KINNETT, K., MCDONALD, C., PANDYA, S., POYSKY, J., SHAPIRO, F., TOMEZSKO, J. & CONSTANTIN, C. 2010a. Diagnosis and management of Duchenne muscular dystrophy, part 1: diagnosis, and pharmacological and psychosocial management. *The Lancet Neurology,* 9**,** 77-93.

BUSHBY, K., FINKEL, R., BIRNKRANT, D. J., CASE, L. E., CLEMENS, P. R., CRIPE, L., KAUL, A., KINNETT, K., MCDONALD, C., PANDYA, S., POYSKY, J., SHAPIRO, F., TOMEZSKO, J. &

CONSTANTIN, C. 2010b. Diagnosis and management of Duchenne muscular dystrophy, part 2: implementation of multidisciplinary care. *Lancet Neurol,* 9**,** 177-89.

BUSHBY, K., MUNTONI, F. & BOURKE, J. P. 2003. 107th ENMC International Workshop: the management of cardiac involvement in muscular dystrophy and myotonic dystrophy. 7th–9th June 2002, Naarden, the Netherlands. *Neuromuscular Disorders,* 13**,** 166-172.

BUSHBY, K. M. 1995. Diagnostic criteria of the limb-girdle muscular dystrophies: report of the ENMC consortium on limb-girdle dystrophies. *Neuromuscul Disord,* 5**,** 71-74.

BUSHBY, K. M., HILL, A. & STEELE, J. G. 1999. Failure of early diagnosis in symptomatic Duchenne muscular dystrophy. *Lancet,* 353**,** 557-8.

BUYSE, G. M., VOIT, T., SCHARA, U., STRAATHOF, C. S., D'ANGELO, M. G., BERNERT, G., CUISSET, J. M., FINKEL, R. S., GOEMANS, N., MCDONALD, C. M., RUMMEY, C. & MEIER, T. 2015. Efficacy of idebenone on respiratory function in patients with Duchenne muscular dystrophy not using glucocorticoids (DELOS): a double-blind randomised placebo-controlled phase 3 trial. *Lancet,* 385**,** 1748-57.

BYDDER, M. & ROBSON, M. D. 2005. Partial fourier partially parallel imaging. *Magnetic Resonance in Medicine,* 53**,** 1393-1401.

CACCHIARELLI, D., LEGNINI, I., MARTONE, J., CAZZELLA, V., D'AMICO, A., BERTINI, E. & BOZZONI, I. 2011. miRNAs as serum biomarkers for Duchenne muscular dystrophy. *EMBO molecular medicine,* 3**,** 258-265.

CAETANO, G. F., FRONZA, M., LEITE, M. N., GOMES, A. & FRADE, M. A. C. 2016. Comparison of collagen content in skin wounds evaluated by biochemical assay and by computer-aided histomorphometric analysis. *Pharmaceutical Biology,* 54**,** 2555-2559.

CANESE, R., MEZZANZANICA, D., BAGNOLI, M., INDRACCOLO, S., CANEVARI, S., PODO, F. & IORIO, E. 2016. In vivo Magnetic Resonance Metabolic and Morphofunctional Fingerprints in Experimental Models of Human Ovarian Cancer. *Front Oncol,* 6**,** 164.

CARAVAN, P. 2006. Strategies for increasing the sensitivity of gadolinium based MRI contrast agents. *Chem Soc Rev,* 35**,** 512-23.

CARAVAN, P., DAS, B., DUMAS, S., EPSTEIN, F. H., HELM, P. A., JACQUES, V., KOERNER, S., KOLODZIEJ, A., SHEN, L. & SUN, W. C. 2007. Collagen‐Targeted MRI Contrast Agent for Molecular Imaging of Fibrosis. *Angewandte Chemie,* 119**,** 8319-8321.

CARAVAN, P., YANG, Y., ZACHARIAH, R., SCHMITT, A., MINO-KENUDSON, M., CHEN, H. H., SOSNOVIK, D. E., DAI, G., FUCHS, B. C. & LANUTI, M. 2013. Molecular magnetic resonance imaging of pulmonary fibrosis in mice. *Am J Respir Cell Mol Biol,* 49**,** 1120-6.

CARLIER, P. G., AZZABOU, N., DE SOUSA, P. L., HICKS, A., BOISSERIE, J. M., AMADON, A., CARLIER, R. Y., WARY, C., ORLIKOWSKI, D. & LAFORET, P. 2015. Skeletal muscle quantitative nuclear magnetic resonance imaging follow-up of adult Pompe patients. *J Inherit Metab Dis,* 38**,** 565-72.

CARLIER, P. G., MARTY, B., SCHEIDEGGER, O., LOUREIRO DE SOUSA, P., BAUDIN, P. Y., SNEZHKO, E. & VLODAVETS, D. 2016. Skeletal Muscle Quantitative Nuclear Magnetic Resonance Imaging and Spectroscopy as an Outcome Measure for Clinical Trials. *J Neuromuscul Dis,* 3**,** 1-28.

CARLSON, G. 2014. *Determination of hydroxyproline content as a measure of fibrosis in nondystrophic and dystrophic skeletal muscle.* [Online]. Treat NMD. Available: http://www.treat-nmd.eu/downloads/file/sops/dmd/MDX/DMD_M.1.2.006.pdf [Accessed 31st of May 2016].

CERQUEIRA, M. D., WEISSMAN, N. J., DILSIZIAN, V., JACOBS, A. K., KAUL, S., LASKEY, W. K., PENNELL, D. J., RUMBERGER, J. A., RYAN, T. & VERANI, M. S. 2002. Standardized Myocardial Segmentation and Nomenclature for Tomographic Imaging of the Heart. *A Statement for Healthcare Professionals From the Cardiac Imaging Committee of the Council on Clinical Cardiology of the American Heart Association,* 105**,** 539-542.

CHAMBERLAIN, J. S., METZGER, J., REYES, M., TOWNSEND, D. & FAULKNER, J. A. 2007. Dystrophin-deficient mdx mice display a reduced life span and are susceptible to spontaneous rhabdomyosarcoma. *The FASEB Journal,* 21**,** 2195-2204.

CHARDON, J. W., SMITH, A. C., WOULFE, J., PENA, E., RAKHRA, K., DENNIE, C., BEAULIEU, C., HUANG, L., SCHWARTZENTRUBER, J., HAWKINS, C., HARMS, M. B., DOJEIJI, S., ZHANG, M., MAJEWSKI, J., BULMAN, D. E., BOYCOTT, K. M. & DYMENT, D. A. 2015. LIMS2 mutations are associated with a novel muscular dystrophy, severe cardiomyopathy and triangular tongues. *Clin Genet*.

CHARLES, J. P., CAPPELLARI, O., SPENCE, A. J., HUTCHINSON, J. R. & WELLS, D. J. 2016. Musculoskeletal Geometry, Muscle Architecture and Functional Specialisations of the Mouse Hindlimb. *PLoS ONE,* 11**,** e0147669.

CHARLESTON, J. S., SCHNELL, F. J., DWORZAK, J., DONOGHUE, C., LEWIS, S., CHEN, L., YOUNG, G. D., MILICI, A. J., VOSS, J., DEALWIS, U., WENTWORTH, B., RODINO-KLAPAC, L. R., SAHENK, Z., FRANK, D. & MENDELL, J. R. 2018. Eteplirsen treatment for Duchenne muscular dystrophy. *Exon skipping and dystrophin production*.

CHEN, H., LIANG, B. M., TANG, Y. J., XU, Z. B., WANG, K., YI, Q., OU, X. M. & FENG, Y. L. 2012. Relationship between 6-minute walk test and pulmonary function test in stable chronic obstructive pulmonary disease with different severities. *Chin Med J (Engl),* 125**,** 3053-8.

CICALA, S., DE SIMONE, G., ROMAN, M. J., BEST, L. G., LEE, E. T., WANG, W., WELTY, T. K., GALLOWAY, J. M., HOWARD, B. V. & DEVEREUX, R. B. 2007. Prevalence and prognostic significance of wall-motion abnormalities in adults without clinically recognized cardiovascular disease: the Strong Heart Study. *Circulation,* 116**,** 143-50.

CLINICAL TRIALS.GOV. 2016. *Safety, Tolerability, and Pharmacokinetics of Single and Multiple Doses of HT-100 in Duchenne Muscular Dystrophy* [Online]. Available: https://clinicaltrials.gov/ct2/show/NCT01847573?term=halofuginone+duchenne&rank=1 [Accessed 24th of May 2016].

CLINICAL TRIALS.GOV. 2017. *Study of SRP-4045 and SRP-4053 in DMD Patients (ESSENCE)* [Online]. Available: https://clinicaltrials.gov/ct2/show/NCT02500381?term=sarepta+duchenne&rank=4 [Accessed 22nd of March 2017].

CLINICAL TRIALS.GOV. 2018a. *Givinostat in Duchenne's Muscular Dystrophy Long-term Safety and Tolerability Study* [Online]. Available: https://clinicaltrials.gov/ct2/show/NCT03373968 [Accessed 14th of February 2018 2018].

CLINICAL TRIALS.GOV. 2018b. *An Open-label Extension Study To Evaluate Safety Of PF-06252616 In Boys With Duchenne Muscular Dystrophy* [Online]. Available: https://clinicaltrials.gov/ct2/show/NCT02907619?term=pfizer&cond=Duchenne+Muscular+Dystrophy&rank=1 [Accessed 14th of February 2018 2018].

CLINICAL TRIALS.GOV. 2018c. *Safety, Tolerability, and Pharmacokinetics of Single and Multiple Doses of HT-100 in Duchenne Muscular Dystrophy* [Online]. Available: https://clinicaltrials.gov/ct2/show/NCT01847573 [Accessed 9th of January 2019 2019].

CLINICAL TRIALS.GOV. 2018d. *A Study to Evaluate the Safety and Tolerability of PF-06939926 Gene Therapy in Duchenne Muscular Dystrophy* [Online]. Available: https://clinicaltrials.gov/ct2/show/NCT03362502?term=pfizer&cond=Duchenne+Muscular+Dystrophy&rank=2 [Accessed].

COHEN, J. 1988. *Statistical power analysis for the behavioral sciences,* Hillsdale, N.J., L. Erlbaum Associates.

COHN, R. D., LIANG, H.-Y., SHETTY, R., ABRAHAM, T. & WAGNER, K. R. 2007. Myostatin does not regulate cardiac hypertrophy or fibrosis. *Neuromuscular Disorders,* 17**,** 290-296.

COLLINS, C. & MORGAN, J. 2003. Duchenne's muscular dystrophy: animal models used to investigate pathogenesis and develop therapeutic strategies. *Int J Exp Pathol,* 84**,** 165-72.

COLLINS, J., SOMMERVILLE, C., MAGRATH, P., SPOTTISWOODE, B., FREED, B. H., BENZULY, K. H., GORDON, R., VIDULA, H., LEE, D. C., YANCY, C., CARR, J. & MARKL, M. 2015. Extracellular Volume Fraction Is More Closely Associated With Altered Regional Left Ventricular Velocities Than Left Ventricular Ejection Fraction in Non-Ischemic Cardiomyopathy. *Circulation. Cardiovascular imaging,* 8**,** e001998.

CONNOLLY, A. M., MALKUS, E. C., MENDELL, J. R., FLANIGAN, K. M., MILLER, J. P., SCHIERBECKER, J. R., SIENER, C. A., GOLUMBEK, P. T., ZAIDMAN, C. M., MCDONALD, C. M., JOHNSON, L., NICORICI, A., KARACHUNSKI, P. I., DAY, J. W., KELECIC, J. M., LOWES, L. P., ALFANO, L. N., DARRAS, B. T., KANG, P. B., QUIGLEY, J., PASTERNAK, A. E. & FLORENCE, J. M. 2015. Outcome reliability in non-ambulatory boys/men with Duchenne muscular dystrophy. *Muscle Nerve,* 51**,** 522-32.

COSTER, W. J. 2013. Making the Best Match: Selecting Outcome Measures for Clinical Trials and Outcome Studies. *The American Journal of Occupational Therapy,* 67**,** 162-170.

CRILLEY, J. G., BOEHM, E. A., RAJAGOPALAN, B., BLAMIRE, A. M., STYLES, P., MUNTONI, F., HILTON-JONES, D. & CLARKE, K. 2000. Magnetic resonance spectroscopy evidence of abnormal cardiac energetics in Xp21 muscular dystrophy. *J Am Coll Cardiol,* 36**,** 1953-8.

CROS, D., HARNDEN, P., PELLISSIER, J. F. & SERRATRICE, G. 1989. Muscle hypertrophy in Duchenne muscular dystrophy. A pathological and morphometric study. *J Neurol,* 236**,** 43-7.

CUI, W., JANG, A., ZHANG, P., THOMPSON, B., TOWNSEND, D., METZGER, J. M. & ZHANG, J. 2015a. Early Detection of Myocardial Bioenergetic Deficits: A 9.4 Tesla Complete Non Invasive 31P MR Spectroscopy Study in Mice with Muscular Dystrophy. *PLoS One,* 10**,** e0135000.

CUI, Z., CRANE, J., XIE, H., JIN, X., ZHEN, G., LI, C., XIE, L., WANG, L., BIAN, Q., QIU, T., WAN, M., XIE, M., DING, S., YU, B. & CAO, X. 2015b. Halofuginone attenuates osteoarthritis by inhibition of TGF-beta activity and H-type vessel formation in subchondral bone. *Ann Rheum Dis*.

D'AMICO, A., PETRINI, S., PARISI, F., TESSA, A., FRANCALANCI, P., GRUTTER, G., SANTORELLI, F. M. & BERTINI, E. 2008. Heart transplantation in a child with LGMD2I presenting as isolated dilated cardiomyopathy. *Neuromuscul Disord,* 18**,** 153-5.

DANIEL, R. M., SVEN, P., DAVID, M. H., KEVIN, W., TIMOTHY, R. J., JOHN, P. R. & MOHAN, U. S. 2006. Human Myocardium: Single-Breath-hold MR T1 Mapping with High Spatial Resolution—Reproducibility Study. *Radiology,* 238**,** 1004-1012.

DE GROOT, J. F., TAKKEN, T., VAN BRUSSEL, M., GOOSKENS, R., SCHOENMAKERS, M., VERSTEEG, C., VANHEES, L. & HELDERS, P. 2011. Randomized Controlled Study of Home-Based Treadmill Training for Ambulatory Children With Spina Bifida. *Neurorehabilitation and Neural Repair,* 25**,** 597-606.

DE JONGE, M. J. A., DUMEZ, H., VERWEIJ, J., YARKONI, S., SNYDER, D., LACOMBE, D., MARRÉAUD, S., YAMAGUCHI, T., PUNT, C. J. A. & VAN OOSTEROM, A. 2006. Phase I and pharmacokinetic study of halofuginone, an oral quinazolinone derivative in patients with advanced solid tumours. *European Journal of Cancer,* 42**,** 1768-1774.

DE PASQUALE, L., D'AMICO, A., VERARDO, M., PETRINI, S., BERTINI, E. & DE BENEDETTI, F. 2012. Increased muscle expression of interleukin-17 in Duchenne muscular dystrophy. *Neurology,* 78**,** 1309-14.

DEN DUNNEN, J. T., GROOTSCHOLTEN, P. M., DAUWERSE, J. G., WALKER, A. P., MONACO, A. P., BUTLER, R., ANAND, R., COFFEY, A. J., BENTLEY, D. R., STEENSMA, H. Y. & ET AL. 1992. Reconstruction of the 2.4 Mb human DMD-gene by homologous YAC recombination. *Hum Mol Genet,* 1**,** 19-28.

DESGUERRE, I., MAYER, M., LETURCQ, F., BARBET, J. P., GHERARDI, R. K. & CHRISTOV, C. 2009. Endomysial fibrosis in Duchenne muscular dystrophy: a marker of poor outcome associated with macrophage alternative activation. *J Neuropathol Exp Neurol,* 68**,** 762-73.

DIAZ-MANERA, J., FERNANDEZ-TORRON, R., J, L. L., JAMES, M. K., MAYHEW, A., SMITH, F. E., MOORE, U. R., BLAMIRE, A. M., CARLIER, P. G., RUFIBACH, L., MITTAL, P., EAGLE, M., JACOBS, M., HODGSON, T., WALLACE, D., WARD, L., SMITH, M., STRAMARE, R., RAMPADO, A., SATO, N., TAMARU, T., HARWICK, B., RICO GALA, S., TURK, S., COPPENRATH, E. M., FOSTER, G., BENDAHAN, D., LE FUR, Y., FRICKE, S. T., OTERO, H., FOSTER, S. L., PEDUTO, A., SAWYER, A. M., HILSDEN, H., LOCHMULLER, H., GRIEBEN, U., SPULER, S., TESI ROCHA, C., DAY, J. W., JONES, K. J., BHARUCHA-GOEBEL, D. X., SALORT-CAMPANA, E., HARMS, M., PESTRONK, A., KRAUSE, S., SCHREIBER-KATZ, O., WALTER, M. C., PARADAS, C., HOGREL, J. Y., STOJKOVIC, T., TAKEDA, S., MORI-YOSHIMURA, M., BRAVVER, E., SPARKS, S., BELLO, L., SEMPLICINI, C., PEGORARO, E., MENDELL, J. R., BUSHBY, K. & STRAUB, V. 2018. Muscle MRI in patients with dysferlinopathy: pattern recognition and implications for clinical trials. *J Neurol Neurosurg Psychiatry,* 89**,** 1071-1081.

DIXON, W. T. 1984. Simple proton spectroscopic imaging. *Radiology,* 153**,** 189-194.

DOGRA, A. C., GUPTA, U., SARKAR, M. & PADAM, A. 2015. Exercise-induced desaturation in patients with chronic obstructive pulmonary disease on six-minute walk test. *Lung India,* 32**,** 320-5.

DOMINGOS, J. & MUNTONI, F. 2018. Outcome measures in Duchenne muscular dystrophy: sensitivity to change, clinical meaningfulness, and implications for clinical trials. *Developmental Medicine & Child Neurology,* 60**,** 117-117.

DONDERS, J. & TANEJA, C. 2009. Neurobehavioral characteristics of children with Duchenne muscular dystrophy. *Child Neuropsychol,* 15**,** 295-304.

DOUST, J. A., PIETRZAK, E., DOBSON, A. & GLASZIOU, P. 2005. How well does B-type natriuretic peptide predict death and cardiac events in patients with heart failure: systematic review. *BMJ,* 330**,** 625.

DROUSIOTOU, A., IOANNOU, P., GEORGIOU, T., MAVRIKIOU, E., CHRISTOPOULOS, G., KYRIAKIDES, T., VOYASIANOS, M., ARGYRIOU, A. & MIDDLETON, L. 1998. Neonatal screening for Duchenne muscular dystrophy: a novel semiquantitative application of the bioluminescence test for creatine kinase in a pilot national program in Cyprus. *Genet Test,* 2**,** 55-60.

DUBOC, D., MEUNE, C., LEREBOURS, G., DEVAUX, J. Y., VAKSMANN, G. & BECANE, H. M. 2005. Effect of perindopril on the onset and progression of left ventricular dysfunction in Duchenne muscular dystrophy. *J Am Coll Cardiol,* 45**,** 855-7.

DUBOC, D., MEUNE, C., PIERRE, B., WAHBI, K., EYMARD, B., TOUTAIN, A., BERARD, C., VAKSMANN, G., WEBER, S. & BECANE, H. M. 2007. Perindopril preventive treatment on mortality in Duchenne muscular dystrophy: 10 years' follow-up. *Am Heart J,* 154**,** 596-602.

DUNN, J. F. & ZAIM-WADGHIRI, Y. 1999. Quantitative magnetic resonance imaging of the mdx mouse model of Duchenne muscular dystrophy. *Muscle Nerve,* 22**,** 1367-71.

E. HEIBERG, J. S., M. UGANDER, M. CARLSSON, H. ENGBLOM, AND H. ARHEDEN, 2010. *Design and Validation of Segment – a Freely Available Software for Cardiovascular Image Analysis.*

EAGLE, M., BAUDOUIN, S. V., CHANDLER, C., GIDDINGS, D. R., BULLOCK, R. & BUSHBY, K. 2002. Survival in Duchenne muscular dystrophy: improvements in life expectancy since 1967 and the impact of home nocturnal ventilation. *Neuromuscul Disord,* 12**,** 926-9.

EMERY, A. E. 2002. The muscular dystrophies. *Lancet,* 359**,** 687-95.

EMERY, A. E. H. 1991. Population frequencies of inherited neuromuscular diseases—A world survey. *Neuromuscular Disorders,* 1**,** 19-29.

ERICKY, C. A. A., AZZABOU, N., VIGNAUD, A., GUILLOT, G. & CARLIER, P. G. 2017. Quantitative ultrashort TE imaging of the short‐T2 components in skeletal muscle using an extended echo‐subtraction method. *Magnetic Resonance in Medicine,* 78**,** 997-1008.

ESAPA, C. T., BENSON, M. A., SCHRODER, J. E., MARTIN-RENDON, E., BROCKINGTON, M., BROWN, S. C., MUNTONI, F., KROGER, S. & BLAKE, D. J. 2002. Functional requirements for fukutin-related protein in the Golgi apparatus. *Hum Mol Genet,* 11**,** 3319-31.

ESCOLAR, D. M., HENRICSON, E. K., MAYHEW, J., FLORENCE, J., LESHNER, R., PATEL, K. M. & CLEMENS, P. R. 2001. Clinical evaluator reliability for quantitative and manual muscle testing measures of strength in children. *Muscle & nerve,* 24**,** 787-793.

EUROPEAN COMMISSION. 2008. *European commission - public health - policy on Rare disease* [Online]. Available: https://ec.europa.eu/health/rare_diseases/policy_en [Accessed 24thof February 2017].

EUROPEAN MEDICINES AGENCY. 2018. *Gadolinium containing contrast agents.* [Online]. Available: https://www.ema.europa.eu/documents/referral/gadolinium-article-31-referral-emas-final-opinion-confirms-restrictions-use-linear-gadolinium-agents_en.pdf [Accessed 18th of December 2018 2018].

EVERETT, R. J., STIRRAT, C. G., SEMPLE, S. I. R., NEWBY, D. E., DWECK, M. R. & MIRSADRAEE, S. 2016. Assessment of myocardial fibrosis with T1 mapping MRI. *Clinical Radiology,* 71**,** 768-778.

FARRAR, C. T., DEPERALTA, D. K., DAY, H., RIETZ, T. A., WEI, L., LAUWERS, G. Y., KEIL, B., SUBRAMANIAM, A., SINSKEY, A. J., TANABE, K. K., FUCHS, B. C. & CARAVAN, P. 2015. 3D molecular MR imaging of liver fibrosis and response to rapamycin therapy in a bile duct ligation rat model. *Journal of Hepatology*.

FATEHI, F., SALORT-CAMPANA, E., LE TROTER, A., LAREAU-TRUDEL, E., BYDDER, M., FOURE, A., GUYE, M., BENDAHAN, D. & ATTARIAN, S. 2017. Long-term follow-up of MRI changes in thigh muscles of patients with Facioscapulohumeral dystrophy: A quantitative study. *PLoS One,* 12**,** e0183825.

FEINGOLD, B., MAHLE, W. T., AUERBACH, S., CLEMENS, P., DOMENIGHETTI, A. A., JEFFERIES, J. L., JUDGE, D. P., LAL, A. K., MARKHAM, L. W., PARKS, W. J., TSUDA, T., WANG, P. J. & YOO, S.-J. 2017. Management of Cardiac Involvement Associated With Neuromuscular Diseases: A Scientific Statement From the American Heart Association. *Circulation*.

FINANGER, E. L., RUSSMAN, B., FORBES, S. C., ROONEY, W. D., WALTER, G. A. & VANDENBORNE, K. 2012. Use of skeletal muscle MRI in diagnosis and monitoring disease progression in Duchenne Muscular Dystrophy. *Physical medicine and rehabilitation clinics of North America,* 23**,** 1-ix.

FINSTERER, J. & STÖLLBERGER, C. 2008. Cardiac involvement in Becker muscular dystrophy. *Can J Cardiol,* 24**,** 786-92.

FISCHER, D., HAFNER, P., RUBINO, D., SCHMID, M., NEUHAUS, C., JUNG, H., BIERI, O., HAAS, T., GLOOR, M., FISCHMANN, A. & BONATI, U. 2016. The 6-minute walk test, motor function measure and quantitative thigh muscle MRI in Becker muscular dystrophy: A cross-sectional study. *Neuromuscular Disorders,* 26**,** 414-422.

FISCHMANN, A., HAFNER, P., GLOOR, M., SCHMID, M., KLEIN, A., POHLMAN, U., WALTZ, T., GONZALEZ, R., HAAS, T., BIERI, O. & FISCHER, D. 2013. Quantitative MRI and loss of free ambulation in Duchenne muscular dystrophy. *J Neurol,* 260**,** 969-974.

FLACKE, S., FISCHER, S., SCOTT, M. J., FUHRHOP, R. J., ALLEN, J. S., MCLEAN, M., WINTER, P., SICARD, G. A., GAFFNEY, P. J., WICKLINE, S. A. & LANZA, G. M. 2001. Novel MRI Contrast Agent for Molecular Imaging of Fibrin: Implications for Detecting Vulnerable Plaques. *Circulation,* 104**,** 1280-1285.

FLETT, A. S., HASLETON, J., COOK, C., HAUSENLOY, D., QUARTA, G., ARITI, C., MUTHURANGU, V. & MOON, J. C. 2011. Evaluation of Techniques for the Quantification of Myocardial Scar of Differing Etiology Using Cardiac Magnetic Resonance. *JACC: Cardiovascular Imaging,* 4**,** 150-156.

FLETT, A. S., HAYWARD, M. P., ASHWORTH, M. T., HANSEN, M. S., TAYLOR, A. M., ELLIOTT, P. M., MCGREGOR, C. & MOON, J. C. 2010. Equilibrium contrast cardiovascular magnetic

resonance for the measurement of diffuse myocardial fibrosis: preliminary validation in humans. *Circulation,* 122**,** 138-44.

FLOREA, V. G., RECTOR, T. S., ANAND, I. S. & COHN, J. N. 2016. Heart Failure With Improved Ejection Fraction: Clinical Characteristics, Correlates of Recovery, and Survival: Results From the Valsartan Heart Failure Trial. *Circ Heart Fail,* 9.

FLORENCE, J. M., PANDYA, S., KING, W. M., ROBISON, J. D., SIGNORE, L. C., WENTZELL, M. & PROVINCE, M. A. 1984. Clinical trials in Duchenne dystrophy. Standardization and reliability of evaluation procedures. *Phys Ther,* 64**,** 41-5.

FLORIAN, A., LUDWIG, A., ENGELEN, M., WALTENBERGER, J., RÖSCH, S., SECHTEM, U. & YILMAZ, A. 2014a. Left ventricular systolic function and the pattern of late-gadolinium-enhancement independently and additively predict adverse cardiac events in muscular dystrophy patients. *Journal of Cardiovascular Magnetic Resonance,* 16**,** 81.

FLORIAN, A., LUDWIG, A., ROSCH, S., YILDIZ, H., SECHTEM, U. & YILMAZ, A. 2014b. Myocardial fibrosis imaging based on T1-mapping and extracellular volume fraction (ECV) measurement in muscular dystrophy patients: diagnostic value compared with conventional late gadolinium enhancement (LGE) imaging. *Eur Heart J Cardiovasc Imaging,* 15**,** 1004-12.

FLORIAN, A., LUDWIG, A., ROSCH, S., YILDIZ, H., SECHTEM, U. & YILMAZ, A. 2014c. Myocardial fibrosis imaging based on T1-mapping and extracellular volume fraction (ECV) measurement in muscular dystrophy patients: diagnostic value compared with conventional late gadolinium enhancement (LGE) imaging. *Eur Heart J Cardiovasc Imaging,* 15.

FLORIAN, A., ROSCH, S., BIETENBECK, M., ENGELEN, M., STYPMANN, J., WALTENBERGER, J., SECHTEM, U. & YILMAZ, A. 2016. Cardiac involvement in female Duchenne and Becker muscular dystrophy carriers in comparison to their first-degree male relatives: a comparative cardiovascular magnetic resonance study. *Eur Heart J Cardiovasc Imaging,* 17**,** 326-33.

FONTANA, M., WHITE, S. K., BANYPERSAD, S. M., SADO, D. M., MAESTRINI, V., FLETT, A. S., PIECHNIK, S. K., NEUBAUER, S., ROBERTS, N. & MOON, J. C. 2012. Comparison of T1 mapping techniques for ECV quantification. Histological validation and reproducibility of ShMOLLI versus multibreath-hold T1 quantification equilibrium contrast CMR. *J Cardiovasc Magn Reson,* 14**,** 88.

FORBES, S. C., WALTER, G. A., ROONEY, W. D., WANG, D. J., DEVOS, S., POLLARO, J., TRIPLETT, W., LOTT, D. J., WILLCOCKS, R. J., SENESAC, C., DANIELS, M. J., BYRNE, B. J., RUSSMAN, B., FINKEL, R. S., MEYER, J. S., SWEENEY, H. L. & VANDENBORNE, K. 2013. Skeletal muscles of ambulant children with Duchenne muscular dystrophy: validation of multicenter study of evaluation with MR imaging and MR spectroscopy. *Radiology,* 269**,** 198-207.

FORBES, S. C., WILLCOCKS, R. J., TRIPLETT, W. T., ROONEY, W. D., LOTT, D. J., WANG, D. J., POLLARO, J., SENESAC, C. R., DANIELS, M. J., FINKEL, R. S., RUSSMAN, B. S., BYRNE, B. J., FINANGER, E. L., TENNEKOON, G. I., WALTER, G. A., SWEENEY, H. L. & VANDENBORNE, K. 2014. Magnetic resonance imaging and spectroscopy assessment of lower extremity skeletal muscles in boys with Duchenne muscular dystrophy: a multicenter cross sectional study. *PLoS One,* 9**,** e106435.

FRATZ, S., CHUNG, T., GREIL, G. F., SAMYN, M. M., TAYLOR, A. M., VALSANGIACOMO BUECHEL, E. R., YOO, S.-J. & POWELL, A. J. 2013. Guidelines and protocols for cardiovascular magnetic resonance in children and adults with congenital heart disease: SCMR expert consensus group on congenital heart disease. *Journal of Cardiovascular Magnetic Resonance,* 15**,** 51-51.

FUCHS, B. C., WANG, H., YANG, Y., WEI, L., POLASEK, M., SCHUHLE, D. T., LAUWERS, G. Y., PARKAR, A., SINSKEY, A. J., TANABE, K. K. & CARAVAN, P. 2013. Molecular MRI of collagen to diagnose and stage liver fibrosis. *J Hepatol,* 59**,** 992-8.

GAETA, M., MESSINA, S., MILETO, A., VITA, G. L., ASCENTI, G., VINCI, S., BOTTARI, A., VITA, G., SETTINERI, N., BRUSCHETTA, D., RACCHIUSA, S. & MINUTOLI, F. 2012. Muscle fat-fraction and mapping in Duchenne muscular dystrophy: evaluation of disease distribution and correlation with clinical assessments. Preliminary experience. *Skeletal Radiol,* 41**,** 955-61.

GARDNER, B. I., BINGHAM, S. E., ALLEN, M. R., BLATTER, D. D. & ANDERSON, J. L. 2009. Cardiac magnetic resonance versus transthoracic echocardiography for the assessment of cardiac volumes and regional function after myocardial infarction: an intrasubject comparison using simultaneous intrasubject recordings. *Cardiovasc Ultrasound,* 7**,** 38.

GARROOD, P., HOLLINGSWORTH, K. G., EAGLE, M., ARIBISALA, B. S., BIRCHALL, D., BUSHBY, K. & STRAUB, V. 2009. MR imaging in Duchenne muscular dystrophy: quantification of T1-weighted signal, contrast uptake, and the effects of exercise. *J Magn Reson Imaging,* 30**,** 1130-8.

GAUR, L., HANNA, A., BANDETTINI, W. P., FISCHBECK, K. H., ARAI, A. E. & MANKODI, A. 2016. Upper arm and cardiac magnetic resonance imaging in Duchenne muscular dystrophy. *Annals of Clinical and Translational Neurology,* 3**,** 948-955.

GEIGER, R., STRASAK, A., TREML, B., GASSER, K., KLEINSASSER, A., FISCHER, V., GEIGER, H., LOECKINGER, A. & STEIN, J. I. 2007. Six-minute walk test in children and adolescents. *J Pediatr,* 150**,** 395-9, 399 e1-2.

GIBERTINI, S., ZANOTTI, S., SAVADORI, P., CURCIO, M., SAREDI, S., SALERNO, F., ANDREETTA, F., BERNASCONI, P., MANTEGAZZA, R. & MORA, M. 2014. Fibrosis and inflammation are greater in muscles of beta-sarcoglycan-null mouse than mdx mouse. *Cell Tissue Res,* 356**,** 427-43.

GIGLIO, V., PUDDU, P. E., CAMASTRA, G., SBARBATI, S., DELLA SALA, S. W., FERLINI, A., GUALANDI, F., RICCI, E., SCIARRA, F., ANSALONE, G. & DI GENNARO, M. 2014. Patterns of late gadolinium enhancement in Duchenne muscular dystrophy carriers. *Journal of Cardiovascular Magnetic Resonance,* 16**,** 45.

GLOVER, G. H. & SCHNEIDER, E. 1991. Three-point Dixon technique for true water/fat decomposition with B0 inhomogeneity correction. *Magn Reson Med,* 18**,** 371-383.

GOSSELIN, L. E. & WILLIAMS, J. E. 2006. Pentoxifylline fails to attenuate fibrosis in dystrophic (mdx) diaphragm muscle. *Muscle Nerve,* 33**,** 820-3.

GOSSELIN, L. E., WILLIAMS, J. E., DEERING, M., BRAZEAU, D., KOURY, S. & MARTINEZ, D. A. 2004. Localization and early time course of TGF-β1 mRNA expression in dystrophic muscle. *Muscle & Nerve,* 30**,** 645-653.

GOTTE, M. J., VAN ROSSUM, A. C., TWISK, J. W. R., KUIJER, J. P. A., MARCUS, J. T. & VISSER, C. A. 2001. Quantification of regional contractile function after infarction: strain analysis superior to wall thickening analysis in discriminating infarct from remote myocardium. *J Am Coll Cardiol,* 37**,** 808-17.

GRAHAM, K. M., SINGH, R., MILLMAN, G., MALNASSY, G., GATTI, F., BRUEMMER, K., STEFANSKI, C., CURTIS, H., SESTI, J. & CARLSON, C. G. 2010. Excessive collagen accumulation in dystrophic (mdx) respiratory musculature is independent of enhanced activation of the NF-κB pathway. *Journal of the Neurological Sciences,* 294**,** 43-50.

GREALLY, E., DAVISON, B. J., BLAIN, A., LAVAL, S., BLAMIRE, A., STRAUB, V. & MACGOWAN, G. A. 2013. Heterogeneous abnormalities of in-vivo left ventricular calcium influx and function in mouse models of muscular dystrophy cardiomyopathy. *Journal of Cardiovascular Magnetic Resonance,* 15**,** 4-4.

GREENBERG, C. R., JACOBS, H. K., HALLIDAY, W. & WROGEMANN, K. 1991. Three years' experience with neonatal screening for Duchenne/Becker muscular dystrophy: gene analysis, gene expression, and phenotype prediction. *Am J Med Genet,* 39**,** 68-75.

GREIL, G. F., GERMANN, S., KOZERKE, S., BALTES, C., TSAO, J., URSCHITZ, M. S., SEEGER, A., TANGCHAROEN, T., BIALKOWSKY, A., MILLER, S. & SIEVERDING, L. 2008. Assessment of left ventricular volumes and mass with fast 3D cine steady-state free precession k-t space

broad-use linear acquisition speed-up technique (k-t BLAST). *J Magn Reson Imaging,* 27**,** 510-5.

GROUNDS, M. D., RADLEY, H. G., LYNCH, G. S., NAGARAJU, K. & DE LUCA, A. 2008. Towards developing standard operating procedures for pre-clinical testing in the mdx mouse model of Duchenne muscular dystrophy. *Neurobiology of Disease,* 31**,** 1-19.

GULATI, A., JABBOUR, A., ISMAIL, T. F., GUHA, K., KHWAJA, J., RAZA, S., MORARJI, K., BROWN, T. D., ISMAIL, N. A., DWECK, M. R., DI PIETRO, E., ROUGHTON, M., WAGE, R., DARYANI, Y., O'HANLON, R., SHEPPARD, M. N., ALPENDURADA, F., LYON, A. R., COOK, S. A., COWIE, M. R., ASSOMULL, R. G., PENNELL, D. J. & PRASAD, S. K. 2013. Association of fibrosis with mortality and sudden cardiac death in patients with nonischemic dilated cardiomyopathy. *JAMA,* 309**,** 896-908.

GUTPELL, K. M., HRINIVICH, W. T. & HOFFMAN, L. M. 2015. Skeletal Muscle Fibrosis in the mdx/utrn+/- Mouse Validates Its Suitability as a Murine Model of Duchenne Muscular Dystrophy. *PLOS ONE,* 10**,** e0117306.

GUYATT, G. H., SULLIVAN, M. J., THOMPSON, P. J., FALLEN, E. L., PUGSLEY, S. O., TAYLOR, D. W. & BERMAN, L. B. 1985. The 6-minute walk: a new measure of exercise capacity in patients with chronic heart failure. *Can Med Assoc J,* 132**,** 919-923.

HAAS, M., VLCEK, V., BALABANOV, P., SALMONSON, T., BAKCHINE, S., MARKEY, G., WEISE, M., SCHLOSSER-WEBER, G., BROHMANN, H., YERRO, C. P., MENDIZABAL, M. R., STOYANOVA-BENINSKA, V. & HILLEGE, H. L. 2015. European Medicines Agency review of ataluren for the treatment of ambulant patients aged 5 years and older with Duchenne muscular dystrophy resulting from a nonsense mutation in the dystrophin gene. *Neuromuscul Disord,* 25**,** 5-13.

HAASS, M., ZUGCK, C. & KUBLER, W. 2000. [The 6 minute walking test: a cost-effective alternative to spiro-ergometry in patients with chronic heart failure?]. *Z Kardiol,* 89**,** 72-80.

HAGENBUCH, S. C., GOTTLIEBSON, W. M., WANSAPURA, J., MAZUR, W., FLECK, R., BENSON, D. W. & HOR, K. N. 2010a. Detection of progressive cardiac dysfunction by serial evaluation of circumferential strain in patients with Duchenne muscular dystrophy. *Am J Cardiol,* 105**,** 1451-5.

HAGENBUCH, S. C., GOTTLIEBSON, W. M., WANSAPURA, J., MAZUR, W., FLECK, R., BENSON, D. W. & HOR, K. N. 2010b. Detection of Progressive Cardiac Dysfunction by Serial Evaluation of Circumferential Strain in Patients With Duchenne Muscular Dystrophy. *The American Journal of Cardiology,* 105**,** 1451-1455.

HAMILTON, D. M. & HAENNEL, R. G. 2000. Validity and reliability of the 6-minute walk test in a cardiac rehabilitation population. *J Cardiopulm Rehabil,* 20**,** 156-164.

HAREL, T., GOLDBERG, Y., SHALEV, S. A., CHERVINSKI, I., OFIR, R. & BIRK, O. S. 2003. Limb-girdle muscular dystrophy 2I: phenotypic variability within a large consanguineous Bedouin family associated with a novel FKRP mutation. *Eur J Hum Genet,* 12**,** 38-43.

HATHOUT, Y., BRODY, E., CLEMENS, P. R., CRIPE, L., DELISLE, R. K., FURLONG, P., GORDISH-DRESSMAN, H., HACHE, L., HENRICSON, E., HOFFMAN, E. P., KOBAYASHI, Y. M., LORTS, A., MAH, J. K., MCDONALD, C., MEHLER, B., NELSON, S., NIKRAD, M., SINGER, B., STEELE, F., STERLING, D., SWEENEY, H. L., WILLIAMS, S. & GOLD, L. 2015. Large-scale serum protein biomarker discovery in Duchenne muscular dystrophy. *Proc Natl Acad Sci U S A,* 112**,** 7153-8.

HAUSMAN, G. J. & POULOS, S. 2004. Recruitment and differentiation of intramuscular preadipocytes in stromal-vascular cell cultures derived from neonatal pig semitendinosus muscles. *J Anim Sci,* 82**,** 429-37.

HELM, P. A., CARAVAN, P., FRENCH, B. A., JACQUES, V., SHEN, L., XU, Y., BEYERS, R. J., ROY, R. J., KRAMER, C. M. & EPSTEIN, F. H. 2008. Postinfarction myocardial scarring in mice: molecular MR imaging with use of a collagen-targeting contrast agent. *Radiology,* 247**,** 788-96.

HENDRIKSEN, R. G. F., HOOGLAND, G., SCHIPPER, S., HENDRIKSEN, J. G. M., VLES, J. S. H. & AALBERS, M. W. 2015. A possible role of dystrophin in neuronal excitability: A review of the current literature. *Neuroscience & Biobehavioral Reviews,* 51**,** 255-262.

HERMANN, P., KOTEK, J., KUBICEK, V. & LUKES, I. 2008. Gadolinium(III) complexes as MRI contrast agents: ligand design and properties of the complexes. *Dalton Trans***,** 3027-47.

HETTERICH, H., BAYERL, C., PETERS, A., HEIER, M., LINKOHR, B., MEISINGER, C., AUWETER, S., KANNENGIESSER, S. A., KRAMER, H., ERTL-WAGNER, B. & BAMBERG, F. 2015. Feasibility of a three-step magnetic resonance imaging approach for the assessment of hepatic steatosis in an asymptomatic study population. *Eur Radiol*.

HICKS, D., SARKOZY, A., MUELAS, N., KOEHLER, K., HUEBNER, A., HUDSON, G., CHINNERY, P. F., BARRESI, R., EAGLE, M., POLVIKOSKI, T., BAILEY, G., MILLER, J., RADUNOVIC, A., HUGHES, P. J., ROBERTS, R., KRAUSE, S., WALTER, M. C., LAVAL, S. H., STRAUB, V., LOCHMULLER, H. & BUSHBY, K. 2011. A founder mutation in Anoctamin 5 is a major cause of limb-girdle muscular dystrophy. *Brain,* 134**,** 171-82.

HIRN, C., SHAPOVALOV, G., PETERMANN, O., ROULET, E. & RUEGG, U. T. 2008. Na(v)1.4 Deregulation in Dystrophic Skeletal Muscle Leads to Na(+) Overload and Enhanced Cell Death. *The Journal of General Physiology,* 132**,** 199-208.

HO, R., NGUYEN, M. L. & MATHER, P. 2016. Cardiomyopathy in becker muscular dystrophy: Overview. *World J Cardiol,* 8**,** 356-61.

HOLLANDER, S. A., RIZZUTO, S., HOLLANDER, A. M., LIN, A., LIU, E., MURRAY, J. M., ALMOND, C. S. & ROSENTHAL, D. N. 2016. Obesity and Premature Loss of Mobility in Two Adolescents with Becker Muscular Dystrophy After HeartMate II Implantation. *ASAIO J,* 62**,** e5-7.

HOLLINGSWORTH, K. G. 2015. Reducing acquisition time in clinical MRI by data undersampling and compressed sensing reconstruction. *Phys Med Biol,* 60**,** R297-322.

HOLLINGSWORTH, K. G., BLAMIRE, A. M., KEAVNEY, B. D. & MACGOWAN, G. A. 2012. Left ventricular torsion, energetics, and diastolic function in normal human aging. *Am J Physiol Heart Circ Physiol,* 302**,** H885-92.

HOLLINGSWORTH, K. G., GARROOD, P., EAGLE, M., BUSHBY, K. & STRAUB, V. 2013a. Magnetic resonance imaging in Duchenne muscular dystrophy: longitudinal assessment of natural history over 18 months. *Muscle Nerve,* 48**,** 586-588.

HOLLINGSWORTH, K. G., WILLIS, T. A., BATES, M. G., DIXON, B. J., LOCHMULLER, H., BUSHBY, K., BOURKE, J., MACGOWAN, G. A. & STRAUB, V. 2013b. Subepicardial dysfunction leads to global left ventricular systolic impairment in patients with limb girdle muscular dystrophy 2I. *Eur J Heart Fail,* 15**,** 986-994.

HOMSI, R., MEIER-SCHROERS, M., GIESEKE, J., DABIR, D., LUETKENS, J., KUETTING, D., NAEHLE, C., MARX, C., SCHILD, H., THOMAS, D. & SPRINKART, A. 2015. 3D-Dixon MRI based volumetry of peri- and epicardial fat. *The International Journal of Cardiovascular Imaging***,** 1-9.

HONG, Y. J., PARK, C. H., KIM, Y. J., HUR, J., LEE, H.-J., HONG, S. R., SUH, Y. J., GREISER, A., PAEK, M. Y., CHOI, B. W. & KIM, T. H. 2015. Extracellular volume fraction in dilated cardiomyopathy patients without obvious late gadolinium enhancement: comparison with healthy control subjects. *The International Journal of Cardiovascular Imaging,* 31**,** 115-122.

HOOIJMANS, M. T., DOORENWEERD, N., BALIGAND, C., VERSCHUUREN, J., RONEN, I., NIKS, E. H., WEBB, A. G. & KAN, H. E. 2017. Spatially localized phosphorous metabolism of skeletal muscle in Duchenne muscular dystrophy patients: 24-month follow-up. *PLoS One,* 12**,** e0182086.

HOR, K. N., TAYLOR, M. D., AL-KHALIDI, H. R., CRIPE, L. H., RAMAN, S. V., JEFFERIES, J. L., O'DONNELL, R., BENSON, D. W. & MAZUR, W. 2013. Prevalence and distribution of late gadolinium enhancement in a large population of patients with Duchenne muscular dystrophy: effect of age and left ventricular systolic function. *J Cardiovasc Magn Reson,* 15**,** 107.

HOR, K. N., WANSAPURA, J., MARKHAM, L. W., MAZUR, W., CRIPE, L. H., FLECK, R., BENSON, D. W. & GOTTLIEBSON, W. M. 2009. Circumferential strain analysis identifies strata of cardiomyopathy in Duchenne muscular dystrophy: a cardiac magnetic resonance tagging study. *J Am Coll Cardiol,* 53**,** 1204-10.

HU, T. C., PAUTLER, R. G., MACGOWAN, G. A. & KORETSKY, A. P. 2001. Manganese-enhanced MRI of mouse heart during changes in inotropy. *Magn Reson Med,* 46**,** 884-90.

HU, X., CHARLES, J. P., AKAY, T., HUTCHINSON, J. R. & BLEMKER, S. S. 2017. Are mice good models for human neuromuscular disease? Comparing muscle excursions in walking between mice and humans. *Skeletal Muscle,* 7**,** 26.

HUANG, H. H., HUANG, C. Y., CHEN, C. N., WANG, Y. W. & HUANG, T. Y. 2018. Automatic regional analysis of myocardial native T1 values: left ventricle segmentation and AHA parcellations. *Int J Cardiovasc Imaging,* 34**,** 131-140.

HUANG, P., ZHAO, X. S., FIELDS, M., RANSOHOFF, R. M. & ZHOU, L. 2009. Imatinib attenuates skeletal muscle dystrophy in mdx mice. *FASEB J,* 23**,** 2539-48.

HUANG, S., CHEN, H. H., YUAN, H., DAI, G., SCHUHLE, D. T., MEKKAOUI, C., NGOY, S., LIAO, R., CARAVAN, P., JOSEPHSON, L. & SOSNOVIK, D. E. 2011. Molecular MRI of acute necrosis with a novel DNA-binding gadolinium chelate: kinetics of cell death and clearance in infarcted myocardium. *Circ Cardiovasc Imaging,* 4**,** 729-37.

HUDSMITH, L. E., PETERSEN, S. E., FRANCIS, J. M., ROBSON, M. D. & NEUBAUER, S. 2005. Normal human left and right ventricular and left atrial dimensions using steady state free precession magnetic resonance imaging. *J Cardiovasc Magn Reson,* 7**,** 775-82.

HUEBNER, K. D., JASSAL, D. S., HALEVY, O., PINES, M. & ANDERSON, J. E. 2008. Functional resolution of fibrosis in mdx mouse dystrophic heart and skeletal muscle by halofuginone. *Am J Physiol Heart Circ Physiol,* 294**,** H1550-61.

HULL, J., ANIAPRAVAN, R., CHAN, E., CHATWIN, M., FORTON, J., GALLAGHER, J., GIBSON, N., GORDON, J., HUGHES, I. & MCCULLOCH, R. 2012. BTS guideline for respiratory management of children with neuromuscular weakness. *Thorax,* 67**,** i1-i40.

IGNAT'EVA, N. Y., DANILOV, N. A., AVERKIEV, S. V., OBREZKOVA, M. V., LUNIN, V. V. & SOBOL', E. N. 2007. Determination of hydroxyproline in tissues and the evaluation of the collagen content of the tissues. *Journal of Analytical Chemistry,* 62**,** 51-57.

ISHIKAWA, Y., BACH, J. R. & MINAMI, R. 1999. Cardioprotection for Duchenne's muscular dystrophy. *Am Heart J,* 137**,** 895-902.

ITO, T., OGAWA, R., UEZUMI, A., OHTANI, T., WATANABE, Y., TSUJIKAWA, K., MIYAGOE-SUZUKI, Y., TAKEDA, S., YAMAMOTO, H. & FUKADA, S. 2013. Imatinib attenuates severe mouse dystrophy and inhibits proliferation and fibrosis-marker expression in muscle mesenchymal progenitors. *Neuromuscul Disord,* 23**,** 349-56.

JACOBS, J., JANSEN, M., JANSSEN, H., RAIJMANN, W., VAN ALFEN, N. & PILLEN, S. 2013. Quantitative muscle ultrasound and muscle force in healthy children: A 4-year follow-up study. *Muscle & Nerve,* 47**,** 856-863.

JANSEN, M., VAN ALFEN, N., NIJHUIS VAN DER SANDEN, M. W., VAN DIJK, J. P., PILLEN, S. & DE GROOT, I. J. 2012. Quantitative muscle ultrasound is a promising longitudinal follow-up tool in Duchenne muscular dystrophy. *Neuromuscul Disord,* 22**,** 306-17.

JARONI, J., MEIER, R., BEER, A., HERRMANN, K., SETTLES, M., RUMMENY, E. J. & HUBER, A. 2013. Three-dimensional magnetic resonance imaging using single breath-hold k-t BLAST for assessment of global left ventricular functional parameters. *Acad Radiol,* 20**,** 987-94.

JEFFERIES, J. L., EIDEM, B. W., BELMONT, J. W., CRAIGEN, W. J., WARE, S. M., FERNBACH, S. D., NEISH, S. R., SMITH, E. O. & TOWBIN, J. A. 2005. Genetic predictors and remodeling of dilated cardiomyopathy in muscular dystrophy. *Circulation,* 112**,** 2799-804.

JOHNSON, K. M., FAIN, S. B., SCHIEBLER, M. L. & NAGLE, S. 2013. Optimized 3D Ultrashort Echo Time Pulmonary MRI. *Magn Reson Med,* 70**,** 1241-50.

JONES, D. E., HOLLINGSWORTH, K., FATTAKHOVA, G., MACGOWAN, G., TAYLOR, R., BLAMIRE, A. & NEWTON, J. L. 2010. Impaired cardiovascular function in primary biliary cirrhosis. *Am J Physiol Gastrointest Liver Physiol,* 298**,** G764-73.

KANAGAWA, M., KOBAYASHI, K., TAJIRI, M., MANYA, H., KUGA, A., YAMAGUCHI, Y., AKASAKA-MANYA, K., FURUKAWA, J. I., MIZUNO, M., KAWAKAMI, H., SHINOHARA, Y., WADA, Y., ENDO, T. & TODA, T. 2016. Identification of a Post-translational Modification with Ribitol-Phosphate and Its Defect in Muscular Dystrophy. *Cell Rep,* 14**,** 2209-2223.

KASPAR, R. W., ALLEN, H. D., RAY, W. C., ALVAREZ, C. E., KISSEL, J. T., PESTRONK, A., WEISS, R. B., FLANIGAN, K. M., MENDELL, J. R. & MONTANARO, F. 2009. Analysis of dystrophin deletion mutations predicts age of cardiomyopathy onset in becker muscular dystrophy. *Circ Cardiovasc Genet,* 2**,** 544-51.

KAWEL, N., NACIF, M., ZAVODNI, A., JONES, J., LIU, S., SIBLEY, C. T. & BLUEMKE, D. A. 2012. T1 mapping of the myocardium: Intra-individual assessment of the effect of field strength, cardiac cycle and variation by myocardial region. *Journal of Cardiovascular Magnetic Resonance,* 14**,** 27.

KELLMAN, P., WILSON, J. R., XUE, H., BANDETTINI, W. P., SHANBHAG, S. M., DRUEY, K. M., UGANDER, M. & ARAI, A. E. 2012. Extracellular volume fraction mapping in the myocardium, part 2: initial clinical experience. *J Cardiovasc Magn Reson,* 14**,** 64.

KEMP, G. J., TAYLOR, D. J., DUNN, J. F., FROSTICK, S. P. & RADDA, G. K. 1993. Cellular energetics of dystrophic muscle. *J Neurol Sci,* 116**,** 201-6.

KEMPEN, J. C., HARLAAR, J., VAN DER KOOI, A. J., DE GROOT, I. J., VAN DEN BERGEN, J. C., NIKS, E. H., VERSCHUUREN, J. J. & BREHM, M. A. 2014. Reliability of the walking energy cost test and the six-minute walk test in boys with Duchenne muscular dystrophy. *Neuromuscul Disord,* 24**,** 216-21.

KHALIL, M. E., BASHER, A. W., BROWN, E. J., JR. & ALHADDAD, I. A. 2001. A remarkable medical story: benefits of angiotensin-converting enzyme inhibitors in cardiac patients. *J Am Coll Cardiol,* 37**,** 1757-64.

KIDO, T., KIDO, T., NAKAMURA, M., WATANABE, K., SCHMIDT, M., FORMAN, C. & MOCHIZUKI, T. 2016. Compressed sensing real-time cine cardiovascular magnetic resonance: accurate assessment of left ventricular function in a single-breath-hold. *J Cardiovasc Magn Reson,* 18**,** 50.

KIERKEGAARD, M. & TOLLBÄCK, A. 2007. Reliability and feasibility of the six minute walk test in subjects with myotonic dystrophy. *Neuromuscular Disorders,* 17**,** 943-949.

KIM, H. K., LAOR, T., HORN, P. S., RACADIO, J. M., WONG, B. & DARDZINSKI, B. J. 2010. T2 mapping in Duchenne muscular dystrophy: distribution of disease activity and correlation with clinical assessments. *Radiology,* 255**,** 899-908.

KIM, H. K., MERROW, A. C., SHIRAJ, S., WONG, B. L., HORN, P. S. & LAOR, T. 2013. Analysis of fatty infiltration and inflammation of the pelvic and thigh muscles in boys with Duchenne muscular dystrophy (DMD): grading of disease involvement on MR imaging and correlation with clinical assessments. *Pediatr Radiol,* 43**,** 1327-35.

KIM, H. K., SERAI, S., LINDQUIST, D., MERROW, A. C., HORN, P. S., KIM, D. H. & WONG, B. L. 2015. Quantitative Skeletal Muscle MRI: Part 2, MR Spectroscopy and T2 Relaxation Time Mapping-Comparison Between Boys With Duchenne Muscular Dystrophy and Healthy Boys. *AJR Am J Roentgenol,* 205**,** W216-23.

KIM, M. M., PAROLIA, A., DUNPHY, M. P. & VENNETI, S. 2016. Non-invasive metabolic imaging of brain tumours in the era of precision medicine. *Nat Rev Clin Oncol*.

KIM, R. J., WU, E., RAFAEL, A., CHEN, E. L., PARKER, M. A., SIMONETTI, O., KLOCKE, F. J., BONOW, R. O. & JUDD, R. M. 2000. The use of contrast-enhanced magnetic resonance imaging to identify reversible myocardial dysfunction. *N Engl J Med,* 343**,** 1445-53.

KINALI, M., ARECHAVALA-GOMEZA, V., CIRAK, S., GLOVER, A., GUGLIERI, M., FENG, L., HOLLINGSWORTH, K. G., HUNT, D., JUNGBLUTH, H., ROPER, H. P., QUINLIVAN, R. M.,

GOSALAKKAL, J. A., JAYAWANT, S., NADEAU, A., HUGHES-CARRE, L., MANZUR, A. Y., MERCURI, E., MORGAN, J. E., STRAUB, V., BUSHBY, K., SEWRY, C., RUTHERFORD, M. & MUNTONI, F. 2011. Muscle histology vs MRI in Duchenne muscular dystrophy. *Neurology,* 76**,** 346-353.

KIRSCHNER, J., SCHESSL, J., SCHARA, U., REITTER, B., STETTNER, G. M., HOBBIEBRUNKEN, E., WILICHOWSKI, E., BERNERT, G., WEISS, S., STEHLING, F., WIEGAND, G., MULLER-FELBER, W., THIELE, S., GRIEBEN, U., VON DER HAGEN, M., LUTSCHG, J., SCHMOOR, C., IHORST, G. & KORINTHENBERG, R. 2010. Treatment of Duchenne muscular dystrophy with ciclosporin A: a randomised, double-blind, placebo-controlled multicentre trial. *Lancet Neurol,* 9**,** 1053-9.

KLINGLER, W., JURKAT-ROTT, K., LEHMANN-HORN, F. & SCHLEIP, R. 2012. The role of fibrosis in Duchenne muscular dystrophy. *Acta Myologica,* 31**,** 184-195.

KLYMIUK, N., BLUTKE, A., GRAF, A., KRAUSE, S., BURKHARDT, K., WUENSCH, A., KREBS, S., KESSLER, B., ZAKHARTCHENKO, V., KUROME, M., KEMTER, E., NAGASHIMA, H., SCHOSER, B., HERBACH, N., BLUM, H., WANKE, R., AARTSMA-RUS, A., THIRION, C., LOCHMULLER, H., WALTER, M. C. & WOLF, E. 2013. Dystrophin-deficient pigs provide new insights into the hierarchy of physiological derangements of dystrophic muscle. *Hum Mol Genet,* 22**,** 4368-82.

KOLE, R. & KRIEG, A. M. 2015. Exon skipping therapy for Duchenne muscular dystrophy. *Advanced Drug Delivery Reviews,* 87**,** 104-107.

KORNEGAY, J. N., BOGAN, J. R., BOGAN, D. J., CHILDERS, M. K., LI, J., NGHIEM, P., DETWILER, D. A., LARSEN, C. A., GRANGE, R. W., BHAVARAJU-SANKA, R. K., TOU, S., KEENE, B. P., HOWARD, J. F., WANG, J., FAN, Z., SCHATZBERG, S. J., STYNER, M. A., FLANIGAN, K. M., XIAO, X. & HOFFMAN, E. P. 2012. Canine Models of Duchenne Muscular Dystrophy and Their Use in Therapeutic Strategies. *Mamm Genome,* 23**,** 85-108.

KOSTAKOW, S. & DERIX, P. 1937. Familienforschung in einer muskeldystrophischen Sippe und die Erbprognose ihrer Mitglieder. . *Dtsch Arch klin Med***,** 180:585.

KRAMER, C. M., BARKHAUSEN, J., FLAMM, S. D., KIM, R. J. & NAGEL, E. 2008. Standardized cardiovascular magnetic resonance imaging (CMR) protocols, society for cardiovascular magnetic resonance: board of trustees task force on standardized protocols. *Journal of Cardiovascular Magnetic Resonance,* 10**,** 35.

KURUVILLA, S., ADENAW, N., KATWAL, A. B., LIPINSKI, M. J., KRAMER, C. M. & SALERNO, M. 2014. Late gadolinium enhancement on cardiac magnetic resonance predicts adverse cardiovascular outcomes in nonischemic cardiomyopathy: a systematic review and meta-analysis. *Circ Cardiovasc Imaging,* 7**,** 250-8.

LAMB, H. J., BEYERBACHT, H. P., VAN DER LAARSE, A., STOEL, B. C., DOORNBOS, J., VAN DER WALL, E. E. & DE ROOS, A. 1999. Diastolic dysfunction in hypertensive heart disease is associated with altered myocardial metabolism. *Circulation,* 99**,** 2261-7.

LAMMINEN, A. E. 1990. Magnetic resonance imaging of primary skeletal muscle diseases: patterns of distribution and severity of involvement. *Br J Radiol,* 63**,** 946-50.

LARCHER, T., LAFOUX, A., TESSON, L., REMY, S., THEPENIER, V., FRANCOIS, V., LE GUINER, C., GOUBIN, H., DUTILLEUL, M., GUIGAND, L., TOUMANIANTZ, G., DE CIAN, A., BOIX, C., RENAUD, J. B., CHEREL, Y., GIOVANNANGELI, C., CONCORDET, J. P., ANEGON, I. & HUCHET, C. 2014. Characterization of dystrophin deficient rats: a new model for Duchenne muscular dystrophy. *PLoS One,* 9**,** e110371.

LAUFFER, R. B., PARMELEE, D. J., DUNHAM, S. U., OUELLET, H. S., DOLAN, R. P., WITTE, S., MCMURRY, T. J. & WALOVITCH, R. C. 1998. MS-325: albumin-targeted contrast agent for MR angiography. *Radiology,* 207**,** 529-38.

LE GUINER, C., MONTUS, M., SERVAIS, L., CHEREL, Y., FRANCOIS, V., THIBAUD, J. L., WARY, C., MATOT, B., LARCHER, T., GUIGAND, L., DUTILLEUL, M., DOMENGER, C., ALLAIS, M., BEUVIN, M., MORAUX, A., LE DUFF, J., DEVAUX, M., JAULIN, N., GUILBAUD, M.,

LATOURNERIE, V., VERON, P., BOUTIN, S., LEBORGNE, C., DESGUE, D., DESCHAMPS, J. Y., MOULLEC, S., FROMES, Y., VULIN, A., SMITH, R. H., LAROUDIE, N., BARNAY-TOUTAIN, F., RIVIERE, C., BUCHER, S., LE, T. H., DELAUNAY, N., GASMI, M., KOTIN, R. M., BONNE, G., ADJALI, O., MASURIER, C., HOGREL, J. Y., CARLIER, P., MOULLIER, P. & VOIT, T. 2014. Forelimb treatment in a large cohort of dystrophic dogs supports delivery of a recombinant AAV for exon skipping in Duchenne patients. *Mol Ther,* 22**,** 1923-35.

LEUNG, D. G., HERZKA, D. A., THOMPSON, W. R., HE, B., BIBAT, G., TENNEKOON, G., RUSSELL, S. D., SCHULERI, K. H., LARDO, A. C., KASS, D. A., THOMPSON, R. E., JUDGE, D. P. & WAGNER, K. R. 2014. Sildenafil does not improve cardiomyopathy in Duchenne/Becker muscular dystrophy. *Ann Neurol,* 76**,** 541-9.

LI, A. M., YIN, J., YU, C. C. W., TSANG, T., SO, H. K., WONG, E., CHAN, D., HON, E. K. L. & SUNG, R. 2005. The six-minute walk test in healthy children: reliability and validity. *European Respiratory Journal,* 25**,** 1057-1060.

LI, G. D., LIANG, Y. Y., XU, P., LING, J. & CHEN, Y. M. 2016. Diffusion-Tensor Imaging of Thigh Muscles in Duchenne Muscular Dystrophy: Correlation of Apparent Diffusion Coefficient and Fractional Anisotropy Values With Fatty Infiltration. *AJR Am J Roentgenol,* 206**,** 867-70.

LIANG, M. H. 2000. Longitudinal construct validity: establishment of clinical meaning in patient evaluative instruments. *Med Care,* 38**,** Ii84-90.

LIN, A. C., STRUGNELL, W., RILEY, R., SCHMITT, B., ZENGE, M., SCHMIDT, M., MORRIS, N. R. & HAMILTON-CRAIG, C. 2016. Higher resolution cine imaging with compressed sensing for accelerated clinical left ventricular evaluation. *J Magn Reson Imaging*.

LIU, J., FENG, L., SHEN, H.-W., ZHU, C., WANG, Y., MUKAI, K., BROOKS, G. C., ORDOVAS, K. & SALONER, D. 2017. Highly-accelerated self-gated free-breathing 3D cardiac cine MRI: validation in assessment of left ventricular function. *Magnetic Resonance Materials in Physics, Biology and Medicine***,** 1-10.

LODI, R., MUNTONI, F., TAYLOR, J., KUMAR, S., SEWRY, C. A., BLAMIRE, A., STYLES, P. & TAYLOR, D. J. 1997. Correlative MR imaging and 31P-MR spectroscopy study in sarcoglycan deficient limb girdle muscular dystrophy. *Neuromuscul Disord,* 7**,** 505-11.

LOEHR, J. A., STINNETT, G. R., HERNANDEZ-RIVERA, M., ROTEN, W. T., WILSON, L. J., PAUTLER, R. G. & RODNEY, G. G. 2016. Eliminating Nox2 reactive oxygen species production protects dystrophic skeletal muscle from pathological calcium influx assessed in vivo by manganese-enhanced magnetic resonance imaging. *J Physiol,* 594**,** 6395-6405.

LOKKEN, N., HEDERMANN, G., THOMSEN, C. & VISSING, J. 2016. Contractile properties are disrupted in Becker muscular dystrophy, but not in limb girdle type 2I. *Ann Neurol,* 80**,** 466-471.

LOUIS, W. M., DAVID, M. H., CARL, N. P., SOPHIE, C., KENNETH, K. H., ANNA, C., ROY, T. & KIEREN, G. H. 2016. Accelerating MR Imaging Liver Steatosis Measurement Using Combined Compressed Sensing and Parallel Imaging: A Quantitative Evaluation. *Radiology,* 278**,** 247-256.

LUMENS, J., DELHAAS, T., ARTS, T., COWAN, B. R. & YOUNG, A. A. 2006. Impaired subendocardial contractile myofiber function in asymptomatic aged humans, as detected using MRI. *Am J Physiol Heart Circ Physiol,* 291**,** H1573-9.

LUSTIG, M., DONOHO, D. L., SANTOS, J. M. & PAULY, J. M. 2008. Compressed Sensing MRI. *IEEE Signal Processing Magazine,* 25**,** 72-82.

MA, J. 2008. Dixon techniques for water and fat imaging. *Journal of Magnetic Resonance Imaging,* 28**,** 543-558.

MACGOWAN, G. A., SHAPIRO, E. P., AZHARI, H., SIU, C. O., HEES, P. S., HUTCHINS, G. M., WEISS, J. L. & RADEMAKERS, F. E. 1997. Noninvasive measurement of shortening in the fiber and cross-fiber directions in the normal human left ventricle and in idiopathic dilated cardiomyopathy. *Circulation,* 96**,** 535-41.

MANKODI, A., AZZABOU, N., BULEA, T., REYNGOUDT, H., SHIMELLIS, H., REN, Y., KIM, E., FISCHBECK, K. H. & CARLIER, P. G. 2017. Skeletal muscle water T2 as a biomarker of disease status and exercise effects in patients with Duchenne muscular dystrophy. *Neuromuscul Disord,* 27**,** 705-714.

MANUS, L. M., STRAUCH, R. C., HUNG, A. H., ECKERMANN, A. L. & MEADE, T. J. 2012. Analytical Methods for Characterizing Magnetic Resonance Probes. *Analytical chemistry,* 84**,** 6278-6287.

MATSUMURA, K., NAKANO, I., FUKUDA, N., IKEHIRA, H., TATENO, Y. & AOKI, Y. 1988. Proton spin-lattice relaxation time of Duchenne dystrophy skeletal muscle by magnetic resonance imaging. *Muscle Nerve,* 11**,** 97-102.

MATTHEWS, E., BRASSINGTON, R., KUNTZER, T., JICHI, F. & MANZUR, A. Y. 2016. Corticosteroids for the treatment of Duchenne muscular dystrophy. *Cochrane Database of Systematic Reviews*.

MAUGHAN, R. J., WATSON, J. S. & WEIR, J. 1983. Strength and cross‐sectional area of human skeletal muscle. *The Journal of Physiology,* 338**,** 37-49.

MAVROGENI, S., PAPAVASILIOU, A., DOUSKOU, M., KOLOVOU, G., PAPADOPOULOU, E. & COKKINOS, D. V. 2009. Effect of deflazacort on cardiac and sternocleidomastoid muscles in Duchenne muscular dystrophy: a magnetic resonance imaging study. *Eur J Paediatr Neurol,* 13**,** 34-40.

MAVROGENI, S., PAPAVASILIOU, A., GIANNAKOPOULOU, K., MARKOUSIS‐MAVROGENIS, G., PONS MARIA, R., KARANASIOS, E., NIKAS, I., PAPADOPOULOS, G., KOLOVOU, G. & CHROUSOS GEORGE, P. 2017. Oedema‐fibrosis in Duchenne Muscular Dystrophy: Role of cardiovascular magnetic resonance imaging. *European Journal of Clinical Investigation,* 47**,** e12843.

MAYHEW, A., MAZZONE, E. S., EAGLE, M., DUONG, T., ASH, M., DECOSTRE, V., VANDENHAUWE, M., KLINGELS, K., FLORENCE, J., MAIN, M., BIANCO, F., HENRIKSON, E., SERVAIS, L., CAMPION, G., VROOM, E., RICOTTI, V., GOEMANS, N., MCDONALD, C., MERCURI, E. & PERFORMANCE OF THE UPPER LIMB WORKING, G. 2013a. Development of the Performance of the Upper Limb module for Duchenne muscular dystrophy. *Developmental Medicine & Child Neurology,* 55**,** 1038-1045.

MAYHEW, A. G., CANO, S. J., SCOTT, E., EAGLE, M., BUSHBY, K., MANZUR, A. & MUNTONI, F. 2013b. Detecting meaningful change using the North Star Ambulatory Assessment in Duchenne muscular dystrophy. *Dev Med Child Neurol,* 55**,** 1046-52.

MAZZONE, E., MARTINELLI, D., BERARDINELLI, A., MESSINA, S., D'AMICO, A., VASCO, G., MAIN, M., DOGLIO, L., POLITANO, L., CAVALLARO, F., FROSINI, S., BELLO, L., CARLESI, A., BONETTI, A. M., ZUCCHINI, E., SANCTIS, R. D., SCUTIFERO, M., BIANCO, F., ROSSI, F., MOTTA, M. C., SACCO, A., DONATI, M. A., MONGINI, T., PINI, A., BATTINI, R., PEGORARO, E., PANE, M., PASQUINI, E., BRUNO, C., VITA, G., WAURE, C. D., BERTINI, E. & MERCURI, E. 2010. North Star Ambulatory Assessment, 6-minute walk test and timed items in ambulant boys with Duchenne muscular dystrophy. *Neuromuscular Disorders,* 20**,** 712-716.

MAZZONE, E. S., MESSINA, S., VASCO, G., MAIN, M., EAGLE, M., D'AMICO, A., DOGLIO, L., POLITANO, L., CAVALLARO, F., FROSINI, S., BELLO, L., MAGRI, F., CORLATTI, A., ZUCCHINI, E., BRANCALION, B., ROSSI, F., FERRETTI, M., MOTTA, M. G., CECIO, M. R., BERARDINELLI, A., ALFIERI, P., MONGINI, T., PINI, A., ASTREA, G., BATTINI, R., COMI, G., PEGORARO, E., MORANDI, L., PANE, M., ANGELINI, C., BRUNO, C., VILLANOVA, M., VITA, G., DONATI, M. A., BERTINI, E. & MERCURI, E. 2009. Reliability of the North Star Ambulatory Assessment in a multicentric setting. *Neuromuscular Disorders,* 19**,** 458-461.

MCCROHON, J. A., MOON, J. C., PRASAD, S. K., MCKENNA, W. J., LORENZ, C. H., COATS, A. J. & PENNELL, D. J. 2003. Differentiation of heart failure related to dilated cardiomyopathy

and coronary artery disease using gadolinium-enhanced cardiovascular magnetic resonance. *Circulation,* 108**,** 54-9.

MCCULLY, K., SHELLOCK, F. G., BANK, W. J. & POSNER, J. D. 1992. The use of nuclear magnetic resonance to evaluate muscle injury. *Medicine and science in sports and exercise,* 24**,** 537-542.

MCDONALD, C. M., HENRICSON, E. K., ABRESCH, R. T., FLORENCE, J. M., EAGLE, M., GAPPMAIER, E., GLANZMAN, A. M., FOR THE, P. G.-D. S. G., SPIEGEL, R., BARTH, J., ELFRING, G., REHA, A. & PELTZ, S. 2013. THE 6-MINUTE WALK TEST AND OTHER ENDPOINTS IN DUCHENNE MUSCULAR DYSTROPHY: LONGITUDINAL NATURAL HISTORY OBSERVATIONS OVER 48 WEEKS FROM A MULTICENTER STUDY. *Muscle & Nerve,* 48**,** 343-356.

MCDONALD, C. M., HENRICSON, E. K., HAN, J. J., ABRESCH, R. T., NICORICI, A., ELFRING, G. L., ATKINSON, L., REHA, A., HIRAWAT, S. & MILLER, L. L. 2010. The 6-minute walk test as a new outcome measure in Duchenne muscular dystrophy. *Muscle Nerve,* 41**,** 500-10.

MCGAHA, T. L., PHELPS, R. G., SPIERA, H. & BONA, C. 2002. Halofuginone, an inhibitor of type-I collagen synthesis and skin sclerosis, blocks transforming-growth-factor-beta-mediated Smad3 activation in fibroblasts. *J Invest Dermatol,* 118**,** 461-70.

MCGIBNEY, G., SMITH, M. R., NICHOLS, S. T. & CRAWLEY, A. 1993. Quantitative evaluation of several partial Fourier reconstruction algorithms used in MRI. *Magn Reson Med,* 30**,** 51-9.

MCINTOSH, L. M., BAKER, R. E. & ANDERSON, J. E. 1998. Magnetic resonance imaging of regenerating and dystrophic mouse muscle. *Biochemistry and Cell Biology,* 76**,** 532-541.

MENDELL, J. R., GOEMANS, N., LOWES, L. P., ALFANO, L. N., BERRY, K., SHAO, J., KAYE, E. M. & MERCURI, E. 2016. Longitudinal effect of eteplirsen versus historical control on ambulation in Duchenne muscular dystrophy. *Ann Neurol,* 79**,** 257-71.

MENDELL, J. R., SHILLING, C., LESLIE, N. D., FLANIGAN, K. M., AL-DAHHAK, R., GASTIER-FOSTER, J., KNEILE, K., DUNN, D. M., DUVAL, B., AOYAGI, A., HAMIL, C., MAHMOUD, M., ROUSH, K., BIRD, L., RANKIN, C., LILLY, H., STREET, N., CHANDRASEKAR, R. & WEISS, R. B. 2012. Evidence-based path to newborn screening for Duchenne muscular dystrophy. *Ann Neurol,* 71**,** 304-13.

MERCURI, E., PICHIECCHIO, A., ALLSOP, J., MESSINA, S., PANE, M. & MUNTONI, F. 2007. Muscle MRI in inherited neuromuscular disorders: Past, present, and future. *Journal of Magnetic Resonance Imaging,* 25**,** 433-440.

MERCURI, E., PICHIECCHIO, A., COUNSELL, S., ALLSOP, J., CINI, C., JUNGBLUTH, H., UGGETTI, C. & BYDDER, G. 2002. A short protocol for muscle MRI in children with muscular dystrophies. *Eur J Paediatr Neurol,* 6**,** 305-7.

MILLER, C. A., NAISH, J. H., BISHOP, P., COUTTS, G., CLARK, D., ZHAO, S., RAY, S. G., YONAN, N., WILLIAMS, S. G., FLETT, A. S., MOON, J. C., GREISER, A., PARKER, G. J. & SCHMITT, M. 2013. Comprehensive validation of cardiovascular magnetic resonance techniques for the assessment of myocardial extracellular volume. *Circ Cardiovasc Imaging,* 6**,** 373-83.

MOAT, S. J., BRADLEY, D. M., SALMON, R., CLARKE, A. & HARTLEY, L. 2013. Newborn bloodspot screening for Duchenne muscular dystrophy: 21 years experience in Wales (UK). *Eur J Hum Genet,* 21**,** 1049-53.

MOON, J. C., MESSROGHLI, D. R., KELLMAN, P., PIECHNIK, S. K., ROBSON, M. D., UGANDER, M., GATEHOUSE, P. D., ARAI, A. E., FRIEDRICH, M. G. & NEUBAUER, S. 2013. Myocardial T1 mapping and extracellular volume quantification: a Society for Cardiovascular Magnetic Resonance (SCMR) and CMR Working Group of the European Society of Cardiology consensus statement. *Journal of Cardiovascular Magnetic Resonance,* 15**,** 1.

MORI, K., MANABE, T., NII, M., HAYABUCHI, Y., KURODA, Y. & TATARA, K. 2002. Plasma levels of natriuretic peptide and echocardiographic parameters in patients with Duchenne's progressive muscular dystrophy. *Pediatr Cardiol,* 23**,** 160-6.

MORROW, D. A., ANTMAN, E. M., TANASIJEVIC, M., RIFAI, N., DE LEMOS, J. A., MCCABE, C. H., CANNON, C. P. & BRAUNWALD, E. 2000. Cardiac troponin I for stratification of early

outcomes and the efficacy of enoxaparin in unstable angina: a TIMI-11B substudy. *Journal of the American College of Cardiology,* 36**,** 1812-1817.

MURPHY, A. & STRAUB, V. 2015. The Classification, Natural History and Treatment of the Limb Girdle Muscular Dystrophies. *Journal of Neuromuscular Diseases,* 2**,** 7-19.

MURPHY, A. P., GREALLY, E., O'HOGAIN, D., BLAMIRE, A., CARAVAN, P. & STRAUB, V. 2018. Noninvasive quantification of fibrosis in skeletal and cardiac muscle in mdx mice using EP3533 enhanced magnetic resonance imaging. *Magn Reson Med*.

NADARAJAH, V. D., VAN PUTTEN, M., CHAOUCH, A., GARROOD, P., STRAUB, V., LOCHMÜLLER, H., GINJAAR, H. B., AARTSMA-RUS, A. M., VAN OMMEN, G. J. B., DEN DUNNEN, J. T. & 'T HOEN, P. A. C. 2011. Serum matrix metalloproteinase-9 (MMP-9) as a biomarker for monitoring disease progression in Duchenne muscular dystrophy (DMD). *Neuromuscular Disorders,* 21**,** 569-578.

NAGAO, H., MORIMOTO, T., SANO, N., TAKAHASHI, M., NAGAI, H., TAWA, R., YOSHIMATSU, M., WOO, Y. J. & MATSUDA, H. 1991. [Magnetic resonance imaging of skeletal muscle in patients with Duchenne muscular dystrophy--serial axial and sagittal section studies]. *No To Hattatsu,* 23**,** 39-43.

NEELEY, C., MORITZ, M., BROWN, J. J. & ZHOU, Y. 2016. Acute side effects of three commonly used gadolinium contrast agents in the paediatric population. *The British Journal of Radiology,* 89**,** 20160027.

NEUMAN, R. E. & LOGAN, M. A. 1950. The determination of hydroxyproline. *J Biol Chem,* 184**,** 299-306.

NICOLAS, A., RAGUÉNÈS-NICOL, C., BEN YAOU, R., AMEZIANE-LE HIR, S., CHÉRON, A., VIÉ, V., CLAUSTRES, M., LETURCQ, F., DELALANDE, O., HUBERT, J.-F., TUFFERY-GIRAUD, S., GIUDICE, E., LE RUMEUR, E. & THE FRENCH NETWORK OF CLINICAL REFERENCE CENTRES FOR NEUROMUSCULAR, D. 2015. Becker muscular dystrophy severity is linked to the structure of dystrophin. *Human Molecular Genetics,* 24**,** 1267-1279.

NIGRO, G., COMI, L. I., POLITANO, L., LIMONGELLI, F. M., NIGRO, V., DE RIMINI, M. L., GIUGLIANO, M. A., PETRETTA, V. R., PASSAMANO, L., RESTUCCI, B. & ET AL. 1995. Evaluation of the cardiomyopathy in Becker muscular dystrophy. *Muscle Nerve,* 18**,** 283-91.

NISHIO, H., WADA, H., MATSUO, T., HORIKAWA, H., TAKAHASHI, K., NAKAJIMA, T., MATSUO, M. & NAKAMURA, H. 1990. Glucose, free fatty acid and ketone body metabolism in Duchenne muscular dystrophy. *Brain Dev,* 12**,** 390-402.

NISKANEN, J. *Aedes a tool for analyzing medical images* [Online]. Available: http://aedes.uef.fi/ [Accessed 1st of February 2016 2016].

NORWOOD, F. L., HARLING, C., CHINNERY, P. F., EAGLE, M., BUSHBY, K. & STRAUB, V. 2009a. Prevalence of genetic muscle disease in Northern England: in-depth analysis of a muscle clinic population. *Brain,* 132**,** 3175-86.

NORWOOD, F. L. M., HARLING, C., CHINNERY, P. F., EAGLE, M., BUSHBY, K. & STRAUB, V. 2009b. Prevalence of genetic muscle disease in Northern England: in-depth analysis of a muscle clinic population. *Brain,* 132**,** 3175-3186.

NOVUS BIOLOGICALS. 2018. *Collagen 1 antibody* [Online]. Available: https://www.novusbio.com/products/collagen-i-alpha-1-antibody_nb600-408 [Accessed 9th of May 2018].

O'HANLON, R., GRASSO, A., ROUGHTON, M., MOON, J. C., CLARK, S., WAGE, R., WEBB, J., KULKARNI, M., DAWSON, D., SULAIBEEKH, L., CHANDRASEKARAN, B., BUCCIARELLI-DUCCI, C., PASQUALE, F., COWIE, M. R., MCKENNA, W. J., SHEPPARD, M. N., ELLIOTT, P. M., PENNELL, D. J. & PRASAD, S. K. 2010. Prognostic significance of myocardial fibrosis in hypertrophic cardiomyopathy. *J Am Coll Cardiol,* 56**,** 867-74.

OGATA, H., ISHIKAWA, Y., ISHIKAWA, Y. & MINAMI, R. 2009. Beneficial effects of beta-blockers and angiotensin-converting enzyme inhibitors in Duchenne muscular dystrophy. *J Cardiol,* 53**,** 72-8.

OLIVIERI, L. J., KELLMAN, P., MCCARTER, R. J., CROSS, R. R., HANSEN, M. S. & SPURNEY, C. F. 2017. Native T1 values identify myocardial changes and stratify disease severity in patients with Duchenne muscular dystrophy. *Journal of Cardiovascular Magnetic Resonance,* 18**,** 72.

OSMAN, N. F., KERWIN, W. S., MCVEIGH, E. R. & PRINCE, J. L. 1999. Cardiac motion tracking using CINE harmonic phase (HARP) magnetic resonance imaging. *Magn Reson Med,* 42**,** 1048-60.

OSMAN, N. F., SAMPATH, S., ATALAR, E. & PRINCE, J. L. 2001. Imaging longitudinal cardiac strain on short-axis images using strain-encoded MRI. *Magn Reson Med,* 46**,** 324-34.

PANE, M., MESSINA, S., BRUNO, C., D'AMICO, A., VILLANOVA, M., BRANCALION, B., SIVO, S., BIANCO, F., STRIANO, P., BATTAGLIA, D., LETTORI, D., VITA, G. L., BERTINI, E., GUALANDI, F., RICOTTI, V., FERLINI, A. & MERCURI, E. 2013. Duchenne muscular dystrophy and epilepsy. *Neuromuscul Disord,* 23**,** 313-5.

PASSAMANO, L., TAGLIA, A., PALLADINO, A., VIGGIANO, E., D'AMBROSIO, P., SCUTIFERO, M., ROSARIA CECIO, M., TORRE, V., DE LUCA, F., PICILLO, E., PACIELLO, O., PILUSO, G., NIGRO, G. & POLITANO, L. 2012. Improvement of survival in Duchenne. *Acta Myol,* 31**,** 121-5.

PEGORARO, E. & HOFFMAN, E. P. 1993. Limb-Girdle Muscular Dystrophy Overview. *In:* PAGON, R. A., ADAM, M. P., ARDINGER, H. H., WALLACE, S. E., AMEMIYA, A., BEAN, L. J. H., BIRD, T. D., DOLAN, C. R., FONG, C. T., SMITH, R. J. H. & STEPHENS, K. (eds.) *GeneReviews(R).* Seattle WA: University of Washington, Seattle.

PERCIVAL, J. M., WHITEHEAD, N. P., ADAMS, M. E., ADAMO, C. M., BEAVO, J. A. & FROEHNER, S. C. 2012. Sildenafil reduces respiratory muscle weakness and fibrosis in the mdx mouse model of Duchenne muscular dystrophy. *J Pathol,* 228**,** 77-87.

PERINI, J. A., ANGELI-GAMBA, T., ALESSANDRA-PERINI, J., FERREIRA, L. C., NASCIUTTI, L. E. & MACHADO, D. E. 2015. Topical application of Acheflan on rat skin injury accelerates wound healing: a histopathological, immunohistochemical and biochemical study. *BMC Complement Altern Med,* 15**,** 203.

PESSINA, P., CABRERA, D., MORALES, M., RIQUELME, C., GUTIÉRREZ, J., L SERRANO, A., BRANDAN, E. & MUÑOZ-CÁNOVES, P. 2014a. *Novel and optimized strategies for inducing fibrosis in vivo: Focus on Duchenne Muscular Dystrophy*.

PESSINA, P., CABRERA, D., MORALES, M. G., RIQUELME, C. A., GUTIERREZ, J., SERRANO, A. L., BRANDAN, E. & MUNOZ-CANOVES, P. 2014b. Novel and optimized strategies for inducing fibrosis in vivo: focus on Duchenne Muscular Dystrophy. *Skelet Muscle,* 4**,** 7.

PETRI, H., SVEEN, M. L., THUNE, J. J., VISSING, C., DAHLQVIST, J. R., WITTING, N., BUNDGAARD, H., KOBER, L. & VISSING, J. 2015. Progression of cardiac involvement in patients with limb-girdle type 2 and Becker muscular dystrophies: a 9-year follow-up study. *Int J Cardiol,* 182**,** 403-11.

PILLEN, S., TAK, R. O., ZWARTS, M. J., LAMMENS, M. M. Y., VERRIJP, K. N., ARTS, I. M. P., VAN DER LAAK, J. A., HOOGERBRUGGE, P. M., VAN ENGELEN, B. G. M. & VERRIPS, A. 2009. Skeletal Muscle Ultrasound: Correlation Between Fibrous Tissue and Echo Intensity. *Ultrasound in Medicine & Biology,* 35**,** 443-446.

PILLEN, S., VERRIPS, A., VAN ALFEN, N., ARTS, I. M. P., SIE, L. T. L. & ZWARTS, M. J. 2007. Quantitative skeletal muscle ultrasound: Diagnostic value in childhood neuromuscular disease. *Neuromuscular Disorders,* 17**,** 509-516.

PINES, M. 2014. Halofuginone for fibrosis, regeneration and cancer in the gastrointestinal tract. *World J Gastroenterol,* 20**,** 14778-86.

PISTILLI, E. E., BOGDANOVICH, S., GONCALVES, M. D., AHIMA, R. S., LACHEY, J., SEEHRA, J. & KHURANA, T. 2011. Targeting the Activin Type IIB Receptor to Improve Muscle Mass and Function in the mdx Mouse Model of Duchenne Muscular Dystrophy. *The American Journal of Pathology,* 178**,** 1287-1297.

POLASEK, M., FUCHS, B. C., UPPAL, R., SCHUHLE, D. T., ALFORD, J. K., LOVING, G. S., YAMADA, S., WEI, L., LAUWERS, G. Y., GUIMARAES, A. R., TANABE, K. K. & CARAVAN, P. 2012.

Molecular MR imaging of liver fibrosis: a feasibility study using rat and mouse models. *J Hepatol,* 57**,** 549-55.

POLASEK, M., YANG, Y., SCHUHLE, D. T., YASEEN, M. A., KIM, Y. R., SUNG, Y. S., GUIMARAES, A. R. & CARAVAN, P. 2017a. Molecular MR imaging of fibrosis in a mouse model of pancreatic cancer. *Sci Rep,* 7**,** 8114.

POLASEK, M., YANG, Y., SCHÜHLE, D. T., YASEEN, M. A., KIM, Y. R., SUNG, Y. S., GUIMARAES, A. R. & CARAVAN, P. 2017b. Molecular MR imaging of fibrosis in a mouse model of pancreatic cancer. *Scientific Reports,* 7**,** 8114.

PONRARTANA, S., RAMOS-PLATT, L., WREN, T. A. L., HU, H. H., PERKINS, T. G., CHIA, J. M. & GILSANZ, V. 2015. Effectiveness of diffusion tensor imaging in assessing disease severity in Duchenne muscular dystrophy: preliminary study. *Pediatric Radiology,* 45**,** 582-589.

POP, M., GHUGRE, N. R., RAMANAN, V., MORIKAWA, L., STANISZ, G., DICK, A. J. & WRIGHT, G. A. 2013. Quantification of fibrosis in infarcted swine hearts by ex vivo late gadolinium-enhancement and diffusion-weighted MRI methods. *Phys Med Biol,* 58**,** 5009-28.

POPPE, M., BOURKE, J., EAGLE, M., FROSK, P., WROGEMANN, K., GREENBERG, C., MUNTONI, F., VOIT, T., STRAUB, V., HILTON-JONES, D., SHIRODARIA, C. & BUSHBY, K. 2004. Cardiac and respiratory failure in limb-girdle muscular dystrophy 2I. *Ann Neurol,* 56**,** 738-41.

POPPE, M., CREE, L., BOURKE, J., EAGLE, M., ANDERSON, L. V., BIRCHALL, D., BROCKINGTON, M., BUDDLES, M., BUSBY, M., MUNTONI, F., WILLS, A. & BUSHBY, K. 2003. The phenotype of limb-girdle muscular dystrophy type 2I. *Neurology,* 60**,** 1246-1251.

POZO, E., VILIANI, D., AGUIRRE, N., AGUDO-QUILEZ, P., OLIVERA, M. J., CABALLERO, P., JIMENEZ-BORREGUERO, L. J. & ALFONSO, F. 2016. Early gadolinium enhancement in hypertrophic cardiomyopathy: a potential premature marker of myocardial damage. *Int J Cardiovasc Imaging*.

PREISLER, N., LUKACS, Z., VINGE, L., MADSEN, K. L., HUSU, E., HANSEN, R. S., DUNO, M., ANDERSEN, H., LAUB, M. & VISSING, J. 2013. Late-onset Pompe disease is prevalent in unclassified limb-girdle muscular dystrophies. *Mol Genet Metab,* 110**,** 287-9.

PUCHALSKI, M. D., WILLIAMS, R. V., ASKOVICH, B., SOWER, C. T., HOR, K. H., SU, J. T., PACK, N., DIBELLA, E. & GOTTLIEBSON, W. M. 2009. Late gadolinium enhancement: precursor to cardiomyopathy in Duchenne muscular dystrophy? *Int J Cardiovasc Imaging,* 25**,** 57-63.

PUNTMANN, V. O., PEKER, E., CHANDRASHEKHAR, Y. & NAGEL, E. 2016. T1 Mapping in Characterizing Myocardial Disease: A Comprehensive Review. *Circ Res,* 119**,** 277-99.

QIAO, C., WANG, C. H., ZHAO, C., LU, P., AWANO, H., XIAO, B., LI, J., YUAN, Z., DAI, Y., MARTIN, C. B., LI, J., LU, Q. & XIAO, X. 2014. Muscle and heart function restoration in a limb girdle muscular dystrophy 2I (LGMD2I) mouse model by systemic FKRP gene delivery. *Mol Ther,* 22**,** 1890-1899.

QUINLAN, J. G., HAHN, H. S., WONG, B. L., LORENZ, J. N., WENISCH, A. S. & LEVIN, L. S. 2004. Evolution of the mdx mouse cardiomyopathy: physiological and morphological findings. *Neuromuscular Disorders,* 14**,** 491-496.

RADUNSKI, U. K., LUND, G. K., STEHNING, C., SCHNACKENBURG, B., BOHNEN, S., ADAM, G., BLANKENBERG, S. & MUELLERLEILE, K. 2014. CMR in patients with severe myocarditis: diagnostic value of quantitative tissue markers including extracellular volume imaging. *JACC Cardiovasc Imaging,* 7**,** 667-75.

RAHIMOV, F. & KUNKEL, L. M. 2013. Cellular and molecular mechanisms underlying muscular dystrophy. *The Journal of Cell Biology,* 201**,** 499-510.

RAMACIOTTI, C., HEISTEIN, L. C., COURSEY, M., LEMLER, M. S., EAPEN, R. S., IANNACCONE, S. T. & SCOTT, W. A. 2006. Left ventricular function and response to enalapril in patients with duchenne muscular dystrophy during the second decade of life. *Am J Cardiol,* 98**,** 825-7.

RAMAN, S. V., HOR, K. N., MAZUR, W., HALNON, N. J., KISSEL, J. T., HE, X., TRAN, T., SMART, S., MCCARTHY, B., TAYLOR, M. D., JEFFERIES, J. L., RAFAEL-FORTNEY, J. A., LOWE, J., ROBLE, S. L. & CRIPE, L. H. 2015. Eplerenone for early cardiomyopathy in Duchenne muscular

dystrophy: a randomised, double-blind, placebo-controlled trial. *Lancet Neurol,* 14**,** 153-61.

RASMUSSEN, M., SCHEIE, D., BREIVIK, N., MORK, M. & LINDAL, S. 2014. Clinical and muscle biopsy findings in Norwegian paediatric patients with limb girdle muscular dystrophy 2I. *Acta Paediatr,* 103**,** 553-8.

RICHARD, I., LAURENT, J.-P., CIRAK, S., VISSING, J., BROWN, S., CAMPBELL, K., CIRAK, S., GICQUEL, E., HOGREL, J.-Y., HONNET, G., KOELMA, N., LAURENT, J.-P., MATHEWS, K., MUNTONI, F., QUIJANO-ROY, S., RICHARD, I., ROBERTSON, A., STEVENSON, H., STOJKOVIC, T., STRAUB, V., TOPALOGLU, H., VAJSAR, J., VISSING, J. & WALTER, M. 2016. 216th ENMC international workshop: Clinical readiness in FKRP related myopathies January 15–17, 2016 Naarden, The Netherlands. *Neuromuscular Disorders,* 26**,** 717-724.

RICOTTI, V., EVANS, M. R. B., SINCLAIR, C. D. J., BUTLER, J. W., RIDOUT, D. A., HOGREL, J.-Y., EMIRA, A., MORROW, J. M., REILLY, M. M., HANNA, M. G., JANICZEK, R. L., MATTHEWS, P. M., YOUSRY, T. A., MUNTONI, F. & THORNTON, J. S. 2016. Upper Limb Evaluation in Duchenne Muscular Dystrophy: Fat-Water Quantification by MRI, Muscle Force and Function Define Endpoints for Clinical Trials. *PLoS ONE,* 11**,** e0162542.

RICOTTI, V., RIDOUT, D. A., PANE, M., MAIN, M., MAYHEW, A., MERCURI, E., MANZUR, A. Y., MUNTONI, F. & ON BEHALF OF, U. K. N. C. N. 2015. The NorthStar Ambulatory Assessment in Duchenne muscular dystrophy: considerations for the design of clinical trials. *Journal of Neurology, Neurosurgery & Psychiatry*.

RIVAS, E., VISSING, J., SCOTO, M., FERNANDEZ-FUENTE, M., VOIT, T., MUNTONI, F. & BROWN, S. 2014. G.P.320: Phenotypic heterogeneity of the c.919T>A FKRP gene mutation in humans and a mouse model. *Neuromuscular Disorders,* 24**,** 918.

ROBERTSON, A. S., MAJCHRZAK, M. J., SMITH, C. M., GAGNON, R. C., DEVIDZE, N., BANKS, G. B., LITTLE, S. C., NABBIE, F., BOUNOUS, D. I., DIPIERO, J., JACOBSEN, L. K., BRISTOW, L. J., AHLIJANIAN, M. K. & STIMPSON, S. A. 2017. Dramatic elevation in urinary amino terminal titin fragment excretion quantified by immunoassay in Duchenne muscular dystrophy patients and in dystrophin deficient rodents. *Neuromuscul Disord,* 27**,** 635-645.

ROMFH, A. & MCNALLY, E. M. 2010. Cardiac Assessment in Duchenne and Becker Muscular Dystrophies. *Current Heart Failure Reports,* 7**,** 212-218.

ROSALES, X. Q., MOSER, S. J., TRAN, T., MCCARTHY, B., DUNN, N., HABIB, P., SIMONETTI, O. P., MENDELL, J. R. & RAMAN, S. V. 2011. Cardiovascular magnetic resonance of cardiomyopathy in limb girdle muscular dystrophy 2B and 2I. *J Cardiovasc Magn Reson,* 13**,** 39.

ROSS, A. J., YANG, Z., BERR, S. S., GILSON, W. D., PETERSEN, W. C., OSHINSKI, J. N. & FRENCH, B. A. 2002. Serial MRI evaluation of cardiac structure and function in mice after reperfused myocardial infarction. *Magn Reson Med,* 47**,** 1158-68.

ROUILLON, J., LEFEBVRE, T., DENARD, J., PUY, V., DAHER, R., AUSSEIL, J., ZOCEVIC, A., FOGEL, P., PEOC'H, K., WONG, B., SERVAIS, L., VOIT, T., PUY, H., KARIM, Z. & SVINARTCHOUK, F. 2018. High urinary ferritin reflects myoglobin iron evacuation in DMD patients. *Neuromuscul Disord*.

SADO, D. M., FLETT, A. S., BANYPERSAD, S. M., WHITE, S. K., MAESTRINI, V., QUARTA, G., LACHMANN, R. H., MURPHY, E., MEHTA, A., HUGHES, D. A., MCKENNA, W. J., TAYLOR, A. M., HAUSENLOY, D. J., HAWKINS, P. N., ELLIOTT, P. M. & MOON, J. C. 2012. Cardiovascular magnetic resonance measurement of myocardial extracellular volume in health and disease. *Heart,* 98**,** 1436-41.

SANDER, M., CHAVOSHAN, B., HARRIS, S. A., IANNACCONE, S. T., STULL, J. T., THOMAS, G. D. & VICTOR, R. G. 2000. Functional muscle ischemia in neuronal nitric oxide synthase-deficient skeletal muscle of children with Duchenne muscular dystrophy. *Proceedings of the National Academy of Sciences,* 97**,** 13818-13823.

SARDONE, V., ELLIS, M., TORELLI, S., FENG, L., CHAMBERS, D., EASTWOOD, D., SEWRY, C., PHADKE, R., MORGAN, J. E. & MUNTONI, F. 2018. A novel high-throughput immunofluorescence analysis method for quantifying dystrophin intensity in entire transverse sections of Duchenne muscular dystrophy muscle biopsy samples. *PLoS One,* 13**,** e0194540.

SATO, K., NAKANISHI, N. & MITSUMOTO, M. 1996. Culture conditions supporting adipose conversion of stromal-vascular cells from bovine intramuscular adipose tissues. *J Vet Med Sci,* 58**,** 1073-8.

SCHELBERT, E. B., HSU, L.-Y., ANDERSON, S. A., MOHANTY, B. D., KARIM, S. M., KELLMAN, P., ALETRAS, A. H. & ARAI, A. E. 2010. Late Gadolinium-Enhancement Cardiac Magnetic Resonance Identifies Postinfarction Myocardial Fibrosis and the Border Zone at the Near Cellular Level in Ex Vivo Rat Heart. *Circulation: Cardiovascular Imaging,* 3**,** 743-752.

SCHELBERT, E. B., PIEHLER, K. M., ZAREBA, K. M., MOON, J. C., UGANDER, M., MESSROGHLI, D. R., VALETI, U. S., CHANG, C. C. H., SHROFF, S. G., DIEZ, J., MILLER, C. A., SCHMITT, M., KELLMAN, P., BUTLER, J., GHEORGHIADE, M. & WONG, T. C. 2015. Myocardial Fibrosis Quantified by Extracellular Volume Is Associated With Subsequent Hospitalization for Heart Failure, Death, or Both Across the Spectrum of Ejection Fraction and Heart Failure Stage. *Journal of the American Heart Association,* 4.

SCHELBERT, E. B., TESTA, S. M., MEIER, C. G., CEYROLLES, W. J., LEVENSON, J. E., BLAIR, A. J., KELLMAN, P., JONES, B. L., LUDWIG, D. R., SCHWARTZMAN, D., SHROFF, S. G. & WONG, T. C. 2011. Myocardial extravascular extracellular volume fraction measurement by gadolinium cardiovascular magnetic resonance in humans: slow infusion versus bolus. *J Cardiovasc Magn Reson,* 13**,** 16.

SCHMIDT, S., HAFNER, P., KLEIN, A., RUBINO-NACHT, D., GOCHEVA, V., SCHROEDER, J., NADUVILEKOOT DEVASIA, A., ZUESLI, S., BERNERT, G., LAUGEL, V., BLOETZER, C., STEINLIN, M., CAPONE, A., GLOOR, M., TOBLER, P., HAAS, T., BIERI, O., ZUMBRUNN, T., FISCHER, D. & BONATI, U. 2018. Timed function tests, motor function measure, and quantitative thigh muscle MRI in ambulant children with Duchenne muscular dystrophy: A cross-sectional analysis. *Neuromuscul Disord,* 28**,** 16-23.

SCHNEIDER, J. E., WIESMANN, F., LYGATE, C. A. & NEUBAUER, S. 2006. How to perform an accurate assessment of cardiac function in mice using high-resolution magnetic resonance imaging. *Journal of Cardiovascular Magnetic Resonance,* 8**,** 693-701.

SCOTT, E., EAGLE, M., MAYHEW, A., FREEMAN, J., MAIN, M., SHEEHAN, J., MANZUR, A. & MUNTONI, F. 2012. Development of a functional assessment scale for ambulatory boys with Duchenne muscular dystrophy. *Physiother Res Int,* 17**,** 101-9.

SHIN, D. G., LEE, H. J., PARK, J., UHM, J. S., PAK, H. N., LEE, M. H., KIM, Y. J. & JOUNG, B. 2016. Pattern of late gadolinium enhancement predicts arrhythmic events in patients with non-ischemic cardiomyopathy. *Int J Cardiol,* 222**,** 9-15.

SICILIANO, G., SIMONCINI, C., GIANNOTTI, S., ZAMPA, V., ANGELINI, C. & RICCI, G. 2015. Muscle exercise in limb girdle muscular dystrophies: pitfall and advantages. *Acta Myol,* 34**,** 3-8.

SIGMA-ALDRICH. 2018. *Halofuginone bromide* [Online]. Available: https://www.sigmaaldrich.com/catalog/search?term=Halofuginone&interface=All&N=0&mode=partialmax&lang=en&region=GB&focus=product [Accessed 8th of May 2018].

SILVERSIDES, C. K., WEBB, G. D., HARRIS, V. A. & BIGGAR, D. W. 2003. Effects of deflazacort on left ventricular function in patients with Duchenne muscular dystrophy. *Am J Cardiol,* 91**,** 769-72.

SLAMAN, J., DALLMEIJER, A., STAM, H., RUSSCHEN, H., ROEBROECK, M. & VAN DEN BERG-EMONS, R. 2013. The six-minute walk test cannot predict peak cardiopulmonary fitness in ambulatory adolescents and young adults with cerebral palsy. *Arch Phys Med Rehabil,* 94**,** 2227-33.

SOSLOW, J. H., DAMON, S. M., CRUM, K., LAWSON, M. A., SLAUGHTER, J. C., XU, M., ARAI, A. E., SAWYER, D. B., PARRA, D. A., DAMON, B. M. & MARKHAM, L. W. 2016. Increased myocardial native T1 and extracellular volume in patients with Duchenne muscular dystrophy. *J Cardiovasc Magn Reson,* 18**,** 5.

SPITALI, P., HETTNE, K., TSONAKA, R., CHARROUT, M., VAN DEN BERGEN, J., KOEKS, Z., KAN, H. E., HOOIJMANS, M. T., ROOS, A., STRAUB, V., MUNTONI, F., AL-KHALILI-SZIGYARTO, C., KOEL-SIMMELINK, M. J. A., TEUNISSEN, C. E., LOCHMULLER, H., NIKS, E. H. & AARTSMA-RUS, A. 2018. Tracking disease progression non-invasively in Duchenne and Becker muscular dystrophies. *J Cachexia Sarcopenia Muscle*.

SPURNEY, C. F., GORDISH-DRESSMAN, H., GUERRON, A. D., SALI, A., PANDEY, G. S., RAWAT, R., VAN DER MEULEN, J. H., CHA, H. J., PISTILLI, E. E., PARTRIDGE, T. A., HOFFMAN, E. P. & NAGARAJU, K. 2009. Preclinical drug trials in the mdx mouse: assessment of reliable and sensitive outcome measures. *Muscle Nerve,* 39**,** 591-602.

SRIVASTAVA, N. K., YADAV, R., MUKHERJEE, S., PAL, L. & SINHA, N. 2017. Abnormal lipid metabolism in skeletal muscle tissue of patients with muscular dystrophy: In vitro, high-resolution NMR spectroscopy based observation in early phase of the disease. *Magn Reson Imaging,* 38**,** 163-173.

STECKLAIR, K. P., HAMBURGER, D. R., EGORIN, M. J., PARISE, R. A., COVEY, J. M. & EISEMAN, J. L. 2001. Pharmacokinetics and tissue distribution of halofuginone (NSC 713205) in CD2F1 mice and Fischer 344 rats. *Cancer Chemother Pharmacol,* 48**,** 375-82.

STEFFENSEN, B., HYDE, S., LYAGER, S. & MATTSSON, E. 2001. Validity of the EK scale: a functional assessment of non-ambulatory individuals with Duchenne muscular dystrophy or spinal muscular atrophy. *Physiother Res Int,* 6**,** 119-34.

STEVENS, E., TORELLI, S., FENG, L., PHADKE, R., WALTER, M. C., SCHNEIDERAT, P., EDDAOUDI, A., SEWRY, C. A. & MUNTONI, F. 2013. Flow Cytometry for the Analysis of α-Dystroglycan Glycosylation in Fibroblasts from Patients with Dystroglycanopathies. *PLOS ONE,* 8**,** e68958.

STRAUB, V., DONAHUE, K. M., ALLAMAND, V., DAVISSON, R. L., KIM, Y. R. & CAMPBELL, K. P. 2000. Contrast agent-enhanced magnetic resonance imaging of skeletal muscle damage in animal models of muscular dystrophy. *Magnetic Resonance in Medicine,* 44**,** 655-659.

STRAUB, V., MURPHY, A. & UDD, B. 2018. ENMC international workshop: Limb girdle muscular dystrophies 2013; nomenclature and reformed classification, 17-19 March 2017, Naarden, The Netherlands. *Neuromuscular Disorders*.

SVAHN, J., STREICHENBERGER, N., BENVENISTE, O., MENASSA, R., MICHEL, L., FAYOLLE, H. & PETIOT, P. 2015. Significant response to immune therapies in a case of subacute necrotizing myopathy and FKRP mutations. *Neuromuscul Disord,* 25**,** 865-868.

SVEEN, M.-L., SCHWARTZ, M. & VISSING, J. 2006. High prevalence and phenotype–genotype correlations of limb girdle muscular dystrophy type 2I in Denmark. *Annals of Neurology,* 59**,** 808-815.

SVEEN, M., THUNE, J., KØBER, L. & VISSING, J. 2008a. CArdiac involvement in patients with limb-girdle muscular dystrophy type 2 and becker muscular dystrophy. *Archives of Neurology,* 65**,** 1196-1201.

SVEEN, M. L., THUNE, J. J., KOBER, L. & VISSING, J. 2008b. Cardiac involvement in patients with limb-girdle muscular dystrophy type 2 and Becker muscular dystrophy. *Arch Neurol,* 65**,** 1196-201.

TANDON, A., VILLA, C. R., HOR, K. N., JEFFERIES, J. L., GAO, Z., TOWBIN, J. A., WONG, B. L., MAZUR, W., FLECK, R. J., STICKA, J. J., BENSON, D. W. & TAYLOR, M. D. 2015. Myocardial Fibrosis Burden Predicts Left Ventricular Ejection Fraction and Is Associated With Age and Steroid Treatment Duration in Duchenne Muscular Dystrophy. *Journal of the American Heart Association: Cardiovascular and Cerebrovascular Disease,* 4**,** e001338.

TANIGUTI, A. P., PERTILLE, A., MATSUMURA, C. Y., SANTO NETO, H. & MARQUES, M. J. 2011. Prevention of muscle fibrosis and myonecrosis in mdx mice by suramin, a TGF-beta1 blocker. *Muscle Nerve,* 43**,** 82-7.

TAYLOR, R. J., MOODY, W. E., UMAR, F., EDWARDS, N. C., TAYLOR, T. J., STEGEMANN, B., TOWNEND, J. N., HOR, K. N., STEEDS, R. P., MAZUR, W. & LEYVA, F. 2015. Myocardial strain measurement with feature-tracking cardiovascular magnetic resonance: normal values. *Eur Heart J Cardiovasc Imaging,* 16**,** 871-81.

TAYLOR, S. C., BERKELMAN, T., YADAV, G. & HAMMOND, M. 2013. A Defined Methodology for Reliable Quantification of Western Blot Data. *Molecular Biotechnology,* 55**,** 217-226.

THAM, E. B., HAYKOWSKY, M. J., CHOW, K., SPAVOR, M., KANEKO, S., KHOO, N. S., PAGANO, J. J., MACKIE, A. S. & THOMPSON, R. B. 2013. Diffuse myocardial fibrosis by T1-mapping in children with subclinical anthracycline cardiotoxicity: relationship to exercise capacity, cumulative dose and remodeling. *J Cardiovasc Magn Reson,* 15**,** 48.

THIBAUD, J. L., MONNET, A., BERTOLDI, D., BARTHELEMY, I., BLOT, S. & CARLIER, P. G. 2007. Characterization of dystrophic muscle in golden retriever muscular dystrophy dogs by nuclear magnetic resonance imaging. *Neuromuscul Disord,* 17**,** 575-84.

TINSLEY, J., AARTSMA-RUS, A., VAN PUTTEN, M., NAGARAJU, K., DE LA PORTE, S., DUBACH-POWELL, J. & CARLSON, G. 2014. *Use of grip strength meter to assess the limb strength of mdx mice* [Online]. TREAT NMD. Available: http://www.treat-nmd.eu/downloads/file/sops/dmd/MDX/DMD_M.2.2.001.pdf [Accessed 13th of March 2018 2018].

TREAT NMD. 2016. *TREAT NMD: Experimental protocols for DMD animal models* [Online]. Available: http://www.treat-nmd.eu/research/preclinical/dmd-sops/ [Accessed 8th of January 2019 2018].

TREAT NMD. 2017. *TREAT-NMD - advancing diagnosis, care and treatment for people with neuromuscular disease round the world* [Online]. Available: http://www.treat-nmd.eu/ [Accessed 24th of February 2017].

TSAO, J. & KOZERKE, S. 2012. MRI temporal acceleration techniques. *J Magn Reson Imaging,* 36**,** 543-60.

TURGEMAN, T., HAGAI, Y., HUEBNER, K., JASSAL, D. S., ANDERSON, J. E., GENIN, O., NAGLER, A., HALEVY, O. & PINES, M. 2008. Prevention of muscle fibrosis and improvement in muscle performance in the mdx mouse by halofuginone. *Neuromuscul Disord,* 18**,** 857-68.

UDELSON, J. E., FELDMAN, A. M., GREENBERG, B., PITT, B., MUKHERJEE, R., SOLOMON, H. A. & KONSTAM, M. A. 2010. Randomized, double-blind, multicenter, placebo-controlled study evaluating the effect of aldosterone antagonism with eplerenone on ventricular remodeling in patients with mild-to-moderate heart failure and left ventricular systolic dysfunction. *Circ Heart Fail,* 3**,** 347-53.

UGANDER, M., OKI, A. J., HSU, L. Y., KELLMAN, P., GREISER, A., ALETRAS, A. H., SIBLEY, C. T., CHEN, M. Y., BANDETTINI, W. P. & ARAI, A. E. 2012. Extracellular volume imaging by magnetic resonance imaging provides insights into overt and sub-clinical myocardial pathology. *Eur Heart J,* 33**,** 1268-78.

UHLIR, O., DVORAK, I., GREGOR, P., MALEK, I., SPINAROVA, L., VOJACEK, J. & VAN NUETEN, L. 1997. Nebivolol in the treatment of cardiac failure: A double-blind controlled clinical trial. *Journal of Cardiac Failure,* 3**,** 271-276.

UK HOME OFFICE. 2018. *Mouse: Decision tree for blood sampling* [Online]. Available: https://www.nc3rs.org.uk/mouse-decision-tree-blood-sampling [Accessed 9th of May 2018].

UPPAL, R., AY, I., DAI, G., KIM, Y. R., SORENSEN, A. G. & CARAVAN, P. 2010. Molecular MRI of intracranial thrombus in a rat ischemic stroke model. *Stroke,* 41**,** 1271-7.

USMAN, M., ATKINSON, D., KOLBITSCH, C., SCHAEFFTER, T. & PRIETO, C. 2015. Manifold learning based ECG-free free-breathing cardiac CINE MRI. *J Magn Reson Imaging,* 41**,** 1521-7.

USMAN, M., RUIJSINK, B., NAZIR, M. S., CRUZ, G. & PRIETO, C. 2017. Free breathing whole-heart 3D CINE MRI with self-gated Cartesian trajectory. *Magn Reson Imaging,* 38**,** 129-137.

VAN DEN BERGEN, J., B H WOKKE, A A JANSON, S G VAN DUINEN, M A HULSKER, H B GINJAAR, J C VAN DEUTEKOM, A AARTSMA-RUS, H E KAN & VERSCHUUREN, J. J. 2014. Dystrophin levels and clinical severity in Becker muscular dystrophy patients. . *J Neurol Neurosurg Psychiatry* 85**,** 747-753.

VAN DER KOOI, A. J., BARTH, P. G., BUSCH, H. F. M., DE HAAN, R., GINJAAR, H. B., VAN ESSEN, A. J., VAN HOOFF, L. J. M. A., HÖWELER, C. J., JENNEKENS, F. G. I., JONGEN, P., OOSTERHUIS, H. J. G. H., PADBERG, G. W. A. M., SPAANS, F., WINTZEN, A. R., WOKKE, J. H. J., BAKKER, E., VAN OMMEN, G. J. B., BOLHUIS, P. A. & DE VISSER, M. 1996. The clinical spectrum of limb girdle muscular dystrophy A survey in the Netherlands. *Brain,* 119**,** 1471-1480.

VAN DER TOORN, A., BARENBRUG, P., SNOEP, G., VAN DER VEEN, F. H., DELHAAS, T., PRINZEN, F. W., MAESSEN, J. & ARTS, T. 2002. Transmural gradients of cardiac myofiber shortening in aortic valve stenosis patients using MRI tagging. *Am J Physiol Heart Circ Physiol,* 283**,** H1609-15.

VAN PUTTEN, M., KUMAR, D., HULSKER, M., HOOGAARS, W. M. H., PLOMP, J. J., VAN OPSTAL, A., VAN ITERSON, M., ADMIRAAL, P., VAN OMMEN, G.-J. B., 'T HOEN, P. A. C. & AARTSMA-RUS, A. 2012. Comparison of skeletal muscle pathology and motor function of dystrophin and utrophin deficient mouse strains. *Neuromuscular Disorders,* 22**,** 406-417.

VAN RUITEN, H. J., STRAUB, V., BUSHBY, K. & GUGLIERI, M. 2014. Improving recognition of Duchenne muscular dystrophy: a retrospective case note review. *Arch Dis Child,* 99**,** 1074-7.

VAN VUGT, J. L., LEVOLGER, S., GHARBHARAN, A., KOEK, M., NIESSEN, W. J., BURGER, J. W., WILLEMSEN, S. P., DE BRUIN, R. W. & JN, I. J. 2017. A comparative study of software programmes for cross-sectional skeletal muscle and adipose tissue measurements on abdominal computed tomography scans of rectal cancer patients. *J Cachexia Sarcopenia Muscle,* 8**,** 285-297.

VAN ZIJL, P. C. M. & YADAV, N. N. 2011. Chemical Exchange Saturation Transfer (CEST): what is in a name and what isn't? *Magnetic resonance in medicine : official journal of the Society of Magnetic Resonance in Medicine / Society of Magnetic Resonance in Medicine,* 65**,** 927-948.

VANDER ELST, L., RAYNAUD, J.-S. & VIVES, V. 2013. *Comparative relaxivities and efficacies of gadolinium-based commercial contrast agents.* [Online]. Available: http://cds.ismrm.org/protected/13MProceedings/files/0746.PDF [Accessed 20th of January 2017].

VANNOY, C. H., XIAO, W., LU, P., XIAO, X. & LU, Q. L. 2017. Efficacy of Gene Therapy Is Dependent on Disease Progression in Dystrophic Mice with Mutations in the FKRP Gene. *Mol Ther Methods Clin Dev,* 5**,** 31-42.

VINCENTI, G., MONNEY, P., CHAPTINEL, J., RUTZ, T., COPPO, S., ZENGE, M. O., SCHMIDT, M., NADAR, M. S., PICCINI, D., CHEVRE, P., STUBER, M. & SCHWITTER, J. 2014. Compressed sensing single-breath-hold CMR for fast quantification of LV function, volumes, and mass. *JACC Cardiovasc Imaging,* 7**,** 882-92.

VOHRA, R., BATRA, A., FORBES, S. C., VANDENBORNE, K. & WALTER, G. A. 2017. Magnetic Resonance Monitoring of Disease Progression in mdx Mice on Different Genetic Backgrounds. *The American Journal of Pathology,* 187**,** 2060-2070.

VOHRA, R. S., LOTT, D., MATHUR, S., SENESAC, C., DEOL, J., GERMAIN, S., BENDIXEN, R., FORBES, S. C., SWEENEY, H. L., WALTER, G. A. & VANDENBORNE, K. 2015. Magnetic Resonance Assessment of Hypertrophic and Pseudo-Hypertrophic Changes in Lower Leg Muscles of Boys with Duchenne Muscular Dystrophy and Their Relationship to Functional Measurements. *PLOS ONE,* 10**,** e0128915.

WAGATSUMA, A. 2007. Adipogenic potential can be activated during muscle regeneration. *Mol Cell Biochem,* 304**,** 25-33.

WALCHER, T., STEINBACH, P., SPIEß, J., KUNZE, M., GRADINGER, R., WALCHER, D. & BERNHARDT, P. 2011. Detection of long-term progression of myocardial fibrosis in Duchenne muscular dystrophy in an affected family: A cardiovascular magnetic resonance study. *European Journal of Radiology,* 80**,** 115-119.

WALSH, T. F. & HUNDLEY, W. G. 2007. Assessment of ventricular function with cardiovascular magnetic resonance. *Cardiol Clin,* 25**,** 15-33, v.

WALTER, M. C., PETERSEN, J. A., STUCKA, R., FISCHER, D., SCHRODER, R., VORGERD, M., SCHROERS, A., SCHREIBER, H., HANEMANN, C. O., KNIRSCH, U., ROSENBOHM, A., HUEBNER, A., BARISIC, N., HORVATH, R., KOMOLY, S., REILICH, P., MULLER-FELBER, W., PONGRATZ, D., MULLER, J. S., AUERSWALD, E. A. & LOCHMULLER, H. 2004a. FKRP (826C>A) frequently causes limb-girdle muscular dystrophy in German patients. *J Med Genet,* 41**,** e50.

WALTER, M. C., PETERSEN, J. A., STUCKA, R., FISCHER, D., SCHRÖDER, R., VORGERD, M., SCHROERS, A., SCHREIBER, H., HANEMANN, C. O., KNIRSCH, U., ROSENBOHM, A., HUEBNER, A., BARISIC, N., HORVATH, R., KOMOLY, S., REILICH, P., MÜLLER-FELBER, W., PONGRATZ, D., MÜLLER, J. S., AUERSWALD, E. A. & LOCHMÜLLER, H. 2004b. FKRP (826C&gt;A) frequently causes limb-girdle muscular dystrophy in German patients. *Journal of Medical Genetics,* 41**,** e50.

WALTON, J. N. & NATTRASS, F. J. 1954. On the classification, natural history and treatment of the myopathies. *Brain,* 77**,** 169-231.

WANSAPURA, J. P., HOR, K. N., MAZUR, W., FLECK, R., HAGENBUCH, S., BENSON, D. W. & GOTTLIEBSON, W. M. 2010. Left ventricular T2 distribution in Duchenne muscular dystrophy. *J Cardiovasc Magn Reson,* 12**,** 14.

WARY, C., AZZABOU, N., GIRAUDEAU, C., LE LOUER, J., MONTUS, M., VOIT, T., SERVAIS, L. & CARLIER, P. 2015. Quantitative NMRI and NMRS identify augmented disease progression after loss of ambulation in forearms of boys with Duchenne muscular dystrophy. *NMR Biomed,* 28**,** 1150-62.

WARY, C., NAULET, T., THIBAUD, J. L., MONNET, A., BLOT, S. & CARLIER, P. G. 2012. Splitting of Pi and other (3)(1)P NMR anomalies of skeletal muscle metabolites in canine muscular dystrophy. *NMR Biomed,* 25**,** 1160-9.

WATTJES, M. P., KLEY, R. A. & FISCHER, D. 2010. Neuromuscular imaging in inherited muscle diseases. *European Radiology,* 20**,** 2447-2460.

WEBER, M. A., NAGEL, A. M., JURKAT-ROTT, K. & LEHMANN-HORN, F. 2011. Sodium (23Na) MRI detects elevated muscular sodium concentration in Duchenne muscular dystrophy. *Neurology,* 77**,** 2017-24.

WEHLING, M., SPENCER, M. J. & TIDBALL, J. G. 2001. A nitric oxide synthase transgene ameliorates muscular dystrophy in mdx mice. *J Cell Biol,* 155**,** 123-31.

WEINMANN, H. J., BRASCH, R. C., PRESS, W. R. & WESBEY, G. E. 1984. Characteristics of gadolinium-DTPA complex: a potential NMR contrast agent. *AJR Am J Roentgenol,* 142**,** 619-24.

WHITE, S. K., SADO, D. M., FONTANA, M., BANYPERSAD, S. M., MAESTRINI, V., FLETT, A. S., PIECHNIK, S. K., ROBSON, M. D., HAUSENLOY, D. J., SHEIKH, A. M., HAWKINS, P. N. & MOON, J. C. 2013. T1 mapping for myocardial extracellular volume measurement by CMR: bolus only versus primed infusion technique. *JACC Cardiovasc Imaging,* 6**,** 955-62.

WICKSELL, R. K., KIHLGREN, M., MELIN, L. & EEG-OLOFSSON, O. 2004. Specific cognitive deficits are common in children with Duchenne muscular dystrophy. *Dev Med Child Neurol,* 46**,** 154-9.

WILLCOCKS, R. J., ARPAN, I. A., FORBES, S. C., LOTT, D. J., SENESAC, C. S., SENESAC, E., DEOL, J., TRIPLETT, W., BALIGAND, C., DANIELS, M. J., SWEENEY, H. L., WALTER, G. A. &

VANDENBORNE, K. 2014. Longitudinal measurements of MRI-T(2) in boys with Duchenne muscular dystrophy: Effects of age and disease progression. *Neuromuscular disorders : NMD,* 24**,** 393-401.

WILLCOCKS, R. J., ROONEY, W. D., TRIPLETT, W. T., FORBES, S. C., LOTT, D. J., SENESAC, C. R., DANIELS, M. J., WANG, D. J., HARRINGTON, A. T., TENNEKOON, G. I., RUSSMAN, B. S., FINANGER, E. L., BYRNE, B. J., FINKEL, R. S., WALTER, G. A., SWEENEY, H. L. & VANDENBORNE, K. 2016a. Multicenter prospective longitudinal study of magnetic resonance biomarkers in a large duchenne muscular dystrophy cohort. *Ann Neurol,* 79**,** 535-47.

WILLCOCKS, R. J., ROONEY, W. D., TRIPLETT, W. T., FORBES, S. C., LOTT, D. J., SENESAC, C. R., DANIELS, M. J., WANG, D. J., HARRINGTON, A. T., TENNEKOON, G. I., RUSSMAN, B. S., FINANGER, E. L., BYRNE, B. J., FINKEL, R. S., WALTER, G. A., SWEENEY, H. L. & VANDENBORNE, K. 2016b. Multicenter prospective longitudinal study of magnetic resonance biomarkers in a large duchenne muscular dystrophy cohort. *Ann Neurol,* 79**,** 535-547.

WILLCOCKS, R. J., TRIPLETT, W. T., FORBES, S. C., ARORA, H., SENESAC, C. R., LOTT, D. J., NICHOLSON, T. R., ROONEY, W. D., WALTER, G. A. & VANDENBORNE, K. 2017. Magnetic resonance imaging of the proximal upper extremity musculature in boys with Duchenne muscular dystrophy. *J Neurol,* 264**,** 64-71.

WILLIAMS SARAH, E., HEEMSKERK ANNERIET, M., WELCH, E. B., LI, K., DAMON BRUCE, M. & PARK JANE, H. 2013. Quantitative effects of inclusion of fat on muscle diffusion tensor MRI measurements. *Journal of Magnetic Resonance Imaging,* 38**,** 1292-1297.

WILLIS, T. A., HOLLINGSWORTH, K. G., COOMBS, A., SVEEN, M. L., ANDERSEN, S., STOJKOVIC, T., EAGLE, M., MAYHEW, A., DE SOUSA, P. L., DEWAR, L., MORROW, J. M., SINCLAIR, C. D., THORNTON, J. S., BUSHBY, K., LOCHMULLER, H., HANNA, M. G., HOGREL, J. Y., CARLIER, P. G., VISSING, J. & STRAUB, V. 2013. Quantitative muscle MRI as an assessment tool for monitoring disease progression in LGMD2I: a multicentre longitudinal study. *PLoS One,* 8**,** e70993.

WILLIS, T. A., HOLLINGSWORTH, K. G., COOMBS, A., SVEEN, M. L., ANDERSEN, S., STOJKOVIC, T., EAGLE, M., MAYHEW, A., DE SOUSA, P. L., DEWAR, L., MORROW, J. M., SINCLAIR, C. D., THORNTON, J. S., BUSHBY, K., LOCHMULLER, H., HANNA, M. G., HOGREL, J. Y., CARLIER, P. G., VISSING, J. & STRAUB, V. 2014. Quantitative magnetic resonance imaging in limb-girdle muscular dystrophy 2I: a multinational cross-sectional study. *PLoS One,* 9**,** e90377.

WINAND, N. J., EDWARDS, M., PRADHAN, D., BERIAN, C. A. & COOPER, B. J. 1994. Deletion of the dystrophin muscle promoter in feline muscular dystrophy. *Neuromuscul Disord,* 4**,** 433-45.

WITTING, N., KRUUSE, C., NYHUUS, B., PRAHM, K. P., CITIRAK, G., LUNDGAARD, S. J., VON HUTH, S., VEJLSTRUP, N., LINDBERG, U., KRAG, T. O. & VISSING, J. 2014. Effect of sildenafil on skeletal and cardiac muscle in Becker muscular dystrophy. *Ann Neurol,* 76**,** 550-7.

WOKKE, B. H., BOS, C., REIJNIERSE, M., VAN RIJSWIJK, C. S., EGGERS, H., WEBB, A., VERSCHUUREN, J. J. & KAN, H. E. 2013. Comparison of dixon and T1-weighted MR methods to assess the degree of fat infiltration in duchenne muscular dystrophy patients. *J Magn Reson Imaging,* 38**,** 619-24.

WOKKE, B. H., HOOIJMANS, M. T., VAN DEN BERGEN, J. C., WEBB, A. G., VERSCHUUREN, J. J. & KAN, H. E. 2014a. Muscle MRS detects elevated PDE/ATP ratios prior to fatty infiltration in Becker muscular dystrophy. *NMR Biomed,* 27**,** 1371-7.

WOKKE, B. H., VAN DEN BERGEN, J. C., VERSLUIS, M. J., NIKS, E. H., MILLES, J., WEBB, A. G., VAN ZWET, E. W., AARTSMA-RUS, A., VERSCHUUREN, J. J. & KAN, H. E. 2014b. Quantitative MRI and strength measurements in the assessment of muscle quality in Duchenne muscular dystrophy. *Neuromuscular Disorders,* 24**,** 409-416.

WONG, T. C., PIEHLER, K., MEIER, C. G., TESTA, S. M., KLOCK, A. M., ANEIZI, A. A., SHAKESPRERE, J., KELLMAN, P., SHROFF, S. G., SCHWARTZMAN, D. S., MULUKUTLA, S. R., SIMON, M. A. &

SCHELBERT, E. B. 2012. Association between extracellular matrix expansion quantified by cardiovascular magnetic resonance and short-term mortality. *Circulation,* 126, 1206-16.

WONG, T. C., PIEHLER, K., PUNTIL, K. S., MOGUILLANSKY, D., MEIER, C. G., LACOMIS, J. M., KELLMAN, P., COOK, S. C., SCHWARTZMAN, D. S., SIMON, M. A., MULUKUTLA, S. R. & SCHELBERT, E. B. 2013. Effectiveness of late gadolinium enhancement to improve outcomes prediction in patients referred for cardiovascular magnetic resonance after echocardiography. *J Cardiovasc Magn Reson,* 15**,** 6.

WOOD, P. W., CHOY, J. B., NANDA, N. C. & BECHER, H. 2014. Left ventricular ejection fraction and volumes: it depends on the imaging method. *Echocardiography,* 31**,** 87-100.

WRAITH, J. E., CLARKE, L. A., BECK, M., KOLODNY, E. H., PASTORES, G. M., MUENZER, J., RAPOPORT, D. M., BERGER, K. I., SWIEDLER, S. J., KAKKIS, E. D., BRAAKMAN, T., CHADBOURNE, E., WALTON-BOWEN, K. & COX, G. F. 2004. Enzyme replacement therapy for mucopolysaccharidosis I: a randomized, double-blinded, placebo-controlled, multinational study of recombinant human alpha-L-iduronidase (laronidase). *J Pediatr,* 144**,** 581-8.

WREN, T. A., BLUML, S., TSENG-ONG, L. & GILSANZ, V. 2008. Three-point technique of fat quantification of muscle tissue as a marker of disease progression in Duchenne muscular dystrophy: preliminary study. *AJR Am J Roentgenol,* 190**,** W8-12.

WU, G., SANDERSON, B. & BITTNER, V. 2003. The 6-minute walk test: how important is the learning effect? *Am Heart J,* 146**,** 129-133.

WU, J. Y., KUBAN, K. C. K., ALLRED, E., SHAPIRO, F. & DARRAS, B. T. 2005. Association of Duchenne Muscular Dystrophy With Autism Spectrum Disorder. *Journal of Child Neurology,* 20**,** 790-795.

WU, K. C., WEISS, R. G., THIEMANN, D. R., KITAGAWA, K., SCHMIDT, A., DALAL, D., LAI, S., BLUEMKE, D. A., GERSTENBLITH, G., MARBÁN, E., LIMA, J. A. C. & TOMASELLI, G. F. 2008a. Late Gadolinium Enhancement by Cardiovascular Magnetic Resonance Heralds an Adverse Prognosis in Nonischemic Cardiomyopathy. *Journal of the American College of Cardiology,* 51**,** 2414-2421.

WU, K. C., WEISS, R. G., THIEMANN, D. R., KITAGAWA, K., SCHMIDT, A., DALAL, D., LAI, S., BLUEMKE, D. A., GERSTENBLITH, G., MARBAN, E., TOMASELLI, G. F. & LIMA, J. A. 2008b. Late gadolinium enhancement by cardiovascular magnetic resonance heralds an adverse prognosis in nonischemic cardiomyopathy. *J Am Coll Cardiol,* 51**,** 2414-21.

WU, R. S., GUPTA, S., BROWN, R. N., YANCY, C. W., WALD, J. W., KAISER, P., KIRKLIN, N. M., PATEL, P. C., MARKHAM, D. W., DRAZNER, M. H., GARRY, D. J. & MAMMEN, P. P. 2010. Clinical outcomes after cardiac transplantation in muscular dystrophy patients. *J Heart Lung Transplant,* 29**,** 432-8.

WYNN, T. A. 2007. Common and unique mechanisms regulate fibrosis in various fibroproliferative diseases. *J Clin Invest,* 117**,** 524-9.

WYNN, T. A. & RAMALINGAM, T. R. 2012. Mechanisms of fibrosis: therapeutic translation for fibrotic disease. *Nature Medicine,* 18**,** 1028-1040.

YILMAZ, A., GDYNIA, H. J., BACCOUCHE, H., MAHRHOLDT, H., MEINHARDT, G., BASSO, C., THIENE, G., SPERFELD, A. D., LUDOLPH, A. C. & SECHTEM, U. 2008. Cardiac involvement in patients with Becker muscular dystrophy: new diagnostic and pathophysiological insights by a CMR approach. *J Cardiovasc Magn Reson,* 10**,** 50.

YOUNG, A. A., COWAN, B. R., THRUPP, S. F., HEDLEY, W. J. & DELL'ITALIA, L. J. 2000. Left ventricular mass and volume: fast calculation with guide-point modeling on MR images. *Radiology,* 216**,** 597-602.

YOUNG, A. A., KRAMER, C. M., FERRARI, V. A., AXEL, L. & REICHEK, N. 1994. Three-dimensional left ventricular deformation in hypertrophic cardiomyopathy. *Circulation,* 90**,** 854-67.

YOUNG, A. A., MEDWAY, D. J., LYGATE, C. A., NEUBAUER, S. & SCHNEIDER, J. E. 2011. Accelerating global left-ventricular function assessment in mice using reduced slice acquisition and three-dimensional guide-point modelling. *J Cardiovasc Magn Reson,* 13**,** 49.

YUSUF, S., PITT, B., DAVIS, C. E., HOOD, W. B., JR. & COHN, J. N. 1992. Effect of enalapril on mortality and the development of heart failure in asymptomatic patients with reduced left ventricular ejection fractions. *N Engl J Med,* 327**,** 685-91.

ZAIDMAN, C. M., MALKUS, E. C. & CONNOLLY, A. M. 2015. Muscle ultrasound quantifies disease progression over time in infants and young boys with duchenne muscular dystrophy. *Muscle Nerve,* 52**,** 334-8.

ZARAISKAYA, T., KUMBHARE, D. & NOSEWORTHY MICHAEL, D. 2006. Diffusion tensor imaging in evaluation of human skeletal muscle injury. *Journal of Magnetic Resonance Imaging,* 24**,** 402-408.

ZERHOUNI, E. A., PARISH, D. M., ROGERS, W. J., YANG, A. & SHAPIRO, E. P. 1988. Human heart: tagging with MR imaging--a method for noninvasive assessment of myocardial motion. *Radiology,* 169**,** 59-63.

ZHANG, J., ZHANG, G., MORRISON, B., MORI, S. & SHEIKH, K. A. 2008. Magnetic resonance imaging of mouse skeletal muscle to measure denervation atrophy. *Experimental Neurology,* 212**,** 448-457.

ZHAO, J., SHI, W., WANG, Y. L., CHEN, H., BRINGAS, P., JR., DATTO, M. B., FREDERICK, J. P., WANG, X. F. & WARBURTON, D. 2002. Smad3 deficiency attenuates bleomycin-induced pulmonary fibrosis in mice. *Am J Physiol Lung Cell Mol Physiol,* 282**,** L585-93.

ZION, O., GENIN, O., KAWADA, N., YOSHIZATO, K., ROFFE, S., NAGLER, A., IOVANNA, J. L., HALEVY, O. & PINES, M. 2009. Inhibition of transforming growth factor beta signaling by halofuginone as a modality for pancreas fibrosis prevention. *Pancreas,* 38**,** 427-35.

ZUBERI, S. M., MATTA, N., NAWAZ, S., STEPHENSON, J. B. P., MCWILLIAM, R. C. & HOLLMAN, A. 1999. Muscle ultrasound in the assessment of suspected neuromuscular disease in childhood. *Neuromuscular Disorders,* 9**,** 203-207.

Limb Girdle Muscular Dystrophy 2I Physiotherapy Assessment Manual

Manual of
Operation
s Clinical
Evaluation

Version 1.0
24th April 2015

Dr Anna Mayhew
Dr Michelle Eagle
Mrs Meredith James

Contents

3

1. ORDER OF TESTS: RECOMMENDED SEQUENCE OF STUDY PROCEDURES

Study procedures should be performed in the same order and at approximately the same time of day for each subject. All procedures should be conducted by a trained physiotherapist.

Test order

a) Timed 10 m walk / run (in shoes)

b) Respiratory Function Test

c) Hand--held Myometry: The dominant side only will be tested

d) Ankle Range of Movement

e) North Star Assessment for Dysferlinopathy (NSAD) (with Timed 10m walk / run and Rise from floor without shoes)

f) Functional and timed tests (Timed UP and Go, Four Stair climb, Four stair descend, Rise from chair)

g) PUL 1.3 Proximal module (optional)

h) 6 minute walk test – **ambulant only**

2. EQUIPMENT AND SPACE REQUIREMENTS FOR EVALUATIONS

Use your own local equipment. Please let us know if you have any queries. Worksheets are required for all tests.

Spirometry	Local spirometry system and bacterial filters
Strength testing	Hand held myometer, MicroFET if available
North Star Assessment for Dysferlinopathy and timed tests	15 cm step A sturdy chair for sit to stand, timed up and go, and stand from sitting on floor. Digital stopwatch A quiet hallway with at least 12 meters of straight, uninterrupted walking space, with a starting line and finish line exactly 10 metres apart. Four step set with hand rails
PUL 1.3 Proximal module	Selection of metric weights. 200g, 500g and 1000g. Plastic cup (vending cup)
Six Minute Walk Test	A quiet hallway of 30m length Small orange cones (12 inch or 20 cm): 2 One 25 metre tape measures Stop watch: 2 Tape Clip board A chair or wheelchair that can be easily moved along the walking course 6MWT worksheet with checklist

3. INTRODUCTION TO PROCEDURES FOR EVALUATIONS

Clinical evaluation will include respiratory testing, muscle strength testing, timed tests including the 6 minute walk test, timed up and go, timed 10 metre / walk, rise from chair, rise from the floor and stairs, functional scales including North Star Assessment for Dysferlinoapthy (NSAD) and PUL 1.3 – Proximal module

Ideally the same evaluator should perform evaluations at subsequent assessments. The evaluator and back up should perform at least the first assessments in pairs.

Tests should be performed at approximately the same time of day and after similar pre--test activities and routines.

Tests should be performed in the order provided in this manual.

To avoid bias, the clinical evaluator (CE) should not review any previous testing results. The testing environment should be standardised.

It is recommended that family members or friends not be present in the room during testing, unless test compliance is affected.

A second CE or staff member may be in the room during testing.

The subject should wear loose clothing. It is preferable for the subject to wear a short--sleeved shirt and shorts.

4. TIMED 10 METRE WALK / RUN (IN SHOES)

Prior to all tests perform a 10 m walk / run following the guidelines within the NSAD (Item 29) but with the patient wearing shoes and if required orthotics. Record whether they used orthoses and aids on the worksheet, grade the test and record the time.

10 m Walk / Run (in shoes)							
Grade	**1**	**2**	**3**	**4**	**5**	**6**	**Time (seconds)**
10 metre walk / run Please circle	Unable	Walk with aids	Walk No extra speed	Walk extra speed	Nearly running No flight	Running	_ _ . _ s

Definition of ambulation: If a patient is able to walk 10 metres with aids and with assistive devices (orthotics) they are defined as ambulant. They should then attempt all other tests. If they are unable to complete 10m walk even with aids the patient is defined as non-ambulant. Do not perform TUG, stair climb and descend and 6MWT.

5. PULMONARY FUNCTION TEST (FVC -- SITTING AND LYING)

Pulmonary function tests are Forced Vital Capacity (FVC) and Forced Expiratory Volume in 1 second (FEV1). They are performed using the same manoeuvre in sitting and in lying.

> Height calculation: For patients able to stand take a height measurement in centimetres in order to calculate percentage predicted FVC and FEV1. For patients unable to stand use an arm span measurement. Use a tape measure from the tip of the longest finger, across each joint (wrist, elbow and shoulder) to the sternal notch. Double this measurement to give an estimated height in centimetres.

The patient should be sitting comfortably in a chair. The evaluator explains /demonstrates the procedure to the subject and explains that they will be performing the test at least 3 times. The specific wording of instructions should be followed closely. These are then repeated in lying. A pillow may be used.

> Please make a note on the worksheet of the type of system you are using to perform the pulmonary function test

Ask the patient to *'take as big a breath in as possible and then blow out through the mouth as hard and as long as you can'*. The evaluator should verbally encourage the subject to keep going for as long as possible. ATS criteria state a 6 second plateau is required.

The test should be repeated three times making sure that the patient has recovered between attempts. If at each attempt there is an improvement in the results further tests can be conducted until the subject has achieved his best result.

The subject can place the mouthpiece in his own mouth unless he is unable to reach his mouth with his hands or flexes his head and shoulders to reach the tube. In this case the evaluator should place the tube into the subject's mouth.

The tube can be placed in the mouth either before the beginning of inspiration (closed circuit technique) or at the end of inspiration just prior to expiration (open circuit technique) whichever the subject finds most comfortable.

Whichever technique is used the same method should be used at each evaluation and documented on the worksheets.

A nose clip should be applied just prior to expiration. If a tight seal cannot be made around the tube then a mask may be used

The subject should not be allowed to flex forward during expiration.

Calibrate the system on the day of testing

MYOMETRY

Testing Guidelines

- Tests should be performed in the order listed on the myometry worksheet.
- The myometer is a very sensitive measuring tool therefore care must be taken to be consistent with test method.
- Allow at least 5 seconds of rest between trials.
- Repeat the test if the subject moves out of the testing position during a trial.
- The subject should be vigorously coached to push or pull in the desired direction while the myometer is held stable by the CE ("make" test).
- If the CE encounters problems during a trial, the trial must be repeated. Three "valid" trials will be performed, and the value from the myometer will be recorded after each trial. The unit of measurement should be the pound, and values should be recorded with 1 decimal place (eg, 1.0 lbs). The test is explained to the patient in a way that they understand. The intent is to build a maximum isometric hold, so the command is effectively 'HOLD' or 'Keep still/don't let me move you'. The words push or pull should not be used.
- The subject will be encouraged verbally to build to and maintain a maximum hold over a period of approximately 5 seconds, to allow for full physiological recruitment of muscle.
- Following one 'trial' test to allow for learning, the best of 3 tests shall be noted. Test results should be fairly closely grouped – a 10% variation is not unusual, e.g. 30lbs +/-- 3
- Any discomfort will limit the patient's ability to offer maximum resistance. As much as is possible, ensure comfort when applying the myometer. The applicator can be padded to allow for comfort.
- If the evaluator does not feel that they have been able to gain compliance from the patient for any reason (e.g. understanding or poor concentration), this should be noted.
- All myometry is performed with the MICROFET2 myometer except for grip and pinch which are performed with the CITEC.
- **Calibrate system on the day of testing**
  Order of Tests

  Supine

  If it is possible to move a non--ambulant subject then attempt all tests if not then document on the worksheet why the test was not performed
    - Hip flexors
    - Hip abduction
    - Hip adduction
    - Ankle dorsiflexion

    - **Ankle dorsiflexion ROM**

  Sitting
    - Knee extension
    - Knee flexion

Supine – Position 1

Hip Flexion (supine)

Patient position	Supine on firm adjustable height plinth with hip and knee at 90º. Femur in neutral rotation. Subject is asked to concentrate on keeping knee steady, not to move foot, as this discourages hamstring involvement
Stabilisation	Under knee and calf to support weight of leg and prevent unwanted hip movement The subject is instructed and encouraged to bring his knee up to his chest pulling into the transducer pad as hard as he can, 'Keep still, don't let me move you'
Myometer Position Therapist position. At side of, sitting or kneeling on plinth. May vary according to weight of leg. Facing the subject. Apply force to resist hip flexion.	Anterior aspect of lower thigh, just proximal to condyles
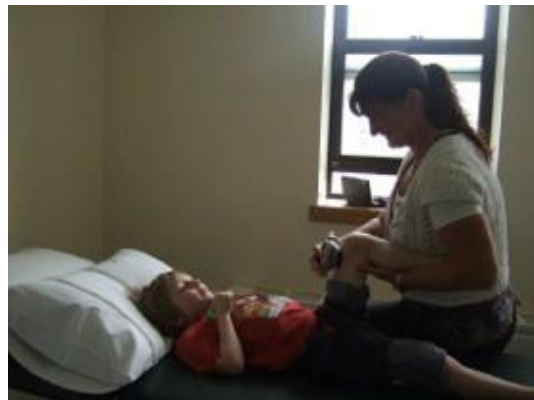
Hip Abduction (supine)

Patient position	Supine, arms by side, leg straight and abducted, knee caps pointing towards the ceiling. Patient is asked to concentrate on keeping knee steady, not to move foot.
Stabilisation	Around heel if necessary or lower leg to prevent excessive rotation from the hip
Myometer Position	Above the knee joint on the lateral aspect of the thigh
Therapist position. Either at end of plinth or standing at edge of plinth on side which is to be tested	

Hip Adduction

Patient position	Supine, arms by side, leg straight, knee caps pointing towards the ceiling. Test leg in adduction, Other leg in abduction. Patient is asked to concentrate on keeping knee steady, not to move foot.
Stabilisation	Around heel if necessary or lower leg to prevent excessive rotation from the hip
Myometer Position	Above the knee joint on medial surface of thigh
Therapist Position Standing at edge of plinth on side which is to be tested	

Ankle Dorsiflexion (supine)

Patient position	Patient in supine. Legs straight with femur in neutral rotation / knee caps pointing to ceiling.
Stabilisation	If needed on lower limb / over knee joint to monitor for trick movements. Watch for: hip external rotation, knee flexion, ankle eversion and inversion
Myometer Position	Anterior surface of foot, just in front of the ankle joint

Therapist Position At end of plinth Or at side of subject	

Sitting – position 2

Knee Extension

Patient position	Patient sitting with thigh supported and hip and knee at 90º, on plinth, chair or in wheelchair. Feet must be clear of the floor. Femur in neutral rotation. Patient can hold onto front of plinth or chair to stabilise himself
Stabilisation	If needed, given by therapist over lower third of thigh, just above knee
Myometer Position	Anterior surface of tibia, at junction between middle and lower third of tibia, place myometer on the lower third of the tibia
Therapist position Sitting in front of subject, on a chair or on floor	

Knee Flexion

Patient position	Patient sitting with thigh supported and hip and knee at 90º, on plinth, chair or in wheelchair. Feet must be clear of the floor. Femur in neutral rotation. Patient can hold onto front of plinth or chair to stabilise himself
Stabilisation	If needed, given by therapist over lower third of thigh, just above knee Watch for: hip external rotation, trunk flexion
Myometer Position	

Therapist Position

Sitting in front of subject, on a chair or on floor

7. GONIOMETRY

1.1 GENERAL ISSUES

Wherever possible the same clinical evaluator should assess and reassess the subject as intra--rater reliability has been found to be better than inter--rater (Pandya *et al*, 1985).
Use an appropriately sized goniometer and measure to the nearest degree.
Passive range is being measured so the subject needs to relax whilst the clinical evaluator ranges the joint.

Measurements should be taken with *a 'moderate' degree of stretch applied and with the patient trying to dorsiflex the foot at the same time.* Ask the patient to count to 10 whilst measuring range*.*
Variations in manual pressure applied have been identified as one of the key factors in inter--rater variability when passive ROM is being monitored (Gajdosik & Bohannon, 1987).

1.2 METHOD: ANKLE DORSIFLEXION

Subject position: Supine. As we are interested in the effects of gastrocnemius shortening on ankle dorsiflexion, this test is undertaken with the knee in full extension. The calcaneum is held in neutral alignment whilst pressure is applied over the mid--section of the foot to dorsiflex the ankle as much as possible, preventing inversion.
Goniometer position:. Stationary arm aligned with the fibular head, along the lateral aspect of the lower leg. "Moving arm" held parallel to the lateral aspect of the 5th metatarsal, aligned with the posterior third of the foot (this is to ensure that gastrocnemius range is being monitored and not that of the planter structures of the foot). Note range of dorsiflexion past plantargrade as +x^o's, range lacking from plantargrade as --x^o's
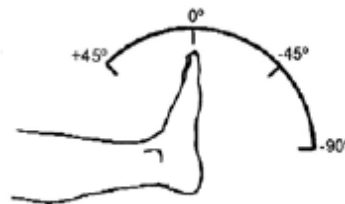
Normal range: 20° dorsiflexion to 50° plantarflexion.
End feel: firm due to joint capsule, Achilles tendon and ligaments.

Assess bilateral ankle dorsiflexion range of movement

8. NORTH STAR ASSESSMENT FOR DYSFERLINOPATHY (NSAD)

The original North Star Ambulatory Assessment was developed for DMD by the Physiotherapy Assessment and Evaluation Group of the North Star Clinical Network in conjunction with Elaine Scott. The North Star Project is supported by Muscular Dystrophy Campaign. The revised NSAD for adults with dysferlinopathy is based on clinical expertise and modern psychometric analysis and has been conducted by Michelle Eagle, Meredith James and Anna Mayhew. It incorporates useful items from the MFM 20 which have been modified to be disease specific. In this manual we have included this revision as it is considered a good approximation of a scale suitable for use in LGMD.

Clear explanations of the methods employed to achieve motor goals are given but it is not possible to be exhaustive in the descriptions, particularly of modifications to activity. One of the goals of this project is to further define common adaptations to movement in people with dysferlinopathy. Generally however activities are graded in the following manner:

> 2 -- 'Normal' – no obvious modification of activity
>
> 1 -- Modified method but achieves goal independent of physical assistance from another
>
> 0 -- Unable to achieve independently

General test instructions

- If you think that the subject is capable of a better performance, it is acceptable to ask for the item to be repeated. Re--score if appropriate. You should attempt all activities at each assessment.
- Do not use a mat unless it is required to gain co--operation. If a mat must be used, make sure it is not heavily padded. Note in comments and do so for all subsequent evaluations
- Shoes and socks should be removed for all items

NOTE: Timed rise from the floor, timed run 10 metres are graded 0--2 for the NSAA but are also further differentiated (see section 'timed graded functional activities'). The items only need to be performed during the NSAD.

Test item 1: Lifts head from supine

Starting position	Supine on a plinth or floor, arms folded across chest. No pillow should be used.	
Instruction	Can you lift your head to look at your toes keeping your arms folded?	
Scoring detail	Ask subject to keep arms crossed over chest during the activity to avoid self--assist. Also ask to look at toes to ensure neck is flexed 'lift your head and look at your toes'	

Activity	1	0
Lifts head from supine	In supine, head must be lifted in mid--line. Chin moves towards chest	Unable. No clearance of head from surface or only partially achieved movement
Photographs / Notes	Score 1 – Chin on chest	Score 0 -- Didn't achieve full range of flexion

Test item 2: Hand to opposite shoulder

Starting position	Supine on a plinth or floor, arms by side. Pillow may be situ.		
Instruction	Can you bring one hand to the opposite shoulder		
Scoring detail	Score best effort R or L and mark on worksheet which arm was used.		

Activity	2	1	0
Hand to opposite shoulder	Raises hands and moves it to opposite shoulder	Raises hand and moves it to opposite shoulder using compensatory movements	Unable
Photographs / Notes	Score 2 no compensation		

Test item 3: Hip flexion in supine			
Starting position	Supine on a plinth or floor, arms by side. Pillow may be situ.		
Instruction	Can you bend one hip and knee up towards your chest?		
Scoring detail			
Activity	2	1	0
Hip flexion supine	In supine flexes hip and knee more than 90° by raising foot through whole movement	Partially flexes hip and knee (<90°, > 20°) or foot remains in contact with mat	Unable
Photographs / Notes	Score 2	Score 1 Partial hip flexion Score 1 Foot in contact with bed	

Test item 4: Bridging in supine

Starting position	Supine on a plinth or floor, arms by side. Pillow may be situ.		
Instruction	Can you bend both hips and knees so your kneecaps point up to the ceiling and your feet stay on the floor?		
Scoring detail	You can help them achieve the crook--lying position. Score 2 – clear lift of bottom off bed with kneecaps pointing up, feet slightly apart and knees not touching. Score 1 – Some wobble is allowed of the legs as they partially raise pelvis but they must not clamp their knees together in order to lift their pelvis off.		

Activity	2	1	0
Bridging in supine	Maintains position of bottom off bed for count of 5, kneecaps pointing up, feet slightly apart, knees not touching	Maintains the starting position for 5 seconds then partially raises the pelvis	Unable
Photographs / Notes	Score 2 Full bridge position	Score 1 Partial elevation of pelvis	

Test item 5: Rolling supine to prone

Starting position	Supine on a plinth or floor, arms by side. No pillow		
Instruction	Can roll onto your tummy?		
Scoring detail	This item can be observed as they perform the MMT part of the assessment.		

Activity	2	1	0
Rolling supine to prone	Turns over into prone and frees both arms from under trunk	Rolls partially / to side	Unable
Photographs / Notes			

Test item 6: Gets to sitting			
Starting position	Starting position supine on the floor, with arms by side. No pillow should be used under head.		
Instruction	Can you get from lying into sitting?		
Scoring detail	Aim is to move into long sitting rather than sitting over the edge of a plinth. Use of one hand or arm is acceptable to achieve a score of 2. Score 1 if subject turns into prone or towards the floor/plinth to work their way into sitting or if uses two arms.		
Activity	2	1	0
Gets to sitting	Starts in supine – may use one hand / arm to push up	Uses two arms / pulls on legs or turns towards floor.	Unable
Photographs /notes
Score 2 – Uses no hands

Score 2 -- Only needs one arm to sit up |
Score 1 -- Pulls with both hands on legs | |

Test item 7: Reaches forward			
Starting position	Sitting on floor or plinth in long sitting. Knees may be flexed to accommodate tight hamstrings. Ball placed on plinth far forward enough so they have to use 30 degrees of trunk flexion to touch ball.		
Instruction	Can you reach forward and touch this ball with both hands?		
Scoring detail	Score 2 – uses both hands to reach forward and touch ball and return to upright sitting Score 1 – uses one hand for balance and one hand to touch ball and also returns to upright sitting.		
Activity	2	1	0
Reaches forward	Without upper limb support, leans forward, touches ball and sits back again	With upper limb support, leans forward, touches ball and sits back again	Unable
Photographs /notes	 Score 2 Reaches forward 30˚ knees flexed Score 2 Reaches forward 30˚ legs extended	 Score 1 Needs hand on bed for support	

Test item 8: Stand up from chair

Starting position	Sitting in chair or on plinth with arms folded across chest and with feet able to reach floor or supported on secure box. Starting position 90º hips and knees.
Instruction	Can you stand up from the chair keeping your arms folded if you can?
Scoring detail	A size--appropriate chair (without armrests) or height adjustable plinth should be used. Alternatively a box step under the feet to achieve the correct starting position could be used. Score 2 -- Arms should be kept crossed throughout the activity to score 2

Activity	2	1	0
Stand up from chair	Able to stand up keeping arms folded	Pushes on thighs or chair using one or two hands / prone turn or alters starting position by widening base	Unable

Photographs/ notes			

Score 2 – keeps arms folded

Score 1 – pushes with hands

Score 0 --Needs to use furniture

Test item 9: Stand to sit on chair			
Starting position	Standing with chair / plinth behind patient (close to or touching legs and secure so chair wont slip) Chair should be at a height so that when patient sits in it their hips and knees are at 90 degrees.		
Instruction	Can you sit down in a controlled way?		
Scoring detail	Score 2 – Does not use hands on chair or body and able to sit down in a controlled fashion Score 1 – uses one or two hands on body or chair to sit down safely		
Activity	2	1	0
Stand to sit on chair	Able to sit down without using arm support in a controlled way	With arm support, able to sit down in chair safely	Unable to sit down without assistance
Photographs /notes			

Test item 10: Stand

Starting position	Feet should be no further than 10cm apart and heels on the ground if possible. Arms by sides. NO shoes should be worn.
Instruction	Can you stand up tall for me for as long as you can and as still as you can for three seconds with your heels flat on the ground?
Scoring detail	When counting to 3 – Use "And 1 -- and 2 -- and 3" so that three seconds is achieved on the word of 3. Best done on the floor rather than on a mat. Whichever is chosen maintain consistency through repeated testing sessions. Score 2 -- Minimum count of 3 seconds.

Activity	2	1	0
Standing	Stands upright, still, symmetrical, without compensation (heels flat legs in neutral) for minimum count of 3 seconds	Stands but with compensation	Cannot stand independently, or needs support (even minimal)

Photographs/ notes	Score 2 -- Symmetrical heels flat	Score 1 -- Asymmetrical, heel up, everted Score 1 --postural adaptation
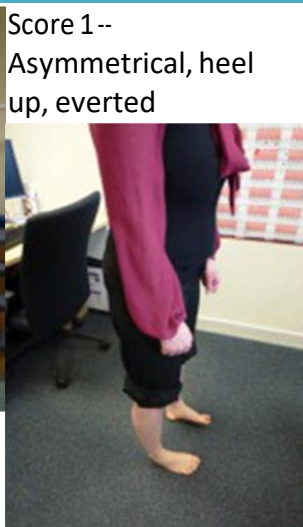
Test item 11: Walk

Starting position	Standing. Observe walk for at least 10 steps in both sagittal and coronal planes.		
Instruction	Can you walk from A to B (state to and where from) for me?		
Scoring detail	Walk without shoes/socks on.		
Activity	2	1	0
Walk 10m	Walks consistently with heel--toe or flat--footed gait pattern	Adapted walking pattern e.g. wide base, altered foot posture, other please define in comments	Loss of independent ambulation or walk short distances with assistance

Score 1 – Externally rotated hips
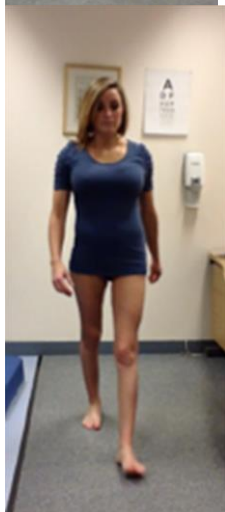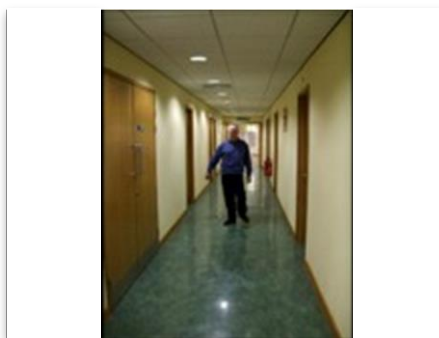
Test item 12 & 13: Stand on one leg R & L

Starting position	Standing. NO Shoes should be worn.
Instruction	Can you stand on your right / left leg for as long as you can?
Scoring detail	Do not use mat. Score 2 – Minimum count of 3 seconds required

Activity	2	1	0
Stand on one leg	Able to stand in a relaxed manner (no fixation) for count of 3 seconds	Stands but momentarily or with trunk side-- flexion or needs fixation e.g. by thighs adducted or other trick	Unable

Photographs / notes			Score 0 --If needs to hold onto a table or person for support or unable to clear foot from the floor

Score 2 – Relaxed and no fixation

Score 1 --Hooks leg behind standing leg

Score 1 --Postural compensation / leaning to side

Test item 14 & 16: Climb box step R &L			
Starting position	A box step 15cm high is used to assess single step climb and descend. Standing in front of box step, toes no more than 20cm away from box step		
Instruction	Can you step onto the top of the box using your right /left leg first?		
Scoring detail	Box step should be approximately 15 cm high. Support may be provided by the use of a height adjustable plinth, or, if not available one 'neutral' hand from the therapist (no taking "weight" of subject).		
Activity	2	1	0
Climbs box step	Faces step – no support needed	Goes up sideways / rotates trunk / circumducts hip or needs support	Unable
Photographs / notes	

Score 1 – Needs | |
| |

support Score 2 – Faces step | | |

Test item 15 & 17: Descend box step R & L			
Starting position	Standing on box step		
Instruction	Can you step down from the box using your right / left leg first?		
Scoring detail	Box step should be approximately 15 cm high. Support may be provided by the use of a height adjustable plinth, or, if not available one 'neutral' hand from the therapist		
Activity	2	1	0
Descends box step	Faces forward, steps down controlling weight bearing leg. No support needed	Sideways, skips down, Pushes on leg, or needs support or uses method that avoids flexing supporting knee (one on the box step)	Unable

Test item 18: Touches floor from standing

Starting position	Standing upright. Arms by sides. Near plinth or chair for support if required.
Instruction	Can you reach down and touch the floor?
Scoring detail	Score 2 – If they are unable to touch the floor due a lack of flexibility in their spine and hips it is acceptable to score 2 if they are short by no more than 20cm off the ground Score 1 – support can be hand(s) on body or plinth or chair

Activity	2	1	0
Touches floor from standing	Without support, touches floor with one hand and stands up again	With support (arm on floor, body, plinth) touches floor with one hand and stands up again	Unable, able to touch floor but cannot get back up again
Photographs/ notes	 Score 2 – Touches floor without using hands or hands on legs	 Score 1 – Uses arm on leg for support	
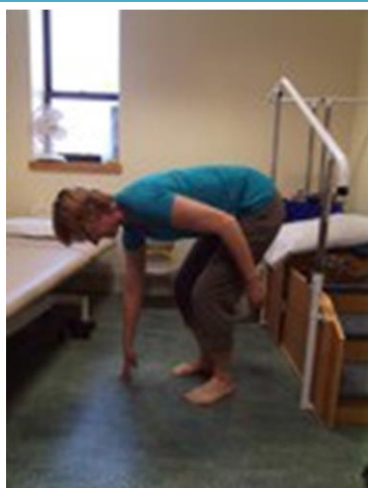
Test item 19: Rise from floor	
Starting position	Starting position in long sitting on floor with arms by sides, legs straight if possible
Instruction	Give the following verbal instructions to the subject: "**When I say GO can you get up as fast as you can and stand up straight with your arms by your side using as little support as possible**". Give the command "**Ready steady – GO**" and start the stopwatch when saying "**GO**". Stop the timer when the subject assumes an upright position with his arms by his side.
Scoring detail / Diagram	Activity should be attempted without use of furniture in the first instance. Score 1: If the person gets to standing independently of any furniture but demonstrates _any part_ of the manoeuvre described below. Components of Gower's manoeuvre: • Turns towards the floor (into a four--point kneeling position or rolls to prone) • Places hands on the floor to assist rising and walks hands back in towards him • Uses one or both arms to push up on legs to achieve upright standing. • Large base of support by abducting hips and extending knees

Test item 19: Rise from floor			
Activity	**2**	**1**	**0**
Rise from floor	No evidence of Gower's maneuver.	Exhibits at least one of the components described above – in particular rolls towards floor, and/**or** use hand(s) on legs	(a) NEEDS to use external support object e.g. chair OR (b) Unable
Photographs / Note	Score 2 -- Doesn't roll. Uses only 1 hand on floor	Score 1 -- Rolled over used hands on floor	Score 0 – Uses chair
	Score 2 No hands on legs to rise	Score 1 -- Didn't roll but used hands	

Test item 20: Stands on heels

Starting position	Standing on the floor. No shoes to be worn.
Instruction	Can you stand on your heels?
Scoring detail	Must clear both feet at the same time to score 2. Watch for inversion. If substantial inversion but forefeet are still lifted – score 1. If only inversion with lateral border of foot still on the ground score 0.

Activity	2	1	0
Stand on heels	Both feet at the same time, clearly standing on heels only (acceptable to move a few steps to keep balance) for count of 3	Only raises forefeet or only manages to dorsiflex one foot or can only evert.	Unable

Photographs / Notes		

Score 2 – Both feet raised

Score 1 -- Both feet raised but only forefoot, everting

Score 1 Raised forefoot only

Score 0 –inversion and feet remain on floor

Test item 21: Jump		
Starting position	Standing on the floor, feet comfortably close together	
Instruction	How high can you jump?	
Scoring detail	Want height, not forward movement. Small amount of forward movement acceptable Score 0 – If unable to leave floor or of they skip jump (one foot then the other)	
Activity	1	0
Jump	Both feet at the same time, clear the ground simultaneously	Unable
Photographs / Notes	Score 1 clears floor, both feet at the same time	Score 0 -- Feet do not leave floor

Test item 22 & 23: Hop R & L leg		
Starting position	Starting position standing on floor on right / left leg. No shoes should be worn.	
Instruction	Can you hop on your right / left leg?	
Scoring detail	Score 1 -- Needs obvious floor clearance.	
Activity	1	0
Hop	Clears forefoot and heel off floor	Unable
Photographs / Notes	Score 2 – Clears foot off floor	Score 0 – not leaving the floor

Test item 24: Squat down			
Starting position	Standing		
Instruction	Can you bend down to the floor bending your knees like this? (show them the manoeuvre)		
Scoring detail	For score 1 please tick whether they used the floor or their hands on their thigh. One tick for one hand, two ticks for two hands. They would score 0 is they used furniture.		
Activity	2	1	0
Squat	Squats down fully with arms free (more than 90° of hip and knee flexion)	Uses one or two hands on thighs or floor to assist full squat On thigh ☐ On floor ☐	Unable

Photographs / Notes

Score 2 – full squat – no hands

° Score 1 – uses hands on floor to assist full squat

Score 0 – Unable to squat

Test item 25: Rise from squat		
Starting position	Squatting	
Instruction	Can you now stand up from that position?	
Scoring detail	For score 1 please tick the boxes to indicate whether they used a hand on the floor or on their thigh. Tick both boxes if they used one hand on the floor and one hand on their thigh. They would score 0 if they first went onto all fours or onto their knees to rise from squat or if they used furniture.	
Activity	2	1	0
Rise from squat	Stands up from full squat without using arms / hands on floor or legs	Uses one or two hands to rise from squat to stand On thigh ☐ On floor ☐	Unable to get back up from squat without assistance or uses furniture
Photographs / Notes	 Score 2 -- No use of arms	 Score 1 – Uses hands on floor to rise from squat	

Test item 26: High kneeling to stand through right leg (leading with left leg)

Starting position	High kneeling, arms free
Instruction	Can you stand up from this position starting with your left leg without using your hands? May need demonstration Have a bench nearby in case the subject requires support for balance or strength
Scoring detail / Diagram	Scores 2: The subject independently transitions from high kneeling to standing via right half kneel without arm support. Half kneeling on the right knee must be used in the transition from high kneeling to stand. Scores 1: Able to stand through R leg (leading with left leg) using hand(s) on body or floor. Scores 0: The subject is unable to achieve standing though half kneel or uses furniture to do so.

Activity	2	1	0
High kneel to stand through right half kneel	Able with arms free	Able to stand up through R half kneeling using hands on floor or legs (Furniture NOT allowed)	Unable
Photographs / Notes	Score 2– Able to rise through half kneeling without using hands	Score 1 -- Subject uses arms to initiate standing and can stand up	

Test item 27: High kneeling to stand through left leg (leading with right leg)

Starting position Instruction	High kneeling, arms free Can you stand up from this position starting with your right leg without using your hands? May need demonstration Have a bench nearby in case the subject requires support for balance or strength
Scoring detail / Diagram	Scores 2: The subject independently transitions from high kneeling to standing via right half kneel without arm support. Half kneeling on the left knee must be used in the transition from high kneeling to stand. Scores 1: Able to stand through L leg (leading with right leg) using hand(s) on body or floor. Scores 0: The subject is unable to achieve standing though half kneel or uses furniture to do so.

Activity	2	1	0
High kneel to stand through right half kneel	Able with arms free	Able to stand up through L half kneeling using hands on floor or legs (Furniture NOT allowed)	Unable

Photographs / Notes	Score 2 Subject stands from high kneeling through left half kneel without the use of arm support (is not using elbow) Score 1 Subject moves from high kneel to left half kneel and uses arm support to stand.

Test item 28: Stand on tiptoes		
Starting position	Standing	
Instruction	Can you stand on your tiptoes?	
Scoring detail	For a score 2, it is possible for the subject to use furniture for balance but not support or weight bearing	
	2	**1**	**0**

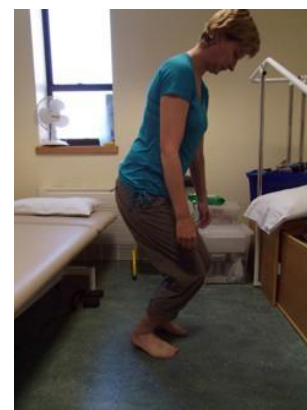| Stand on tip toes	Tiptoes on one foot, clearly on toes for count of 3, knee straight	Both feet at the same time, clearly on toes for count of 3, knees straight	Unable / momentarily / knees flexed

Photographs / Notes

Score 2 Single heel raise, flexed Knee straight

Score 1 – Up on toes of both feet for count of 3, knees straight

Score 0: Knees to lift heels

Score 2 Single heel raise, rail for balance onl...

Test item 29: Run (10 metres)	
Starting position	Standing
Instruction	Give the following verbal instructions to the subject: "When I say GO you go as fast as you safely can all the way to me." Give the command "ready steady – GO" and start the stopwatch when saying "GO". Give encouragement as necessary. Stop the timer when the second foot clears the finish line.
Scoring detail	A straight 10m walkway should be clearly marked in a quiet department or corridor. A stopwatch should be used to time the walk. Preferably no shoes to be worn. Ensure safety of subject. They should self select speed after being asked to go 'as fast as they can'. Score 1 – Faster than a walk but no time in 'flight' Both feet are never off the ground at the same time. May use excessive use of arms, trunk rotation, substantial 'waddle'. No real 'push--off'

Activity	2	1	0
Run	Both feet off the ground (no double stance phase during running)	Faster than a walk.	Walk

Photographs / Notes	
Score 2 -- Both feet off the ground Definite 'run'	Score 1 -- Picks up speed but waddles and always has double stance

9. TIMED FUNCTIONAL TESTS

Order of Tests

WITHIN NSAD WITHOUT SHOES

- Timed Rise from floor
- Timed 10 metre walk /run

WITH SHOES

- Timed up and go (TUG)
- Stair Ascend
- Stair Descend
- Timed rise from chair

Rise from floor (NSAD Item 19)

- **No shoes or socks to be worn**
- Place the subject in a long sitting position on the floor with his arms by his sides and his legs in front of him.
- Give the following verbal instructions to the subject: "**When I say GO you get up as fast as you can and stand up straight with your arms by your side**".
- Give the command "**Ready steady – GO**" and start the stopwatch when saying "**GO**".
- Stop the timer when the subject assumes an upright position with his arms by his side.
- Only provide a chair after the subject has attempted to stand from the floor for 30 seconds and failed.
- Time recorded to the nearest 1/10th of a second? _ _. _ seconds

Grading Rise from floor

Assign 1 of the following grades:

1= Unable to stand from supine, even with use of a chair

2= Assisted Gower's – requires furniture for assist in arising from supine to full upright posture

3= Rolls over, stands up with both hands "climbing up" the legs to achieve full upright posture.

4= Rolls over, stands up with 1 hand support on leg

5= Rolls to the side and stands up with one or both hands on the floor to start to rise but does not touch legs

6= Stands up without rolling over or using hands on legs

10 metre walk/run without shoes (NSAD Item 29)

Preparation	•	**No shoes, socks or orthoses should not be worn** for this test
	•	NOTE: An additional timed walk/run is performed to determine ambulatory status at the beginning of the assessment in shoes and using any orthotics and walking aids.

Mark out 10m distance in quiet area if possible

Starting position   Standing at start of marked distance

Instructions   On the word "GO" go as fast as you can to "x". Define point x.

Timing   Start timing on the word go and stop when the second foot passes the 10 metre mark.

Grading
Timing-- to the nearest 1/10th of second

Timing-- to the nearest $1/10^{th}$ of second

10 m Walk / Run (in shoes)							
Grade	**1**	**2**	**3**	**4**	**5**	**6**	**Time (seconds)**
10 metre walk / run Please circle	Unable	Walk with aids	Walk No extra speed	Walk extra speed	Nearly running no flight	Running	_ _ . _ s

Timed up and go

| Preparation | **Shoes to be worn**. Place a piece of tape or other marker on the floor 3 metres away from the chair so that it is easily seen by the subject. The chair should be stable and positioned such that it will not move when the subject moves from sitting to standing.

The subject wears their **regular footwear**, may use any gait aid that they normally use during ambulation, but may not be assisted by another person. There is no time limit. They may stop and rest (but not sit down) if they need to. Please mark on the worksheet what orthotics and aids they use.

Normal healthy elderly usually complete the task in ten seconds or less.
The subject should be given a practice trial that is not timed before testing |
|---|---|
| Starting position | Subject sitting in a **chair with arms**. The subject's back should rest on the back of the chair. |
| Instructions | On the word "GO" you will stand up, go as fast as you safely can to the line on the floor, turn around and come back to the chair and sit down. |
| Timing | Start timing on the word "GO" and stop timing when the subject is seated again correctly in the chair with their back resting on the back of the chair. Time taken recorded to the 1/10th second |

Stair Climb

Preparation	**Shoes to be worn**. Use standard steps four steps with handrail where possible

|	
Starting position	Standing upright at bottom of steps. Arms by side

Instructions
When I say "GO" climb the stairs as quickly as you can, safely and stand up straight with your arms by your side when you get to the top

Timing Start the watch on the word go and stop it when they are standing straight with their arms by their side. Time recorded to 1/10th second

Grading

1. Unable to climb 4 standard stairs

2. Climbs 4 standard stairs "marking time" (climbs one foot at a time, with both feet on a step before moving to next step), uses **both arms** on one or both handrails or uses 1 handrail and the other arm pushes on the leg.

3. Climbs 4 standard stairs "marking time" (climbs one foot at a time, with both feet on a step before moving to next step), using one arm on one handrail or one arm on a leg or body

4. Climbs 4 standard stairs "marking time" (climbs one foot at a time, with both feet on a step before moving to next step), not needing handrail

5. Climbs 4 standard stairs alternating feet, needs handrail for support or uses arms on body or legs.

6. Climbs 4 standard stairs alternating feet, not needing handrail support
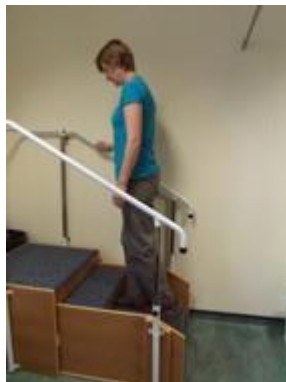
Grade 5

Stair Descend

Preparation   **Shoes to be worn**. As stair ascend

Starting position   Standing at the top of the stairs with arms by side (not hands in pockets)

Instructions
When I say "GO" go as fast as you can down the stairs safely and at the bottom, stand up straight with your arms by your side

Timing
Start the watch on the word go and stop it when they are standing straight with their arms by their side.
Time taken recorded to the nearest 1/10th second

Grading

1. Unable to descend 4 standard stairs

2. *Descends 4 standard stairs "marking time" (descends one foot at a time, with both feet on a step before moving to next step), requires both arms on one or both handrails or uses 1 handrail and the other arm pushes on the leg.*

3. Descends 4 standard stairs "marking time" (descends one foot at a time, with both feet on a step before moving to next step), requires one arm on a handrail or one arm on a leg or body

4. Descends 4 standard stairs "marking time" (descends one foot at a time, with both feet on a step before moving to next step), not needing handrail

5. Descends 4 standard stairs alternating feet in both directions, needs handrail for support or uses arms on body or legs

6. Descends 4 standard stairs alternating feet, not needing handrail support

Grade 5

Rise from chair

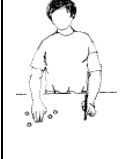|	
Preparation	**Shoes to be worn**. The chair should be stable and positioned such that it will not move when the subject moves from sitting to standing. The subject wears their **regular footwear**, may use any gait aid that they normally use during ambulation, but may not be assisted by another person.
Starting position	Subject sitting in a **chair without arms**. The subject's back should rest on the back of the chair.
Instructions	On the word "GO" you will stand up, go as fast as you can.
Timing	Start timing on the word "GO" and stop timing when the subject is standing fully upright.
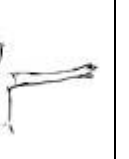
Rise from Chair Record height of chair from floor to middle of cushion or pad …………….cm						
Timed rise from chair Please circle Standard chair with no arms	Unable	Stand up using additional furniture or person	Uses two hands to stand up	Uses one hand to stand up	Adapts standing position to stand	Gets up normally	_ _ . _ s

10. PERFORMANCE OF UPPER LIMB SCALE PUL 1.3 –PROXIMAL MODULE ONLY

Relationship of Entry Item A to Brooke score.

The Brooke Upper Extremity Functional Rating Scale was developed specifically for use in DMD [Brooke 1989] and has been used frequently as an outcome measure in the disease [Lue 2006]. The original instrument grades arm and shoulder function from to 1 to 6, with higher values indicating less function. The adapted version is reversed to reflect the majority of functional rating scales where a higher score means higher function. An additional score of 4 has been added in

Adapted Brooke Score	0	1	2	3	4	5	6
	No useful function of hands.	Can use hands to hold pen or pick up a coin or drive a powered chair	Can raise 1 or 2 hands to mouth but cannot raise a cup with a 200g weight in it to mouth	Can raise standardized plastic cup with 200g weight in it to mouth using both hands if necessary.	Can raise both arms (elbows to shoulder height with or without compensation. Elbow bent or in extension	Can raise both arms simultaneously above head only by flexing the elbow shortening circumference of the movement /using accessory muscles)	Can abduct both arms simultaneously elbows in extension in a full circle until they touch above the head.
Original Brooke Score	6	5	4	3	3	2	1

Introduction to PUL 1.3 (Proximal module only)

The **Performance of the Upper Limb** (PUL) **Scale** has been devised to assess motor performance in the upper limb for individuals with dystrophinopathies (Becker and Duchenne muscular dystrophy). Details of the conceptual framework of the scale are detailed in the manual and elsewhere (Mayhew et al. [Dev Med Child Neurol.](#) 2013 Nov;55(11):1038-45). PUL has been devised by the PUL Physiotherapy Working Group (Anna Mayhew, Michelle Eagle, Elena Mazzone, Marion Main, Maria Ash, Meredith James, Marlene Vandenhauwe, Katrijn Klingels, Tina Duong, Julaine Florence, Valerie Decostre). Work is on-going to improve the content, validity and reliability of the scale. This version (1.3) has been updated to reflect on-going psychometric analysis of the scale properties.

Conceptual Framework of PUL

Intended population
Ambulant and non-ambulant individuals with dystrophinopathies from childhood to adulthood. The scale is recommended from 7 years of age onwards. This has been included to assess proximal arm function in LGMD2I.
The purpose of an upper limb scale for use in dystrophinopathy is to assess change that occurs in motor performance of the upper limb over time from when a boy is still ambulant to the time he loses all arm function when non-ambulant. Motor performance in dystrophinopathy is defined as a demonstrated ability to perform a skill under certain test conditions. This performance changes with disease progression and /or intervention (including surgery) and is based on the observed response on the day. Motor performance will be impacted by muscle strength, contractures and maturational development (puberty) and the scale aims to incorporate performance of shoulder, elbow, wrist and hand function. Specific domains have yet to be established precisely but domains may relate to functional workspace. I.e. high level shoulder dimension, mid-level elbow dimension, distal wrist and hand dimension. **These may however lie on a continuum of ability.** Items measuring motor performance will relate to meaningful functional activities (as detailed in a related Patient Reported Outcome measure (PROM) developed through patient focus groups)

Proposed Conceptual framework for Performance of Upper Limb Scale

Muscle strength

Maturation development ———————→ Motor Performance

Contractures
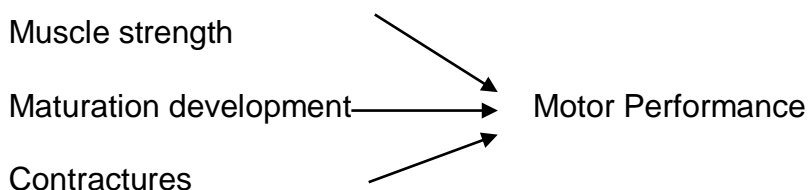
Equipment Required

General Instructions

- In general items are scored without compensation, if there is compensation score lower
- Ideally the same evaluator should perform evaluations at subsequent assessments
- Items should be performed in the order provided in this manual
- The subject should wear loose clothing, T shirt etc.
- For ambulant individuals and those still able to transfer with minimal assistance use a chair with a backrest but no armrests and ensure their feet are supported / on the floor
- For individuals in a powered chair unable to transfer easily ensure their chair has the seat positioned as horizontally as possible, the backrest in an upright position if tolerated and

that the feet are supported, no armrests if possible

- No assistive devices are to be used for any of the tests
- We recommend that a plinth / adjustable table is not used to sit **on** for the tests (as there is no back support)
- On the worksheet, mark whether the right or left were chosen to perform the test. The same hand must be used throughout and at successive visits unless both hands are used together
- If starting position cannot be maintained because of contractures, score is 0 unless stated that starting position can be adapted.

In the worksheet, indicate:
- Preferred arm is defined as the one used to draw or write or, if unable, the arm most frequently used to perform tasks.
  Items of the PUL scale can be performed by the preferred arm (dominant or not) but must be the same one throughout and at successive visits.
- Make a note of significant elbow contractures and mark on the worksheet if the score was limited by these. Elbow contracture should be expressed as its degrees from full elbow extension e.g. -10
- Ambulant is defined as able to walk 10m without any kind of support and non ambulant as unable to walk 10m without any kind of support

Entry item – Adapted Brooke Score

Equipment:	200g weight and plastic cup. Coin and a pencil if necessary.
Starting position:	Sitting, start with hands on lap, no table in front of them. If ambulant use a chair with a back rest but with no armrests. If they are non-ambulant and it's not practical to transfer them they can remain in their wheelchair with seat as horizontal as possible and backrest upright as possible.
Instruction:	**"Lift your hands and arms as high as you can**." Trunk side flexion can be up to 20°. If they bend their head to their hands instruct them to keep their head up if they can. For individuals less able you can start by asking them: **"Can you bring your hands to your mouth?"** For the most able individuals, demonstrate abduction of both arms simultaneously with elbows in extension.
Scoring details	Score 4: Defined as elbow to shoulder height. Score 2 and 3. They should not do this by bringing their mouth to their hands. If they use significant head and trunk flexion in order to complete the task means they cannot score 2 or 3 for this item.

1. Shoulder abduction arms above head (scored from Entry item A)

Equipment:	Seated in chair, no arm rests
Starting position:	Sitting, Preferably with no arm rests on chair. Start with their hands in their lap and elbows unsupported.
Final position	Both arms extended above head through abduction
Instruction:	"Raise your arms above your head out to the side – try and keep straight elbows"
Scoring details	This item is scored from the entry item above. A score of 2 is the equivalent of a score 6 in the entry item and a score 1 is equal to a score of 5 in the entry item. 4 or below in the entry item scores 0 in this item.

Item	Description	0	1	2
1 Score from Entry item above	**Shoulder abduction both arms above head** "Raise your arms above your head out to the side – try and keep straight elbows"	Unable	Can raise both arms simultaneously **above head** only by flexing the elbow (using compensation)	Can abduct both arms simultaneously elbows in extension in a full circle until they touch above the head

2. Shoulder flexion above shoulder height (no weight)

3. Shoulder flexion above shoulder with 500g weight

4. Shoulder flexion above shoulder with 1 kg weight

Equipment:	Weights
Starting position:	Sitting, preferably with no arm rests on chair. Start with their hands in their lap. And elbows unsupported, ask them to use a full palmar grasp to hold the weight. NO table in front. Position yourself to make sure that trunk is not assisting e.g at the side of the subject.
Finish position	Arm extended in front (elbow to eye level) – through flexion Note: **the arm should be in neutral not pronated or supinated.** The movement is a combination of almost simultaneous forward flexion and elbow extension
Testing sequence	Test using no weight first – Item 2. Proceed to both additional items as they may be able to complete the task using compensation.
Instruction:	Item 2:"Reach out and touch my hand" –elbow to eye level Item 3 and 4: "Hand on lap – give me the weight" Always take weight from them once they have reached maximum height (to avoid eccentric muscle work).
Scoring details	The proper movement without compensation is a simultaneous combination of shoulder flexion and elbow extension. Absence or asynchrony of one of these components or additional movement is considered as compensation. They score 2 if they do not use compensation. They score 1 if they use compensation but still achieve the correct end position. Other arm must remain in the individuals lap

Item	Description	0	1	2
2	**Shoulder flexion above shoulder height (no weights)** "Reach out and touch my hand" –elbow to eye level	Unable	Able **with** compensation	Able **without** compensation
3	**Shoulder flexion above shoulder height with 500 g weight** Hand on lap – "give me the weight" –elbow to eye level	Unable	Able to lift 500g weight **with compensation**	Able to lift 500g weight **without compensation**
4	**Shoulder flexion above shoulder with 1 kg weight** Hand on lap – "give me the weight" –elbow to eye level	Unable	Able to lift 1 kg weight **with compensation**	Able to lift 1 kg weight **without compensation**

5. Shoulder abduction above shoulder height (no weight)

6. Shoulder abduction above shoulder with 500g weight

7. Shoulder abduction above shoulder with 1 kg weight

Equipment:	Weights
Starting position:	Sitting, preferably with no arm rests on chair. Start with their hands in their lap. And elbows unsupported, ask them to use a full palmar grasp to hold the weight. NO table in front. Position yourself to make sure that trunk is not assisting e.g at the side of the subject.
Finish position	Arm extended too side (elbow to eye level) – through abduction Note: **the arm should be in neutral not pronated or supinated.** The Movement is a combination of almost simultaneous abduction and elbow extension
Testing sequence	Test using no weight first – Item 5. Proceed to both additional items as they may be able to complete the task using compensation.
Instruction:	Item 5:"Reach out and touch my hand" –elbow to eye level Item 6 and 7: "Hand on lap – give me the weight" Always take weight from them once they have reached maximum height (to avoid eccentric muscle work).
Scoring details	The proper movement without compensation is a simultaneous combination of shoulder abduction and elbow extension. Absence or asynchrony of one of these components or additional movement is considered as compensation. They score 2 if they do not use compensation. They score 1 if they use compensation but still achieve the correct end position. Other arm must remain in the individuals lap

Item	Description	0	1	2
5	**Shoulder abduction above shoulder height (no weights)** "Reach out and touch my hand" –elbow to eye level	Unable	Able **with** compensation	Able **without** compensation
6	**Shoulder abduction above shoulder height with 500 g weight** Hand on lap – "give me the weight" –elbow to eye level	Unable	Able to lift 500g weight **with compensation**	Able to lift 500g weight **without compensation**
7	**Shoulder abduction above shoulder with 1 kg weight** Hand on lap – "give me the weight" –elbow to eye level	Unable	Able to lift 1 kg weight **with compensation**	Able to lift 1 kg weight **without compensation**

11.6--MINUTE WALK TEST

This evaluation is a modified version of the 6MWT adapted from the protocol specifically designed for DMD in the PTC 124 2b trial (ATS, 2002, Ref Henriksen, Mc Donald).

Testing Guidelines

- Subjects should wear comfortable clothing and appropriate shoes for walking (ie, trainers, tennis shoes, etc). Since subjects will be tested at multiple time points, they should make an effort to wear the same type of shoes each time.

- A light meal or snack is permissible at least 1 hour before testing.

- A walking stick or aid may be used if the patient feels this is required for safety. Please mark use of a walking aid or orthotics clearly on the worksheet.

Course Set up

- The test should be performed indoors, along a flat, straight, enclosed, and seldom travelled corridor at least 6 feet wide with a hard surface. The test area will be marked with a 25--metre tape line. The tape line should be placed in the middle of the corridor. Arrows indicating the counterclockwise direction and path of movement should be placed in a half--circle at the ends of the course. Note that due to the possibility of subject falls, the course should be within easy access of appropriate medical assistance.

Testing Directions

- Set the stopwatch to zero.

- Ask the subject to stand quietly with his toes at the starting line, immediately adjacent to axis of the "home" cone.

- The following information should be imparted to the subject in a way they will understand

  "Remember, you will be walking back and forth around these cones without crossing the line in the middle. You will walk around the cone in a half circle without slowing down. Then you will go back the other way. Remember that the object of this test is to walk as fast and as far as you can for six minutes without running."

- The clinical evaluator should follow the subject whilst he is walking around the course.

- When the subject is ready, say "Ready, set, go!", and start the stopwatch.

- Every time the subject reaches the each end of the course, mark the worksheet to record the time at each 25 metres completed.

- Give positive verbal encouragement as appropriate.

- Let the subject know how long he has been walking. For example "three minutes done, only three to go, you are half way there, one minute left"

  - If the subject stops to rest, say:

- "You can lean on the wall or stand to rest. Just start walking again as soon as you feel like you can."
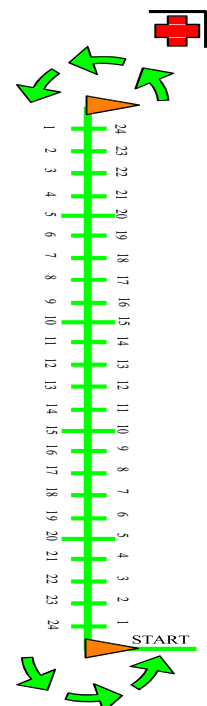
If the subject falls:

Record the time of fall

- The evaluator should ensure that the subject is OK, and then should assist him back to a standing position as soon as it is safe to do so.

- If the subject is injured or cannot rise from the floor, the test is over. Total time and distance should be recorded, and any necessary medical attention should be given to the subject.

- If the subject is uninjured, he should resume walking as soon as he is able. Say:

"If you are alright, you should start walking again as soon as you feel like you can."At the final seconds of the test count down, the timer will announce:

"Five fifty seven, five fifty--eight, five fifty--nine, six minutes! Great job, you can stop now." Bring a chair or wheelchair for him to sit and rest. Offer the subject a drink of water.

- Measure the distance from the final cone passed to the point at which the subject stopped at 6 minutes. Multiply by 25 the number of completed 25 metre laps and add to the distance reached on the final lap. This is recorded as the total distance walked in 6 minutes.

- Document the number of falls during the 6 minute walk test

Safety Considerations and Additional Information

- Subjects should have medical clearance from the study investigator prior to testing.

- Testing staff should know the location of the nearest resuscitation cart and institutional emergency care procedures. Emergency contact numbers should be immediately accessible.